TECHNISCHE UNIVERSITÄT MÜNCHEN

Lehrstuhl für Analytische Lebensmittelchemie

Manganese:
Species Pattern and Mechanisms of Brain Injury

Katharina Theresa Neth

Vollständiger Abdruck der von der Fakultät Wissenschaftszentrum Weihenstephan für Ernährung, Landnutzung und Umwelt der Technischen Universität München zur Erlangung des akademischen Grades eines

Doktors der Naturwissenschaften

genehmigten Dissertation.

Vorsitzender: Univ.-Prof. Dr. rer. nat. Erwin Grill

Prüfer der Dissertation:

1. apl. Prof. Dr. agr. habil. Philippe Schmitt-Kopplin
2. Univ.-Prof. Dr. rer. nat. Michael Rychlik
3. Hon.-Prof. Dr. rer. nat. Bernhard Michalke
   (Technische Universität Graz/ Österreich)

Die Dissertation wurde am 15.09.2015 bei der Technischen Universität München eingereicht und durch die Fakultät Wissenschaftszentrum Weihenstephan für Ernährung, Landnutzung und Umwelt am 13.01.2016 angenommen.

To Simon & Lisa-Marie

…And until we meet again,
May God hold you in the palm of His hand.

Acknowledgments

Summary

Manganese (Mn) is an essential trace element being involved in many important functions within the body. Already in 1873 symptoms of a neurological disorder have been described in welders exposed to Mn-dust, which comprised similarities to Parkinson´s Disease, and were termed manganism. Besides of the occupationally exposed cases, other endangered individuals have been described (e.g. anemic persons or patients, who received long-time parenteral nutrition). Many studies are concentrating on the elucidation of the mechanism of Mn-induced injury of neural tissue in various exposure models both *in vivo* and *in vitro*. The overall aim is, to exactly understand the preliminary mechanisms for early detection of the onset of manganism and for appropriate intervention or even therapy.

In this work, this aim was pursued from the analytical perspective, whereby the focus was on the application of Mn-concentrations in the range of non-toxic but elevated levels at the edge of toxicity. For this purpose, two different animal models in rats were carried out: one with increased, subchronic exposure (almost 2 month) via the fodder as well as one single intravenous injection of Mn. Elemental levels of Mn, iron (Fe), copper (Cu) and zinc (Zn) in serum and brain were monitored by ICP-OES or -MS, and revealed alterations dependent on the exposure condition. The same dependency was true for AchE activity and glutamate concentrations in brain. Mn-speciation by SEC-ICP-MS in serum and brain extracts revealed an increase in low molecular mass compounds as possible binding partners for Mn when compared to the respective controls. This increase, however, was dependent on the exposure method. The determination of the oxidation state of Fe in brain by IC-ICP-OES showed for the first time that the highly toxic Fe(II)-species is increased by a subchronic Mn-exposure, contributing to the development of oxidative stress in neural tissue. Furthermore, a non-targeted analysis of the brain by means of ESI-ICR/FT-MS revealed changes in several pathways due to the Mn- exposure, which all indicated a diminished ability of protection against oxidative stress. For the first time, the connectivity between Mn-species in serum or brain with alterations in metabolites of the brain was examined by correlation studies. That approach showed that certain Mn-species could be possible indicators of the emerging disease of neural tissue. Finally, a LA-ICP-MS method was developed within this work for localization of Mn, Fe, Cu and Zn within brain slices. Initial results revealed the distribution of these elements after a single Mn-injection compared to control by elemental imaging.

In summary, the knowledge of Mn-induced injury of neural tissue from previous studies could be underlined, connected and even expanded by the combination of metallomics and metabolomics.

Zusammenfassung

Mangan (Mn) ist ein essentielles Spurenelement, welches viele verschiedene Funktionen im Körper einnimmt. Bereits 1873 wurden in Schweißern, die mit Mn-Staub exponiert waren, Anzeichen einer neurologischen Störung mit Parkinson-ähnlichem Erscheinungsbild beschrieben, welches als Manganismus bezeichnet wurde. Neben beruflich exponierten Individuen zählen auch z.B. Menschen mit Anämie oder mit langzeit-parenteraler Ernährung zu gefährdeten Gruppen. Ziel aller Studien zur Aufklärung der Mechanismen der Mn-induzierten Schädigung von neuronalem Gewebe ist es, die vorherrschenden Mechanismen genau zu verstehen, um Manganismus möglichst frühzeitig zu detektieren und mit geeigneten Therapien zu intervenieren.

In der vorliegenden Arbeit wurde dieses Ziel aus der analytischen Perspektive verfolgt. Hierbei stand im Mittelpunkt, dass die verwendeten Mn-Konzentrationen nicht im toxischen, aber im erhöhten Bereich an der Schwelle zur Toxizität lagen. Es wurden zwei verschiedene Tiermodelle in der Ratte durchgeführt: eine erhöhte, subchronische Exposition (~ 2 Monate) über das Futter sowie eine einmalige i.v. Injektion von Mn. Konzentrationen an Mn, Fe, Cu und Zn in Serum und Gehirn wurden mittels ICP-OES/-MS bestimmt und ergaben Veränderungen abhängig von der Expositionsmethode. Gleiches bestätigte sich für die AchE Aktivität sowie Glutamat Konzentrationen im Gehirn. Durch Mn-Speziation mittels SEC-ICP-MS in Serum und Gehirn konnte eine Erhöhung von niedermolekularen Verbindungen als Mn-Bindungspartner im Vergleich zu den Kontrollen beobachtet werden. Die Bestimmung der Oxidationsstufen von Fe im Gehirn mittels IC-ICP-OES konnte zum ersten Mal zeigen, dass die hoch toxisches Fe(II) durch subchronische Mn-Exposition erhöht ist, was zur Entstehung von oxidativem Stress im Gehirngewebe beitragen kann. Zudem zeigte eine nicht-zielgerichtete Untersuchung des Gehirns mittels ESI-ICR/FT-MS Veränderungen in verschiedensten Metabolismen aufgrund der Mn-Exposition, welche alle auf einen verminderten Schutz gegen oxidativen Stress hindeuteten. Zum ersten Mal wurde der Zusammenhang von Mn-Spezies in Serum und Gehirn mit Metaboliten im Gehirn anhand von Korrelationsstudien untersucht. Dieses Verfahren zeigte, dass Mn-Spezies als Indikatoren einer entstehenden Erkrankung des neuronalen Gewebes dienen könnten. Abschließend wurde eine LA-ICP-MS Methode entwickelt, um die Verteilung von Mn, Fe, Cu und Zn nach einmaliger i.v. Injektion von Mn in Gehirnschnitten mittels eines bildgebenden Verfahrens zu untersuchen.

Zusammenfassend konnte somit das Wissen über die Mn-induzierte Schädigung von neuronalem Gewebe aus vorangehenden Studien durch die Verbindung von *Metallomics* und *Metabolomics* belegt, aber auch erweitert und Zusammenhänge geknüpft werden.

List of scientific Communications

Original Research Articles

<u>Fernsebner K</u>, Zorn J, Kanawati B, Walker A, Michalke B. **Manganese leads to an increase in markers of oxidative stress as well as to a shift in the ratio of Fe(II)/(III) in rat brain tissue.** Metallomics, 2014, 6(4): 921-31.

<u>Neth K</u>, Lucio M, Walker A, Kanawati B, Zorn J, Schmitt-Kopplin P, Michalke B. **Diverse Serum Manganese Species affect Brain Metabolites depending on Exposure Conditions.** *Chemical Research in Toxicology*, 2015, *28* (7): 1434–1442.

<u>Neth K</u>, Lucio M, Walker A, Zorn J, Schmitt-Kopplin P, Michalke B. **Changes in Brain Metallome/Metabolome Pattern due to a Single *i.v.* Injection of Manganese in Rats.** PLoS One, 2015, accepted

Review Article

Michalke B, <u>Fernsebner K</u>. **New insights into manganese toxicity and speciation.** Journal of Trace Elements in Medicine and Biology, 2014, 28(2):106-16.

Book Chapter

<u>Neth K</u>, Bornhorst J, Michalke B. **Neurodegeneration with focus on Manganese and Iron speciation.** In: Metallomics: Analytical Techniques and Speciation Methods, 2015, Manuscript submitted

Oral presentations

30. Jahrestagung der Gesellschaft für Mineralstoffe und Spurenelemente e.V. (GMS) 2014, Freising-Weihenstephan, Germany: **Elemental Speciation in Biological Matrices.** <u>Neth K</u>, Michalke B

29. Jahrestagung der Gesellschaft für Mineralstoffe und Spurenelemente e.V. (GMS) 2013, Berlin, Germany: **Explorating the Mechanism of Mn-induced dopaminergic Injury.** <u>Fernsebner K</u>, Walker A, Kanawati B, Schmitt-Kopplin P, Michalke B.

Anorganica 2013 der Firma Perkin Elmer, Frankfurt, Düsseldorf, Hamburg, Berlin und München, Germany: **Einsatz von Kopplungstechniken in der ICP-MS/-OES: Praktische Erfahrungen mit HPLC, CE & Laser**. <u>Fernsebner K</u>

Poster Presentations

European Winter Conference on Plasma Spectrochemistry 2015, Münster, Germany: **Manganese: Species pattern and Mechanism of action in Neuroinflammation during acute and chronic exposure in rats.** Neth K, Lucio M, Walker A, Kanawati B, Zorn J, Schmitt-Kopplin P, Michalke B.

5th Congress of the Federation of European Societies on Trace Elements and Minerals (FESTEM) 2013: Investigations on the Mechanisms of Mn-Induced Injury of Dopaminergic Neurons. Fernsebner K, Lucio M, Walker A, Kanawati B, Zorn J, Schmitt-Kopplin P, Michalke B.

European Winter Conference on Plasma Spectrochemistry 2013, Krakau, Polen: **Dissecting the Role of Manganese in Dopaminergic Neurotoxicity**. Fernsebner K, Walker A, Kanawati B, Schmitt-Kopplin P, Michalke B.

Poster Presentations

List of Abbreveations

ANOVA	Analysis of variance
CSF	Cerebrospinal fluid
(O)PLS-DA	(Orthogonal) Partial least square-discriminative analysis
+Mn_Food	Samples from animals, which were supplemented with increased Mn by food
+Mn_Inj (_1h/_4d)	Samples from animals, which received $MnCl_2$ injection (one hour or four days after injection)
AchE	Acetylcholinesterase
AD	Alzheimer´s Disease
ANOVA	Analysis of variance
ARA	Arachidonic acid
b.w.	Body weight
Cit	Citrate
cps	Counts per second
CRF	Certified reference standards
DA	Dopamine
DHA	Docosahexanoic acid
DMT-1	Divalent metal transporter-1
DRC	Dynamic reaction cell
ESI-ICR/FT-MS	Electrospray ionization-ion cyclotron resonance/Fourier transform-mass spectrometry
GPx	Glutathione peroxidase
GS	Glutamine synthetase
GSH/GSSG	Reduced/oxidizes glutathione (glutathione disulfide)
HCA	Hierarchical cluster analysis
HMM	High molecular masses
HSA	Human serum albumin
IC-ICP-OES	Ion chromatography-inductively coupled plasma-optical emission spectrometry
ICP-sf-MS	Inductively coupled plasma-sector field-mass spectrometry
Int.	Intensity
IS	Internal standard
i.v.	intravenously
KED	Kinetic energy discrimination
LA-ICP-MS	Laser ablation-inductively coupled plasma-mass spectrometry
LMM	Low molecular masses
LoD	Limit of detection
m/z	Mass to charge ratio
PCA	Principal component analysis

PD	Parkinson´s Disease
PGB	Prostaglandin
PPP	Pentose-Phosphate-Pathway
PUFAs	Poly unsaturated fatty acids
ROS	Reactive oxygen species
RT	Retention time
S/N	Signal to noise ratio
SEC-ICP-MS	Size exclusion chromatography-inductively coupled plasma-mass spectrometry
Tf	Transferrin
TfR	Transferrin receptor
TH	Tyrosine hydroxylase
TOF	Time of flight
VIP	Variable importance in projection

List of Figures

List of Tables

.

A   Introduction

A.1   Metallomics - Studying the Metallome

A.1.1   Definitions

In 2001 Williams referred to the term *metallome* as an element distribution, equilibrium concentrations of free metal ions or as free element content in a cellular compartment, cell or organism (Williams 2001). Hence, an organism is not only described by its genome, proteome or metabolome but also by an elemental compartment, the metallome (Figure 1). This seems somehow natural as fundamental bio-
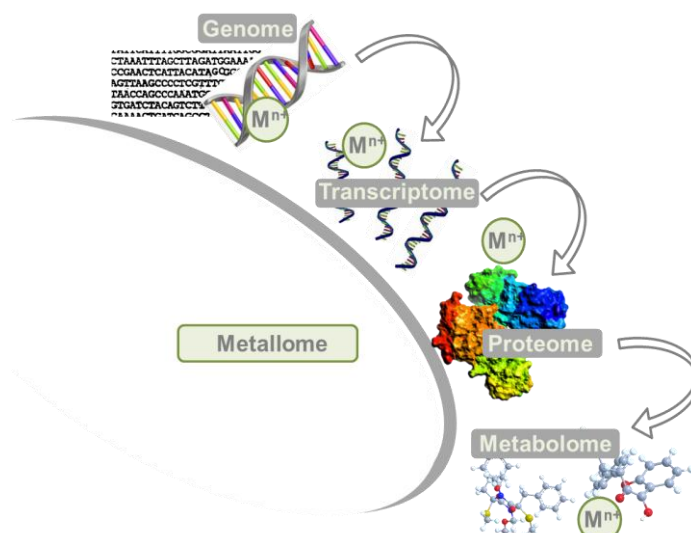
Figure 1   Metals or metal species (M^{n+}) play a role in various steps in formation of organisms.

logical processes make use of metal ions for vitality, e.g. Fe^{2+} as central ion of heme b for oxygen transport in blood or Ca^{2+} for vesicle transport in neurotransmission. For example, one-third of all proteins is believed to require a metal as cofactor, with enzymes leading the way (Goodacre 2007; Tainer et al. 1991). However, in many situations it's not only the inorganic metal itself, but rather metal complexes, i.e. –species, that account for biological function. Therefore, the extension of the term metallome to the entirety of metal- and metalloid species present in a cell or tissue, or general in a biological system, seemed appropriate (Goodacre 2007; Lobinski et al. 2010; Szpunar 2004). At about the same time, the term *metallomics* entered the field of language used in "-omics" life sciences. Metallomics incorporates "the study of the metallome, interactions, and functional connections of metal ions and other metal species with genes, proteins, metabolites, and other biomolecules in biological systems" (Lobinski et al. 2010).

Opening a new research field, the study of mechanisms by which metals are regulated, distributed and incorporated in metalloproteins and thus affecting physiological processes becomes more and more important. This requires the combination of elemental and biomedical analytics, over all elemental speciation. The various combinatorial analytical possibilities in metallomics research are illustrated in Figure 2.
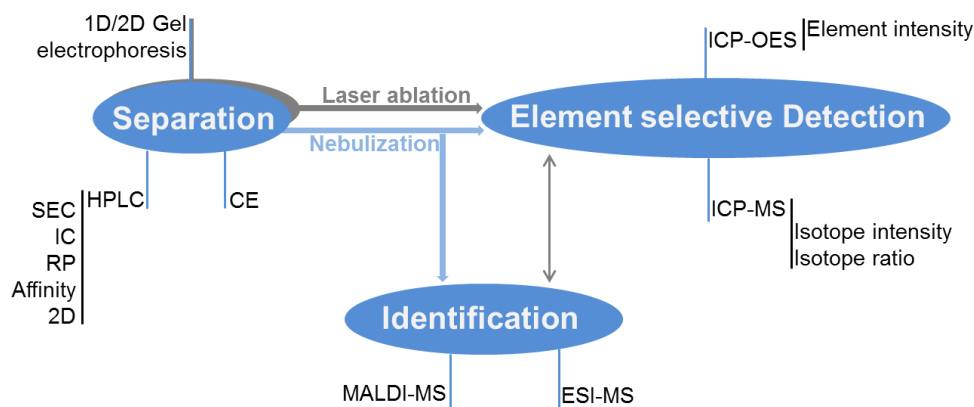
Figure 2   Analytical techniques in metallomics
(modified according to (Lobinski et al. 2006), with permission)

A.1.2   Element selective spectrometry

Determination and quantification of (trace) elements requires complete destruction of all molecular structures in a sample. Contrary to organic mass spectrometry, ionization sources in inorganic spectrometry facilitate the removal of those molecular connections (Gross 2013). Different ionization sources are available, such as thermal, spark source or glow discharge ionization. However, one of the most applied ionization methods in element selective spectrometry is the use of inductively coupled plasma (ICP).

A.1.2.1 Inductively coupled plasma (ICP) as ionization source

Developed in the mid-1960s, the ICP is not only used in optical emission spectrometry, but also an excellent ion source in mass spectrometry (Fassel 1986). The core of an ICP represents a so called torch (Figure 3). It is an assembly of three concentric fused-silica tubes, referred to as inner, intermediate and outer gas tube. A water-cooled copper coil (load coil) is surrounding the torch at its upper part, which is further connected to a RF generator (commonly 27 MHz). An argon (Ar) stream in the outer tube of 12-20 l/min is ignited by electric glow discharge producing "seed" electrons and ions. Furthermore, the gas gets more and more heated by the electric energy of the magnetic field maintained by the load coil. This in turn forces ion movement in the gas as well as collision with Ar atoms sustaining a continuous streaming, high temperature plasma. Additionally, an auxiliary gas flow is provided through the intermediate tube, feeding the plasma. The resulting plasma has an annular shape under these conditions as also shown in Figure 3.
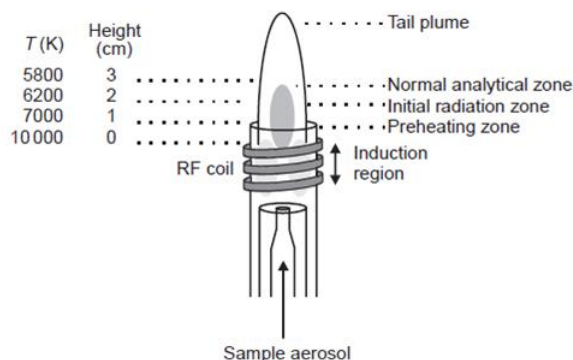
Figure 3   Construction of an ICP torch.
Three concentric tubes surrounded by a RF coil for sustenance of the magnetic field. Also shown are
the different plasma zones as well as the different temperature zones depending on the height above
the coil ((Hou and Jones 2000), with permission).

Aqueous sample introduction into the plasma is performed by a nebulizer, which is fitted into a spray chamber. The type of nebulizer used, mainly depends on viscosity and available volume of the sample. In each case, the nebulizer is operated by an Ar carrier gas flow of 1-1.5 l/min. When entering the plasma, the sample droplets undergo three major steps: (1) desolvation – removal of solvents from droplets; (2) vaporization – decomposition of particles into gaseous-state molecules; (3) atomization and excitation/ionization – breaking of molecules into atoms, which are then excited and/or ionized. Starting at 10000 K right at the induction region of the plasma, downstream excitation of atoms takes place at about 7500 K, while finally, atoms are ionized at around 6500 K.

ICP is characterized by high efficiency and reproducibility as well as by its applicability to a broad spectrum of elements in various matrices. Compared to other plasma sources (e.g. laser induced plasma, microwave induced plasma or direct current plasma) the ICP is advantageous with regard to less noise, cheaper manufacturing as well as its inert nature due to an electrode free source and therefore not contaminating samples (Hou and Jones 2000). In inorganic or element analysis the ICP can be the ionization method of an optical emission spectrometer (OES) or a mass spectrometer (MS). The choice of one or the other instrument is dependent on the elements of interest, their concentrations and the sample matrix.

A.1.2.2 Inductively coupled plasma – optical emission spectrometry (ICP-OES)

As the name ICP-OES indicates, the principle of element determination is based on measurement of radiation emission. Therefore, electrons are excited in the plasma to leave their ground state towards the excited state and emit light of a certain wavelength (λ) by returning to the ground state. According to Planck´s law ($E=h*v=h*(c/\lambda)$), the emitted wavelength is

inversely proportional to the energy. Noteworthy, every element has respective energy levels and has therefore a unique emission spectrum enabling element selective detection by ICP-OES. However, elements with similar wavelength are still prone for showing interferences. Depending on the position in the plasma and therefore the prevalent temperature, emission from the atomic or the ionic excited state is possible, which is illustrated in Figure 4.
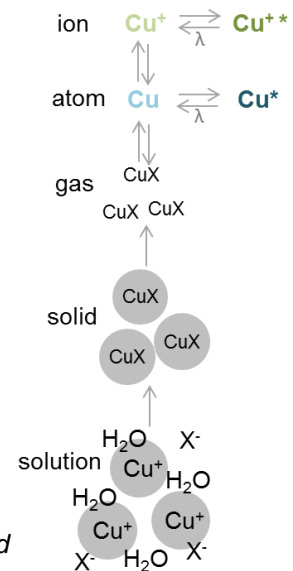
Figure 4   Processes in plasma exemplarily shown by a Cu-solution. After desolvation and vaporization, molecules are atomized and/or ionized emitting light from both excited states.

Different possibilities for observation of the emission from the ICP exist as shown in Figure 5. Depending on the manufacture of the instrument there is either a radial (side-on) or axial (end-on) viewing of the plasma. In the radial operation, the plasma is built up vertically and the analytical zone is observed from the side. The advantage of it is, that observation is restricted only to the normal analytical zone (see Figure 3) and therefore spectral or background interferences are reduced. In the axial view, the plasma is formed horizontally as is the observation direction from the end of the plasma. Due to the longer viewing path along the plasma axis, sensitivity is improved, providing better limit of detection (LoD) than the radial view (Lichte and Koirtyohann 1976). However, this view is more prone to interferences from spectra or background. Modern instruments often combine both applications (dual view, Figure 6) for optimum measurement conditions.

Figure 5   Radial and axial plasma viewing in ICP-OES. (adopted from Perkin Elmer brochure (Perkin)).

Very simplified, an ICP-OES instrument consists of three major parts: the plasma, a spectrometer and a detector. To summarize, the analyte is excited in the plasma emitting light of a certain wavelength when returning to the ground state. This light is fragmented by a grat-

ing or prisma and then examined by the detector. In reality, the optical and detection systems are much more complicated as the correct wavelengths need to be filtered out and detected simultaneously with up to 70 possible elements. As a detailed description of the various available mono-/ polychromator-based and detection systems is beyond of the scope of this thesis, the optical and detection system of the ICP-OES instrument (Optima 7300DV, Perkin Elmer, Rodgau, Germany) used during this work is only summarily described (Figure 6). As Figure 6 shows, this IPC-OES makes use of a combination of different dispersive systems. After merging of axial and radial viewed emission, the radiation is focused through an entrance slit. Then the radiation beam is dispersed by both an echelle grating as well as perpendicular to it another grating and a prism. The result at the exit plane is a two dimensional order with wavelength at the one direction and spectral order at the other. These systems are hallmarked by good efficiency as well as excellent resolution due to operation in higher spectral orders.
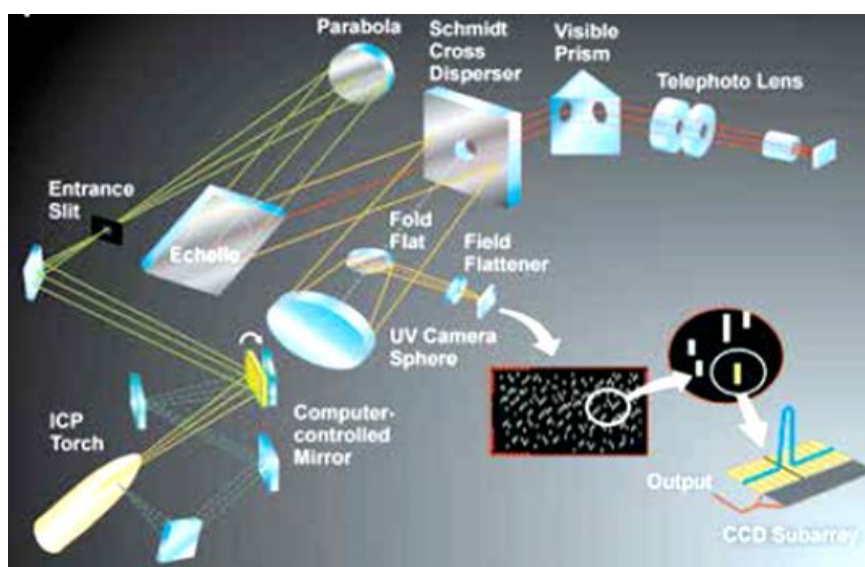
*Figure 6   Optical system and detector of the herein applied ICP-OES instruments.
            (adopted from Perkin Elmer instrument brochure (Perkin))*

In general, ICP-OES offers a wide range of applications due to the fact that many elements can be measured at once in very short time as well as in very low concentrations down to trace levels. Furthermore, a variety of samples can be measured from different fields like nutrition, agriculture, geology, biology or medicine up to analysis of oil. The information about ICP-OES given herein is interpreted based on the book (Boss and Fredeen 2004).

A.1.2.3 Inductively coupled plasma - mass spectrometry (ICP-MS)

In spite of the versatile advantages of ICP-OES, some applications in inorganic analysis require measurement by a mass spectrometer, especially when it comes to very low elemental concentrations in samples. Basically, most of the elements in the periodic table can be measured by ICP-MS at or below the ppt range. Other important fields of application are archeology, paleontology, geology and forensic, where isotope ratio analysis is used to determine age or ancestry (Vankaecke et al. 2006).

In ICP-MS, the ion beam is focused into the so called interface before entering the high vacuum area of the mass analyzer after ionization. The interface represents a kind of shield between the very high plasma temperatures operating at atmospheric pressure and the area of normal temperature but high vacuum (10^{-6} - 10^{-9} mbar), which is needed by the ion lens and mass spectrometer. The interface consists of two or three so called cones (sampler, skimmer and hyperskimmer cone) possessing a small orifice made of Ni or Pt, which focus the ion beam. The further constitution of the instrument depends on which kind of mass analyzer is incorporated and the respective type of manufacturer. Three major systems for mass separation are applied in inorganic analysis, namely time of flight (TOF), sector field (SF) and quadrupole instruments. For better illustration of the functional principles, the quadrupole and sector field instruments applied during this work will be described shortly. A schematic of the quadrupole based ICP-MS (Nexion300D, Perkin Elmer) applied for Mn speciation is shown in Figure 7.
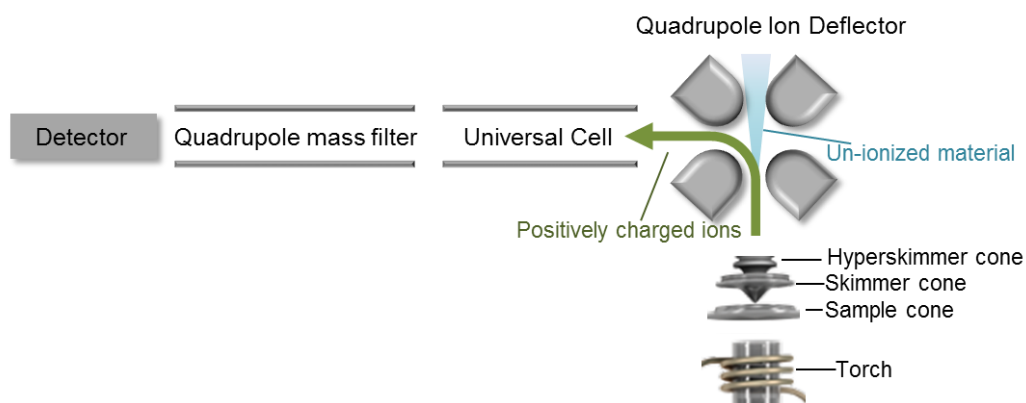
Figure 7   Schematic of the ion optic path of the herein applied quadrupole ICP-MS (Nexion 300D from Perkin Elmer ; modified from the brochure (Perkin))

After passing the interface the ion beam is deflected by a first quadrupole (Q1), where also un-ionized material is filtered off. Stability improvement and removing of background are major aims by this first filtering. The second quadrupole, which is passed by the ions, is an

universal cell constructed to remove interferences. It can be used in three different modes, depending on the element(s) of interest: during the standard mode, no cell gas is active, which is the mode of action for high throughput analysis with few interferences; in the collision mode (KED-kinetic energy discrimination) a non-reactive gas such as He is introduced into the cell, which collides with interfering ions reducing their kinetic energy and removing them; the dynamic reaction mode (DRC) introduces a reactive gas such as NH_3 producing predictable reactions, where arising side reactions or new interferences are removed by a scanning quadrupole and only elements of interest are allowed to pass. The following quadrupole then is the analyzing one. Each isotopic mass, which was set to be analyzed, has its own voltage and radio frequency setting at the analyzing quadrupole and only these will be passed through to the detector. The capability of the quadrupole to scan more than 5000 atomic mass units per second allows a fast determination of many different elements. Finally, the ions reach the detector, which is nowadays mostly a dual detector, including a digital as well as an analog mode. The prevalent mechanism is a dynode electron multiplier, where ions strike a first dynode of the detector, leading to a release of electrons, which starts an amplification process. The final electronic signal is then measured.

As indicated above, ICP-MS analysis is often prone for interferences. Such common ICP-MS interferences are shown in Table 1. Mostly, it is a matter of polyatomic isobaric interferences, which means formation of molecular species with the same nominal mass-to-charge ratio as the analyte isotope of interest. Sources for these interferences are the plasma itself (Ar), the atmosphere with components like C, N or O, or the sample matrix (H_2O) (Thomas 2002).

Isotope	Interferences
^{55}Mn	^{40}Ar^{14}N^{1}H$^+$, ^{40}Ar^{15}N$^+$, ^{38}Ar^{16}O^{1}H$^+$, ^{38}Ar^{17}O$^+$, ^{37}Cl^{18}O$^+$, ^{37}Cl^{17}O^{1}H$^+$
^{56}Fe	^{40}Ar^{16}O$^+$, ^{38}Ar^{18}O$^+$, ^{38}Ar^{17}O^{1}H$^+$, ^{37}Cl^{18}O^{1}H$^+$
^{63}Cu	^{36}Ar^{12}C^{14}N^{1}H$^+$
^{64}Zn	^{32}S^{16}O$_2$
^{75}As	^{40}Ar^{35}Cl
^{80}Se	^{40}Ar^{40}Ar

Table 1   Typical polyatomic isobaric interferences for ^{55}Mn, ^{56}Fe, ^{63}C, ^{64}Zn, ^{75}As and ^{80}Se in ICP-MS. These can arise by reaction with constituents from matrix, plasma and carrier gas (adopted from (May and Wiedmeyer 1998)).

The disadvantage of a quadrupole mass analyzer is therefore its resolution, which depends on instrumental tuning, but typically is in the range of 0.5-1 amu. Hence, this "unit" resolution is based on the capability to distinguish only between two nominal masses like ^{56}Fe and ^{57}Fe, but not between ^{56}Fe and ^{40}Ar^{16}O. This is the reason for development and application

of the above described cell techniques. Another possibility to circumvent these interferences in ICP analysis is application of high resolution instruments, like a double focusing sector field - MS. The basic construction of the herein applied ICP-sf-MS (Element2, Thermo Fisher Scientific, Bremen, Germany) is shown in Figure 8.
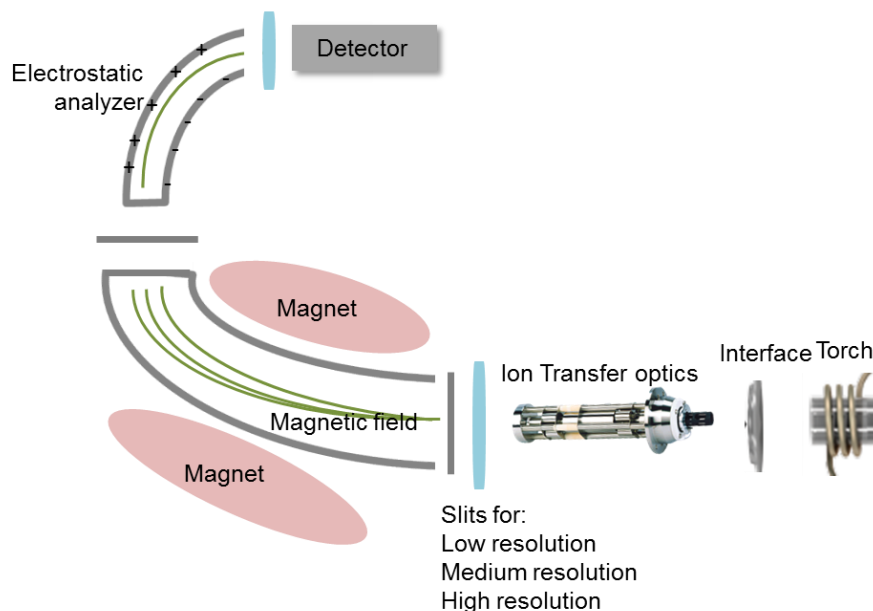
Figure 8   Basic construction of the herein applied ICP-sf-MS (Element2).
(modified according to the instrument´s brochure (Thermo))

The capability of high resolution in a double focusing sector field MS is based on the combination of the sector field mass analyzer with an electrostatic analyzer. The theoretic principle of the magnetic sector can be explained as follows: if an ion is moving in a direction perpendicular to a magnetic field, it is subjected to the Lorentz force ($F_L = z*e*v*B$). This ion is also following a certain orbit with a radius r. The Lorentz force and centripetal force (F_C) are equal according to:

$$F_L = z \cdot e \cdot v \cdot B = \frac{m \cdot v^2}{r} = F_C \ or \ r = \frac{m \cdot v^2}{e \cdot z \cdot B}$$

As the equations show, the separation of ions in the magnetic field is dependent on the radius r, which in turn is a result of the impulse *m*v* of ions and therefore dependent on m/z. Hence, Gross suggested to rather term the magnetic sector impulse analyzer instead of mass analyzer (Gross 2013). The so called dispersion of velocity or energy within the magnetic field results from aberration in the radii of ions due to their different velocity. The result is a broadening of the ion beam as illustrated by the green lines in Figure 8. The subsequent electrostatic analyzer is constructed of two capacitor plates with direct current. It serves for focusing of the ion beam by reducing the dispersion of velocity/energy emerged in the magnetic field. Therefore, slower (positively charged) ions are more attracted by the negative potential and move faster through the electric field due to the shorter path length. Opposite,

the faster ions enter the electric field deeper and need more time to pass the analyzer. At the exit slit, the homogeneity between ions is therefore rebuilt and the ion beam is more focused. Due to this double focusing of the ion beam, the resolution is much higher (up to R=10000) as compared to quadrupole instruments. Most of the instruments possess the feature to choose between low, medium and high resolution (LR, MR and HR) facilitated by two slits before the first and after the second analyzer. Depending on the width of entrance and exit slit, more or less ions are allowed to pass through. In general, LR (R=300) is applied at non-interfered analysis, MR (R=4000) for example at analysis of transition elements as those are prone for interferences at 27-70 amu, and HR (R=10000) for highly interfered analyses, e.g. separation of As and Se from Ar-dimer or Ar-Cl interferences (Jakubowski et al. 1998). One drawback of enhancement in resolution can be a decrease in ion transmission, which means compromised detection limits in certain cases.

A.1.3   Hyphenated techniques for elemental analysis

As indicated in Figure 2, hyphenated techniques play a major role in the study of the metallome. Even the definition of metallomics reveals that often not only the concentration of a certain element itself but rather an elemental species is crucial for biological function.

A.1.3.1 Elemental speciation by liquid chromatography (LC)-ICP-MS/-OES

According to the IUPAC definitions (Templeton et al. 2000), "chemical species are specific forms of an element defined as to isotopic composition, electronic or oxidation state, and/or complex or molecular structure (i.e. colloids, metal-organo-complexes, oxidation states)". "Speciation" of an element means the distribution of an element amongst defined chemical species in a system. The knowledge of chemical species therefore allows for assessment of the mobility, bioavailability as well as biological pathways, which an element accomplishes within a biological system (Caruso et al. 2003). Furthermore, a chemical species might also serve as biomarker, because an element might have sound or harmful effects on a biological system dependent on its oxidation state or binding partner. To reveal this, speciation analysis has to be carried out, which includes "all analytical activities for identification and/or quantification of one or more individual chemical species in a sample". These analytical activities demand hyphenation of species-appropriate separating techniques with element selective detectors like ICP-OES or –MS.

Besides hyphenation of gas chromatography and capillary electrophoresis, the main applied separation technique in biological or environmental speciation is liquid chromatography (LC) (Francesconi and Sperling 2005). While searching for the optimum LC technique, the stabil-

ity of the elemental species has always to be considered. LC techniques offer extended variability in separation mechanisms (Michalke 2002). One of the most gentle separation methods is size exclusion chromatography (SEC), which is applied to very labile or weak metal-complexing biopolymers. In SEC the retention depends on the molecular size of the analytes although mass calibration of columns is often assigned to the molecular weight. More information about SEC is given in the Mn-speciation part in *Experimental Procedures (chapter D.7)*. One rarely used separation method in speciation analysis is adsorption chromatography. Due to the highly polar stationary phase and the highly apolar mobile phase, species are prone to attach irreversibly to the stationary phase leading to species alteration. However, adsorption chromatography might be used for selective enrichment of single species. Compared to SEC, ion exchange chromatography (IEC) is hallmarked by high separation efficiency. The separation principle is based on the exchange between charged analyte ions and the oppositely charged stationary phase, totally independent from molecular mass. As IEC was applied for speciation of Fe(II)/(III) within this work, more information on the methodology is given in *Experimental Procedures (chapter D.6)*. Another possible separation method is reversed phase (RP) chromatography, which is one of the most commonly applied LC techniques. The majority of columns is also based on silica gels, but the hydroxyl groups are modified by alkyl chains providing an unpolar stationary phase. Various lengths of alkyl chains up to C18 can be supplied and need to be chosen adapted for the analytes of interest. In general, the longer the alkyl chain, the more hydrophobic analytes will be retained. This kind of polar stationary phase requires very polar eluents like water, methanol or acetonitrile. However, these carbon-rich eluents are very incompatible with the plasma source. They are prone to extinguish the plasma or lead to deposition on the interface cones. In ICP-MS/-OES, organic eluents can only be applied in low concentrations, which might not be sufficient for optimum column operating conditions, what makes RP-LC not really attractive for elemental analysis. Although techniques like membrane desolvation of eluents are available, these membranes are prone to adsorb analytes. Moreover, organic solvents can lead to unfolding and re-complexation of weak element-protein complexes during analysis, making RP chromatography only applicable for covalently bound elemental species. Advantages and disadvantages of online hyphenation to an element selective detector are summarized in Table 2.

Advantages	Disadvantages
no storage of fractions; circumvent storage problems like species instability or adsorption to storage cases	often compromise between optimized separation and good detection (S/N ratio, interferences)
less contamination	optimal interface: fulfill all requirements (buffer, salt load, organic modifiers); no dead volume (quantitative transfer)
lower losses: decreased risk of oxidation or degradation by bacteria	

Table 2   Advantages and Disadvantages of online hyphenation of LC with ICP. (modified according to (Szpunar 2000)).

As indicated before, the major problem in hyphenation of LC to ICP is the eluent transfer. Some applications like IEC require buffers highly concentrated in salts. These can in turn plug the nebulizer or the cones. Too high concentrations of sodium can change the Ar plasma into a Na plasma, which has a totally different ionization character. High salt intake may also cause even more polyatomic interferences or increase detection noise, so that low concentrated species are not detected any more. As discussed during RP chromatography, the use of organic modifiers also changes ionization characteristic and can even lead to plasma extinction. A carbon deposition on the torch may cause flashovers, also shutting down the ICP (Andrle et al. 1997). Moreover, flow rates have to be adopted to avoid too high liquid intake. The easiest way to circumvent high salt or organic intake into the plasma is post-column dilution, where the dilution of the samples has to be considered. This might not be desired for low concentrated species. Cooling of the spray chamber also reduces organic vapor, even more when the nebulizer gas contains small amounts of oxygen reducing ArC+ interferences (Caruso et al. 2003). The use of microconcentric nebulizers (30-150 μl/min) in combination with microbore LC can also produce relief for these problems (Makarov and Szpunar 1999). Interestingly, small amounts of MeOH in the eluent (3%v/v) were shown to improve signal intensities as well as the LoD in arsenic speciation (Larsen and Sturup 1994).

Mostly important is the quantitative sample transfer from the LC to the ICP. To ensure quantity, species stability has to be considered already during sampling, sample storage and sample pretreatment. Both, short sampling under inert gas as well as short sample storage time at low temperatures (-80°C) is suggested to avoid species transfer reactions. Any sample pretreatment like dilution or pre-concentration can change species equilibria. If the element of interest contains more than one isotope, isotope dilution is beneficial. By measuring of isotope ratios, the quantity of the element can be controlled throughout the whole procedure from sampling to detection. However, it might also come to exchange of the elemental isotope with the natural one at the binding position. Another challenge of quality control in

elemental speciation, above all in the field of neurodegenerative diseases, is the lack of commercial available, well characterized standards (Michalke et al. 2009). The respective standards have to be prepared in-house by mixing of the investigated element with the ligand. The guarantee of full complexation is not given. Moreover, spiking of samples with these standards for recovery analysis can lead to changes in stoichiometric equilibria of the natural sample due to excess free ligand in the standard. Characterization of the elemental species solely on its retention time determined with these standards might therefore be not sufficient for describing the chemical form of the species. The combination of element selective detection with molecule selective detection (e.g. ESI-MS) should be applied as far as possible. However, low concentrated and instable species can be the reason, why approaches like ESI-MS are not applicable. Other so-called 2D approaches for precise description of chemical species can involve combination of different separation methods, e.g. by collecting fractions of a SEC separation and analyzing those by a CE-ICP-MS approach. Overall, every speciation analysis requires modification to the respective problems depending on the elemental species of interest as no general protocols exist.

A.1.3.2 Laser Ablation-ICP-MS (LA-ICP-MS)

Beside the classical speciation of elements in various kind of samples, imaging or mapping of elemental distribution on solid sample surfaces has gained high interest in life sciences (Becker et al. 2009). As such imaging mass spectrometric technique, the hyphenation of a laser ablation (LA) system to an ICP-MS detector can be applied for elemental and isotope selective trace analysis of solid materials (Fernández et al. 2007; Pisonero et al. 2009). Since the first publication on the use of LA-ICP-MS in 1985 (Gray 1985) it has gained growing attention by the wide range of application from bioimaging, environmental analysis, material analysis over archaeology through to forensics. To the main advantages of LA-ICP-MS account (Koch and Gunther 2011): ease of use, high sample throughput, almost no sample preparation, high spatial resolution (10-200 µm), high accuracy and precision as well as nondestructive on macroscopic scale due to small material uptake (<0.1 µg/s).

A general setup of LA-ICP-MS coupling is shown in theory and practice in Figure 9. The laser set up consists of a pulsed laser source, optics for beam delivery, an air tight ablation cell, an aerosol transport line and the ICP detector. The major steps during LA-ICP-MS are therefore ablation, transportation, ionization and detection.
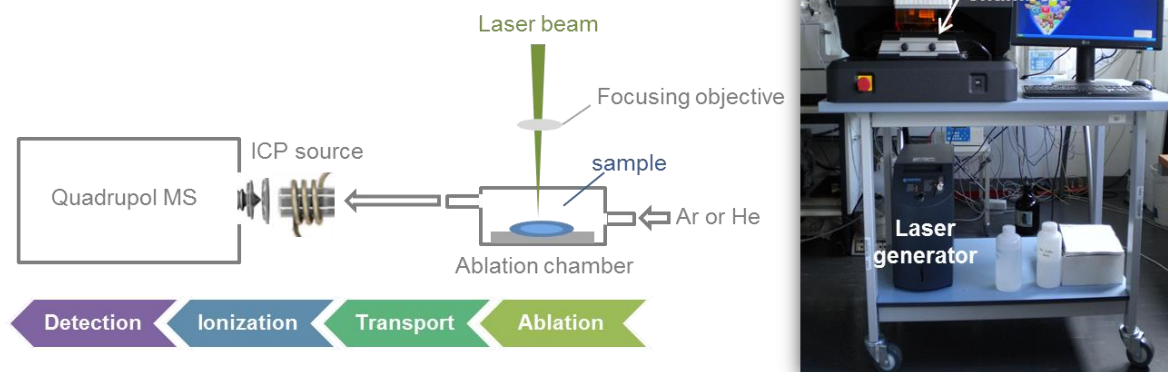
Figure 9   Setup for LA-ICP-MS in theory (left side) and in practice (right picture).

For analysis of biological tissue, microtome thin tissue slices of 5-100 µm are mounted on an object slide, which is placed in the ablation chamber (Becker 2013). Before analysis, the chamber has to be purged with the inert carrier gas to remove oxygen. For aerosol transportation either argon (Ar) or helium (He) can be used. Each of those gases has its advantages, with He having higher transport efficiency (Gunther and A. Heinrich 1999) whereas Ar showing faster washout of the ablation chamber (Hare et al. 2009). When using He as transportation gas it has to be mixed with Ar downstream the laser before introduction into the ICP, because the plasma is not compatible with too high He input. In general, transport efficiency was shown to lie between 75-95% for either applied carrier gas (Carmen C. Garcia et al. 2007; C. C. Garcia et al. 2008). The ablation chamber is directly coupled to the ICP by a connection tube, which should be made of polytetrafluorethylen (Teflon®) due to low memory effects of this material. For ablation itself, Nd:YAG (neodymium-doped yttrium aluminium garnet) laser sources emitting nanosecond pulses (5-10 ns) in the UV spectral range at 213 or 266 nm are commonly used (Günther and Hattendorf 2005). The laser beam can be applied in different patterns, either as single spot or as raster, detecting line by line for concentration profiling, resulting in 2D- or 3D-imaging by evaluation with respective software.

A major problem in LA-ICP-MS can arise at the point of quantification. The applied quantification procedure must be reliable when comparing control with diseased tissue. The problems, which can arise during vaporization, transportation, atomization and ionization in the plasma, are mainly dependent on the matrix. Thus, standards used for quantification of elements should match the sample matrix accurately. In most cases, these standards have to be prepared in-house. One possibility is the direct ablation of pressed pellets of certified biological reference material (Jackson et al. 2006). Another, more matrix-matched possibility, is the use of either certified reference material or other tissue with known elemental concentra-

tions doped with different concentrations of the element(s) of interest to obtain a calibrating curve (Zoriy et al. 2006). Important in this approach is a homogenous distribution of standards within the base material. If possible, the method of choice for quantification in LA-ICP-MS is isotope dilution due to its powerful accuracy (Sussulini et al. 2013). Another approach is solution-based calibration, where micronebulizers are inserted in the ablation chamber for simultaneous delivery of standard aerosol with tissue aerosol into the ICP (Becker et al. 2005a). Various applications for calibration in LA-ICP-MS have been described by authors and current approaches are reviewed in (Miliszkiewicz et al. 2015)

Similar to the different developments of quantification procedures, various technical developments have been accomplished over the last years depending on the scope of research. Cryogenically cooled laser ablation chambers for fresh wet tissue analysis (Feldmann et al. 2002) or laser microdissection coupled to ICP-MS for highest spatial resolution analyzing at single cell level are only two examples (Becker et al. 2010). Especially in the field of neurological diseases, LA-ICP-MS is of great interest for analysis of elemental distribution as small amounts of certain metal ions, such as Cu, protect the brain from various insults, over all oxidative stress. Moreover, LA-ICP-MS can be useful in the development or monitoring of metal-containing drugs, e.g. detection of Pt in cisplatin-treated cancer (Egger et al. 2014). A very comprehensive application is the combination of LA-ICP-MS with another imaging mass spectrometric technique such as matrix assisted laser desorption ionization (MALDI)-MS reaching the field of proteomics. Therefore, metal distribution in a tissue slide can be monitored with simultaneous detection of phosphoproteins or metal-containing proteins (Becker et al. 2004; Becker et al. 2005b). Such approaches will be a challenging task for future applications in the life sciences (Becker et al. 2007).

A.2   Metabolomics by means of ESI-ICR/FT-MS

As indicated in Figure 1, the metabolome is the endpoint of the "-*omics*" cascade and therefore the closest to the respective phenotype. Studying changes in phenotype caused by environmental influences, disease or changes in genotype is the foundation of metabolomics (Dettmer et al. 2007). Herein, metabolomics by means of ESI-ICR/FT-MS analysis of brain extracts was carried out to study the affected brain metabolisms after Mn exposure.

A.2.1   Definitions, Applications and Techniques in Metabolomics

With *metabolome* being the "complete set of metabolites in an organism", *metabolomics* is concerned with the comprehensive analysis of low-molecular weight compounds (less than

2000 Da) in a biological system (Nicholson and Wilson 2003; Patti et al. 2012; Ramautar et al. 2013). When working in metabolomics, the chemical diversity of measured metabolites has to be considered, which not only include endogenous but also exogenous compounds originating from nutrients, microbiota, drugs and other sources (Ramautar et al. 2013). This is aggravated by the fact that metabolites are often present in a very wide dynamic range of concentrations.

Two major approaches are commonly applied in metabolomics, which is also demonstrated in Table 3. Targeted metabolomics can also be termed as quantitative metabolite profiling. It brings along the analysis of a very limited number or a specific group of metabolites, whose certain biological observation is of interest, such as compounds of the amino acid metabolism (Fiehn 2002). Moreover, metabolic profiling can also be part of pharmaceutical research and development by monitoring the fait or effects of a newly designed drug (Goodacre 2007). Such targeted analysis requires very sensitive and direct techniques, mostly application of MS^n analysis. Non-targeted metabolomics or global metabolic fingerprinting is another approach, which was also termed *metabonomics* in the beginning work of Nicholson (Nicholson et al. 1999). Here, the aim is not to detect every single metabolite but to compare patterns of metabolites as response to disease, toxin exposure or environmental alterations (Dettmer et al. 2007). It is a global screening approach intended to find discriminating metabolites and can involve direct measurement of samples without any pre-separation. Commonly applied are (ultra)high resolving instruments such as Q-ToF-MS, ICR/FT-MS and NMR. Establishment of methods, which describe those discriminating metabolites in more detail, will lead to the linkage of targeted and non-targeted approaches.

Metabolomics: Comprehensive analysis of all metabolites		
Quantitative metabolite profiling or targeted	*Global metabolic fingerprinting or non-targeted*	
Focus on certain metabolites or a group of metabolites (e.g. amino acids); also within pharmaceutical applications	Global evaluation of biochemical fingerprint caused by disease, toxins or other alterations; metabolic footprinting focuses on the extracellular metabolome	
Selective metabolite extraction	Comprehensive metabolite extraction	
HILIC LC-CE	(HP)LC/GC/CE-MS	NMR FT-IR	DI-MS (ToF, ICR/FT) MALDI-MS
BIOLOGICAL UNDERSTANDING	SAMPLE CLASSIFICATION	
	Develop list of quantitative methods	

Table 3   Strategies in metabolomics and applied analytical techniques (adopted from (Goodacre 2007) and (Dettmer et al. 2007)).

Metabolomics facilitates a direct read-out of the physiological status of an organism and can therefore ideally be used to describe the human health status. By giving insight into biochemical mechanisms of disease, it can deliver diagnostic biomarkers for detection and prognosis of disease and predict the efficacy and safety of a pharmaceutical therapy (Kaddurah-Daouk and Weinshilboum 2014; Mamas et al. 2011). In the first instance, healthcare management makes use of single molecules to predict a disease process, such as cholesterol in atherosclerosis or glucose in diabetes. However, in multifactorial processes such as neurodegenerative disorders the need for reliable and all types of biomarkers is really urgent for intervention of disease already at the onset. The phenotype of such onsets is very complex due to influences from genetics as well as the environment. Thus, the need for detecting these cross-compartment communications can be fulfilled by application of metabolomics. In the future, that approach will allow a more personalized medicine with focus on prevention rather than diagnosis (van der Greef et al. 2013). Additionally, humans are meanwhile generally considered as superorganisms or human-microbe hybrids with a non-underestimating amount of 90% bacteria in and on our body (Sekirov and Finlay 2006; Wilson and Sober 1989). It was shown that the microbiome diversity is huge and intersubject variability is significant (Eckburg et al. 2005). That fact even more reinforces the need of metabolic approaches at a very individual level to predict disease onset and progression and to be able to understand the multifactorial manner of diseases also on the basis of interaction with the microbiome. The site specific metabolite pathways along the gastrointestinal tract by the influence of the respective predominant microbiome was for example discussed by Heinzmann et al. (Heinzmann and Schmitt-Kopplin 2015).

As indicated in Table 3, a variety of technical approaches can be applied for studying a metabolome. Advantages of NMR-spectroscopy are its applicability in a full automated, reproducible, high-throughput manner as well as its nondestructive nature (Ala-Korpela et al. 2012). It can be applied without any complex sample pretreatment in a variety of biological samples, including fluids, cells and intact tissues (Nicholson et al. 1999). Another advantage compared to MS techniques is the possibility of quantification of metablites. Often, NMR is used as a first screening method, followed by a subsequent identification of certain resonances, which are different between samples. These can then be used as targets for more specified analysis. NMR is thought to stay a leading tool in metabolomics in future, due to the broad chemical information, which can be drawn from such analysis. However, due to the relative week sensitivity, only medium to high abundant metabolites will be detected. With focus on high sensitivity as well as dynamic mass range, mass spectrometry (MS) techniques are commonly applied in metabolomics (Soga et al. 2003). Due to their improving accuracy, MS-based approaches can also help to identify unknown metabolites in complex

matrices. Samples can either be directly infused into the MS or separated before, reducing complexity of the mass spectra and adding information about the physico-chemical properties of the metabolites (Dettmer et al. 2007). The need for sample preparation in MS-based metabolomics has to be considered well, as the preparation steps can lead to metabolite losses. Moreover, the MS ionization technique has to be suitable so that there is no loss of information of specific metabolite classes. Different LC techniques from reversed phase up to hydrophilic interaction liquid chromatography (HILIC) as well as capillary electrophoresis (CE) or gas chromatography (GC) can be applied for coupling to MS. Methods have to be developed and the separation technique has to be appropriate for the sample and the purpose. A detailed description of the various separating and hyphenating techniques would exceed the scope of this thesis. During this work, an untargeted ESI-ICR/FT-MS analysis should serve for an overview of alterations in neural metabolisms due to Mn exposure. Therefore, this technique will be explained in more detail in the following chapter.

A.2.2   Electrospray ionization ion cyclotron resonance Fourier transform mass spectrometry (ESI-ICR/FT-MS)

As one of the currently most applied ionization techniques in MS, electrospray ionization (ESI) facilitates ionization of molecules under atmospheric pressure (Dole 1997). ESI is a mild ionization process, where ions from liquid phase are transferred into gaseous phase. It is very applicable for analysis of a wide range of analytes from non-volatile, easy chargeable molecules like proteins or nucleic acids up to smaller polar molecules or ionic metal complexes (Cristoni and Bernardi 2003; Traeger 2000).

The working principle of ESI is illustrated in Figure 10. The first step is the generation of an electrically charged spray: the analyte solution (10^{-3}-10^{-5} mol/L) is vaporized by N_2 through a thin capillary needle into a strong electric field, which is maintained by the capillary tip and a counter electrode. This leads to ionization of analyte molecules and separation of the charged analyte solution forming a cone shape, the so called *Taylor Cone*. The next step is the reduction of the droplet size facilitated by the counter streaming, heated sheath gas (N_2), which leads to evaporation of the volatile solvents. During evaporation, the charge on the surface increases until the so called *Rayleigh Limit* is reached, were the electrostatic repulsion is bigger than the surface charge leading to even smaller droplets (Kebarle 2000). At the end, the complete desolvated ions are released and transferred to the ion source of the MS reaching the high vacuum zone in a step-wise manner.
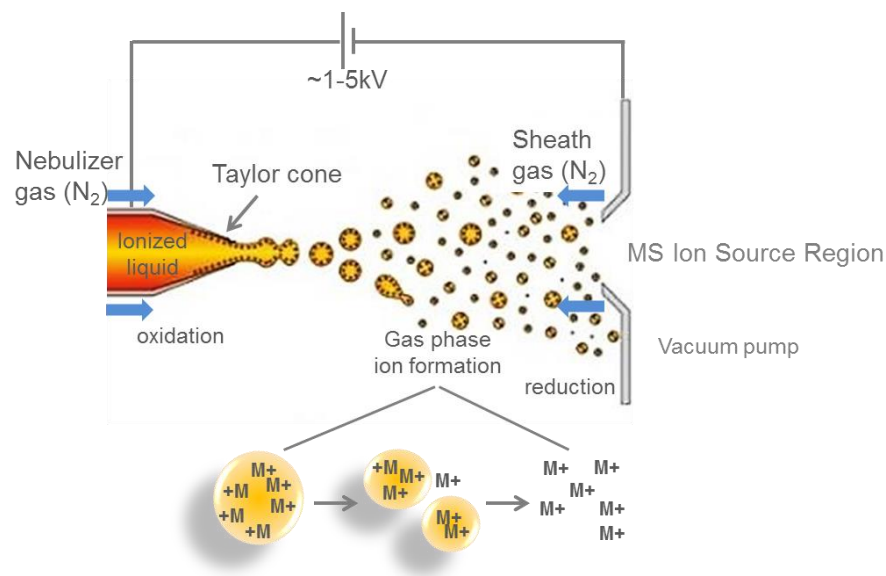
Figure 10 Principle of Electro spray ionization (ESI).
The analyte molecules are ionized by the high voltage applied at the tip of the introducing capillary needle. A heated, counter flowing sheath gas leads to desolvation of charged analyte droplets and finally to release of ions.

Dependent on the electric field, either positive ionization (oxidation) or negative ionization (reduction) of molecules occurs at the tip of the capillary needle. Furthermore, different types of ions can be formed dependent on the polarity of the analyte, the solvent (polarity, pH) and the presence of contaminants like salts. In metabolomics, the m/z (mass per charge) range of interest is generally between 100 and 1000, where multiple charges are rarely observed (Gross 2013). ESI sources can in general be applied to every kind of MS.

With respect to ultra-high resolution in combination with highest mass accuracy, ion cyclotron resonance-Fourier transform (ICR/FT)-MS is the outstanding mass detector in MS. Since its breakthrough in 1974 (Comisarow and Marshall 1974), development of performance has been continuously proceeded. With the application of superconducting magnets, modern ICR/FT-MS instruments have a resolving power of $R=10^5$-10^6 (He et al. 2001) and a mass accuracy of $\Delta m=10^{-4}$-10^{-3}u (Schaub et al. 2008). Resolving power is defined as the observed mass centroid divided by the mass peak width at 50% height ($m/\Delta m_{50\%}$). The mass accuracy can be determined by the difference of calculated and experimental determined mass of a given sum formula:

$$\left(\frac{m_{\,measured} - m_{\,calculated}}{m_{\,calculated}}\right) \times 1.000.000 \text{ in ppm}$$

A detailed description of the physical theory of the technique of ICR/FT-MS is beyond the scope of the thesis and has recently been given by Nikolaev et al. (Nikolaev et al. 2014). In this work, the solariX™ (Bruker, Bremen, Germany) has been applied, which is illustrated in

Figure 11. In short, ions generated in the ESI source are guided through ion optics into a quadrupole zone (Q1 and Q2). The first quadrupole can be used to select ions of interest whereas the second one can also be applied as collision cell for ion enrichment. Finally, ions are trapped in the ICR detection cell.
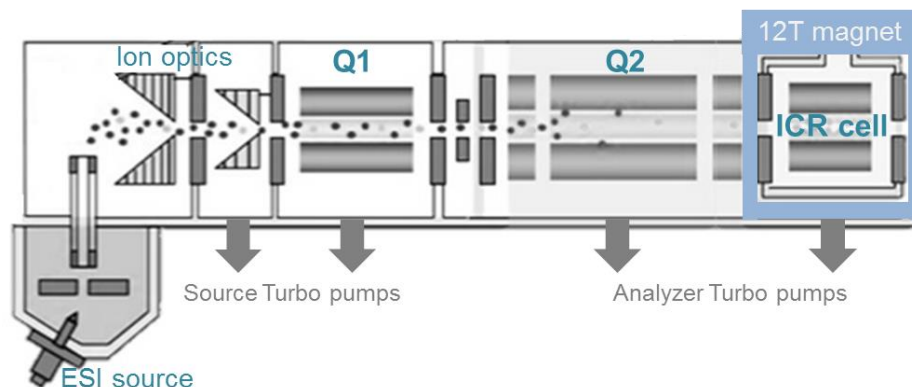
Figure 11 Schematic view of the applied ICR/FT-MS SolariX^{TM} (adopted from (Bruker 2012).
 Ions are generated in the ESI source and guided through the ion optics and quadrupoles (Q1, Q2) towards the ICR cell. Frequencies of orbiting ions are detected in the ICR cell and mathematically transferred by Fourier transformation into intensities of m/z.

The ICR detection is embedded within a homogenous magnetic field. As soon as the charged ions enter the ICR cell they start to oscillate due to the effect of the Lorentz force and ion velocity vector in the magnetic field (Forcisi et al. 2013). The resulting movement is also called cyclotron motion and is defined by the following equation

$$F = m \frac{dv}{dt} = q v \; x \; B$$

(F=Lorentz force, m=mass, q=charge, v=velocity, B=magnetic field strength)

The respective cyclotron frequency (w_c), which is specific for each mass to charge ratio, is yielded by rearrangement of the equation and described by

$$w_c = \frac{qB}{m}$$

As a result, the cyclotron frequency is independent from the initial velocity of the ions, but it is proportional to their charge and the magnetic field as well as indirect proportional to their mass (Gross 2013). In order to detect measurable current, the orbital radius of the ions has to be increased to move them closer to the detector plates. This so called *resonant excitation* is facilitated by a pair of opposed arranged RF electrodes building up a transversal electric field, which changes according to the cyclotron frequency. The resulting spiral movement of ions is recorded as an oscillating electric voltage over time by two orthogonally arranged detector plates and converted into frequency by Fourier transform. A final mathematical

treatment gives the m/z ratios of a mass spectrum (Barrow et al. 2005). The mechanism of detection and signal conversion is illustrated in Figure 12.
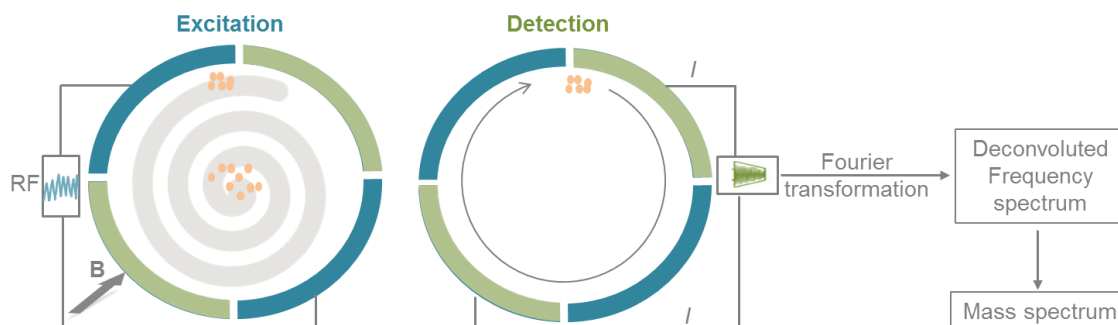
Figure 12 ICR cell excitation and detection.
The ICR cell is constructed of two pairs of orthogonal plates for excitation and detection with an or-thogonally acting magnetic field (B). During excitation, an orbital movement of ions with increasing radius is generated by applying radio frequency (RF). After excitation, the ion current is monitored by the detection plates and mathematically transformed to a mass spectrum.

With this technique thousands of ionic molecules in a wide range of concentration can be scanned at the same time, which is a prerequisite in metabolomics. ICR/FT-MS is best ap-plied in direct injection with an ESI source delivering constant ion flows and enhancing sensi-tivity as well as mass accuracy, which usually results in very high resolution and a mass accuracy of <0.1 ppm. ICR/FT-MS has therefore been applied in various fields of research to describe metabolic alterations in disease such as obesity or diabetes (Walker et al. 2014; Wörmann et al. 2012), to observe alterations in metabolisms during host-pathogen interac-tions (Muller et al. 2013; Witting et al. 2014) or to describe chemical alterations due to ex-traordinary storage conditions of wine (Jeandet et al. 2015).

A.2.3   Analysis of generated ICR/FT-MS data

The resulting spectra of the ICR/FT-MS measurement compose several thousands of indi-vidual masses demanding a special preprocessing of data before statistical analysis and visualization.

In general, noise is reduced by choosing a certain signal to noise ratio and a signal thresh-old, which is considered for all spectra (from each sample). Moreover, peak alignment and spectra calibration with regard to known metabolite masses is the next step. When all peaks are "in line", a matrix of all detected masses is build up, which serves for annotation via a database. The normal case in annotation is 5-30% of known metabolites in a typical MS-based dataset, leaving 70-95% of unknown or novel metabolites (Witting and Schmitt-Kopplin 2014). This matrix of annotated and unknown metabolites is then further taken as basis for statistical analysis of obtained data. Importantly, data have to be transformed (e.g.

log transformation) and scaled (e.g. unit variance scaling) avoiding the influence of high abundant signals on the applied statistical model.

The aim of statistical data analysis of metabolomics data is basically one or more of the following objectives: to visualize relationship between groups (samples and metabolites); to determine if an effect leads to a significant difference between groups (e.g. effect of treatment on metabolites); and over all to find out, which metabolites are responsible for this differentiation (De Ioro et al. 2007). Multivariate analysis (MVA) as one of the most powerful tools for interpretation of biological phenomena is therefore applied on the data matrix herein (Lucio 2008). MVA not only captures changes of single metabolites between groups but makes also use of the dependency between individual molecules (Bartel et al. 2013). These analyses can be separated into supervised and unsupervised methods. Belonging to the unsupervised methods, principal component analysis (PCA) in general represents a first exploratory step in data analysis. It is a linear mixture model, which attempts to uncover hidden internal structures by defining principal components describing the maximal variance within a dataset (Boccard et al. 2010). Another unsupervised method is hierarchical cluster analysis (HCA), which helps to divide the dataset in its natural subgroups or clusters. Observations, which are similar to each other, group together in a hierarchical structure. Belonging to the group of supervised methods, partial least square data analysis (PLS-DA) has the power to build structures with a certain prediction power by maximization of the covariance between data and class assignment (Boccard et al. 2010). Group separation can then be sharpened and variables, carrying the class separation information (i.e. biomarkers) can be determined (Fernández Pierna et al. 2003). All herein applied data processings and statistical models are described in more detail in *Experimental Procedures (chapters D.8.2. and D.8.3)*.

A.3   The trace element Manganese (Mn)

Manganese (Mn) is a group 7 element in the periodic table and the 12th most abundant element in the biosphere. Its concentration in the ocean crust is about 60% greater than in the continental one and it is widely distributed in soil, sediment, water as well as in biological materials (M. Aschner et al. 2007). The most common form is the inorganic one, where Mn can occur in 11 oxidation states from -3 to +7 (USEPA 1984). In living tissue, mainly Mn^{2+} and Mn^{3+} (possibly Mn^{4+}) were found to be the predominant oxidation states (Archibald and Tyree 1987).

A.3.1   Essentiality vs. Toxicology

Being an essential trace element, Mn has to be taken up by the body for proper human development. It has variable biological functions such as activation of certain metalloenzymes, involvement in function of immunological system, nervous system and reproductive hormone signaling (ATSDR 2000; IOM 2011). Mn is cofactor of a variety of enzymes, including those with antioxidant properties like mitochondrial superoxide dismutase (Mn-SOD) or acetylcholine esterase (AchE). Many metabolisms require Mn such as carbohydrate, cholesterol, amino acid as well as energy metabolism, where Mn is a component of pyruvate carboxylase in gluconeogenesis. The enzyme arginase catalyzes the recycling of ammonia by the urea cycle in the liver, where Mn is a further cofactor (Christianson 2005). Bone and connective tissue growth is also dependent on Mn as the formation of proteoglycans is promoted by glycosyltransferase, another Mn containing enzyme. Focusing on the brain, small amounts of Mn are needed for proper brain development as well as for metabolism of glutamate to glutamine, facilitated by the enzyme glutamine synthetase (GS). Additionally Mn containing enzymes are involved in neurotransmitter synthesis and metabolism (K. M. Erikson and Aschner 2003; Stallings et al. 1991). The various biological functions of Mn are illustrated in Figure 13.
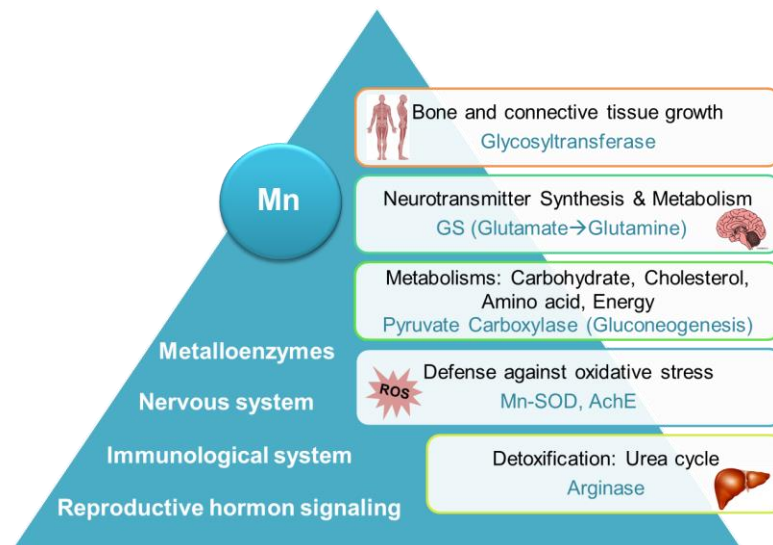
Figure 13 Biological functions of Mn.
Mn participates for example in the function of metalloenzymes, immunological system, nervous system and reproductive hormone signaling. Mn-containing enzymes or which get activated by Mn are shown in cyan.

While Mn deficiencies only rarely occur in humans, higher levels of Mn can be very harmful to the body. Independent from the way of exposure, Mn toxicity is mainly manifesting in the central nervous system (CNS), and after inhalation, also in lung tissue (J. Crossgrove and Zheng 2004). Excess Mn in brain may develop a neurotoxic disease called manganism,

which resembles idiopathic Parkinson Disease (iPD) (Hudnell 1999; Iregren 1999). In manganism, the primary targeted brain regions are the globus pallidus and striatum of the basal ganglia, whereas in iPD mainly the substantia nigra is affected by neurodegeneration (Calne et al. 1994; Walter et al. 2003). However, the common cellular mechanisms in both diseases are an increased accumulation of Mn within mitochondria leading to oxidative stress as well as dopaminergic neurotoxicity (M. Aschner et al. 2009; Racette et al. 2005). One of the hallmarks of iPD is α-synuclein aggregates, so called Lewy bodies. An increase in fibril formation by α-synuclein can also be prompted by Mn leading to neuronal death (Avila et al. 2013). Recent studies also suggest several genetic factors to be associated with both diseases. In general, it was observed, that manganism occurs in response to acute Mn exposure, whereas iPD arises due to long-term exposure to relatively low Mn concentrations (Stredrick et al. 2004). Psychiatric symptoms such as emotional liability, mania, hallucinations, humor changes as well as mild motor impairment occur at the initial stage of manganism. At the established disease, disturbances of the extrapyramidal system become prominent such as mask-like face, mild tremors, limb rigidity and disturbances of balance as well as a cock-like walk – symptoms also observed in iPD. Mn was also found to play a role in the etiology of other neurological diseases such as Amyotrophic Lateral Sclerosis (ALS), Alzheimer´s Disease (AD) as well as Huntington´s Disease (HD) (reviewed in (Avila et al. 2013).

A.3.2   Sources of exposure

Today, Mn is the fourth most widely used metal in the world (Takeda 2003) with 90% of all pure produced Mn is used in steel industry, production of dry-cell batteries, glass or textile bleaching (Flynn and Susi 2009). Therefore, the main anthropogenic sources of environmental Mn include municipal wastewater discharges, sewage sludge, mining and mineral processing as well as emissions from ferroalloy-, steel- and iron production. Mn is also used in an organic compound called MMT (methylcyclopentadienyl-Mn-tricarbonyl) as anti-knock agent in gasoline. It is therefore released by fuel combustion, which can be a major problem for humans in areas with high traffic (Lynam et al. 1999; Zayed 2001). Manganese ethylene-1,2-dithiocarbamate (MANEB) is a Mn containing fungicide, which is applied in agriculture, increasing the environmental concentrations of Mn in air, soil and plants (Ferraz et al. 1988). Another use of Mn is the application of Mn-containing contrast agents (Mangafodipir) in magnetic resonance imaging for medical purposes (Pan et al. 2010). Dermal absorption and inhalation are the major routes of environmental Mn exposure raising concerns about health risks due to the broad application of Mn. Another exposure route is dietary intake of Mn via food or drinking water. The estimated safe and adequate intake of Mn for adults is 2-5 mg

per day recommended by the U.S. National Research Council´s (USEPA 1984). As Mn essentiality varies in humans depending on life-stage, age and also sex, adequate intake for men is 2.3 mg Mn per day and for women 1.8 mg Mn per day. Dietary Mn sources include black tea, wheat germs, hazelnuts, oatmeal, soya beans, flaxseed, blueberries and rye (concentrations of Mn in descending order) (Ekmekcioglu and Merktl 2006). Of course, Mn is also taken up by drinking water, which usually contains less than 100 µg Mn per L (WHO 1996). Nevertheless, concentrations of Mn in food or drinking water are dependent on the territorial location. As examples: spices from West Bengal (India) showed much higher Mn concentration than the respective vegetables (Roychowdhury et al. 2003); and elevated Mn concentrations in tap water from Quebec (Canada) were positively correlated with impairment of school children (M. F. Bouchard et al. 2011). Although intoxication with Mn by oral route is on rare occasion, it should be kept in mind, that the results of oral chronically low exposure to Mn are not fully known yet (Michalke and Fernsebner 2013).

A.3.3   Sensitive populations and Epidemiology

Sensitive populations include occupationally exposed humans like welders or miners, which are not correctly protected from inhaling Mn dust (Guilarte 2010). It was shown that the prevalence of developing PD was higher among welders than in control persons of the general population of the same age (Racette et al. 2001). Also infants fed with Mn-containing formulas are at higher risk due to an incomplete functionality of the blood brain barrier (BBB) as well as reduced liver enzymes activity (critically reviewed in (J. L. Aschner and Aschner 2005)). Here has to be considered that infant formulas often contain substantially higher levels of Mn than either human´s or cow´s milk (Stastny et al. 1984). Not only infants, but also reports of children with Mn toxicity including cognitive effects are documented (M. F. Bouchard et al. 2011; Herrero Hernandez et al. 2003). Patients with hepatic encephalopathy and those receiving long-term parenteral nutrition were also observed to accumulate Mn in the body without any relevant exogenous exposures (Bertinet et al. 2000; Fabiani et al. 2007). One additional major risk factor for increase Mn uptake and accumulation is chronic Fe deficiency (reviewed in (Roth and Garrick 2003). This is based mainly on the common transport systems of Fe and Mn within the body as well as on their comparable chemical nature. As Fe deficiency affects almost 10 million people in Germany (WHO 2005) and almost 2 billion in USA (S. J. Garcia et al. 2006), the fact of Mn accumulation without any relevant exogenous exposure should not be underestimated. Additionally, certain genetic predispositions have also been taken into account in recent studies to be causative for development of manganism (Avila et al. 2013).

Due to the increasing use of Mn in pesticides and fuel, the situation might be changing from occupational towards environmental exposure. Therefore, also the general population has to be considered to be at higher risk for accumulating Mn in the body in elevated concentrations (Zatta et al. 2003). Epidemiological studies depict the public health concern due to increasing environmental Mn concentrations. Lucchini and coworkers carried out excessive studies in Valcamonica (province of Brescia, Italy), where four ferro-alloy industries had been operating until 2001 (R. G. Lucchini et al. 2007; Zacco et al. 2009). In general they concluded that lifetime low-dose Mn exposure resulting from these industries may be a risk factor for development of neurological disorders like PD in inhabitants living nearby. The effect of environmental Mn was also studied in Toronto and Hamilton (Canada), where MMT is applied in gasoline since 1976. According to the authors, exposure to ambient Mn advances the age of PD diagnosis (Finkelstein and Jerrett 2007). Interestingly, Mn may also have lasting consequences long after occupational exposure, which was addressed in a follow-up study in workers from a ferro-alloy plant in Quebec (Canada) (M. Bouchard et al. 2007). Providing a sufficient risk assessment, thus, is one major goal of nowadays studies to expand testing from occupational to general exposed populations (Rohlman et al. 2008).

A.3.4   Resorption, Metabolism and Transportation

With absorption being usually tightly regulated, approximately 1-5% of dietary Mn is resorbed in the intestine as Mn^{2+} or Mn^{4+} (Barceloux 1999). Mn is then transported to the target organs bound to different transport molecules in blood/plasma. Excretion takes place with 97% via the bile, which is driven by concentration gradients (Takeda et al. 1995). Inhaled Mn can either be directly transported into the brain through the olfactory neurons and bulb or it is released into the blood system via the lungs (reviewed in (Dorman and Foster 2014). Highly soluble $MnCl_2$ and $MnSO_4$ are thought to enter the blood system and brain faster than for example MnO_2 (Dorman et al. 2001). Exposure to high Mn concentrations overwhelms homeostatic control mechanisms and the usually stable tissue levels will be increased. Additionally it is known, that iron (Fe) deficiency can increase Mn absorption due to the shared binding and transport properties, as well as liver failures can lead to accumulation due to reduced excretion (Fitsanakis et al. 2008).

Transportation of Mn in blood is facilitated by specific carrier proteins such as transglutaminase, β-globulin, transferrin (Tf), human serum albumin (HSA) and α-2-macroglobulin. While some authors describe Mn(III)-Tf to be the predominant Mn-species in plasma and serum, others reported that over 80% of Mn is bound to the two latter proteins (Cotzias and Papavasiliou 1962; Scheuhammer and Cherian 1985). In general, the oxidation level of Mn

is the determinant for the final binding form and transport properties (M. Aschner et al. 2006), although the aqueous chemistry is dominated by Mn(II)-complexes (Ronconi and Sadler 2008). Mn transportation into the brain was found to occur by facilitated diffusion and active transport via high affinity to metal transporters crossing the neuronal barriers (Yokel and Crossgrove 2004). An in vitro study carried out by Bornhorst et al. reported that the blood cerebrospinal fluid barrier was the preferred route over the blood brain barrier (BBB) when applying different Mn concentrations (Bornhorst et al. 2012b). Discussed transporters include Ca^{2+} channels, ZIP8/14, transferrin receptors and DMT-1, while latter is not the major mediator for Mn uptake (J. S. Crossgrove and Yokel 2004). Moreover, Tf-receptor mediated influx into brain was also suggested for Mn(III)-Tf complexes by controlled mechanisms (M. Aschner et al. 2006). Also Mn-citrate tridentate complexes are thought to be transported by a monocarboxylate transporter or ATP-binding cassette superfamilies. Interestingly, intravenously injected Mn was found to enter the brain as the free ion. Mn-efflux from brain tissue seems to be mediated by diffusion mechanisms (Yokel 2009). The mentioned transporters for Mn into the brain are summarized in Figure 14. Failure in these controlled transport procedures under the influence of increased Mn concentrations are discussed, while analysis of these changes in transport procedures was a major aim within this work.
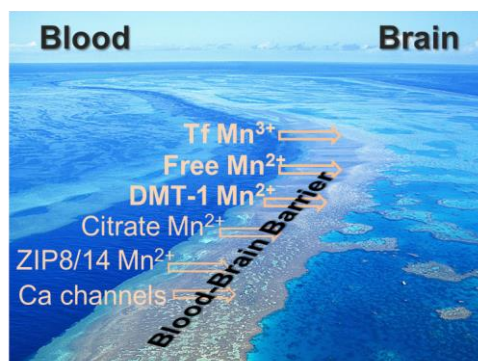
Figure 14 Mn transporters at BBB which are discussed in literature.

As mentioned before, mitochondria in liver and brain are thought to be the primary pool for Mn, where it is transported into the cell via the Ca^{2+} uniporter (Kalia et al. 2008). Determination of the oxidation state of Mn within brain mitochondria, neuron-like cells, and astrocytes proofed the presence of mainly Mn(II)-complexes, diminishing earlier suggestions of a possible oxidation of Mn(II) to Mn(III) and its role for neuronal toxicity (Thomas E. Gunter et al. 2006).Regarding the cellular import of Mn, beside the named transporters across neural barriers, also the ATPase ATP13A2m, which is encoded by the park9 gene, seems to be parti-cipating. Interestingly, this gene was found to be responsible for the early onset of PD (Gitler et al. 2009). Intracellular Mn transporter further include voltage regulated or glutamate-activated ion channels, which are usually responsible for Ca^{2+} transport, and

Hip14/14L, which can of course also mediate transportation of other divalent metals (Avila et al. 2013). Cellular Mn-efflux is supposed to be regulated by ferroportin-1 (Madejczyk and Ballatori 2012). However, if this mechanism is also the efflux mode of action in neural cells remains to be evaluated.

A.3.5   The disease Manganism

The disease manganism was firstly described in 1837 by James Couper, who observed paraplegia mostly in the lower extremities in five Scottish men working on grinding MnO_2 ore (Couper 1837). Cases of diseased workers from all over the world were reported since then (e.g. (Iregren 1999; Roels et al. 1987; Wang et al. 1989), reviewed in (Flynn and Susi 2009)). Exact numbers of prevalence are not known, but in China, a 0.5-2% prevalence rate was reported amongst exposed workers (Gao et al. 2003), where metal poisoning ranks among the 10 leading occupational diseases (Liang and Xiang 2004). Large cohort studies are therefore designed to take remedial actions (Lv et al. 2014). The early stage of the disease is termed "manganese madness" as affected persons show emotional lability accompanied by weakness, anorexia, behavioral and psychiatric disturbances (P. Chen et al. 2014). After an onset, the disease is progressive and irreversible. The occurring neurodegenerative mechanisms are versatile and still not fully understood and research is progressing. The main supposed modes of action should therefore be shortly explained in the following chapters, and are also summarized in Figure 15.

A.3.5.1 Supposed molecular mechanisms of neurodegeneration

As Mn is part of various biological functions in the body (Figure 13), it becomes obvious that mechanisms leading to neurodegeneration during manganism or Mn-induced Parkinsonism have to be multifactorial. These mechanisms are by far not completely understood and the individual severity depends on several factors such as level and route of exposure, dosage, age of exposed individual as well as exposure duration (Dobson et al. 2003). However, the common thread of all supposed modes of action is the formation of oxidative stress. Very comprehensive literature about the neurotoxicology of Mn has recently been published in a book (Costa and Aschner 2014).

A.3.5.1.1 Mitochondrial dysfunction and oxidative stress

As mentioned before, the primary target organelles for Mn accumulation are mitochondria. Once Mn concentrations are elevated, Mn^{2+} is oxidized to Mn^{3+}, which has greater pro-oxidant activity leading to generation of reactive oxygen species (ROS) even in trace amounts (C. J. Chen and Liao 2002). Moreover, Mn^{3+} is a potent inhibitor of complex I of the

mitochondrial electron transfer chain, which causes a reduced ATP production, increased leakage of electrons and oxygen radical formation (S. Zhang et al. 2004). Interestingly, anti-oxidants were shown to attenuate these ROS-producing effects of Mn on mitochondria (Gavin et al. 1990). Additionally, enzymes with anti-oxidative properties are disturbed in their functionality by excess Mn. Neuroblastoma cells treated with $MnCl_2$ showed decreased activities of Mn-SOD, Cu/Zn-SOD, catalase and glutathione peroxidase (GPx) (Yassine Chtourou et al. 2011). Activity of AchE seems to be dependent on duration of exposure as high sub-acute Mn doses led to an increase in its activity whereas chronically treatment decreased activity (Michalke and Fernsebner 2013). However, mediators of inflammation such as pros-taglandines and F2-isoprostanes were elevated and ATP levels were depleted due to in-creased oxidative stress resulting from imbalanced activity of anti-oxidant enzymes (Santos et al. 2012).

A.3.5.1.2 Alteration in neurotransmitter levels

Mn-induced disruption of the glutamate-glutamine cycling seems to occur due to a preferred accumulation of Mn in astrocytes, whose functionality is essential for normal neuronal activi-ty (Avila et al. 2013). Glutamate homeostasis is altered to the effect that glutamate uptake by astrocytes is decreased as well as the expression of astrocytic glutamate: aspartate trans-porter (GLAST) is reduced (M. Sidoryk-Wegrzynowicz et al. 2009). Finally, excitatory neuro-toxicity is emerging (K. M. Erikson and Aschner 2003). One of the most abundant catechol-amine in brain is dopamine (DA) controlling locomotion, emotion and the neuroendrocrine system. The PD-resembling symptoms observed in manganism are a result of degenerating nigrostriatal DAergic neurons (Racette et al. 2001). A decrease in DA transporters as well as declined pre-synaptic DAergic functioning was observed after postnatal Mn exposure (McDougall et al. 2008). However, effects on DA metabolism seem to be dependent of sev-eral factors such as route of administrations and exposure time or duration (Avila et al. 2013). Mn-induced effects on DA cycling also include free radicals. As mentioned above, the oxidation of Mn^{2+} to Mn^{3+} generates ROS catalyzing autoxidation of DA (Graumann et al. 2002). Moreover, this DA oxidation induced by Mn involves much more complex steps impli-cating semiquinone, aminochrome intermediates, L-cysteine, copper and NADPH (Stredrick et al. 2004). Thus, DAergic cell death by DA autoxidation might be facilitated due to genera-tion of cytotoxic quinones and ROS adding all up to oxidative damage. The effect of Mn on glutamate, dopamine and γ-aminobutyric acid (GABA) is reviewed in (Fitsanakis et al. 2006).

A.3.5.1.3 Effects on molecular and genetic levels

Focusing on the molecular toxicology of Mn, an inhibition of poly(ADP-ribosyl)ation in human astrocytes failed to repair Mn-induced DNA strand breaks (Bornhorst et al. 2010). Clastogen-

icity and DNA strand breaks were also induced by Mn treatment in human lymphocytes, re-ducing the mitotic index as well as inducing chromosome aberrations (Lima et al. 2008). Moreover, cellular energy related nucleotides ATP, NAD+, NADH as well as the NAD+/NAD ratio were decreased after MnCl$_2$ in a human lung cell line (Bornhorst et al. 2012a). These results on molecular level are further enlarging the knowledge about Mn-induced toxicologi-cal mechanisms; however, further studies in that direction in brain derived cell types are needed for reinforcement. Interestingly, Mn seems to facilitate the capacity for ions through the mitochondrial permeability transition pore (Dejan Milatovic et al. 2007). Opening of this pore activates extracellular signal-regulated kinases (ERK) such as caspase-3, finally lead-ing to chromatin condensation and DNA fragmentation. This activation of ERK and caspase-3 was also observed in Mn-treated astrocytes.

As indicated above, genetic predisposition seems to be one factor contributing to a preferred accumulation of Mn leading to parkinsonian disturbances. The genetic implication was al-ready observed 1987, where occupationally exposed Aborigines (Groote Eylandt, Northern Australia) showed higher blood Mn levels as well as neurological signs compared to workers from other ethnicities (Cawte et al. 1987). Nowadays studies focus on PD-involved genes such as Park2, -6, or -7. Recessive mutations in Park2 were shown to increase environmen-tal sensitivity to Mn exposure with an increase in ROS and mitochondrial fragmentation (Aboud et al. 2012). Moreover, both Park2 and -7 were decreased in DAergic brain areas in rodents exposed to Mn containing welding fumes (Sriram et al. 2010). Mn-induced genotoxi-city is reviewed in (P. Chen et al. 2014).
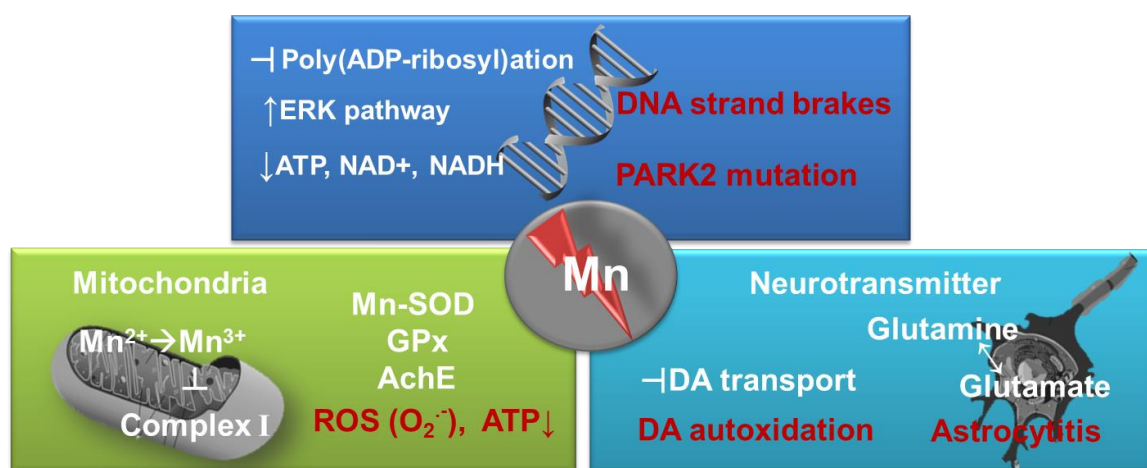
Figure 15 Main supposed mechanisms of Mn-induced neurodegeneration.
Mn-induced toxicity in neural tissue is mediated by its accumulation primarily in mitochondria inhibiting of complex I of the respiratory chain and of anti-oxidative enzymes like SOD, which leads to genera-tion of ROS. Besides, astrocytitis and dopamine (DA) autoxidation was shown to be induced by Mn. Also on molecular level, DNA strand brakes as well as genetic mutations can result from increased neural Mn.

A.3.5.2 Biomonitoring and treatment attempts of exposed persons

The problem in monitoring exposed persons is the discrepancy of Mn levels in blood and the target tissue, e.g. brain. Therefore, Mn assessment scenarios have to be appropriate to the respective situation. Biomonitoring attempts of Mn intoxications are reviewed in (Zheng et al. 2011). In summary, total Mn concentrations in blood are suggested to be only useful for distinguishing Mn-exposed from unexposed subjects on a group comparison basis. At the individual level, a MRI scan of the brain might be helpful. Due to the paramagnetic properties of Mn, bilateral symmetrical increases in brain signal intensities during accumulation of Mn ions can be observed on T1-weighted MRI. Here, the "pallidus index" (PI) is defined as the ratio of the signal intensity in the globus pallidus to that in the subcortical frontal white matter in axial T1-weighted MRI planes multiplied by 100, and serves as a measure value for Mn accumulation in globus pallidus (Krieger et al. 1995). However, this PI is only useful for comparing observations within one study as it depends on exact image parameters and is known to vary significantly between studies. On group comparison basis or in combination with the noninvasive assessment of GABA, the MRI of exposed active workers might be indicative even in the absence of clinical symptoms of Mn-intoxication. It remains, however, only a proportional measure of Mn concentrations.

For low-dose residential or historical exposed persons, monitoring is much more complex. In such case, authors suggest determination of Mn/Fe ratios (so-called MIR) in plasma or erythrocytes due to the adverse effects in concentrations of those two elements under exposure. One prerequisite for that is the determination of cut-off values in the general population, which need to be established first. Moreover, the MIR rather signals the biological response to Mn exposure (e.g. altered Fe concentrations) than the steady-state burden of Mn or Fe.

As Mn is essential for development of connective tissue and bone, approximately 40% of Mn accumulates in the latter. X-ray fluorescence and neutron-based spectroscopy, hence, might represent a novel non-invasive method for assessing historical Mn exposure. The *in vivo neutron activation analysis* (IVNAA) was tested in a pilot study in occupationally exposed welders compared to a control non-exposed group of humans. The authors found significantly elevated Mn levels in the occupationally exposed group. One drawback was that the determined value for the control group was below the minimum detection limit. However, improvement and optimization in the method might be worthwhile to obtain reliable reference values for measuring Mn levels in the body non-invasively in exposed persons.

Effects of treatment of Mn-intoxication are controversial and unrevealing. While Levodopa is used as state of the art treatment in PD, there is commonly no response of manganism cases (Koller et al. 2004). As with treatment of many metal poisonings, the primary treatment strategy in highly Mn-exposed individuals is chelating therapy. Here, the calcium disodium salt $CaNa_2EDTA$ should be applied preferential over EDTA, as latter was shown to induce hypocalcemia (M. Aschner et al. 2009). Some other agents were tested mostly in *in vitro* studies, which mainly attenuated signs of oxidative stress or showed neuroprotective activity. Examples of examined agents and their observed effects are summarized in Table 4.

Agent	Cells	Effect(s)	Reference
Indomethacin/ para-Aminosalicilic acid	Primary rat cortical neurons	Antiinflammatory: isoprostanes, PGE2↓	(D. Milatovic et al. 2011)
17β-Estradiol (estrogen) and tamoxifen	Primary rat cortical astrocytes	NF-κB, NOS2↓ GLAST mRNA ↑	(Lee et al. 2009)
Tamoxifen/ MK801 (NMDA antagonist)	Rat striatum	Glutamate excitotoxicity↓	(B. Xu et al. 2010)
Melissa officinalis/ Silymarin	Murine neuroblastoma cells	Oxidative stress↓	(Yassine Chtourou et al. 2011; Y. Chtourou et al. 2012)

Table 4　Attempts for Treatment of manganism.
Listed agents and their molecular effects were tested in in vitro or direct injection studies of Mn-induced neurotoxicity.

Even after primary retaining of high concentrated Mn from the body by chelating agents, neurological symptoms can worsen also after years of cessation of chronic exposure. Additional cases are reported, where the symptoms of manganism emerged only years after retirement. Finding of biomonitoring and treatment possibilities in Mn-induced neurodegeneration, preferably at the onset of disease, is therefore one major goal of nowadays studies. Elucidation of cellular and molecular mechanisms of action in their totality is therefore likely the major task.

A.4　Aims and Objectives within this work

Overexposure to Mn either occupationally or environmentally has been proven to lead to neurodegeneration in the area of basal ganglia. The resulting disease called manganism or Mn-induced Parkinsonism has historically been monitored by measuring of total Mn concentrations in blood or other body fluids like urine. Studies have shown, though, that total concentrations of Mn in the body are only valid in a group comparing manner or even when it might already be too late. The formation of low molecular mass (LMM) carriers of Mn in the body, towards and across neural barriers during overexposure has been discussed for some

years now. However, studies on the formation of these Mn-compounds within the body *in vivo* are rarely as available literature focusses on environmental aspects such as Mn-speciation or fractionation in soil and dust (Borgese et al. 2013; Okonkwo et al. 2009; Salmanzadeh et al. 2015), in aquatic organisms (Hernandez et al. 2011b; Vitoulova et al. 2011), in plants (Weber and Konieczyński 2003), or reports about Mn-species in environmental pollutants (Keane et al. 2010; Ressler et al. 2000; Thomassen et al. 2001). This is aggravated by the fact that the availability of human samples such as CSF is very limited due to medicinal regulations. That fact necessitates the implementation of animal studies if further information about formation of Mn-species within a biological system should be found. Several animal studies have been carried out in the context of neurochemical and behavioural effects of Mn, where the common aim was the investigation of the occurring alterations in neuronal mechanisms during Mn-intoxication (e.g. investigation on the dopamine cycling after Mn-exposure in monkeys by positron emission tomography (PET) imaging (M. K. Chen et al. 2006; Guilarte et al. 2006; Shinotoh et al. 1995)). However, internal cumulated Mn concentrations in animal studies often extend the doses at which neurological symptoms were observed in occupationally exposed humans (10-15 mg/kg b.w., cumulative) by two orders of magnitude. These problems are described in a literature evaluation carried out by Gwiazda et al., where the authors concluded that most animal studies might not be relevant for risk assessment of chronically, and low-level Mn exposure in humans (Gwiazda et al. 2007). Bearing this result in mind, the focus of animal studies should therefore be on lower concentrated Mn-exposure models similar to those concentrations, which individuals can nowadays be exposed to during lifetime for example by environmental pollution (R. Lucchini and Zimmerman 2009).

Based on that, two different animal studies were designed in this work. One study served as **(sub)chronic exposure** study, where rats received elevated but not toxic levels of Mn by their fodder compared to a control group which received standard fodder. For this feeding study, a pre-feeding study was carried out to elucidate applicable concentrations of Mn to be fed. The other animal study was based on a previous injection study where rats received a **single low-dose injection of Mn *i.v.*** mimicking an accident or a single direct exposure to elevated, but not toxic Mn levels. The first major aim of this work was therefore to investigate **Mn-species distribution in serum and brain** by SEC-ICP-MS in these two different animal studies. Moreover, mechanisms of Mn-induced neural injury and their connections are not fully understood, yet. With the applied concentrations of Mn in a nontoxic range, the possible impact of Mn on alterations in neural mechanisms should be addressed such as it is for example the case in environmentally increased concentrations. Hence, the second aim in this work was the examination of neural mechanisms leading to neuronal injury even at these

very slightly increased Mn concentrations. Different questions were addressed such as: are there changes in **concentrations of other elements like Cu, Fe or Zn in serum or brain**, and whether **AchE activity and glutamate concentrations might be altered in the brain**. Moreover, possible changes in the **ratio of Fe(II) and Fe(III) in the brain** were investigated with regard to arising oxidative stress in the brain. For this, a valid **separation and hyphenation technique** had to be found before. A non-targeted analysis of brain by ESI-ICR/FT-MS served for elucidation of the **various possible involved alterations in neural mechanisms** in its entirety. One goal was therefore, to address eventually occurring interlinkages between different mechanisms in the brain. By doing so, another aim was the investigation of possible occurring **correlations from Mn-speciation with detected brain metabolites** by ESI-ICR/FT-MS combining metallomics with metabolomics. One further aim during this work was the investigation of **elemental distribution in the brain after the single injection of Mn by LA-ICP-MS**. Due to limitations in time, only preliminary results will be shown.

The structure of the thesis addressing the above mentioned aims is illustrated in Figure 16.
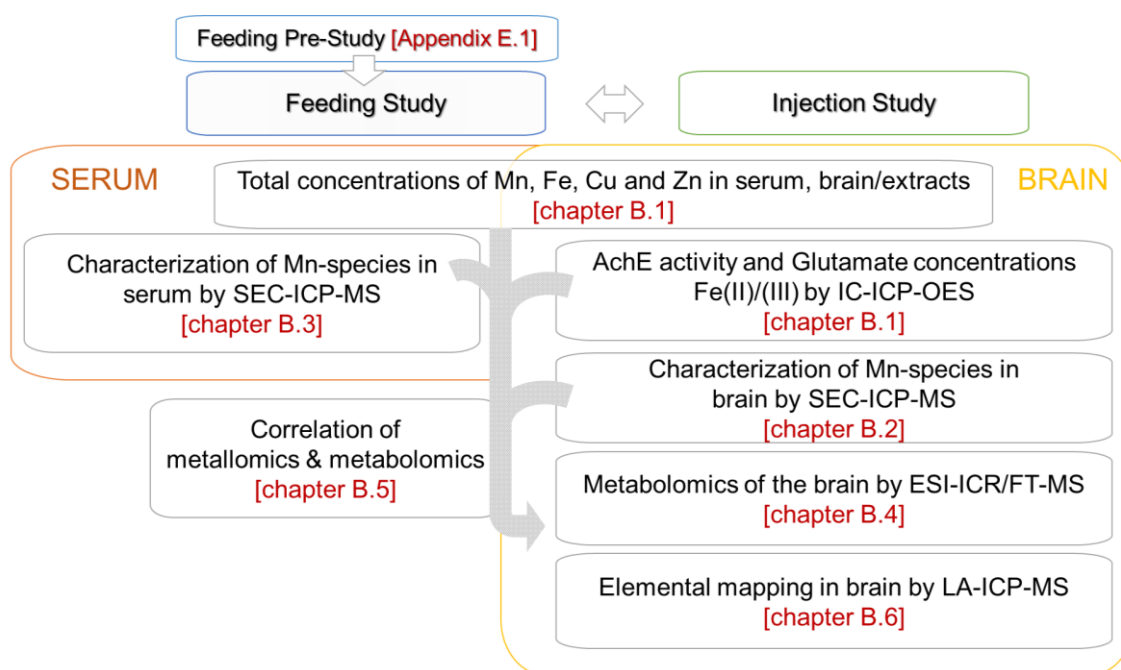
Figure 16 Structure of the thesis with chapter details.

B   Results and Discussion

B.1   Mn-exposure: Feeding vs. Injection

The following chapter describes the comparison of the single $MnCl_2$ injection with the low-dose chronic feeding of Mn in rats with respect to the following questions:

➢   Does the applied Mn exposure affect concentrations of Fe, Cu and Zn in serum or brain? (chapter *B.1.1*)

➢   Are there changes in glutamate concentrations in brain due to Mn exposure? (chapter *B.1.2*)

➢   Is the activity of acetylcholinesterase (AchE) influenced by Mn? (chapter *B.1.3*)

➢   Are there changes in the Fe(II)/(III) ratio in brain due to Mn exposure? (chapter *B.1.4*)

These will be concluded at the end of the chapter.

B.1.1   Determination of Mn, Fe, Cu and Zn in serum and brain

To monitor Mn concentrations and to unravel potential effects of Mn substitution on elemental levels of Fe, Cu and Zn, concentrations of these elements were measured in serum and brain. Serum was obtained after centrifugation of blood taken from the *aorta abdominalis* at animal sacrifice (serum_feeding and serum_Inj4d) or from the *vena sublingualis* by punctuation one hour after $MnCl_2$ injection (serum_Inj1h). The serum was aliquoted and stored at -80°C until analysis. Taken brains at animal sacrifice were shock frozen with liquid N_2 and a nitric acid digestion was carried out. Serum was diluted 1:20 and brain digestions were measured undiluted by standard solution analysis with ICP-OES or ICP-sf-MS as described in chapter *D.3*. The obtained concentrations for Mn, Cu, Fe and Zn are summarized in Table 5.

As the table shows, a significant increase of **Mn** concentrations in serum could only be observed one hour after injection (7 ± 2 µg/l compared to 194 ± 49 µg/l, p<0.001). Levels of Mn in serum were already balanced in Mn-exposed animals four days later at time of sacrifice (6.0 ± 1.5 µg/l in control and 6.7 ± 1.3 in +Mn_Inj). The same was true for Mn concentrations in serum in the feeding study as no significant difference between control and Mn-fed rats was observed (4.5 ± 0.8 µg/l in control and 4.7 ± 0.7 µg/l in +Mn_Food). Interestingly, the increase of Mn in total brain was similar after feeding (~17%) or injection (~19%) of Mn in Mn-exposed animals compared to controls (feeding: 368 ± 25 ng/g vs 429 ± 57 ng/g, p<0.05; injection: 360 ± 20 ng/g vs 429 ± 17 ng/g, p<0.001; control vs Mn-exposed, respectively).

The concentrations of Mn in the brain found in Mn-exposed animals showed less variance in the injection study. This might be due to controlled exposure by injection, where every animal received exact the same Mn concentration. Therefore, the only influence left was the individual distribution of Mn in the body by the blood system. Controversy in the feeding study, Mn concentrations in the brain of Mn-exposed rats showed higher variance due to the individual intake of food as well as possible variations in homogeneity of Mn distribution in the fodder. These intersubjective variations in Mn uptake, which is also susceptible to digestion, added to the variation in the individual distribution of Mn in the body resulted in such distributed values. However, a clear increase of Mn in brain of treated animals was observed both in the feeding as well as in the injection study. This was not the case in serum Mn levels. An effective increase of total Mn in serum was only observed one hour after injection. Already four days later and also after the almost two months of feeding of Mn, concentrations in serum of exposed rats were comparable to the control animals. These results contradict many studies, where only total Mn concentrations in serum or blood are determined. As observed herein, an increase in total Mn concentration in serum occurs only after direct exposure. An increase of serum Mn after prolonged exposure might only be meaningful on basis of group comparison to non-exposed individuals. This problem was also reported by Smith et al. (D. Smith et al. 2007). The authors tried to find correlations between Mn concentrations in air and blood Mn concentrations in exposed workers. However, they found only limited relationship between Mn in air and blood. The less utility of Mn concentrations in blood as biomarker of exposure will further be discussed in chapter *B.5* in a wider context.

Concentrations of Fe, Cu and Zn in serum and brain showed differences depending on the applied exposure. In serum and brain, feeding of Mn led to a significant decrease of **Fe** concentrations compared to control (80% lower in serum, $p < 0.001$: 3.1 ± 0.7 vs. 0.6 ± 0.1 mg/l and 30% lower in brain, $p < 0.001$: 13.0 ± 0.5 vs. 9.0 ± 0.5 µg/g). This decrease in serum was also implied in the injection study, but was not significant (16% and 40% lower than in control one hour and four days after injection, respectively). A decrease in brain Fe due to injection was not observed. Controversy, **Cu** was highly increased in serum by 88% and also in brain by 17% after feeding of Mn compared to control (serum: 128 ± 108 vs. 1024 ± 300 µg/l, $p < 0.001$; brain: 1.4 v 0.1 vs. 1.9 ± 0.4 µg/g, $p < 0.01$). The injection of Mn led to a slight decrease of Cu in serum 25-30% one hour and four days after injection, which was only significant four days after injection (95 ± 22 vs. 73 ± 14 µg/l in serum, $p < 0.05$). In brain, no difference in Cu concentrations between control and Mn-injected rats could be observed due to injection of Mn. **Zn** was significantly reduced in serum in both feeding (40% lower compared to control, 0.5 ± 0.2 vs. 0.3 ± 0.6 µg/l, $p < 0.001$) and injection study (23% lower compared to control, four days after injection, 1.3 ± 0.1 vs. 1.0 ± 0.1 µg/l, $p < 0.05$). In brain, however, con-

centrations of Zn showed no difference compared to control both in the feeding as well as in the injection study.

Mn, Fe, Cu and Zn all belong to the group of essential metals serving critical roles in physiological functions. Imbalances in these essential metals may have adverse effects on biological processes, and have been associated with neurological diseases (S. J. Garcia et al. 2006). Dietary intake of metals critically influences brain metal uptake and concentrations of other metals. It is known that Fe deficiency enhances Mn accumulation while Mn treatment can likewise alter Fe homeostasis (K. A. Erikson et al. 2002; E. A. Smith et al. 2013). Therefore, daily $MnCl_2$ treatment of rats for one month decreased Fe concentrations in plasma and increased Fe in CSF (Smyth et al. 1973). Garcia et al. observed decreases in brain Fe and increased brain Mn and Zn by a supplemented Mn diet via mothers milk during lactation, from postnatal day 4 to 21 (S. J. Garcia et al. 2006). Similar results were obtained in an earlier study of $MnCl_2$ injection in rats, where Mn and Cu accumulated in brain, while Fe and Zn were decreased (Riojas-Rodriguez et al. 2010), which is concordant to our observations in the feeding study. The decrease in Zn was also found in a study where rats received a Fe-deficient diet (Lynam et al. 1999). As described in literature, Fe deficiency can enhance Mn uptake (K. A. Erikson et al. 2002; Kim et al. 2012; Kwik-Uribe et al. 2000; Seo et al. 2013). This can be a major problem for people with diagnosed iron deficiency living in regions where high exposure to Mn is given, such as by food, drinking water or air. Interestingly, this interaction of Fe and Mn might not always be true as found in a study by Fitsanakis et al. (Fitsanakis et al. 2008). Mn was *i.v.* applied for two weeks (3 mg/kg b.w.) in three feeding groups of rats, namely control, Fe-deficient and Fe-rich diet. Concentrations of Mn in blood and brain were determined and were found to be increased in both, Fe-deficient as well as Fe-rich fed animals. The concentration and duration of Mn uptake as well as the way of uptake (*i.v.* or oral) might have diverse effects on Fe levels independent from the body Fe status before.

An increase in Cu concentrations in brain and plasma was also described by Fordahl et al. after Mn-exposure of rats by drinking water with 1 g Mn/L for six weeks (Fordahl et al. 2012). A chronic exposure (~6 months) of Mn in non-human primates also increased Cu concentrations in the brain, primarily in structures of the basal ganglia (Guilarte et al. 2006). Interestingly, also in CSF of PD patients, metals seem to be subject to variations with an increase in Cu and a decrease in Fe being commonly observed (Dusek et al. 2014). The similarity of Mn-induced alterations in brain elemental status with alterations observed in CSF of PD patients is a further common factor of these two neurological disorders. However, post mortem analysis of brain tissue showed adverse results with increased Fe and decreased Cu. Keep-

ing these studies in mind, an effect on metal imbalances in brain seems to require a pro-longed or a very high concentrated administration of Mn. Therefore, the results of the feeding study with decreased levels of Fe and increased levels of Cu are in line with the mentioned studies of Mn-exposure although an effect on the neural Zn pool was not observed in this study. The effect of increased Mn-exposure on variation of elemental concentrations in blood might occur already after a short intervention as observed herein. A later time point of measurement would have been interesting in respect of rebalancing or further alteration of elemental concentrations of Fe, Cu and Zn due to the single MnCl$_2$ injection. Overall, it seems astonishingly that increased but non-toxic concentrations of Mn can already alter Fe, Cu and Zn levels in that extend both in serum and brain, while latter seems to be more prone to such changes after a prolonged or chronic Mn-exposure.

		Serum				Total Brain	
		1h after injection		4d after injection/ 53 days feeding			
		Co	+Mn	Co	+Mn	Co	+Mn
Feeding	Mn			4.5±0.8	4.7±0.7 n.s.	368±25	429±57*
	Fe			3.1±0.7	0.6±0.1***	13.0±0.5	9.0±0.5***
	Cu			128±108	1024±300***	1.4±0.1	1.9±0. **
	Zn			0.5±0.2	0.3±0.6***	11.5±0.7	11.4±0.5 n.s.
Injection	Mn	7±2	194±49***	6.0±1.5	6.7±1.3 n.s.	360±20	429±17***
	Fe	2.5±0.5	2.1±0.9 n.s.	5.3±3.0	3.1±1.2 n.s.	13.0±0.6	13.5±0.7 n.s.
	Cu	132±31	105±20 n.s.	95±22	73±14*	1.6±0.1	1.7±0.1 n.s.
	Zn	1.1±0.2	1.2±0.1 n.s.	1.3±0.1	1.0±0.1*	11.1±0.4	11.2±0.5 n.s.

Mn: µg/l (serum) or ng/g (brain); Fe: mg/l (serum) or µg/g(brain); Cu/Zn: µg/l (serum) or µg/g (brain)

Table 5   Total concentrations of Mn, Fe, Cu and Zn in serum and total brain determined by ICP-OES and ICP-sf-MS.
Statistical significantly altered concentrations are shown in red (Student t-test between control and Mn-exposed animals, *p<0.05, **p<0.01, ***p<0.001, n.s. not significant)

B.1.1.1 Concentrations of Mn and Fe in aqueous brain extracts

As described in the Experimental procedure section (chapter *D.2.2.1*), for Mn-speciation in brain as well as for application of the *in vitro* kits, an aqueous brain extraction was carried out. This extraction was established by Diederich et al. (Diederich and Michalke 2011) and was proven to be highly specific in terms of maintaining Mn- as well as Fe-species which are natively abundant in brain. This is one prerequisite for a reliable characterization of Mn-species in the brain. Beside a suitable chromatographic system, a species-specific sample

preparation is inevitable to prohibit species alterations in the matrix. Therefore, the extraction was carried out under exclusion of O_2 in an Ar atmosphere with He purged extraction buffer on ice. Step-wise procedure was carried out with only small sample amounts per step (three brain samples yielding six extracts per step). Extracts were aliquoted, stored at -80°C and allowed to thaw at 4°C overnight before analysis to prohibit species alterations during thawing. Pellets obtained during extraction were microwave digested with nitric acid. Total concentrations of Mn and Fe in extracts and pellets were determined by measurement with ICP-sf-MS (for Mn) as well as ICP-OES (for Fe). The results are shown in Table 6, listing the determined concentrations of Mn (ng/g brain FW) and Fe (µg/g brain FW) in brain extracts, pellets and total brain. Besides that, "extract+pellet in %" reflects the recovery of Mn or Fe concentrations in extracts and pellets in sum compared to total Mn or Fe concentrations in brain. The extraction efficiency (EE, %) reflects the obtained concentrations in extracts compared to total concentrations in brain.

		Mn		Fe	
		Co	**+Mn**	**Co**	**+Mn**
Feeding	**Extract**	112.9 ± 13.8	134.7 ± 14.9**	6.9 ± 1.0	3.7 ± 0.5***
	Pellet	253.4 ± 28.2	292.8 ± 31.4**	7.0 ± 0.6	5.8 ± 0.6***
	Total	368.1 ± 24.6	429.2 ± 56.8*	13.4 ± 0.5	9.0 ± 0.5***
	Extract+Pellet (%)	99.9 ± 9.7	100.4 ± 9.2	104.1 ± 10.7	106.2 ± 7.2
	EE (%)	30.8 ± 3.9	31.9 ± 5.4	52.0 ± 8.7	41.5 ± 3.8
Injection	**Extract**	108.6 ± 14.6	173.5 ± 60.9**	8.0 ± 1.2	7.6 ± 1.2[n.s.]
	Pellet	262.4 ± 16.1	288.3 ± 63.5[n.s.]	7.3 ± 0.7	6.1 ± 1.5*
	Total	360.1 ± 19.7	429.1 ± 17.4***	13.1 ± 0.6	13.5± 0.7[n.s.]
	Extract+Pellet (%)	103.4 ± 9.4	104.3 ± 9.8	116.8 ± 8.8	104.7 ± 16.8
	EE (%)	30.3 ± 4.6	37.2 ± 17.2	61.0 ± 8.2	56.3 ± 7.7

Extract, pellet and total: Mn in ng/g and Fe in µg/g brain FW

Table 6   Mn and Fe concentrations in brain extracts and pellets (n=12 per group).
The sum of concentrations in extracts and pellets were compared to total concentrations in brain (n=18 per group). Extract+Pellet (%) reflects the recovery. The extraction efficiency (EE (%)) was obtained by division of concentrations in extracts by total concentrations in brain. (Student t-test between control and Mn-exposed (+Mn), *p<0.05, **p<0.01, ***p<0.001, n.s. not significant)

The extraction efficiency (EE%) for Mn in the feeding study was for both groups (control and +Mn) 26.9-37.3% (median 31.5%). In the injection study, the extraction efficiency for Mn was in average 25.7-54.1% where a slightly higher average value was obtained for +Mn_Inj

samples, mainly due to one outlier. In median the EE for Mn in the injection study was comparable to the feeding study with 32.6%. Compared to the developed method of Diederich et al., the EE for Mn from brain herein was slightly higher (28% vs 32% in median), showing an appropriate extraction of Mn from brain tissue. The increase in brain Mn in +Mn samples was still given in the extracts compared to control. The recovery for Mn (Extract+Pellet (%)) was 90.2-109.6% in the feeding study and 91.2-126.4% in the injection study. Despite of the outlier in the injection study and with respect to measurement uncertainty, median values for recovery of Mn were comparable between the feeding and the injection study with 101.5% and 103.7%, respectively. This very good recovery led to the conclusion that there were no losses or major contamination with Mn during extract preparation.

Obtained values for extraction efficiency of Fe were 37.7-60.7% (median 46.8%) in the feeding study and 48.6-69.2% (median 57.4%) in the injection study. Median values showed slightly higher extraction efficiency for Fe in the injection study. However, compared to the median EE value for Fe of 51.3% value reported by Diederich et al., the herein found EE was comparable good. The significantly lower Fe concentration in +Mn_Food total brain were also found in extracts and pellets. Recovery for Fe was 93.4-114.9% (median 105.2%) in the feeding study and 87.9-125.5% (median 110.1%) in the injection study. Recoveries were therefore comparable in both studies and showed no losses of Fe during extraction procedure.

B.1.1.2 Quality Control

For quality control of brain digestion and measurement, certified reference material (CRM) was digested and measured in line with samples. The CRM applied throughout the work was BCR185, which was pulverized bovine liver. This approach included digestion of a comparable amount of BCR185 in line with samples in the Seif apparatus or the microwave and subsequent measurement in line with the digested samples. Table 7 summarizes the mean concentrations of Mn, Fe, Cu and Zn of five digestion controls in comparison with the reference values. The obtained values (in average 95% for Mn, Fe, Cu and Zn) were in good agreement with the target values with respect to measurement uncertainty and age of the applied CRM. The distribution from digestion up to measurement is reflected by the SD, which was below 1% for Mn, Fe and Cu. Only for Zn the found SD was 1.4%, which is still in an acceptable range. Therefore, the accuracy of the applied digestion and ICP-OES measurement was proven.

	Mean ± SD	BCR185 target mean ± SD	% (found/target)
Mn (µg/g)	8.8 ± 0.2	9.3 ± 0.3	94.7 ± 0.9
Fe (mg/g)	203.8 ± 2.4	214 ± 5	95.1 ± 0.9
Cu (µg/g)	178.0 ± 2.7	189 ± 4	94.5 ± 0.5
Zn (mg/g)	133.0 ± 0.8	142 ± 3	93.7 ± 1.4

*Table 7   Digestion of CRM by Seif apparatus and measurement by ICP-OES (n=5).
Obtained values were compared to target values of the CRM 185 (bovine liver).*

Another factor giving indication of the quality of a measurement is the comparability of ICP-OES and ICP-sf-MS. For this, concentrations of Mn, Fe, Cu and Zn of four brain extracts measured by both instruments were compared. As Figure 17 shows, almost equal values on both instruments were obtained for Mn, Cu and Zn. Moreover, standard deviations of Mn measurement were also in the same range on both instruments. Standard deviations for Cu and Zn were slightly higher in the measurement by ICP-sf-MS. Concentrations found for Fe were higher in the ICP-sf-MS measurement, although SD was small. The increased Fe concentrations in ICP-sf-MS can be explained by potentially occurring polyatomic interferences as described in the Introduction. Overall, ^{56}Fe is interfered by $^{40}Ar^{16}O^+$, which is one constituent of the plasma or $^{40}Ca^{16}O^+$, which might occur in the matrix of brain extracts. Such kind of interferences could explain the slightly increased concentrations of Fe. Moreover, calibration lines found for Fe, Cu and Zn in measurements by ICP-sf-MS sometimes showed relatively worse linearity ($r^2<0.99$), which could be caused by interferences in medium resolution for these elements. Due to these observations, results for Mn in serum and brain extracts herein are referred to the concentrations obtained by ICP-sf-MS, which was found to be the more accurate with respect to abundant low concentrations of Mn in the samples and very linear calibrations. Mn concentrations in the remaining samples (fodder, feces, brain digestion and brain pellet digestion) as well as concentrations for Fe, Cu and Zn in all samples are referred to the values determined by ICP-OES due to the more robust and linear measurement.
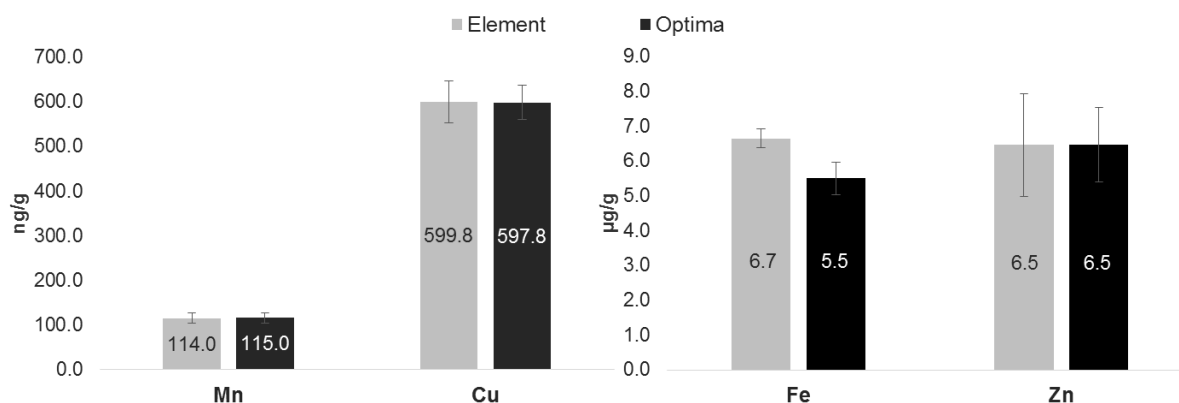
Figure 17 Comparability of ICP-OES (Optima7300) and ICP-sf-MS (Element2).
Four brain extracts were measured on both instruments. Determined concentrations and the respective SD were compared showing good agreement for Mn. SD for Cu and Zn were higher at the measurement by ICP-sf-MS as well as Fe concentrations were higher possibly due to occurring interferences.

B.1.2   Glutamate concentrations in brain

As described in the Introduction, the glutamate-glutamine cycling is one possible neurotransmitter system affected during Mn exposure. To unravel the effect of low-dose Mn-feeding and the single Mn-injection on glutamate concentrations in the brain, a commercial available glutamate determination assay was applied in the aqueous brain extracts as described in chapter *D.4.*

<u>Feeding study:</u>

Due to chronical Mn feeding, glutamate concentrations in brain extracts were significantly increased by 19% compared to control animals (1.85 and 2.21 mmol/g brain, p=0.028; Figure 18A). The correlation of these results with the respective Mn concentrations in the brain extracts revealed a weak, but linear positive correlation (y=0.015x+0.1744, R^2=0.4309), which was also found to be highly significant (p=0.0005) as shown in Figure 18B. A correlation between brain glutamate concentrations with total concentrations of Mn in serum or in whole brain was also carried out. However, serum Mn concentrations were not correlated with brain glutamate concentrations (Figure 18C). Correlation with Mn concentrations in total brain revealed a weak but not significant correlation with glutamate concentrations (Figure 18D). This result reflects the importance of the surrounding matrix for certain measurements. As glutamate was determined in the brain extracts, it only shows correlation with Mn concentrations in brain extracts and only weak correlation with Mn concentrations in total brain, where the matrix was different due to nitric acid digestion.
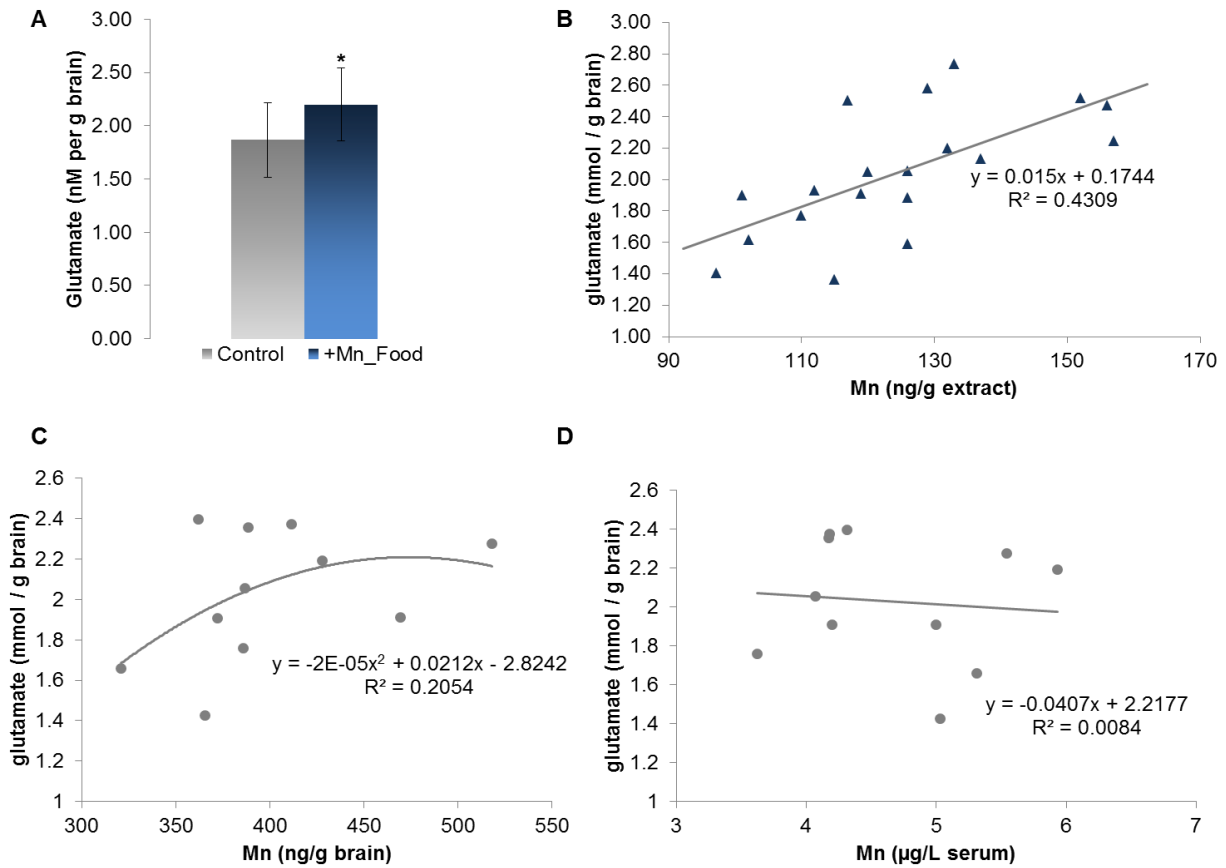
Figure 18 Determination of glutamate concentrations in brain extracts of the feeding study.
A: Glutamate concentrations were significantly increased in Mn-fed rats (p=0.028), N=12 extracts per group.
B: Glutamate concentrations showed a linear positive correlation with Mn concentrations in the brain extracts (p=0.0005; R^2=0.4309).
C: Glutamate concentrations showed a weak correlation with total Mn in brain (n.s.; R^2=0.2054).
D: Glutamate concentrations were not correlated with Mn concentrations in serum.

Injection study:

Due to the single time injection of Mn, no significant difference in brain glutamate concentrations was observed between test and control animals (Figure 19).
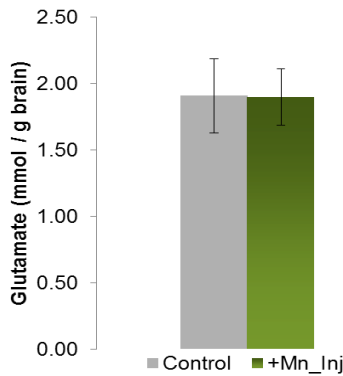
Figure 19 Determination of glutamate concentrations in brain extracts of the injection study.
No difference in glutamate concentrations between control and Mn-injected animals was found (N=12 extracts per group).

With glutamate (Glu) being the major excitatory neurotransmitter in the CNS, an over activation of neurons has also been linked to neurodegenerative diseases like ALS, HD, AD and PD (Lau and Tymianski 2010). The glutamate/glutamine-GABA-cycle (GGC) is maintained by the active communication of astrocytes and neurons in the CNS: glutamine is metabolized to Glu in neurons, indirectly generating GABA and the TCA cycle intermediate α-ketoglutarate. Various Glu transporters can then shuttle Glu to astrocytes, where it is amidated to glutamine by glutamine synthetase (GS), an enzyme exclusively found in astrocytes (Norenberg and Martinez-Hernandez 1979). Hence, the major role of the GGC is to circumvent too high extracellular glutamate levels (Marta Sidoryk-Wegrzynowicz and Aschner 2013). Mn toxicity is known to disrupt both glutamine influxes in neurons as well as glutamine efflux from astrocytes (M. Sidoryk-Wegrzynowicz et al. 2009). For example, accumulation of Mn in cultured rat astrocytes led to a decrease in the GLAST and taurine transporter (K. Erikson and Aschner 2002). This reduction in Glu transporters was confirmed *in vivo* in long-term airborne Mn-exposed rhesus monkeys both on mRNA and protein level (K. M. Erikson et al. 2008). The resulting extracellular increased Glu levels can then promote excitatory neurotoxicity, which was also observed in rat neonatal primary astrocytes. However, in rat neuronal-derived cells treated with low-level $MnCl_2$, extracellular and intracellular Glu levels were significantly increased (Crooks et al. 2007), which was also observed in other *in vitro* studies in astrocytes treated with Mn (Mutkus et al. 2005; Zwingmann et al. 2003a). Due to the preferred accumulation of Mn in astrocytes, an increase in Glu concentrations can also be reasoned in an impaired conversion of Glu to glutamine by an inactive GS enzyme. This inhibition of GS was described by Deng and colleagues (Deng et al. 2012). A chronically lasting oral input of low-dose Mn can result in an increase of Glu levels in brain as confirmed herein, what might lead to chronic excitotoxicity. Although Glu-mediated excitotoxicity was also observed during acute situations like traumatic brain injury, Glu concentrations seemed not to be influenced by the single Mn injection herein. Interestingly, the effect of Mn on Glu concentrations might further be dependent on the acting concentration as 20 mg Mn/kg fodder per day resulted in an increase in brain Glu levels, whereas 6 mg Mn/kg fodder per day decreased Glu levels (Lipe et al. 1999). Hence, the single low dose injection of $MnCl_2$ might not have been sufficient to increase/decrease Glu concentrations effectively or the time between injection and sacrifice was too short to be able to observe such changes. The exact Glu-mediated neurotoxicity seems to be versatile as both, apoptotic as well as necrotic cell death was observed. The underlying pathways include various molecular players such as cysteine proteases, mitochondrial endonucleases, peroxynitrite, PARP-1 and GAPDH. For Mn-mediated disruption of Glu and glutamine transport, the mechanism implicates caspase-3 and PKCδ inhibition (Nissen-Meyer and Chaudhry 2013). Moreover, excessive Glu release from astrocytes might also be reasoned by NO causing excitotoxic death of

neurons. An increase in NO production in turn was shown in astrocytes after Mn treatment (X. Liu 2006; Spranger et al. 1998).

B.1.3   AchE activity in brain

With AchE being one crucial enzyme for maintaining an anti-oxidative milieu, it´s activity under the impact of Mn was of great interest. For determination, a commercial available assay kit was applied at the aqueous brain extracts.

Feeding study:

As illustrated in Figure 20A, AchE activity was significantly increased by 9% in Mn-fed rats compared to controls (896 mU/ml and 979 mU/ml per g brain respectively, p=0.026). The correlation of AchE activity with Mn concentrations in brain extracts revealed a highly significant correlation curve (y=-0.1352x^2+39.09-1797.3, R^2=0.7083, p=1.22E-5). Interestingly, the progression of the correlation indicated a saturation curve with increasing Mn concentrations in brain extracts as illustrated in Figure 20B.
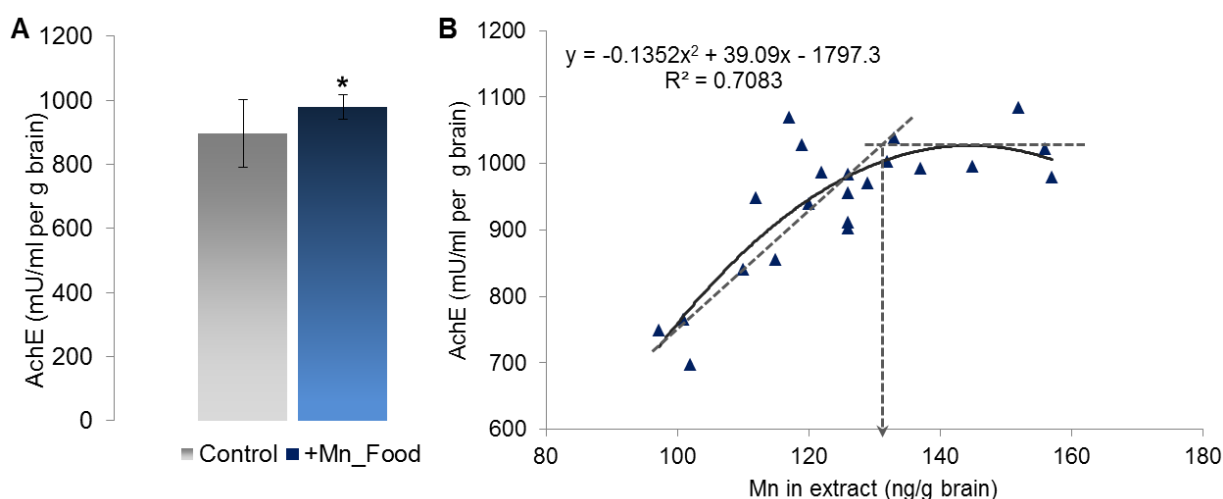
Figure 20 AchE activity in the feeding study.
A: AchE activity was significantly increased by 9% in test (Mn-fed) rats (p=0.026, N=12 extracts per group)
B: Correlation of AchE activity with Mn concentrations in brain extracts revealed a regression line indicating a saturation curve (R^2=0.7083, p=1.22E-5, N=22 extracts, 11 per group)

Injection study:

Due to *i.v.* injection of MnCl$_2$, AchE activity was significantly increased by 15% in +Mn_Inj rats compared to control rats (1054 mU/ml and 919 mU/ml per g brain respectively, p=0.033) as shown in Figure 21A. Correlation of AchE activity with Mn concentrations in brain extracts also revealed a similar shape of correlation curve, which tended towards a decrease at very high Mn concentrations, as shown in Figure 21B. The correlation was not as strong as in the feeding study, but also significant (y=-0.0298x^2+10.961+67.602, R^2=0.2967, p=0.007).
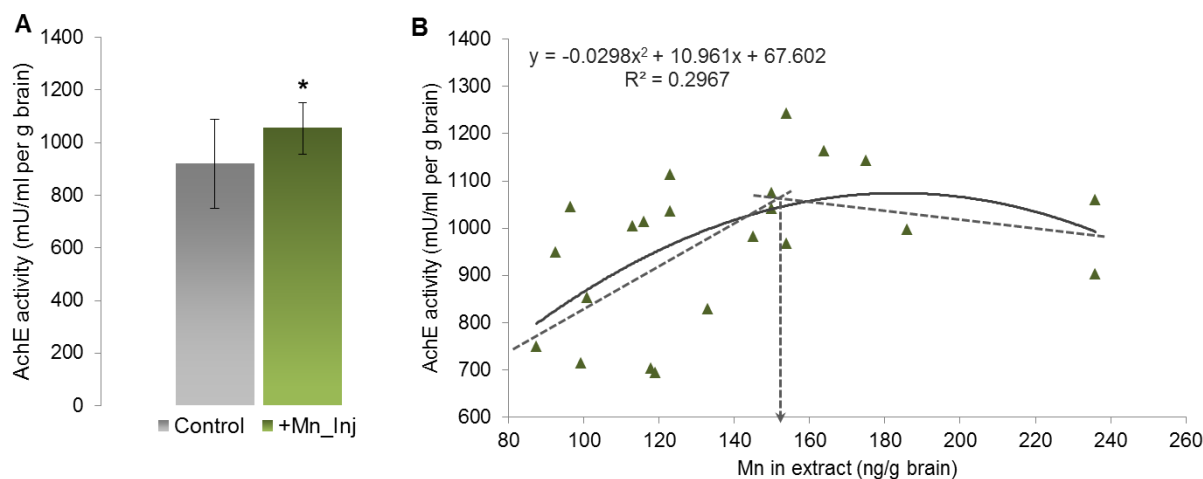
Figure 21 AchE activity in the injection study.
A: AchE activity was significantly increased by 15% in Mn-injected animals compared with control (p=0.033; N=12 extracts per group).
B: correlation of AchE activity with Mn concentrations in brain extracts was weak and tended towards a decrease from at high Mn concentrations (R^2=0.355, p>0.05; N=22 extracts, 11 per group).

The main function of AchE is the hydrolysis of acetylcholine in the periphery and the nervous system, being expressed in cholinergic neurons as well as neuromuscular junctions (Touitou et al. 1986). Beside this, AchE exhibits non-cholinergic functions, where it is accountable for cell adhesion, neurite formation, axonal outgrowth neuronal migration and synaptogenesis (Antonini et al. 2006; M. Aschner 2000).

The effect of Mn on AchE activity and protein levels of AchE was focus of recent studies. Daily *i.p.* injections of 6 mg Mn/kg b.w. in rats for 20 days increased AchE activity significantly compared to control animals (Lebda et al. 2012). This was also the case for daily injections of 50 mg Mn/kg b.w. for one week (Liapi et al. 2008). Moreover, male wistar rats receiving 20 mg Mn/ml drinking water for one month had increased AchE activity as well as AchE protein expression in cerebellum (Y. Chtourou et al. 2012). Interestingly, this was accompanied by an increase in inducible nitric oxide synthase (iNOS) as well as NO. Controversial to those more or less short term exposures, chronic exposure to Mn via drinking water in rats (10 mg/ml for eight months (Martinez and Bonilla 1981) and 1 mg/ml for two years (Lai et al. 1981)) resulted in decreased AchE activity. Herein, the increase in AchE activity compared to control levels was slightly stronger after the single injection of $MnCl_2$ compared with the chronic feeding for almost two months (15% compared to 9%). Based on the observed parallel increase of iNOS mentioned above, AchE activity might be increased due to oxidative stress in the first instance with increased Mn concentrations. However, in both studies, the correlation of AchE activity with respective Mn concentrations in the applied brain extracts revealed a plateau from which on AchE activity seemed to be stagnant. In the feeding study this plateau was found at Mn concentrations of around 130 ng/g brain (in the brain extract)

whereas in the injection study that value was slightly higher at around 150 ng/g brain. This could mean that AchE activity during Mn exposure is not only dependent on duration of exposure but maybe also on the effective concentration of Mn reaching the brain.

The stagnation or even decline of AchE activity as observed herein could be seen as neuronal response to increasing oxidative stress in the brain tissue due to increasing Mn concentrations. Interestingly, an inhibition of AchE showed neuroprotective effects in a neonatal rat model of oxygen toxicity. Inhibitors of AchE reduced its hyperoxia-triggered activity, neural cell death and pro-inflammatory cytokine up-regulation as well increased the reduced/oxidized GSH ratio (Foradori et al. 1967). Moreover, AchE was linked to activation of dopaminergic neurons leading to a release of dopamine from dendrites in the substantia nigra as well as from neurons in midbrain (Apostoli et al. 2000). The observed loss of dopamine during Mn-induced brain injury, hence, might be dependent on the activity of AchE. Latter seems to be tightly regulated dependent on the concentration of Mn rather than exposure conditions. A possible interplay of Mn concentrations, AchE activity and dopamine excretion is illustrated in Figure 22. To prove these dependencies, further studies with different applied concentrations of Mn would be required with parallel determination of Mn concentrations, AchE activity and dopamine levels in the brain tissue.
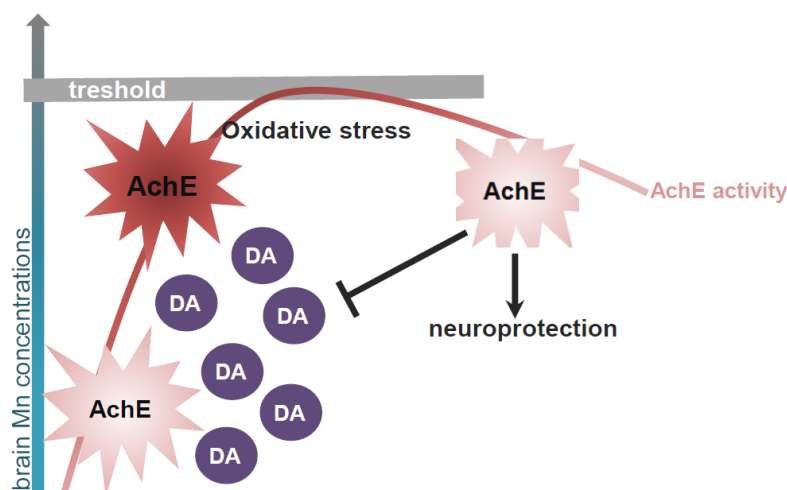
Figure 22 Possible effect mechanism of Mn on AchE activity.
AchE shows normal activity with normal Mn concentrations activating neurons to release dopamine (DA). Activity increases with imbalanced Mn concentrations in brain leading to/due to oxidative stress. From a certain Mn threshold on, AchE is stagnating and may even be decreasing resulting in reduced DA release and activation of neuroprotective mechanisms.

B.1.4   Fe(II)/(III) concentrations in brain

In terms of Mn-induced oxidative stress in brain tissue, the neural Fe(II)/(III) ratio was of interest in this work. An imbalance in the two oxidative Fe states is discussed to prompt neuroinflammation by oxidative stress. For this, aqueous rat brain extracts were prepared from frozen brain and analyzed by IC-ICP-OES as described in chapter *D.6*.

B.1.4.1 General considerations regarding the IC-ICP-OES method

Colorimetric assays are conventionally applied for assessment of total Fe or ferrous Fe (Fe(II)) in geological or biological samples. The two most famous ones are the so-called ferrozine and phenanthroline methods. In the ferrozine assay, Fe(II) has to be extracted with ammonium oxalate or HCl to form a violet complex with ferrozine showing absorption at 560 nm (Stookey 1970). The phenanthroline assay includes masking of Fe(III) with an agent (e.g. phosphate), while the remaining Fe(II) forms an orange complex with 1,10-phenanthroline comprising an absorption at 508 nm (Fortune and Mellon 1938). Besides the drawback of high time-consumption by these assays due to the multi-step procedures, some other possible problems have to be considered, which can contribute to disturbances of measurement: extraction by HCl can oxidize Fe(II) to Fe(III); metabolic products can form strong complexes with both Fe species, which might be dissolved by phenanthroline but not by ferrozine (S. W. Taylor et al. 1994); high concentrations of sulfide in the sample can affect ferrozine complexes (Chapin et al. 2002). Overall for determination of Fe(II) an overestimation of concentrations was found for both assays due to decreasing reliability of both assays with decreasing concentrations (Braunschweig et al. 2012).

A possibility for determination of Fe(II) and Fe(III) simultaneously in biological samples is the application of ion chromatography with post-column reaction with PAR ([4-(2-pyridylazo)resorcinol]) and subsequent detection by UV. The metal-PAR complexes elute at different times and their absorbance can be determined at a certain wavelength. However, full complexation of PAR with Fe is required for quantitative analysis and sensitivity of UV detection might not be sufficient in some applications. Herein, after separation of Fe(II) and Fe(III) in rat brain extracts by ion chromatography, the detection method of choice was ICP-OES. Compared with the other mentioned ways for determination of Fe(II) and Fe(III), ICP-OES is advantageous with respect to sensitivity. Moreover, being an element selective detector, no post-column reaction with PAR was needed. A further prerequisite to the simultaneous determination of Fe(II) and Fe(III) was the comparable low analysis time of around 5 minutes.

B.1.4.2 LoD and Recoveries

Retention times of Fe(II) and Fe(III) were verified by the respective standard solutions (Fe(II)Cl$_2$ and Fe(III)citrate) and potent carryover was monitored during analysis. For determination of LoD, peak intensities of measured standard solutions were compared with blank intensities. The LoDs were calculated according to the 3σ criteria and were obtained to be 6.33 µg/l for Fe(III) and 9.11 µg/l for Fe(II), which was in good accordance to the concentrations measured in the brain extracts (range Fe(II): 368.8-822.5 µg/L, range Fe(III): 122.2-470.0 µg/L). Compared with an UV detection method, where the absorption of a Fe(III)-quercetin complex was measured in Fe(II) samples, the LoD for Fe(III) was 60 µg/l (Balcerzak et al. 2008). This seems suitable for samples with high concentrations but also shows the advantage of ICP-OES detection with LoD for Fe(III) herein being lower by a factor of 10 compared to the mentioned method. ICP-MS detection might also have been applicable, but the LoDs in ICP-OES were significant and operation is simpler, less prone for interferences in Fe and also cheaper. For calculation of recoveries, peak areas of standard solutions were compared with peak areas of samples. The recovery obtained for Fe(III) was 43-66% while it was 83-105% for Fe(II). The comparable low recovery for Fe(III) might be due to the problems with the Fe(III)citrate standard. As described in Experimental procedure, these standards solutions had to be added with a small amount of HNO$_3$ to verify full decomplexation of Fe(III) from the citrate complex. The resulting pH in the standard solution therefore differed from the physiological one found in the brain extracts. Nevertheless, the good recovery for Fe(II) proofed the method to be appropriate.

The finally applied method IC-ICP-OES method revealed a Fe(III) peak at around 1 minute elution time and a Fe(II) peak at around 5 minutes elution time (described in chapter *D.6.2*). The comparison of a control and a +Mn_Food brain extract are shown by the chromatograms in Figure 23.
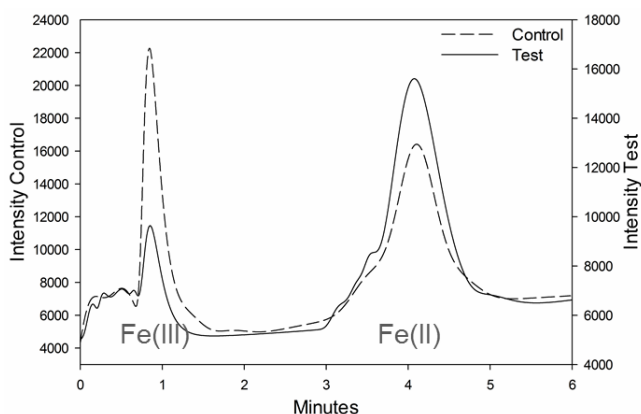
Figure 23 Example of chromatograms of a control and a +Mn_Food brain extracts by ICP-ICP-OES for Fe(II)/(III) determination.

B.1.4.3 Analysis of brain extracts

B.1.4.3.1 Determination of Fe(II)/Fe(III) in brain extracts from the feeding study

Obtained peak areas in IC-ICP-OES were compared with standard measurements prior each analysis of samples and respective concentrations of Fe(II) and Fe(III) were calculated. Analysis of brain extracts revealed significantly higher concentrations of Fe(II) both in control and Mn-fed samples compared to Fe(III) concentrations (Fe(II) vs. Fe(III): Control: 4.47 vs. 2.13 µg/g brain, $p<0.001$; +Mn_Food: 3.08 vs. 0.63 µg/g brain, $p<0.001$). Due to lower total Fe concentrations in the brain of Mn-fed rats, results are shown in percent in Figure 24 for better comparability. A significant increase of Fe(II) in +Mn_Food rat brain extracts was observed compared to control rats (70% in control vs. 83% in +Mn_Food samples, $p<0.05$), accompanied by a significant decrease of Fe(III) in +Mn_Food samples (30% in control and 17% in +Mn_Food samples, $p<0.05$).
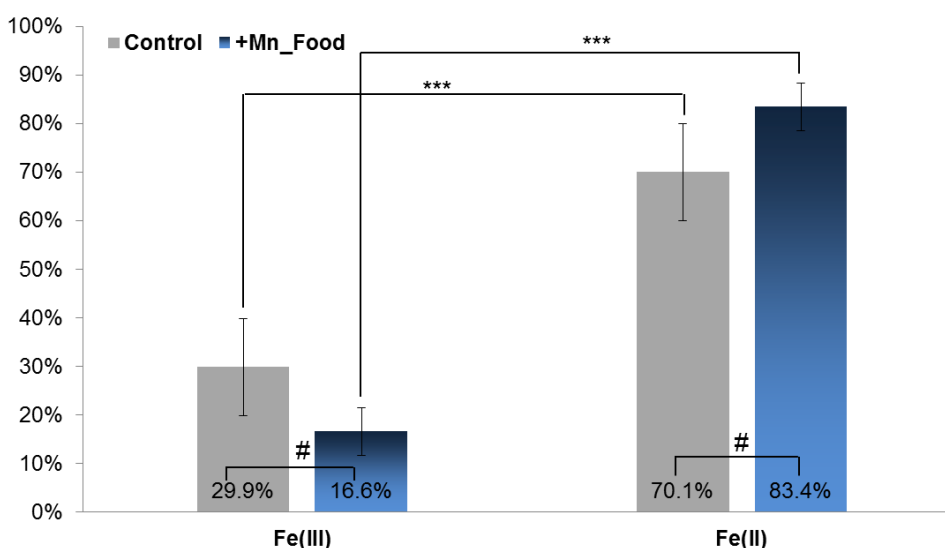
Figure 24 Determination of Fe(II)/(III) in the feeding study.
Fe(II) was significantly elevated both in control and +Mn_Food brain extracts (***p<0.001). Fe(II) in +Mn_Food samples was significantly higher (83.44 vs 70.09%, #p<0.05) and Fe(III) significantly lower (16.56 vs 29.91%, #p<0.05) compared to control samples indicating a shift towards an increased Fe(II)/(III) ratio (N=12 extracts per group, mean±SD).

The respective concentrations of Fe(II) and Fe(III) in brain extracts in µg/l were calculated and correlated to Mn concentrations in brain extracts. The results for linear correlation of control samples is shown Figure 25A and respectively for +Mn_Food samples in Figure 25B. In both cases, Fe(II) and Fe(III) showed a positive linear correlation with Mn concentrations in brain extracts. However, Fe(II) correlation was in both cases stronger – expressed by a higher R^2 – and it was also significant, which was not true for correlation of Fe(III). These results show that after chronic Mn-feeding, Fe(II) increases with accelerating Mn concentrations in brain.
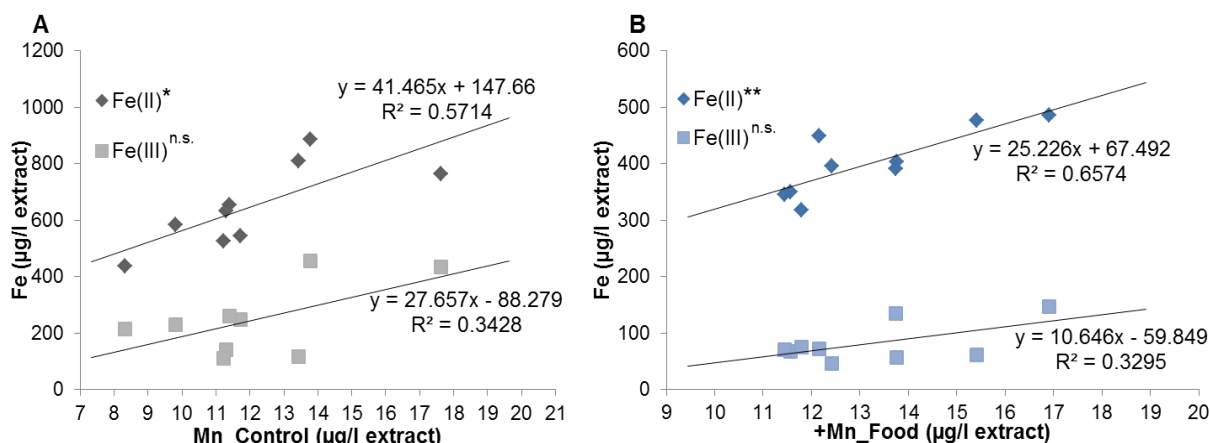
Figure 25 Correlation of Fe(II) and Fe(III) with Mn concentrations in the feeding study.
A: Correlation of Fe(II) and Fe(III) concentrations with Mn concentrations in brain extracts of control samples revealed a linear positive correlation. Correlation of Fe(II) was stronger (R^2=0.5714 vs. R^2=0.3428) and significant (*p<0.05).
B: Correlation of Fe(II) and Fe(III) concentrations with Mn concentrations in brain extracts of +Mn_Food samples revealed a linear positive correlation. Correlation of Fe(II) was stronger (R^2=0.6574 vs. R^2=0.3295) and significant (**p<0.01).

B.1.4.3.2 Determination of Fe(II)/Fe(III) in brain extracts from the injection study

After the single injection of $MnCl_2$, the majority of neural Fe was present as Fe(III) (90% and 91% in control and +Mn_Inj, respectively). Fe(III) was significantly higher than Fe(II) concentrations both, in control and +Mn_Inj samples (p<0.001) as shown in Figure 26. Overall, no increase or decrease in one or the other Fe species between control and Mn-injected brain samples could be observed.
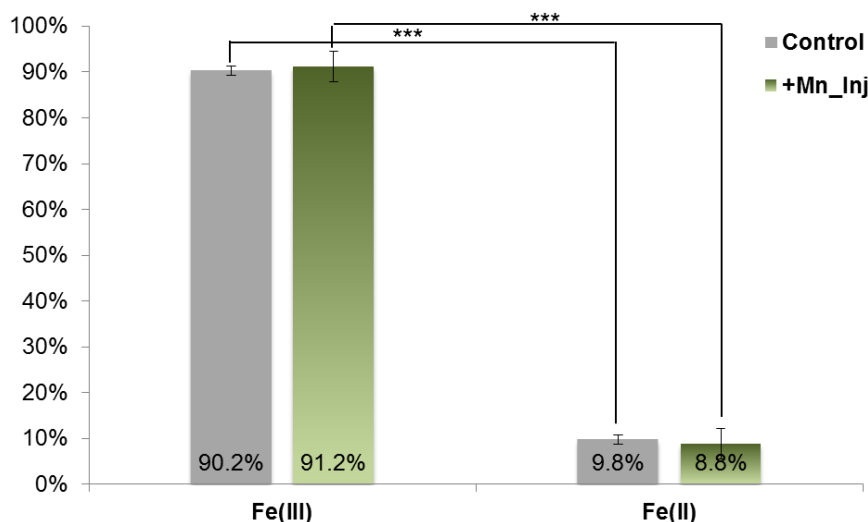
Figure 26 Determination of Fe(II)/(III) in the injection study.
Fe(III) was significantly increased in both, control and +Mn_Inj samples with around 90% (***p<0.001). No difference in Fe(II) or Fe(III) between control and Mn-exposed animals could be observed (N=12 extracts per group, mean±SD).

Figure 27A illustrates the correlation of Fe(II) in control and +Mn_Inj as well as Fe(III) in control and +Mn_Inj separately. Interestingly, Fe(III) in control samples showed a linear positive correlation, which was not given in +Mn_Inj samples anymore (R^2=0.375 in control and R^2=0.0002 in +Mn_Inj, respectively), while both correlations were not significantly. In contrast, Fe(II) in +Mn_Inj samples showed a significant linear correlation with Mn concentrations, which was not given for control samples (R^2=0.4901, p<0.05 and R^2=0.0219). Interestingly, this illustration indicated a switching point at around 13 µg Mn/l extract (~120 ng Mn/g brain in extract), where correlation behavior changed (black arrow in Figure 27A). Correlation of compiled concentrations for Fe(II) and Fe(III) independently from control or treated group with Mn concentrations is shown in Figure 27B. In the average, Fe(II) showed a significant positive linear correlation with increasing Mn concentrations in brain extracts (R^2=0.4488, p<0.01). On the other hand, Fe(III) correlation was also significant (R^2=0.5873, p<0.05), and the shape of the trendline indicated an increase in Fe(III) with increasing Mn concentrations up to a certain Mn concentration from which on Fe(III) seemed to decline. Without the intention of any over interpretation of data, these results bare some interesting observations, which again suggest an increase in Fe(II) with increasing Mn concentrations although the difference in total Fe(II) between control and +Mn_Inj samples was not given.
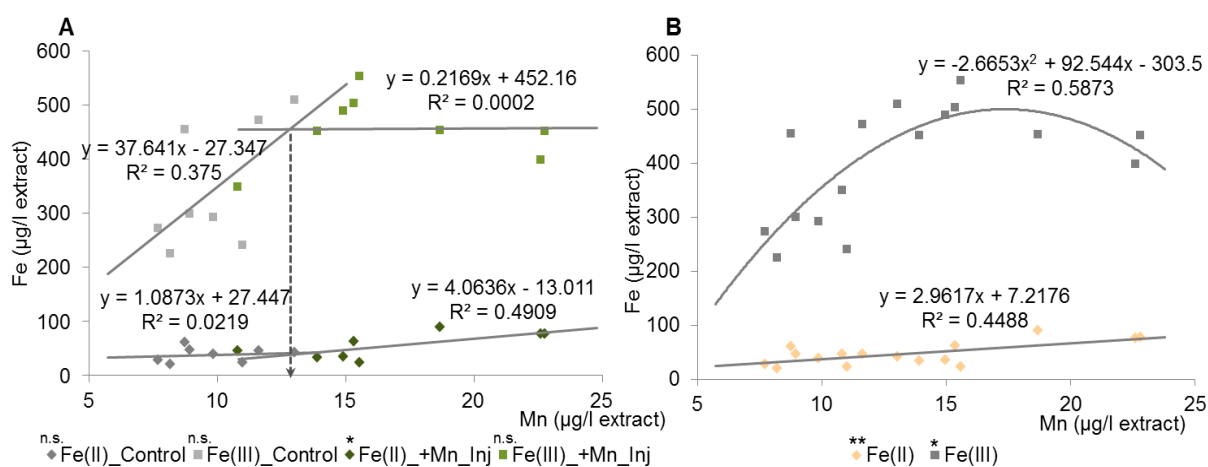
Figure 27 Correlation of Fe(II) and Fe(III) with Mn concentrations in the injection study.
*A: Correlation of Fe(III) in control and +Mn_Inj brain extracts with Mn concentrations in brain extracts independently from each other showed a positive linear correlation in control samples which was not given any more in +Mn_Inj samples at higher Mn concentrations (both not significant (n.s.)). Correlation of Fe(II) showed no correlation in control samples but a positive linear and significant correlation (*p<0.05) with increasing Mn concentrations in +Mn_Inj samples. Interestingly, that kind of correlation implied a switching point at a certain Mn concentration (~13 µg/l).*
*B: Taking all samples together for correlation (control and +Mn_Inj) showed a significant linear correlation of Fe(II) with increasing Mn concentrations (**p<0.01). Correlation of Fe(III) with Mn concentrations (*p<0.05) indicated an increase in Fe(III) up to a certain Mn concentration and a decrease from this concentration on (accompanied by an increase in Fe(II)).*

Correlation itself only led to plausible results by correlation of Fe(II) or Fe(III) in µg/l extract. Transforming the data on total concentrations in brain (ng/g) did not show any reliable correlation behavior. This shows the importance of suitable extraction procedures in speciation analysis. Moreover, the existing concentrations of Fe(II)/(III) species in the extracts might not be so easily translated to total brain concentrations. The same effects were also described for correlation of glutamate concentrations with Mn concentrations in total brain (chapter *B.1.2*).

When comparing the results from the feeding with the injection study, it is notable that under both exposure conditions Fe(II) concentrations in brain seemed to increase with increasing Mn concentrations substantiated by significant correlations as well as comparative good R^2 values. Due to chronic feeding, Fe(III) concentrations were also positively correlated with Mn concentrations, but correlations were weaker. Controversy in the injection study, Fe(III) first increased with accelerating Mn concentrations but tended to decline with even higher Mn above a certain concentration (switching point at around 13 µg Mn/l extract ≙ 120 ng Mn/g total brain). However, referring to total concentrations of Fe(II) and Fe(III) in brain extracts, a significant shift towards Fe(II) could only be observed in the feeding study whereas no difference was observed in the injection study. These results lead to some presumptions: (i) a short intervention of Mn as imitated in the injection study may not be sufficient to change the neuronal Fe(II)/(III) ratio; (ii) this shift might have occurred at a later time point of measurement (longer than four days after injection) over all as the correlation study revealed tendencies for changes primary towards Fe(III); (iii) prolonged increased feeding of Mn could lead to the shift towards Fe(II) in brain tissue; (iv) this shift towards Fe(II) as observed in the feeding study might not solely be based on Mn intake but even prompted by the decrease in total Fe in Mn-substituted rats. In many ways, all of the mentioned points could be conceivable. A definite statement is not possible under the given experimental conditions, but overall it seems as if a change in the Fe(II)/(III) ratio requires a certain concentrations of Mn which is acting on the body or brain. A prolonged acting might in the end prompt this shift to a greater extend second to a Mn-induced shift in total neural Fe. As discussed above, this decrease in total Fe in the brain has been described during studies of Mn exposure before. However, determination of Fe(II) and Fe(III) has to our knowledge not been carried out in Mn exposure models yet. Hence, the mentioned suggestions lack in comparison to other studies, but the findings herein can contribute to a better understanding of Mn-induced neurodegenerative mechanisms. After all, Fe concentrations and the effect of high Fe(II) were described in other studies of neural diseases, within which frame the results obtained herein can be discussed.

Acute brain injuries such as ischemia are known to induce release of Fe from mitochondrial heme into neurons by degradation of heme. In more detail, this degradation prompts the release of Fe(II), which might then accelerate neuronal damage by formation of hydroxyl radicals, which are neutralized under physiological conditions by SOD or GPx (Moos and Morgan 2004). In the case of ischemia, it was shown that the inhibition of detoxifying enzymes such as SOD or GPx prevented the oxidation of Fe(II) to Fe(III), leading to an increase in Fe(II) concentrations. Free Fe(II) can then accumulate in neural tissue and induce the highly reactive Fenton reaction (eq. 1)):

$$Fe(II) + H_2O_2 \rightleftharpoons FeOH^{2+} + {}^{\bullet}OH \qquad (eq. 1)$$
$$Fe(III) + {}^{\bullet}O_2^- \rightleftharpoons Fe(II) + O_2 \qquad (eq. 2)$$
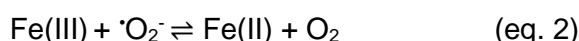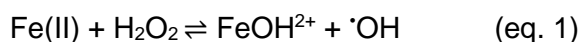
All in all this describes a vicious cycle as more than one factor might contribute to the activation of the Fenton reaction: on the one hand Mn-induced increase of Fe(II) concentrations as observed in the chronic feeding study can react with H_2O_2 according to (eq. 1) producing ${}^{\bullet}OH$, which belongs to the group of ROS. On the other hand, possible Mn-induced inhibition of SOD can increase highly toxic ${}^{\bullet}O_2^-$ (Yassine Chtourou et al. 2011), which might further reduce Fe(III) according to (eq. 2) producing even more Fe(II). Therefore, increased Mn can contribute via several ways to increased Fe(II) concentrations and the harmful outcome of it. In this context, a PD model in monkeys is of interest (Goto et al. 1996), where Fe-containing microglia infiltrated the substantia nigra accompanied by a disappearance of dopaminergic neurons. The destruction of dopaminergic neurons is also described as major mechanism during Mn-exposure. Moreover, no ferritin is found in neurons of substantia nigra in PD but the vicinity of dopaminergic neurons was rich in ferritin-containing microglia (Mirza et al. 2000). Interestingly, in acute brain injuries Fe is released from ferritin in microglia and oligodendrocytes (Moos and Morgan 2004). A local accumulation of highly reactive Fe(II) in specific cell types of substantia nigra is conceivable as transport by ferritin or heme might be disturbed. Such mechanisms might also be occurring during Mn-induced neuroinflammation due to the molecular similarities between PD and manganism. In the pathogenesis of PD, the accumulation of divalent metal ions such as Fe^{2+} or Cu^{2+} in neuromelanin granula of the substantia nigra is discussed (Sadrzadeh and Saffari 2004). The formation of radicals in these structures is described for increased concentrations of Fe or Cu during neurodegenerative diseases. In the case of Mn-(over)exposure, an interaction of increased Mn concentrations with lowered total Fe but increased Fe(II) in the substantia nigra could prompt such neurotoxic reactions.

There is still debate whether Fe is increased or decreased in neurodegenerative diseases such as PD (Moos and Morgan 2004; Salvador 2010), which is also the case for Mn-induced neurodegeneration (see chapter B.1.1). Knowledge about the existing Fe-species together

with determination of Mn concentrations might therefore help to understand the proceeding of neuroinflammation with regard to oxidative stress induced by the interplay of Fe(II) and Mn e.g. in substantia nigra by the Fenton reaction.

B.1.5   Conclusion

This chapter was intended to answer various questions in a comparative manner of the single $MnCl_2$ injection as well as the chronic low-dose feeding of Mn in rats. The following lines serve as conclusion for above discussed findings.

➢ *Does the applied Mn exposure affect concentrations of Fe, Cu and Zn in serum or brain? (B.1.1)*

The observations on Mn affecting metal balances of Fe, Cu and Zn in serum and brain herein showed accordance with the majority of discussed literature. It seems as if inducement of imbalances of these essential metals in brain requires repeated or chronic exposure to Mn. If so, Fe concentrations will be decreased while Cu levels will be increased in brain. Studies from literature also found decreased Zn levels while no alteration of Zn was found herein. The alterations of Fe, Cu and Zn were concordant with measurement of these elements in CSF of PD patients, underlining the similarity of Mn-induced neurodegeneration with the one in PD. In serum, besides the effect on Fe and Cu, also Zn was decreased in both applied Mn exposure conditions. Interestingly, after the single injection of $MnCl_2$ some alterations in serum were observed: Fe (not significant), Cu and Zn seemed to be decreased while Cu was highly increased in the feeding study. Therefore, alterations in blood elemental levels might occur already shortly after Mn intervention whereas for changes in brain, longer lasting impact is needed. With respect to different findings for Cu in serum, the concentration at a later time point of measurement after injection would have been interesting to find out if such changes might emerge later on or if elemental concentrations might have already been balanced again due to clearance of Mn from the body.

➢ *Are there changes in glutamate concentrations in brain due to the applied Mn exposure? (B.1.2)*

Changes on glutamate concentrations in the brain were only observed after chronic feeding of Mn. The increase in neural glutamate was also positively correlated with increasing Mn concentrations in the brain. No correlation was found with Mn concentrations in serum what can be explained by very similar concentrations of Mn in serum between control and Mn-fed rats. An increase in glutamate is related to excitotoxicity including production of NO, what connects Mn-induced neurotoxicity also to NO-mediated mechanisms. Moreover, a single

injection of Mn might not be sufficient to alter glutamate concentrations in the brain – however, changes might have been detectable at a later time point of measurement after injection.

> *Is AchE activity influenced by Mn? (B.1.3)*

AchE activity was increased in both feeding and injection study, while this increase was slightly higher in the latter. Correlation of AchE activity with brain Mn concentrations showed in both cases a saturation line with a plateau from a certain Mn concentrations on. A deactivation of AchE activity with even higher increasing concentrations of Mn might be possible. Therefore, a first increase of Mn could activate AchE due to or trigger oxidative stress in neural tissue while a lasting Mn exposure might lead to an inactivation for reasons of neuroprotection. An inactive AchE is further known to inhibit DA release from neurons, eventually contributing to the observed DA reduction in Mn exposure.

> *Are there changes in the Fe(II)/(III) ratio in brain due to Mn exposure? (B.1.4)*

The herein applied method for separation of Fe(II) and Fe(III) by IC-ICP-OES was advantageous with respect to simplicity, short analysis time as well as good LoDs. It was also the first time that Fe(II)/(III) was determined in a Mn exposure study enlarging the knowledge of mechanisms leading to oxidative stress and neurodegeneration in manganism or Mn exposure scenarios. Chronic feeding of Mn led to a significant increase of the Fe(II)/(III) ratio in brain showing stronger correlation of Fe(II) with increasing Mn concentrations than Fe(III). Although the majority of Fe was present as Fe(III) both in control as well as in the Mn injected rats, some interesting observations in the correlation study could be made. A kind of switching point was revealed from which Mn concentration on (~120-140 ng/g in brain extract) Fe(II) was positively correlated and Fe(III) not any more, while Fe(III) also tended to decrease. Therefore, a shift in Fe(II)/(III) ratio might depend on total Mn concentrations in brain where a dramatic effect could be observed in chronic exposure to Mn. Increases in Fe(II) can promote activation of the Fenton reaction leading to production of ROS. These can in turn contribute to Mn-induced neural inflammation, and can reduce Fe(III) by production of Fe(II).

B.2   Characterization of Mn-species in brain by SEC-ICP-MS

The characterization of Mn-species in brain under Mn-exposure was one major task of this work. As it was shown that total Mn concentrations in brain were increased in similar manner in both exposure studies, possible binding partners of Mn in the brain were of interest. For aqueous extraction of these inherently labile species from the brain tissue, a specific extraction protocol was applied, which was established for this task in the laboratory of Prof. Michalke (Helmholtz Zentrum München, Neuherberg, Germany).

B.2.1   Column mass calibration

For separation of Mn-species, two SEC columns were combined in line. A Biobasic SEC300 with an exclusion limit of 700 kDa was applied for separation of HMM molecules and a Peek column body filled with TSK HW40S with an exclusion limit of 10 kDa for separation of LMM compounds. For column mass calibration, following standards were applied: alpha-2-macroglobulin (725 kDa), ferritin (440 kDa), γ-globulin (190 kDa), arginase (107 kDa), transferrin (Tf, 78 kDa), human serum albumin (HSA, 66 kDa), glutamine synthetase (42 kDa), oxidized glutathione (GSSG, 612 Da), reduced glutathione (GSH, 307 Da), L-Cystine (120 Da), citrate (192 Da), L-glutamic acid (147 Da) and inorganic Mn (55 Da). In matching with UV signals, retention times for the respective standards were recorded and ln MW (kDa) was plotted against those. The obtained linear equations describing the first column was *ln MW = -0.5775 * RT + 14.865* for compounds eluting before 20 minutes and for the second column *ln MW = -0.2414 * RT + 3.8975* for compounds eluting after 20 minutes. Standards with respective MW and retention times are listed in Table 8.

Standard	MW (kDa)	RT (min)	ln MW (kDa)
α-2-Macroglobulin	725	14.2	6.5862
Ferritin	440	15.2	6.0868
γ-Globulin	190	15.9	5.2470
Arginase	107	16.8	4.6728
Tf	78	17.2	4.3567
HSA	66	18.3	4.1897
Glutamine synthetase	42	19.5	3.7376
GSSG	0.612	20	-0.4780
GSH	0.307	20.5	-1.1809
Citrate	0.192	22	-1.6503
L-Glutamic acid	0.147	25	-1.9173
L-Cysteine	0.120	26	-2.1203
Mn	0.055	28	-2.9004

Table 8   Column mass calibration for analysis of aqueous brain extracts by SEC-ICP-MS.

B.2.2   Assignment of peaks in aqueous brain extracts

According to analysis of standards, separation of Mn-species was satisfactory. As an example, Figure 28 shows the native chromatogram of a brain extract from the feeding study (green line). Superposed (grey line) is the chromatogram of this brain extract spiked with a solution of Mn-citrate and Mn-Tf. With this, retention times of Tf and citrate as well as inorganic Mn were checked, which showed an increase in intensities compared to the other peaks, which were reduced in intensity due to dilution effect of standard solution addition. With the use of PeakFit™ software, chromatograms of analyzed brain extracts were aligned. The final peak assignment resulted in six size fractions (Table 9) referring to the size classification of Mn-species characterization in serum. Also here, the named compounds are only possible binding partners of Mn based on retention time of the applied standards and based on knowledge from literature. Of course, other Mn-binding compounds might have eluted at the same time frame as SEC only allows setting of eluting fractions. Moreover, the separation was satisfactory due to the clear separation of the citrate peak, which was supposed to play an important role in Mn-transportation in the brain after exposure.
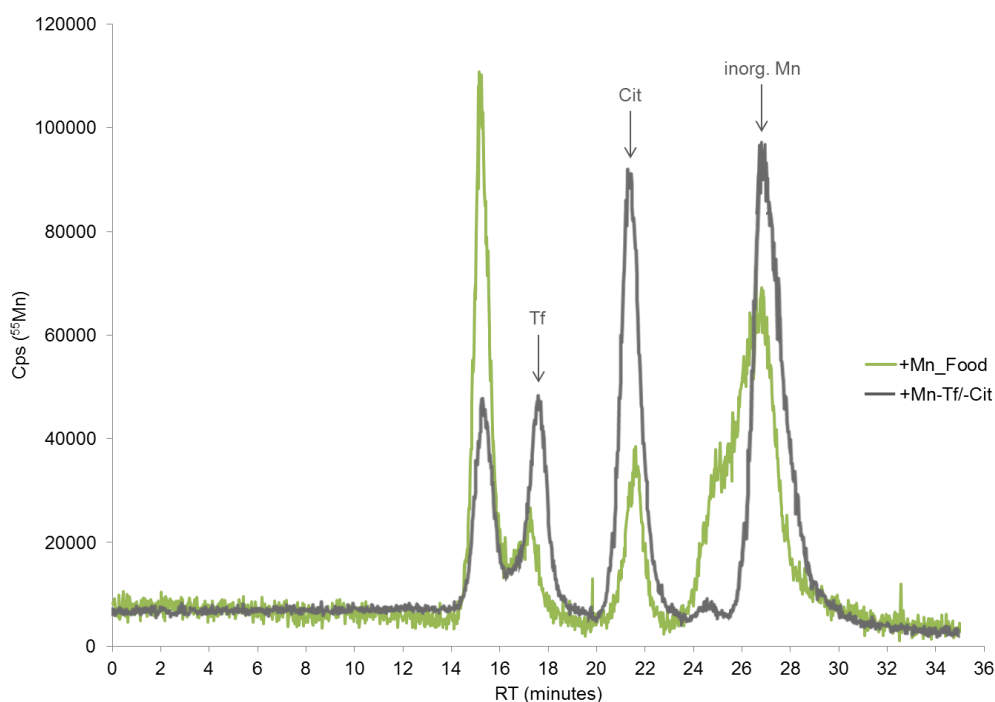
Figure 28 Example of a chromatogram of a brain extract from the feeding study (green line).
The extract was spiked with a solution of Mn-Tf and Mn-citrate and analyzed again (grey line). With this, retention times of Tf, citrate and inorganic Mn were tested within the matrix of the aqueous extracts.

	SEC-fraction	Size	Assignment
HMMs	fraction A	650-400 kDa	α-2-macroglobulin
(High molecular	fraction B	400-200 kDa	γ-globulin
masses)	fraction C	200-70 kDa	transferrin
LMMs	fraction D	350-150 Da	Mn-citrate
(Low molecular	fraction E	150-60 Da	amino acids
masses)	fraction F	<60 Da	inorganic Mn

Table 9   Assignment of SEC fractions for characterization of Mn-species in aqueous brain extracts. For better comparability with serum size fractions, the labelling with fractions A-F corresponds to the same assignment as in serum Mn-speciation.

B.2.3   Analysis of brain extracts

For characterization of Mn-species in rat brain, aqueous extracts were prepared and stored at -80°C until analysis. The amount of brain extracts to be analyzed at one day was allowed to thaw at 4°C overnight. Aqueous brain extracts from both exposure studies (feeding and injection) were applied undiluted at the above described column combination in random order. One major indicator for column pollution was an increase of the first HMM peak, which was observed with increasing numbers of analyzed brain extracts. Therefore, not more than six samples were analyzed per day with a cleaning step (100% eluent B for 10 minutes) in between. Columns were further cleaned overnight as described in chapter *D.7.2*.

B.2.3.1 Characterization of brain Mn-species from the feeding study

After feeding of animals for 53 days, brains were taken at time point of sacrifice and immediately deep frozen in liquid nitrogen. Brain extracts were prepared the after next day and stored at -80°C until analysis. The obtained peak areas in percentage obtained by SEC-ICP-MS were transferred into concentration of Mn (ng/g brain) for each size fraction according to the total Mn concentrations in the respective brain extracts. The results for concentrations of Mn bound to the diverse carriers in the brain are shown in Figure 29. As the comparison of brain extracts from control with Mn-fed rats by the student t-test revealed, SEC fraction A and B were significantly decreased due to Mn-feeding (0.4-fold, $p<0.001$ and 0.8-fold, $p<0.01$, respectively). For Mn concentrations of fraction C no differences between control and Mn-exposed rats were observed. On the other hand LMM SEC fractions D and E were increased in the brain extracts of Mn-fed rats compared with control (1.6-fold, $p<0.001$ and 1.7-fold, $p<0.001$, respectively). Also inorganic Mn (fraction F) was increased in the aqueous brain extracts due to feeding of Mn (1.7-fold, $p<0.001$). The results indicated that consequently to chronic low-dose feeding of Mn, changes in Mn-carrying molecules in the brain occurred. These changes included a reduction in HMM molecules like α-2-Macroglobulin or γ-globulines and an increase in LMM compounds like citrate or amino acids. Also free inor-

ganic Mn seemed to be increased after this feeding procedure. Interestingly, the importance of Tf as Mn-carrier in the brain seemed not as prominent as concentrations were similar in control and Mn-exposed rat brain extracts.
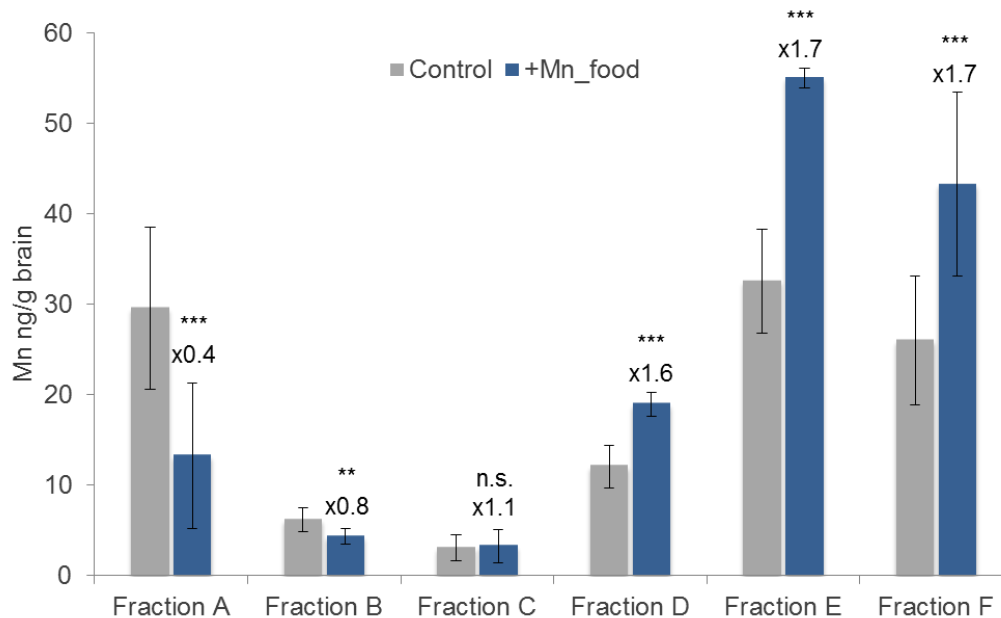
Figure 29 Characterization of Mn-species in the brain of the feeding study.
Fractions A and B were significantly decreased in Mn-fed rats compared to LMM fractions D and E and also inorganic Mn, which were significantly increased in Mn-exposed rats. Fraction C showed no difference between both groups. (Student t-test, *p<0.05, **p<0.01, ***p<0.001).

Following the elaboration methods from Mn-speciation in serum, the results from the Mn-speciation in the brain were further analyzed by another statistical method. After log transformation of the data, a two-way ANOVA was applied. In general, this method has more strength than a t-test. The t-test only includes analysis of the influence of one factor whereas by a two-way ANOVA the interaction of two factors is considered. In the case herein, these two factors comprise the interaction effect of group (control and Mn-fed) with the SEC fraction (A-F). The respective p-values from this analysis are shown *Appendix* in Table 26. The only SEC fraction, which revealed to be significantly between control and Mn-fed rat brain extracts, was the decreased Fraction A. Although the lines between LMM fraction D, E and F looked very steep (meaning significance) at the first instance, the corresponding p-values could not confirm the significance.

Unless the outcome of the two-way ANOVA, more comparative conclusions can further be drawn from the total Mn bound to HMM or LMM molecules in percentage compared to total Mn in brain extracts, which is illustrated in Figure 30. In average, Mn bound to HMM compounds in brain of +Mn_Food samples was significantly lowered compared to control rats

(15.4±2.5% vs. 34.8±3.4%, respectively). On the other hand LMM carriers seemed to bind Mn in significantly higher amounts due to feeding of Mn with 54.8±1.0% compared to 40.1±3.7% in control samples. Moreover, higher levels of free inorganic Mn were found in the brain extracts of +Mn_Food samples than in control samples (32±8% vs. 23.4±6%, respectively). Over all, the results from Mn-speciation in the brain of the feeding study indicated a decreased transportation of Mn by HMM molecules like α-2-Macroglobulin but an increased transportation of Mn by LMM molecules like citrate or amino acids. Due to the enhanced low-dose feeding of Mn, also more free inorganic Mn seemed to occur in the brain compared to normal fed rats as revealed by SEC-ICP-MS.
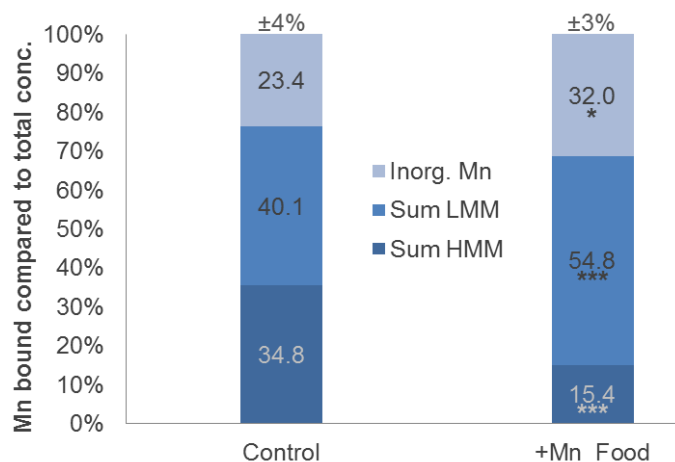
Figure 30 Percental amount of Mn bound according to SEC-ICP-MS in brain extracts of the feeding study.
The concentration of Mn bound to each size fraction was calculated in percentage and summed up for HMM, LMM and inorganic Mn. The average SD in percentage is given at the top of each column. Mn bound to HMM molecules was significantly lowered, while Mn bound to LMM as well as inorganic Mn was significantly increased in Mn-fed rat brain extracts (Student t-test between control and +Mn_Food of sum of fractions from each sample ***p<0.001, *p<0.05).

B.2.3.2 Characterization of brain Mn-species from the injection study

Four days after the single injection of $MnCl_2$ (or isotonic saline in control rats), rats were sacrificed. Brains were taken, immediately shock frozen in liquid nitrogen and brain extracts were prepared, which were stored at -80°C until analysis by SEC-ICP-MS. Mn concentrations found at each SEC size fraction were calculated with regard to the respective peak areas. The results are shown in Figure 31. According to SEC-ICP-MS, Mn was significantly increased in the rat brain samples in every size fraction (A-F) compared to controls. The x-fold increases were strongest for fractions D and E (1.8-fold each) and decreased in following order: fraction C (1.5-fold) > fraction A and F (1.4-fold) > fraction B (1.2-fold). Based on these fold-changes, the LMM carriers in brain seemed to transport Mn during increased neu-

ral Mn concentrations. Also fraction C (Tf) could act as possible Mn-carrier due to this single exposure to Mn.

The increase in fraction A (α-2-Macroglobulin) was rather unexpected. However, it is known that α-2-Macroglobulin can have either neuroprotective or neurodegenerative effects (Kovacs 2000). As observed in Alzheimer's´ Disease, increased concentrations of α-2-Macroglobulin were observed in hippocampal plaques. Human neuroblastoma cells activated with α-2-Macroglobulin increased Aβ-mediated toxicity (Fabrizi et al. 1999). An acute inflammation could eventually be an explanation for increased Mn-transportation by this HMM molecule in brain. Interestingly, HMMs were also increased 1.7-fold in the injection study by Diederich et al. in Mn-speciation of brain extracts.
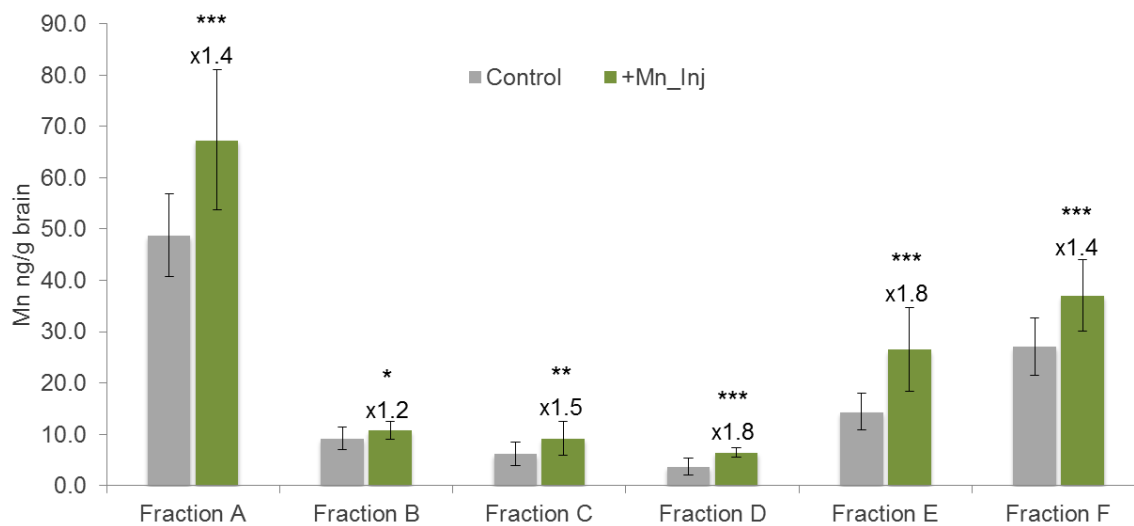
Figure 31 Characterization of Mn-species in brain from the injection study.
Mn of all SEC fractions of the brain were increased in +Mn_Inj rats with Fractions D and E showing the greatest increase compared to control. (Student t-test *p<0.05, **p<0.01, ***p<0.001)

Also here, a two-way ANOVA was carried out to examine possible significant interaction effects for group (control or +Mn_Inj) and SEC-fraction (Figure 32, p-values in the Appendix, Table 27). According to the p-values, Fractions C, D and E showed significance between control and +Mn_Inj samples, substantiating the results from fold-changes of the t-test shown above.
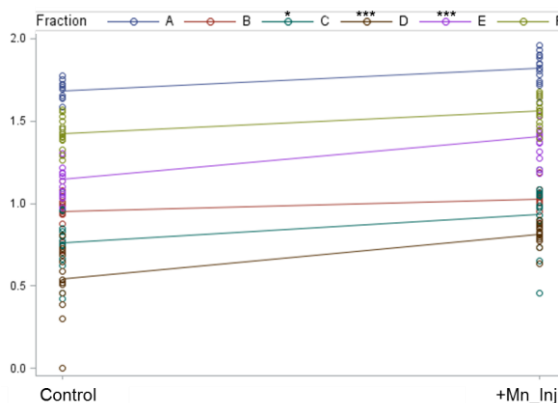
Figure 32 Two-way ANOVA of data from Mn-speciation in the brain of the injection study.
A significant interaction effect (group*SEC-fraction) was observed for Fractions C, D and E between control and +Mn_Inj (*p<0.05, ***p<0.001).

From the comparison of each fraction between control and Mn-exposed rats, it seemed as if the LMM fractions D and E as well as the fraction C had greatest importance for carrying of Mn in the brain under exposure conditions. This means that during the single exposure to very low concentrations of Mn, it is preferentially bound to citrate or amino acids for transportation in the brain. A binding to Tf could also be possible, overall for transportation into the brain by a Tf receptor-mediated influx.

For better comparability, the sum of Mn bound to HMM, LMM and inorganic Mn in percentage compared to total concentrations in the brain extracts is shown in Figure 33. The sum of Mn bound to HMM molecules in brain was comparable between control and exposed rats (58.4±4% vs. 54.8±4%, respectively). Also the percentage of inorganic Mn in brain extracts was comparable between control and Mn exposed rats (24.7±5% vs. 23.2±5%, respectively). However, the sum of Mn bound to LMM carriers in the brain was significantly higher in brains of injected rats compared to controls (20.7±3% vs. 16.5±2%, respectively). Overall, these results indicate that already due to the very low and single exposure to Mn *i.v.* a shift towards LMM carriers of Mn in the brain could be observed. The comparable high amount of HMM carriers in the brain found in control as well as treated rats in this injection study was somehow strikingly. Repetition of SEC-ICP-MS analysis of the samples, however, showed the same peak distribution with greater peaks of the first three size fractions compared for example to the inorganic peak (*Appendix*, Figure 87). Two possible reasons for that outcome would be: either there was a species transformation already in the sample or during chromatography leading to an accumulation of these HMM compounds in the first column. Or, these rats inherently possessed more HMM molecules in the brain carrying Mn.
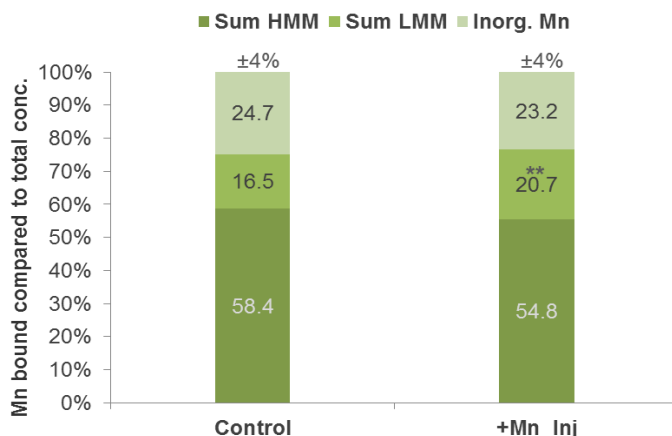
Figure 33 Bound Mn in percentage compared to total Mn in the brain extracts from SEC-ICP-MS in brain of the injection study.
The concentration of Mn bound to each size fraction was calculated in percentage and summed up for HMM, LMM and inorganic Mn. The average SD in percentage is given at the top of each column. Mn bound to HMM molecules as well as inorganic Mn in brain was comparable between control and Mn-exposed rats. Mn bound to LMM carriers was significantly increased compared to control (Student t-test between control and +Mn_Inj of sum of fractions from each sample **p<0.01).

B.2.4   LoD and Mn recovery

For determination of the column limit of detection (LoD) solutions of a Mn single standard (Spex CertiPrep, Middlesex, UK) in eluent A were applied on the column in five different concentrations (0.5, 1, 10, 25, 100 µg/l). Peak intensities (heights) were recorded and three blank runs were measured. LoD for Mn was then calculated according to the 3σ criterion [3*SD (blank intensities) * conc. Standard / (peak height standard-peak height blank)] and was found to be 0.050 µg/l for the applied column combination. Measured values for Mn in brain extracts size fractions were between 3-75 µg/l.

For column recovery, a brain extract was spiked with different concentrations of the same Mn single standard (10, 50, 250 and 500 µg/l). These solutions as well as the unspiked sample were applied at the column combination and total peak areas were plotted against the concentrations of Mn in the standard solutions. The resulting calibration curve was used for calculation of recoveries of the applied samples. In average, the recovery for Mn in brain extracts analyzed at that column combination was 105±22%. This recovery was accepted as being conclusive and the SEC-ICP-MS method was proofed to be reliable for Mn-speciation in the brain extracts.

B.2.5   Discussion by comparison of Mn-species in brain in the feeding and injection study

The two Mn-exposure studies carried out in this work revealed some interesting insights into Mn-species formation in the brain. Due to the prolonged feeding of low-dose Mn, a significant decrease in HMM compounds and an increase in LMM compounds could be observed by SEC-ICP-MS. About 15% of total Mn in the brain extracts was still bound to HMM carriers like α-2-macroglobulin or γ-globulin. Interestingly, concentrations of Mn in the Tf fraction were comparable to control samples. About 55% of Mn were found at the LMM size fractions, like citrate or amino acids in the brain extracts of exposed animals. These findings are in line with results from Yokel and Crossgrove, where a three-fold higher influx co-efficient across BBB was found for Mn-citrate compared with Tf (Yokel and Crossgrove 2004). Also the amount of inorganic Mn was significantly higher compared to control rat brain extracts after feeding of Mn, which underlines the suggestion of transportation of free Mn across neural barriers.

Oppositely to the feeding study, total Mn was significantly higher in all SEC fractions of brain extracts from Mn-exposed rats. These results were also observed in the previous injection study carried out by Diederich et al. (Diederich et al. 2012). Herein, however, the percentage amount of Mn bound to HMM molecules in the brain extracts was similar between control and exposed samples. The same was true for inorganic Mn. In line with the results from the feeding study was the fact that the percentage amount of Mn bound to neural LMM carriers like citrate or amino acids was significantly increased due to Mn exposure.

Both exposure modes therefore led to a shift of Mn bound to LMM molecules like citrate or amino acids. The only difference was that a clear decrease in HMM molecules as well as an increase in free inorganic Mn revealed by SEC-ICP-MS was only observable after a prolonged exposure to Mn (feeding study). In general, these findings correspond very well with Mn-speciation studies in human CSF. The samples in the study of Nischwitz et al. were drawn from healthy individuals presenting an average concentration of 1 µg/l Mn in CSF. A Mn-speciation by SEC-ICP-MS revealed Tf as the biggest HMM molecule comprising 9% of total Mn. 91% of total Mn were assigned to LMM molecules (15% citrate, 12% unknown), including 64% inorganic Mn. Unless the findings for the HMM compounds and concentrating on the LMM carriers (without inorganic Mn), these results correspond very well with the observations herein. Under prolonged exposure by food 54% of Mn in brain extracts was assigned to LMM molecules, which was even higher than in the injection study (21%). This finding is not unreasonable as a prolonged exposure might lead to an even bigger shift to-

wards LMM Mn-carriers in brain. The results therefore substantiate previous findings of Mn-speciation in CSF carried out in the group of Prof. Michalke. In another study of Mn-speciation in human CSF by CZE-ICP-MS, about 26% of total Mn was assigned to citrate (Michalke et al. 2007). But the authors also found various amino acids as possible Mn-carriers in the brain, which was also found to be true herein. As mentioned above, the amount of Mn bound to HMM molecules was much more higher in the injection study both in control as well as in brain extracts from exposed animals. The discrepant concentrations of HMMs as well as for inorganic Mn can also be observed in other studies. As just discussed, Nischwitz et al. found 64% inorganic Mn in CSF, Diederich et al. 12-13% in rat brain extracts, herein 23-32% and a study by Michalke et al. found inorganic Mn below LoD in human CSF. The problem with inorganic Mn for sure traces back to conditions at sample drawing and storage, which cannot be monitored when samples are drawn in the clinic (e.g. CSF). Even taking blood by a metal needle instead of punctuation as carried out in the injection study led to higher Mn concentrations in the serum (personal observation, data not shown). In this mentioned study by Michalke et al. 44% of Mn was bound to HMM when total concentrations of Mn were below 1.55 µg/l in CSF (Michalke et al. 2013). Above that concentration, HMMs decreased to 13%, which is very in line with the results from Mn-speciation in brain extracts from the feeding study. Moreover, Mn bound to LMM molecules increased from 42% to 60% above that 1.55 µg/l of total Mn. These are again similar values to the ones found herein in the feeding study.

B.3   Characterization of Mn-species in serum by SEC-ICP-MS

Besides gaining knowledge about formed Mn-species in brain under Mn-exposure, a further task of this work was the determination of Mn-species in serum. This meant, finding characteristic serum compounds, to which Mn is bound for transportation. Based on the two different Mn-exposure studies, differences or similarities in serum Mn-species even between these two studies were of interest.

B.3.1   Column Mass Calibration

As described in chapter *D.7.2.1*, the Biobasic SEC300 column, which was used for Mn-speciation in brain extracts, showed ageing phenomena as test runs with serum revealed no good separation. Therefore, for characterization of Mn-species in serum, this first column was exchanged by a Peek column filled with SEC material, separating high molecular mass compounds (HMM, exclusion limit 700 kDa). The second column was the same as applied for Mn-speciation in brain but was packed freshly with SEC material separating low molecular masses (LMM, exclusion limit 10 kDa). Mn-containing standards as well as standards

without Mn in the expected size range were applied for column mass calibration. The ln of the molecular weight (ln MW) was plotted against obtained retention times (RT) resulting in two equations, which described the two columns: $\ln(y) = -0.645 \cdot x + 15.627$ for HMM compounds eluting before 19 minutes and $\ln(y) = -0.1264 \cdot x + 1.1565$ for LMM compounds eluting after 19 minutes. These equations were used to characterize the eluting Mn-species in serum according to the respective RT. Applied standards are listed in Table 10 and the resulting column mass calibration is shown in Figure 34. According to the results of column mass calibration, separation of Mn-species was satisfactory.

Standard	MW (kDa)	RT (min)	ln MW (kDa)
α-2-Macroglobulin	725	14.2	6.5862
Ferritin	440	15.2	6.0868
γ-Globulin	190	15.9	5.2470
Arginase	107	16.8	4.6728
SOD	80	17.2	4.3820
Tf	78	17.2	4.3567
HSA	66	18.3	4.1897
GSH	0.307	19.2	-1.1809
Citrate	0.192	20.4	-1.6503
L-Glutamic acid	0.147	25.9	-1.9173
L-Cysteine	0.120	26.5	-2.1120
Mn	0.055	31	-2.9004

Table 10 Column mass calibration for Mn-speciation in serum.
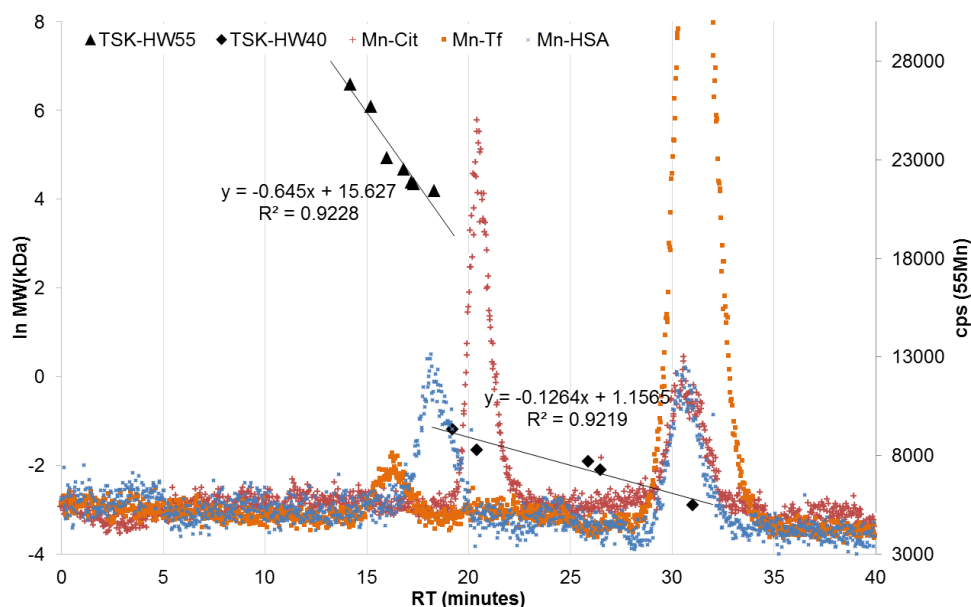
Figure 34 Equations of Column mass calibration for Mn-speciation in serum.
The first column (filled with TSK-HW55S) described separation of HMM compounds such as Tf (orange squares) or HSA (blue crosses). The second column (filled with TSK-HW40S) described separation of LMM compounds such as Mn-citrate (red crosses). Tf, HSA and citrate were incubated with inorganic Mn, giving an inorganic Mn peak at 31 minutes. The secondary vertical axis showing counts per second (cps) of ^{55}Mn is scaled to improve visualization of the protein peaks.

B.3.2   Assignment of serum peaks

With results from column mass calibration, separation of serum Mn-compounds with this column combination looked promising. However, the influence of the sample matrix applied to a column, is shown as an example in Figure 35 by a serum sample from the injection study. The pure serum (grey line) revealed one big peak with maximum height at around 16 minutes in the front including all HMM, a clear citrate peak at 21 minutes, one peak between citrate and inorganic Mn at 31 minutes. Dilutions of 1:10 and 1:50 were carried out to check if the first big peak could be separated into more peaks. However, even the 1:50 dilution showed no improvement of the separation. It rather had the disadvantage of flattening the peaks at the end of the chromatogram, including citrate, making determination of LMM peaks nearly impossible. For further examination of compounds contributing to this first HMM peak, fractions were collected according to the vertical lines in Figure 35, lyophilized, diluted in eluent A and analyzed again at the same column combination. By this, a matrix removal and additional dilution of HMM compounds was intended.
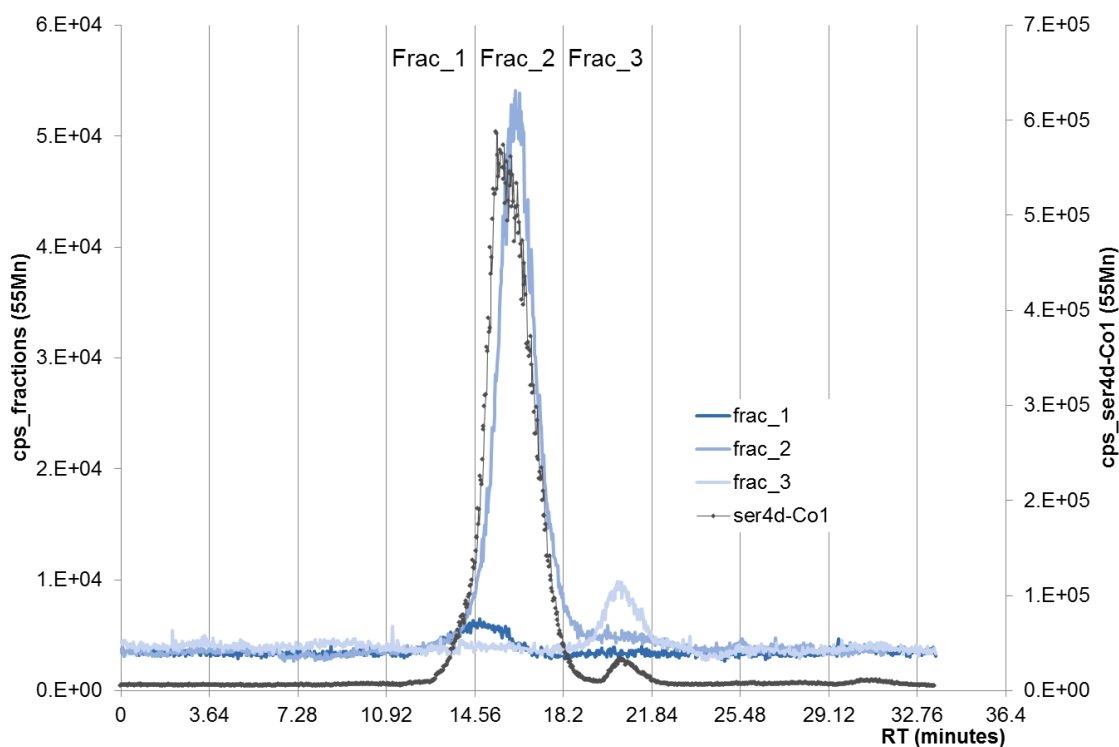
Figure 35 Application of a serum sample from injection study at the described column combination. (ser4d-Co1, grey line). As dilution was unrewarding for further separation of the first peak including all HMM compounds at around 16 minutes, fractions were collected at the time points indicated by the vertical black lines and fractions 1-3 were analyzed at the same column combination after lyophilization and dilution in eluent A (blue lines).

By the applied timing of fraction collection the first serum peak was cut at 14.56 minutes and analysis of this first fraction revealed therefore a peak at this time frame with a flat top from

14 to around 15.5 minutes (dark blue line in Figure 35). This fraction therefore co-eluted with α-2-Macroglobulin. The second fraction (middle blue line) included the major part of this big serum peak and couldn´t be separated any better as shown in Figure 35. The maximum of the peak was around 16 minutes but showed a broad eluting time frame. According to retention times of standards, this fraction included among others γ-Globulin or Tf. Analysis of the third fraction (light blue line) proved retention time of citrate as shown in Figure 35. Although the first big peak couldn´t be separated any better, the separation from citrate from the remaining peaks was satisfying, and therefore the column combination was applied to the serum samples. By application of PeakFit™ software, the first peak was therefore divided into three size fractions, referring to chromatography of brain extracts for better comparability. The final size classification of serum samples is illustrated in Figure 36. Referred to the applied standards for column characterization, the first size fraction (Fraction A, 700-350 kDa) included α-2-macroglobulin, the second size fraction (Fraction B, 350-100 kDa) included γ-globulin, the third size fraction (Fraction C, 150-60 kDa) mainly transferrin, the fourth size fraction (Fraction D, 280-170 Da) Mn-citrate, the fifth size fraction (Fraction E, 150-100 Da) amino acids, and eluting at last was inorganic Mn (Fraction F, <60 Da) (summarized in Table 11). It has to be mentioned that the applied standards are possible binding partners of Mn according to obtained retention times and literature. Of course, other molecules, which were not examined, might also be eluting in the same time frame as SEC only allows setting eluting time frames due to its limited resolution. However, it is still the most suitable separation method for the inherently very labile Mn-species.

	SEC-fraction	Size	Assignment
HMMs	fraction A	700-350 kDa	α-2-macroglobulin
(High molecular	fraction B	350-100 kDa	γ-globulin
masses)	fraction C	100-60 kDa	transferrin
LMMs	fraction D	280-170 Da	Mn-citrate
(Low molecular	fraction E	150-100 Da	amino acids
masses)	fraction F	<60 Da	inorganic Mn

Table 11   SEC-fraction assignment.
According to retention times of applied standards and with the aid of PeakFit™ software, serum samples were separated into six size fraction referred to the main compounds listed in the last column.
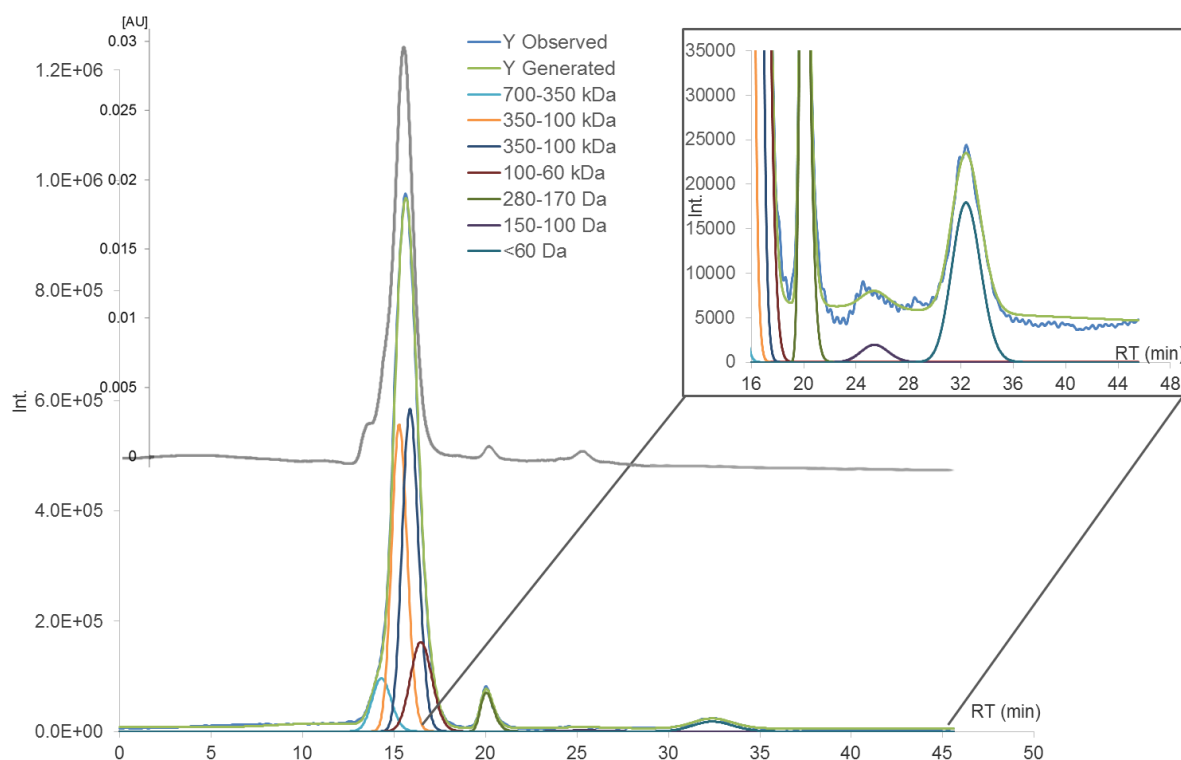
Figure 36 Peak assignment for analysis of serum samples by SEC-ICP-MS.
Peak alignment was carried out by use of PeakFit^TM software (Y observed and Y generated). The first
peak was separated into three size fractions: 700-350 kDa, 350-150 kDa and 150-60 kDa. A further
peak at 280-170 Da and 150-100 Da as well as an inorganic Mn peak (<60 Da) were generated. Su-
perimposed in grey is the UV signal at 220 nm.

B.3.3   Analysis of serum samples

Every serum sample to be analyzed at one day was allowed to thaw at 4°C overnight and
was diluted in eluent A 1:4 (v/v) before analysis at the above described column combination.
Serum samples from the feeding and the injection study were analyzed in random order.
After every third run, columns were cleaned as serum is known to be a matrix burdening the
column material. The obtained peak areas (%) of chromatograms were converted into con-
centration of Mn bound to each serum compound with respect to the total Mn concentration
in the respective serum sample.

B.3.3.1 Characterization of serum Mn-species from the feeding study

In the feeding study, blood (~4 ml) was collected from the *aorta abdominalis* at time of sacri-
fice of animals after feeding for 53 days of standard fodder for control rats and Mn-enriched
fodder (500 mg/kg) for Mn-exposed rats. Blood was centrifuged at 4°C and serum was tak-
en, aliquoted and stored at -80°C until analysis by SEC-ICP-MS. The results for Mn-species
characterization in the feeding study are shown in Figure 37 in comparison of control and
+Mn-fed samples according to student t-test of calculated Mn concentrations of the respec-
tive serum fractions (µg/l). Serum Fraction A showed no significant difference between the

two groups (2.06±0.29 µg/l in control and 2.27±0.29 µg/l in +Mn_Food), whereas fractions B and C were found to be significantly lowered due to Mn feeding (B: 1.19±0.06 µg/l and 0.99±0.16 µg/l, 0.8-fold, p<0.05; C: 0.99±0.20 µg/l and 0.41±0.20 µg/l, 0.4-fold, p<0.001; for control and +Mn_Food, respectively). On the other hand, serum fractions D, E and F were increased in Mn-exposed animals (D: 0.12±0.03 µg/l and 0.38±0.18 µg/l, 3.2-fold, p<0.01; E: 0.03±0.04 µg/l and 0.11±0.07 µg/l, 4.4-fold, p<0.05; F: 0.01±0.003 µg/l and 0.08±0.04 µg/l, 5.3-fold, p<0.01; for control and +Mn_Food, respectively). However, it has to be mentioned here that Mn concentrations in fraction F of control samples was below LoD.

Beside the t-test, another evaluation model applied included a multiple analysis. Therefore data were log transformed to obtain normality. A general linear model (GLM) was used to calculate least square means for each SEC fraction (A-F) for each group (control and +Mn_Food). Comparing these, the contrast in the different SEC fractions between groups could be observed as shown in Figure 38 (respective LS means can be found in the *Appendix,* Table 24). By this analysis, the results from the t-test were expanded as the model also included the interaction effect. This examines the simultaneous interaction of the two factors *group* (control or Mn-fed) and *SEC fraction,* strengthening the outcome. HMM SEC fractions A, B and C showed no significant difference between the groups as shown by the almost parallel lines in the interaction plot in Figure 38A. Controversy, Fractions D, E and F showed significant differences between both groups as shown by the interaction plot as well as in the box plot. Compared to the t-test, this analysis strengthens the fact that the main effects for serum Mn-species distribution after feeding came from the LMM SEC fractions.
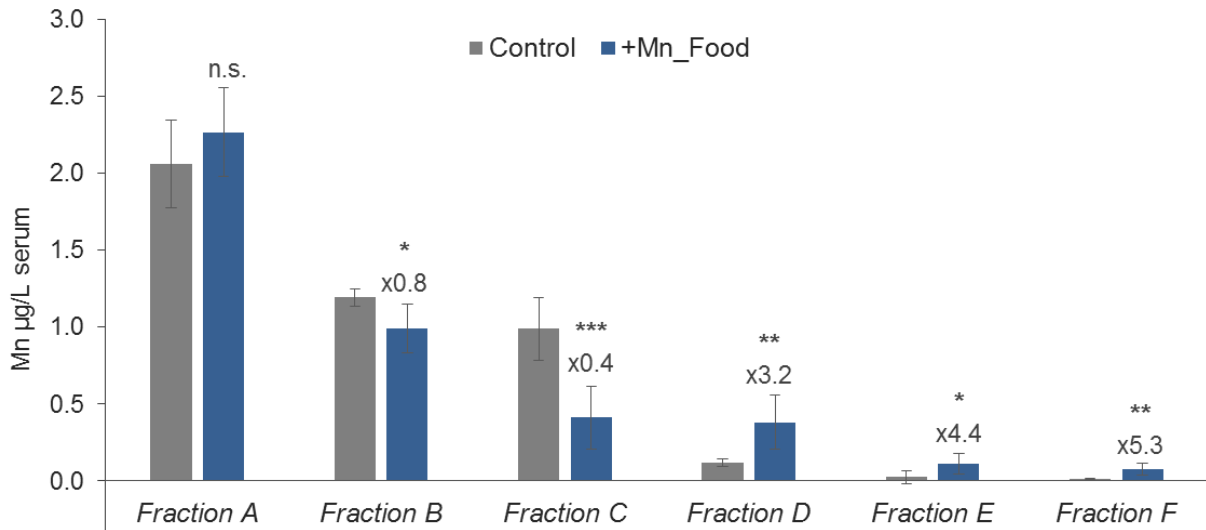
Figure 37 Comparison of SEC serum fractions obtained for control and +Mn animals in the feeding study.
HMM serum fractions B and C were found to be significantly decreased in +Mn_Food serum (x0.8 and x0.4, respectively) whereas LMM fractions D, E and F were found to be significantly increased due to Mn feeding (x3.2, x4.4 and x5.3, respectively). (Student t-test *p<0.05, **p<0.01, ***p<0.001)
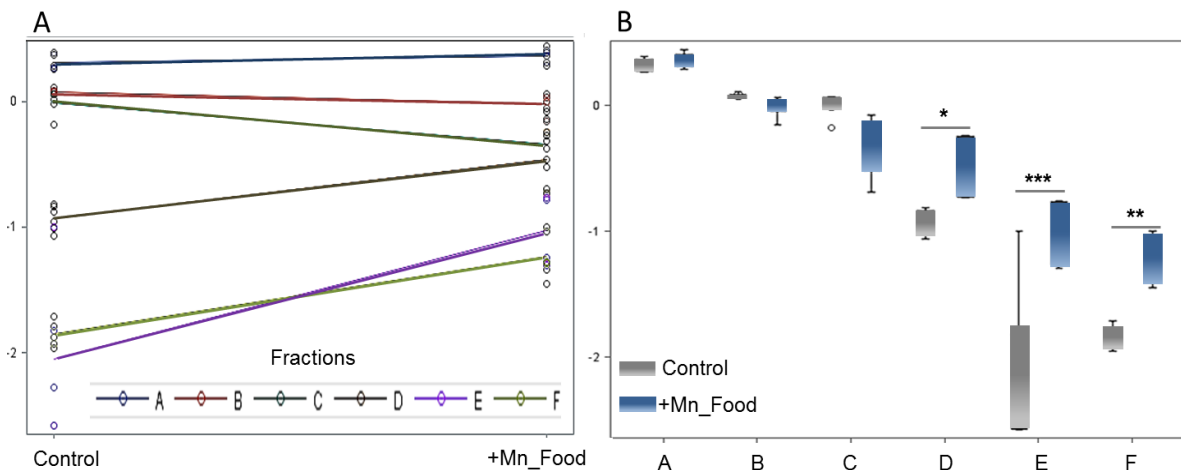
Figure 38 General linear model to test the effect of SEC-fractions between control and +Mn-Food serum.
After log transformation of data, a general linear model tested the contrast in SEC Fractions between control and +Mn_food serum. That kind of statistical analysis is more valid compared to a t-test. Due to statistical significance, the main effects on Mn-species distribution serum came from the LMM fractions D, E and F, which were significantly increased in serum of Mn-fed animals. This is shown by the interaction plot (A) due to a significant slope in the interaction lines of Fractions D, E and F as well as by the box plots (B) (*p<0.05, **p<0.01, ***p<0.001).

After Tukey-Kramer adjustment of the log transformed data, a two-way ANOVA was applied. This analysis also included the so-called interaction effect, where the simultaneous interaction of the two factors *group* (control or Mn-fed) and *SEC fraction* was tested. The results are summarized in Table 12, where every SEC fraction from one group (control or Mn-fed) can be compared with every SEC fraction from the other group on the basis of the interaction of the two factors. This kind of analysis strengthens the analysis of such an experiment com-

pared to application of only the t-test, by which only one factor is considered. According to the table, SEC fractions A, B and C showed no significant interaction effect (p-values shown in red), neglecting the importance of these fractions for describing the experiment. On the other hand, SEC fractions D, E and F showed a significant interaction effect (p-values shown in blue). Also this test substantiated the importance of these LMM fractions for Mn-species distribution in serum after subchronic feeding.

Least Square Means of two-way ANOVA for effect group (Control vs. Mn-fed)*SEC-fraction Pr > |t| for H0: LSMean(i)=LSMean(j) Dependent Variable: Mn						
Fraction	Co_A	Co_B	Co_C	Co_D	Co_E	Co_F
Co_A		0.9043	0.5587	<.0001	<.0001	<.0001
Co_B	0.9043		1.0000	<.0001	<.0001	<.0001
Co_C	0.5587	1.0000		<.0001	<.0001	<.0001
Co_D	<.0001	<.0001	<.0001		<.0001	<.0001
Co_E	<.0001	<.0001	<.0001	<.0001		0.9677
Co_F	<.0001	<.0001	<.0001	<.0001	0.9677	
+Mn_A	1.0000	0.6702	0.2722	<.0001	<.0001	<.0001
+Mn_B	0.4559	0.9999	1.0000	<.0001	<.0001	<.0001
+Mn_C	0.0015	0.1571	0.4848	0.0029	<.0001	<.0001
+Mn_D	<.0001	0.0157	0.0855	**0.0467**	<.0001	<.0001
+Mn_E	<.0001	<.0001	<.0001	1.0000	**<.0001**	0.0001
+Mn_F	<.0001	<.0001	<.0001	0.5256	<.0001	**0.0027**

Table 12 Excerpt of the least square means table of the two-way ANOVA of the serum Mn-species in the feeding study.
This two-way ANOVA included the interaction effect between group (control or Mn-fed) and SEC-fractions, strengthening the analysis of the experiment. Exemplarily are significantly different serum fractions D, E and F (bold numbers) between control and +Mn_Food serum samples. This result showed that the main effect for Mn-species distribution in serum after feeding of Mn came from the LMM serum fractions.

E.3.3.2 Characterization of serum Mn-species from the injection study

In the injection study, control rats received 100 µl of isotonic saline and Mn-exposed rats received a solution of 100 µl of 1.5 mg Mn/kg b.w. for one single time. Blood was drawn at two time points: one hour after injection, blood was taken from the *vena sublingualis* by punctuation and centrifuged to obtain serum, which was stored at -80°C until analysis (serum_1h). The second time point for drawing of blood was four days after injection from the *aorta abdominalis* at the time point of sacrifice (serum_4d). For each time point, Mn-speciation was carried out in the respective serum by SEC-ICP-MS.

As shown in Figure 39 (first third) every serum fraction was increased in +Mn_Inj_1h samples consequently to *i.v.* injection of $MnCl_2$ with respect to the increase in total Mn (µg/l). Comparing the x-fold increases, fractions were increased as follows in descending order: fraction F (x422) > fraction E (x82) > fraction C (x63) > fraction D (x27) > fraction B (x25) >

fraction A (x21), where the last three named fractions were increased by similar factors (~20-fold). To obtain a better overview, the Mn concentrations of each SEC Fraction (µg/l) was divided by that factor by which total Mn in serum was increased one hour after injection compared to control levels (factor 28, 7±2 µg/l compared to 194±49 µg/l, see Table 5). These "normalized" values were further compared with the values for serum Mn-species of the control samples shown in the last third of the panel chart in Figure 39. Applying this kind of normalization revealed only two serum fractions, which were significantly altered in Mn-injected serum samples. Inorganic Mn (Fraction F) remained highly increased in +Mn_Inj_1h samples (15-fold). The second significantly increased serum fraction was Fraction C (x2.3). According to the SEC fraction assignment, Fraction C included Tf as serum protein, which eluted at that time point. The obtained results indicate that besides being abundant in its inorganic form, Mn was mainly bound to Tf 1h after Mn injection.
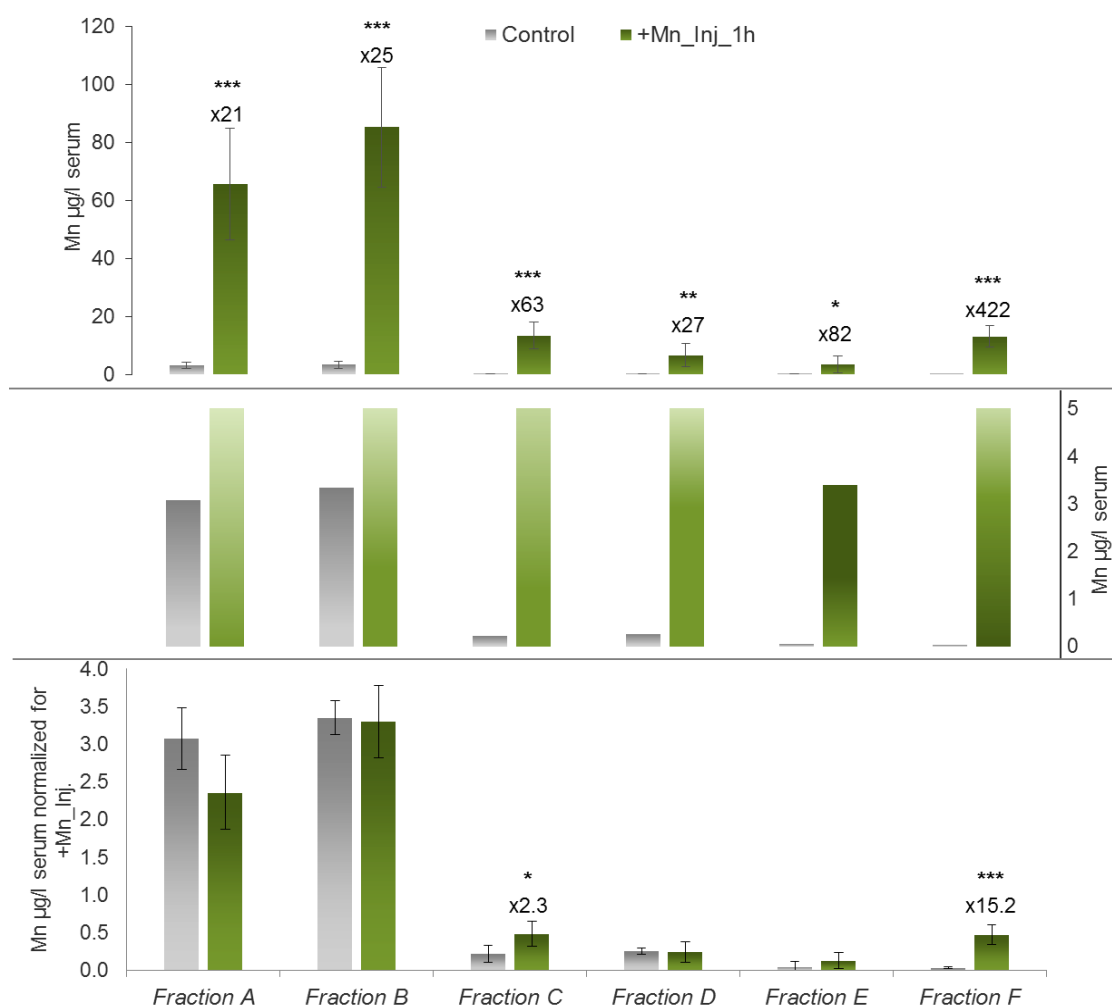
Figure 39 Comparison of serum Mn-species between control and +Mn_Inj_1h by SEC-ICP-MS. The upper part of the panel chart shows the not zoomed view with x-fold increases whereas the middle part shows the bars of control samples zoomed out. The lower part depicts a kind of normalization for better overview: Mn concentrations of respective serum fractions were divided by the factor by which total Mn in serum was increased compared to control (~ x27.8). This revealed Fractions C and F significantly increased in Mn-injected serum samples. (Student t-test, *p<0.05, **p<0.01, ***p<0.001)

The distribution of Mn amongst serum compounds four days after the injection, at time point of animal sacrifice, is shown in Figure 40. Although there was no significant difference in total Mn in serum four days after the injection any more (6.0±1.5 µg/l compared to 6.7±1.3 µg/l, see Table 5), serum Mn-species seemed to be still altered. According to the results of the student t-test, serum fractions A and F were significantly reduced in +Mn_Inj_4d samples. The remaining fractions (B, C, D and E) were significantly increased compared to control with fractions B and D showing similar increase (x1.7). Fractions C and E were still increased the most compared to the remaining fractions (x2.5 and x4.2, respectively) in +Mn_Inj_4d serum.
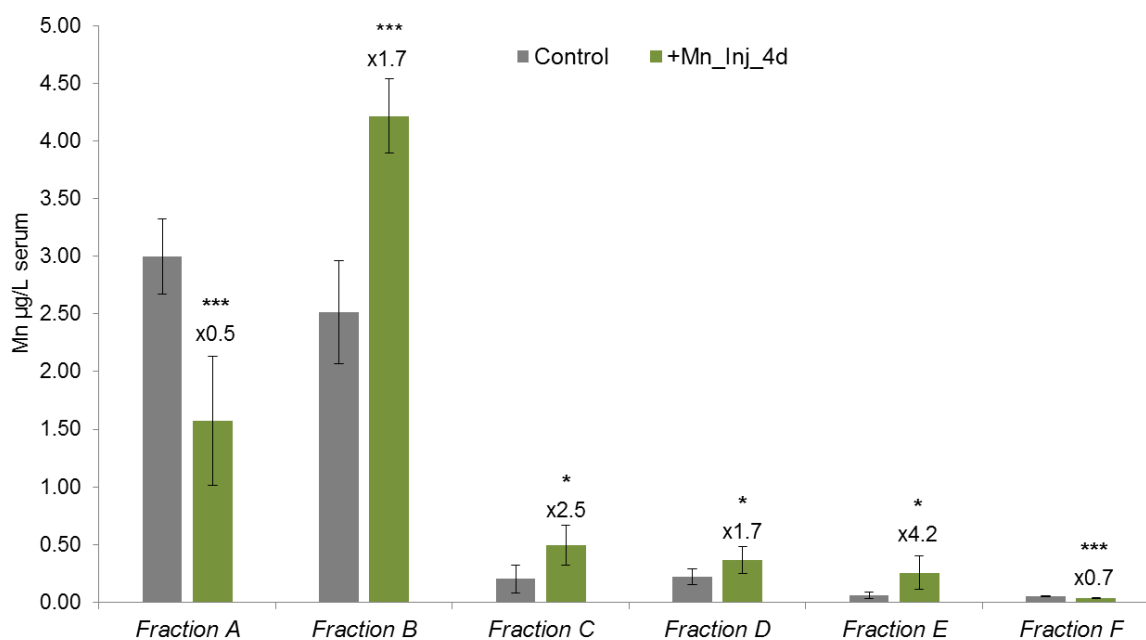
Figure 40 Comparison of serum SEC fractions four days after MnCl$_2$ injection between control and +Mn_Inj serum samples obtained by SEC-ICP-MS.
All serum fractions were significantly altered in +Mn_Inj_4d serum with fractions A and F being decreased and B, C, D, E being increased. Fractions B and D were increased in similar manner (x1.7) while fractions C and E were increased stronger (x2.5 and x4.2, respectively). (Student t-test, *p<0.05, ***p<0.001)

Further evaluation of the serum speciation data of the injection study included a general linear model with repeated measures. For this, data were also log transformed to obtain normality. As above, the model also included the interaction effect between group (control or Mn-exposed) and SEC-fraction, having higher validity than the t-test. The results are shown in Figure 41 with respective least square means being summarized in the *Appendix,* Table 25. As the interaction plot and the box plot one hour after injection shows (Figure 41 A), every SEC fraction was significantly increased in +Mn_Inj serum due to the i.v. injection. Four days after the injection (Figure 41B), the main effects for Mn distribution in serum came from the Fractions C and E, which showed also strong increase in +Mn_Inj serum according to t-

test (Figure 40). Therefore, four days after injection, Mn seemed to be transported in serum still by Tf (Fraction C) and also by LMM compounds like amino acids (Fraction E).
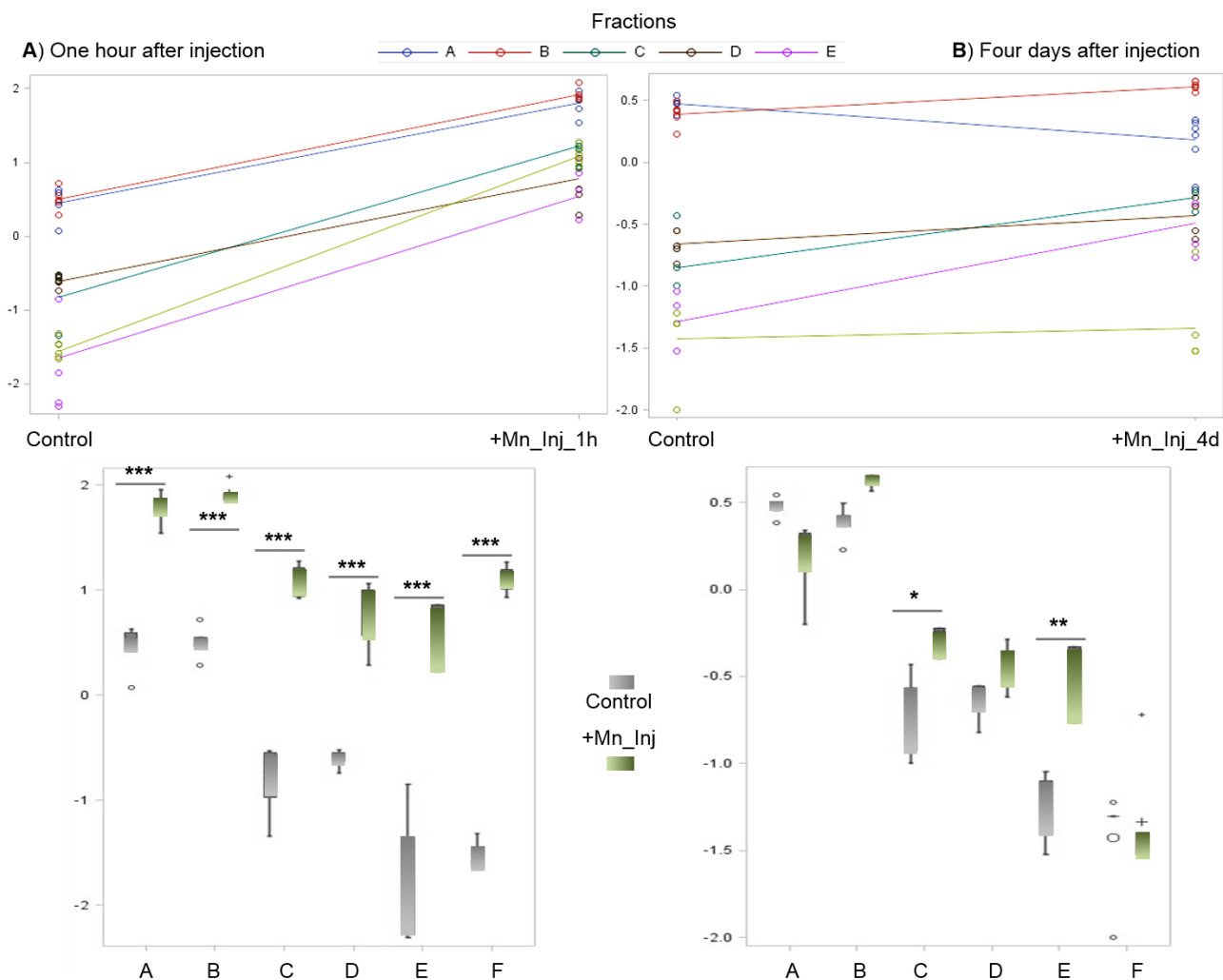
Figure 41 General linear model with repeated measures of data from the serum Mn-speciation in the injection study.
One hour after injection each fraction was significantly increased due to i.v. injection of $MnCl_2$ (A) as shown by the interaction plot as well as the box plot. Four days after injection the main effects came from serum fractions C and E, which showed significance compared to control (B).

B.3.4   LoD and Mn recovery

For determination of the column limit of detection (LoD) solutions of a Mn single standards (Spex CertiPrep, Middlesex, UK) in eluent A were applied on the column in five different concentrations (0.1, 0.5, 1, 10, 50 µg/l). Peak intensities (heights) were recorded and three blank runs were measured. LoD for Mn was then calculated according to the 3σ criterion [3*SD (blank intensities) * conc. Standard / (peak height standard-peak height blank)] and was found to be 0.017 µg/l for the applied column combination. Measured values for Mn in the fractions for all serum samples were between 0.01 and 120.95 µg/l.

For determination of column recovery, serum samples were spiked with different concentrations of a Mn single standard. The aim was to compare the total peak areas of the samples with the total peak areas of the spiked samples with regard to applied Mn concentrations and found Mn concentrations in the samples after SEC-ICP-MS. However, peak areas of spiked samples were not increasing in a linear manner according to applied Mn standards. Therefore, total areas of samples were subtracted from total areas of the spiked samples remaining the net increase in area of the inorganic peak. This area respective to the applied concentrations was then compared with the area of the inorganic peak of the sample obtaining the respective concentration of Mn. By comparison of the obtained concentration with the total Mn concentration in the serum sample, the recovery was calculated. In average, the recovery for Mn of the SEC-ICP-MS method was obtained with 90±36% (n=28). These variations in recovery seem strikingly at the first instance. However, the problem with recovery of Mn in serum after Mn-speciation is well known. As the chromatograms showed, the high abundant HMM molecules in serum were eluting within a very short time frame. This high load of proteins is discussed to cause interferences such as isobaric cluster ions during ICP-MS detection (Nischwitz et al. 2008). In that study, the authors report a mean recovery for Mn in serum of 230±82% (n=17). They further analyzed Fe, Cu and Zn, where recoveries lied in an acceptable range. According to the authors, the problem with interferences of HMM molecules is less critical for these elements as they are abundant in higher concentrations in the serum compared to Mn. Compared with the stated study in human serum and keeping in mind the known problems with Mn recovery in serum, the recovery for Mn in serum obtained herein lies in an acceptable range.

B.3.5   Discussion by comparison of Mn-species in serum in the feeding and injection study

For comparing the results from characterization of Mn-species in serum of the feeding and the injection study, the sum of Mn concentrations assigned to HMM compounds (SEC fractions A-C), to LMM compounds (SEC fractions D and E) and inorganic Mn (SEC fraction F) were compared as percent respective to total Mn in serum (Figure 42).

In the feeding study, the majority of Mn was bound to HMM in both control (96%) and +Mn_food (87%) serum, whereas this amount was slightly lower in the +Mn_Food group. Due to feeding of Mn, significantly 4-fold more Mn was bound to LMM (12% compared to control with 3%, p<0.01) in serum. Also inorganic Mn in the speciation was significantly higher compared to control serum (2% vs. 0.3%). These summed up results are in line with findings from the total concentrations, where all applied evaluation models revealed a signifi-

cant increase of LMM fractions D (citrate) and E (amino acids) as well as inorganic Mn. De-spite of missing significant differences in total Mn in serum, the applied subchronic feeding of Mn led to a shift in serum Mn compounds, where overall Mn-citrate and Mn bound to amino acids as well as inorganic Mn were the most abundant species found in serum according to SEC-ICP-MS.

In the injection study, the majority of Mn was also bound to HMM compounds in comparable manner between control and +Mn_Inj serum with 95% in control (both 1h and 4d after injec-tion) and in average 90% in +Mn_Inj at both time points. On hour after injection a considera-ble amount of 7% existed as inorganic Mn in +Mn_Inj rats. This was balanced already four days after injection with comparable values to control serum (0.5%), which was also true for total Mn concentrations in serum (Table 5, chapter *B.1.1*). According to SEC-ICP-MS, the amount of LMM compounds were comparable to control one hour after injection (4% and 5%) but as inorganic Mn decreased for days after injection, Mn bound to LMM compounds significantly increased by almost a factor of two compared to control serum (9% in +Mn_Inj vs. 5% in control, $p < 0.05$).
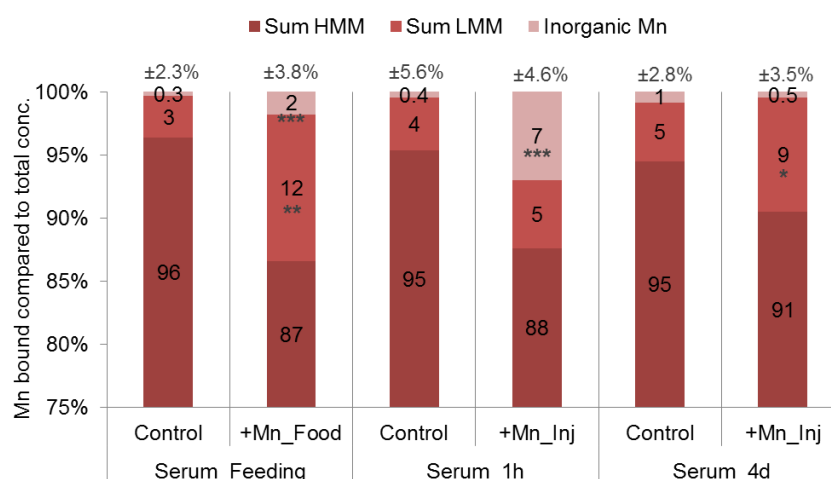
Figure 42 Comparison of Mn bound to HMM/LMM and inorganic Mn in percent to total Mn in serum from feeding and injection study.
Concentrations of Mn bound to HMM and LMM were summarized and compared between the studies in percentage (Serum_Feeding and Serum_1h/_4d). The average SD for each sum is given above each column. Significant differences between control and +Mn serum were found for: LMM and inor-ganic Mn in the feeding study, inorganic Mn in the injection study_1h, LMM in the injection study_4d (Student t-test *p<0.05, **p<0.01, ***p<0.001).

Overall, the subchronic feeding of Mn led to an observable shift of LMM Mn-carrying mole-cules in serum like citrate or amino acids in a greater extent than the single injection of Mn. However, these LMM fractions were also significantly increased four days after the injection. Regarding the acute intervention of Mn, Tf could further act as an important Mn-carrying protein in serum as observed both one hour and four days after injection. The inorganic Mn fraction was of course increased one hour after injection, but interestingly it was also higher

due to prolonged feeding. These results indicate that during a prolonged low-dose exposure to Mn, more LMM compounds transport Mn than under normal conditions. This loading of citrate or amino acids may already occur very early as seen four days after injection.

The results of Mn-species characterization in serum from the injection study herein cannot be transferred so easily to the one carried out by Diederich et al (Diederich et al. 2012). In this previous injection study, the majority of Mn in serum was found as inorganic Mn both one hour and four days after injection (94% and 63%, respectively) in the Mn-exposed animals, which was not the case herein. Moreover, Mn-species distribution in Mn-exposed rats was determined to be comparable to control serum four days after injection, what was also not the case herein. In line with the previous results from Mn-species characterization in rat serum after i.v. injection is that Tf was found to play a major role in Mn transportation. Also an increase in LMM compounds, presumably Mn-citrate complexes, as well as the amino acid fraction was described one hour after injection in the study of Diederich et al. Together with the results from the feeding study found herein, Mn binding in serum to amino acids seems to occur both under acute as well as under chronic exposure to Mn. Under acute exposure, Tf may trap the majority of Mn while under chronic exposure also LMM carriers like citrate seem to transport Mn in serum. This might be reasoned in an overload of HMM carriers in serum. The majority of Mn was still bound to HMM molecules in serum under normal and exposed conditions in the feeding and the injection study. The size fraction from >350-60 kDa (including α-2-Macroglobulin, γ-globulin, pyruvate carboxylase, arginase and Tf/HSA) carried most Mn. These serum proteins are all known to be typical Mn carrier molecules in blood, where the binding to one or the other depends on the oxidation state of Mn (either Mn(II) or Mn(III)) (WHO 2006). In general, the highest amount of Mn will be found at Tf and α-2-Macroglobulin in blood. Such a clear assignment was sophisticated herein as the transition from one size fraction to the other in this HMM range was fluent due to the elution of these HMM molecules as one major peak. Other speciation studies also assigned the majority of Mn to HMM molecules (~70-80%) by SEC-ICP-MS in human serum samples from healthy individuals (Michalke et al. 2013; Nischwitz et al. 2008). Michalke et al. determined inorganic Mn in human serum below LoD in the respective SEC-ICP-MS method, whereas Nischwitz et al. found around 29% as inorganic Mn. In comparison, inorganic Mn was found between 0.5 and 7% herein. Therefore, concentrations of inorganic Mn determined by SEC-ICP-MS seem to depend on variety of factors such as the kind of Mn-exposure (e.g. occupational or acute), origin of sample (human/rodent, place of living, sex), sample-taking (e.g. contamination of serum by use of metal needles), sample storage, and handling as well as age of samples. Even short storage times at inappropriate conditions can lead to changes in species equilibria. Unfortunately, only very little is known about Mn-species in serum. Addi-

tionally, so far analyzed human serum is gained from unexposed people complicating the finding of statements for Mn-species distribution in serum under exposed conditions. In the study by Michalke et al., however, HMM Mn carriers like Tf or HSA were found to correlate positively with total Mn in serum until a certain Mn concentration, from which on Mn-citrate in serum correlated positively. This finding indicated a certain Mn concentration in (human) serum, were binding partners seemed to switch. These observations for correlations of total concentration of Mn in serum with determined Mn-species in serum were not plausible herein. Both, the sample number as well as the low differences between total serum Mn concentrations made it impossible to find any reliable trend in correlation behavior. One further major drawback in this study was the very long sample storage time, which was based in the prolonged time for development of an applicable separation method. Nevertheless, the findings for Mn-species in serum after chronic and acute low dose Mn-exposure can contribute to the understanding of transport procedures dependent on time of exposure. More interesting was the fact that even at these low concentrations of Mn, trends and changes is Mn-species were observable in serum although total Mn concentrations were comparable. Overall, a trend towards LMM Mn-carriers in serum was clearly observed depending on exposure conditions, which substantiates previous findings.

B.3.6   Conclusion on Mn-speciation: Pattern of Mn-species in serum and brain under differed exposure scenarios

One major task of this work was the characterization of Mn-species in serum and brain after Mn-exposure of rats. This exposure included two different low-dose Mn-exposure models. The first study comprised a low-dose subchronic feeding with Mn for 53 days simulating a persistent intake (e.g. individuals living in areas with naturally higher abundant Mn in drinking water or foodstuff grown in soil). The second study comprised a single low-dose *i.v.* injection of Mn in rats simulating a short intervention with this metal (e.g. occupational accident or use of Mn-containing contrast agents for MRI).

In both studies, the majority of Mn in serum was assigned to HMM molecules like α-2-Macroglobulin or Tf, while the latter was significantly increased only due to the single injection compared to control but not during feeding. These HMM compounds were still relatively abundant in brain in the samples from the injection study both in control and +Mn brain extracts. However, due to the subchronic feeding the significant reduction in the amount of Mn bound to HMM carriers in the brain was concomitant with a significant increase in LMM molecules, namely Mn-citrate and Mn bound to amino acids. This shift towards LMM molecules

in brain was also observed due to the single injection, but was found to be more prominent in the feeding study. Moreover, also in serum more Mn was bound to LMM carriers during increased feeding and injection. An exposure to Mn might therefore lead to the shift of Mn-species towards LMM molecules already in serum, passing neural barriers in that form more easily without any control mechanisms. Additionally, Mn previously bound to HMM in serum might get uncoupled at the BBB and be attached to LMM carriers at the neural site. Despite to the injection of Mn, a prolonged oral intake could also lead to increased free inorganic Mn in serum as well as in brain. This might be due to an overload of other transport molecules if Mn is chronically abundant in the body.

These findings substantiate previous research in our group and give even more insight into formation and pattern of Mn-species due to the different exposure parameters. As assumed, the main LMM species in neural tissue is Mn-citrate. Two possible complexes of Mn and citrate at physiological pH were studied by Matzapetakis et al. (Matzapetakis et al. 2000). Referring to the authors, in both cases Mn is six-coordinated and bound to two citrate molecules. In the Mn(II) state, the citrate is triply deprotonated whereas in the Mn(III) state, citrate is completely deprotonated. The oxidation state of Mn does for sure influence the uptake into brain. Some authors also suggest that Mn(III) is taken up by Tf-receptor-mediated processes whereas Mn(II) is readily taken up into CNS in its free form (Zheng et al. 2003). However, the Mn-citrate route seems to be preferred over the Tf route under exposure (J. S. Crossgrove et al. 2003). Accounting to the LMM fractions, the herein also highly abundant Mn-amino acids complexes, both in serum and brain, seem even conclusive for easy transport across neural barriers. As observed for other metals like Zn or Cu, a certain sulfur affinity can prompt binding of these metals to sulfur rich amino acids like cysteine or methionine as well as Mn was shown to likely bind to the carboxyl groups of amino acids in proteins (R. E. Gunter et al. 1975; T.E. Gunter and Puskin 1975). Moreover, after metal-induced deprotonation, also the nitrogen atom such as in histidine is free for coordination (Apostoli 2006). These complexations seem also to be plausible in the case of Mn, and would have eluted in the respective time frame of the applied SEC-ICP-MS method.

To conclude, the distribution of Mn into brain is mainly affected by its chemical species. Changes towards LMM carriers of Mn might already occur in serum – so before neural barriers. Already in 2000, Apostoli mentioned the measurement of different fractions and species as an important tool for understanding Mn toxicity (Apostoli et al. 2000). The difficult task regarding this issue is the development of standardized methods for analysis of this species in biological tissue, including very low concentrations, species changes and matrix interferences.

B.4   Changes in brain metabolism after Mn-exposure

So far, quite a number of studies addressing Mn-induced mechanisms of neuroinflammation or neurodegeneration on cellular and molecular level exist. Often, applied concentrations of Mn are in a toxicological range, where any neural damaging effects would be observed anyhow due to the applied concentration of Mn. Moreover, studies often concentrate on few endpoint metabolites or makers, where the connectivity between different possible mechanisms reveals missing. One major task of the work herein was therefore, to elucidate versatile neural mechanisms, which might be affected by a rather low-dosed Mn-exposure, applying non-targeted metabolomics. An aliquot of the neural tissue from rats of the feeding and the injection study were extracted with methanol and analyzed by ESI-FT/ICR-MS as described in chapter *D.8*.

B.4.1   Statistical analysis

With the objective to examine group separation behavior and to elucidate some discriminative masses, different statistical analysis were applied on the data matrix gained by matrix generator after calibration of mass spectra (see chapter *D.8.2*). Masses, which were abundant in less than two samples, were filtered out. In sum, 2644 masses remained in the matrix of the feeding study and 9865 masses remained in the matrix of the injection study. It should be repeated here, that the samples from the feeding study were measured separately from the samples of the injection study. As the matrix of the feeding study comprised such a low number of detected masses, measurement was repeated in the same samples and in additional fresh extracts (three per group) from residual brain tissue. The data matrix resulting from the new extracts included also only 2584 masses. The repeated measurement in the old extracts now gave 3535 masses within the matrix. Although the same extraction protocol was used for both studies (feeding and injection), the extraction in the feeding study seemed less effective or quantitative. It is conceivable that the residual brain tissue was not representative for the metabolite quantity of the whole brain due to the comparable low yield in all extracts and measurements from the feeding study. Due to these problems and unrepresentative data, an extensive comparison of feeding and injection study such as carried out in the preceding chapters could not be fulfilled. However, if changes in certain metabolite changes are given in both studies, this will be mentioned and explained (chapter *B.4.2.*).

Unsupervised data analyses were carried out for first overviews on possible group separation of data. Figure 88 in the *Appendix* shows the score scatter plots from PCA and Figure

43 shows observations from HCA. Data matrices from both studies (feeding and injection study) revealed no clear group separation by this unsupervised statistical analysis.
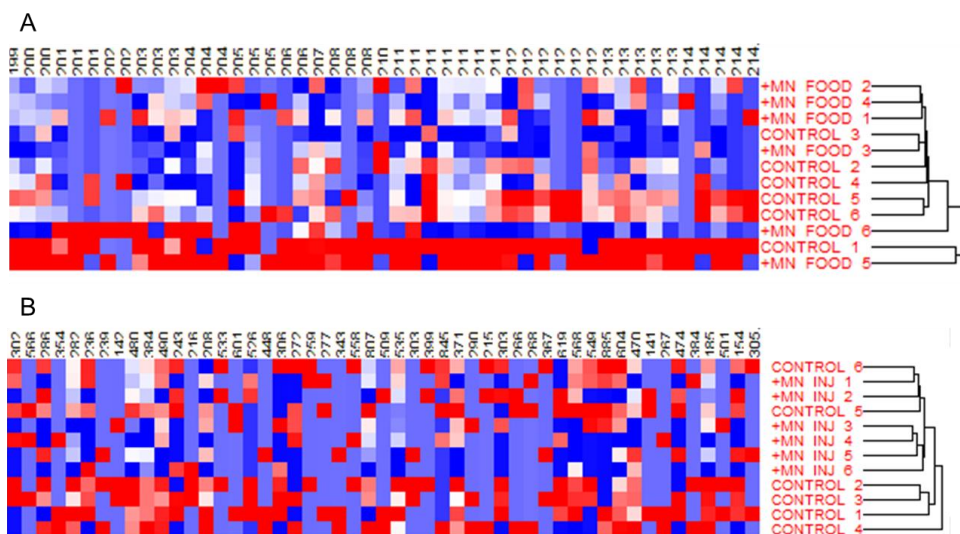
Figure 43 Unsupervised analysis of ICR/FT-MS data by HCA (except of the heat map).
Neither data from the feeding study (A) nor data from the injection study (B) showed a clear group separation by PCA or HCE.

Applying PLS-DA on the data resulted in a group separation between control and Mn-exposed animals according to the first component in both studies. Figure 44 shows score scatter plots for the PLS-DA analyses, which revealed a good model for the feeding study (R^2Y(cum)=0.578 and Q^2(cum)=0.692, Figure 44A)) and an excellent model for the injection study (R^2Y(cum)=0.98 and Q^2(cum)=0.728, Figure 44B).
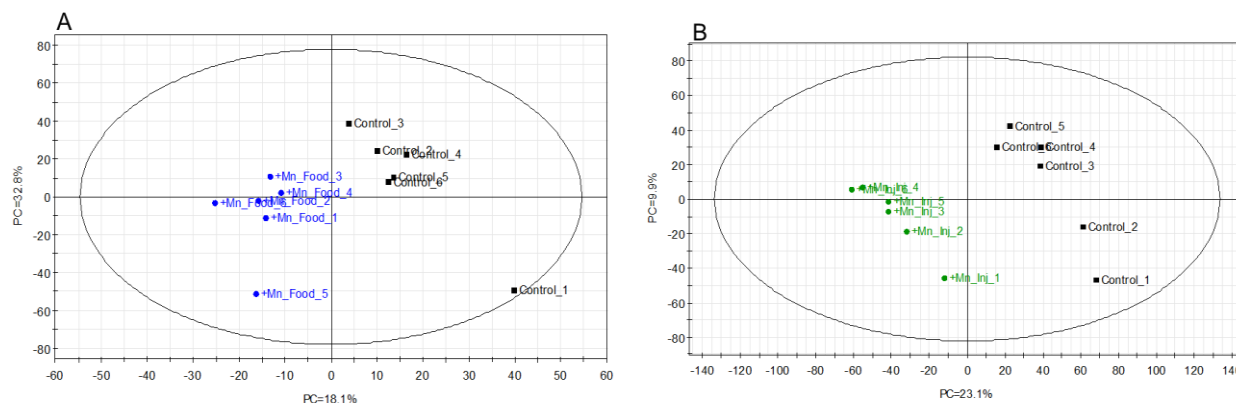
Figure 44 Supervised analysis of ICR/FT-MS data by PLS-DA (score scatter plots).
Both, feeding study (A) and injection study (B) revealed a group separation between control and Mn-exposed group according to the first component.

To obtain masses, which were discriminant for treated and untreated groups, OPLS-DA on the data was carried out. For this, data were scaled to unit variance and 7-point cross validated. Both exposure studies revealed good models according to values for the goodness of prediction and of fit (Feeding study: R^2Y(cum)=0.9 and Q^2(cum)=0.9; Injection study:

R^2Y(cum)=0.9 and Q^2(cum)=0.6; score scatter plots can be found in the *Appendix, chapter E.3,* Figure 89).

The masses from the data matrices were uploaded to MassTrix webserver as described in chapter *D.8.2* for annotation. For overview of numbers of detected, annotated and "important" masses according to statistical data analysis, Table 13 summarizes these features. The table reflects above mentioned problems with the data from the feeding study. As described, indeed a very small number of masses was detected at all in the samples from the feeding study. The part of annotated masses was comparable high (19.5%), but data showed in general no high significance between samples from control and Mn-fed animals (only 42 annotated masses had a p-value ≤ 0.05). For comparison, in the injection study 1332 masses were annotated from which 378 showed a p-value ≤ 0.05. The high variance between the samples from the feeding study was also seen in the differences in intensities of masses. The reason for this presently is not clear. A possible explanation could be an inhomogeneous extraction of tissue. Also conceivable is that the neural changes in metabolites were so different among each animal due to the uptake of Mn by food. Hence, every animal ingested other concentrations and metabolized differently from the other – compared to the injection, where every animal received exactly the same concentration of Mn and circumvented the influence of the gastrointestinal tract.

	Feeding Study	Injection Study
	All / annotated	
Detected masses	2644 / 515	9865 / 1332
p-value ≤ 0.05	161 / 42	2013 / 378
VIP ≥ 1.5 (OPLS-DA)	553 / 92	1377 /178
VIP ≥ 1.0 (OPLS-DA)	1973 / 356	3642 / 461

Table 13 Numbers of all detected, annotated and important masses of ICR/FT-MS analysis.

B.4.2   Pathway analysis

Non-targeted ESI-ICR/FT-MS analysis of brain samples served for investigation if also such minor concentrations of Mn could already alter the physiology of neural mechanisms. Neural mechanisms, which might have been affected by the applied Mn-exposure, were explored by pathway analysis via KEGG Mapper (http://www.genome.jp/kegg/tool/map_pathway2.html). This pathway analysis was therefore indicated for eventual detection of new mechanisms of

action of Mn-induced neural injury, whereby these mechanisms should be interlinked as far as possible.

Annotated masses, which had VIP values ≥1.5 according to OPLS-DA (discriminative masses) and a p-value ≤0.05 were considered for pathway analysis in the injection study. As the table above (Table 13) indicates, very few masses from the feeding study showed a VIP value ≥1.5 (only 92 annotated). To expand the working range, masses with VIP values ≥1.0 were considered for pathway analysis of the feeding study. However, in the following figures, results from the feeding study are only shown for relevant metabolites.

Pathways showing highest numbers of detected metabolites in uploaded data lists were considered as being important for describing metabolic changes in the brain due to Mn-exposure. Figure 45 compares the number of detected metabolites in the shown pathways according to uploaded annotated masses (KeggID) with regard to settings of VIP- and p-values. Under every criteria setting (VIP, p-value or both), the most metabolites counted belong to carbohydrate, amino acids, lipid and nucleotide metabolism. This was the case both in the injection as well as in the feeding study. Again it should be emphasized, that including VIP-values≥1.0 for data of the feeding study might result in some kind of over-interpretation of data and should only be seen as comparison/countercheck to the injection study.

Alterations in carbohydrate and amino acid metabolism might be a sign of failures in protein synthesis as well as energy production. A disturbed lipid metabolism is observed during lipid oxidation occurring under conditions of oxidative stress, which is also true for alterations in GSH metabolism. Additionally, alterations of the nucleotide metabolism can result in impaired RNA- or DNA synthesis. These possible mechanisms of action in neural tissue due to Mn-exposure will be discussed in more detail in the following subchapters in the frame of knowledge about neurodegenerative mechanisms in PD or Mn-exposure.
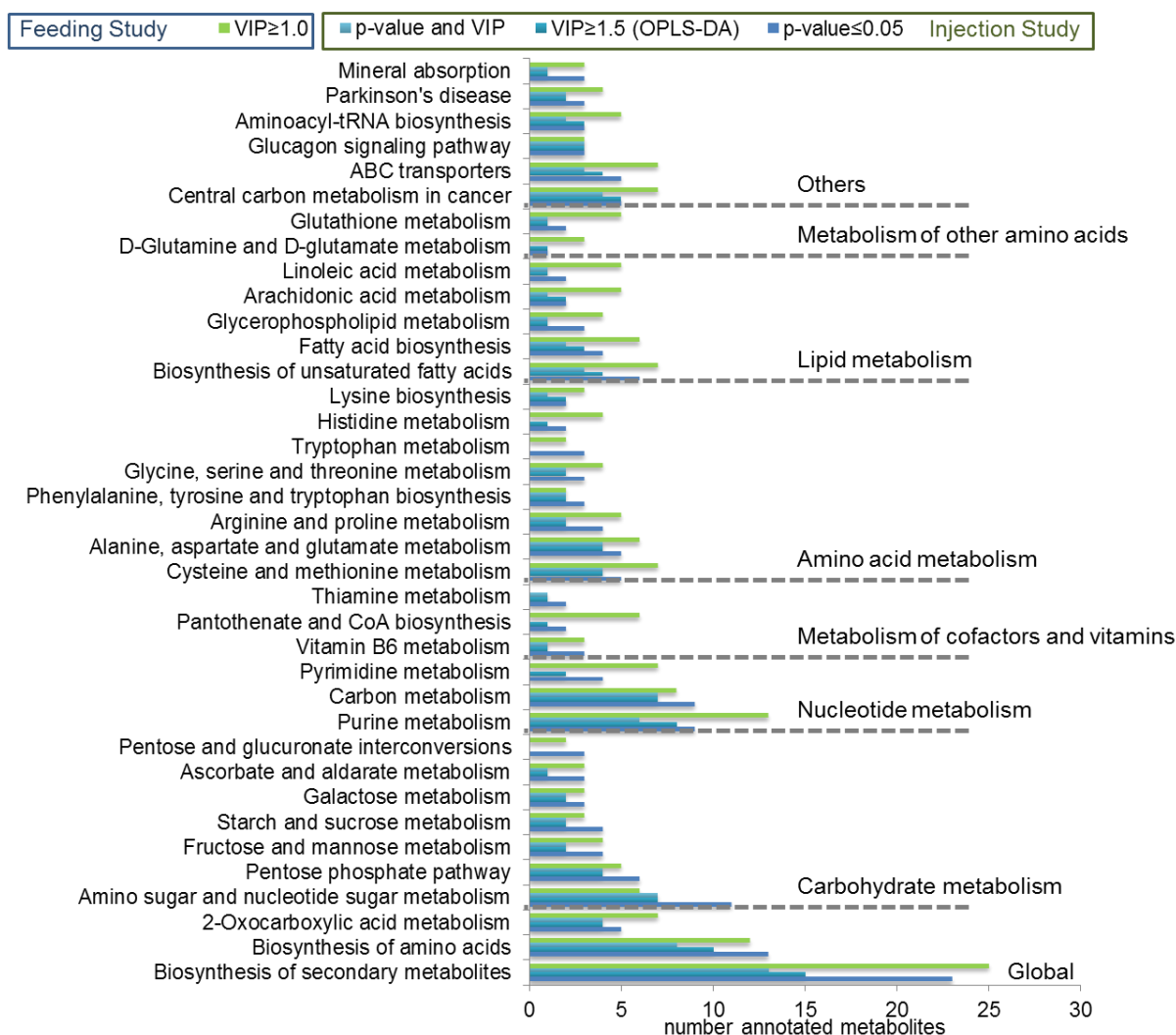
Figure 45 Pathway analysis via KEGG mapper.
In the injection study annotated masses with VIP- values≥1.50 (OPLS-DA), with p-values (Intensities)≤0.05 and annotated masses fulfilling both criteria were examined for comparison of number of annotated metabolites. In the feeding study annotated masses with VIP-values≥1.0 were also noted and pathway annotations were compared with the injection study to reveal an overview of important metabolisms.

B.4.2.1 Alterations in nucleotide metabolism

As shown in Figure 45, several metabolites belonging to the nucleotide metabolism were categorized as discriminative metabolites according to OPLS-DA (VIP values ≥1.5 and p-values≤0.05). Referring to classification by KEGG, pyrimidine, purine as well as carbon metabolisms rank among the nucleotide metabolism. Interestingly, nearly all detected metabolites belonging to the group of pyrimidines and purines were decreased in the brain extracts of Mn-injected animals (Figure 46A). Notable is the significant decline in the major purines guanosine, xanthosine, inosine and adenosine (Figure 46B), whereby adenosine and inosine were also significantly decreased in the brain of Mn-exposed animals in the feeding study.

Besides providing precursors for RNA- or DNA- synthesis, purine nucleosides are involved in a variety of neuronal processes (Hasko et al. 2004). Nucleotides such as adenosine, guanosine, inosine and uridine were also observed to have neuroprotective effects in several neurological insults, above others also during the pathophysiological insults in PD (K. Xu et al. 2005). For adenosine it was shown to possess anti-inflammatory properties by reducing toxic effects of oxygen radicals (Stone 2002). Failure in keeping up adenosine concentrations as observed herein could prompt formation of free radicals further exacerbating oxidative stress in the brain.

With inosine being the breakdown product of adenosine, their effects are mediated by adenosine receptors (A_1, A_{2A}, A_{2B}, A_3). A_{2A}-receptors are known to form heteromeric complexes with dopamine- and A_1-receptors enabling purines to fine-tune neurotransmission in the basal ganglia, the main affected brain area during Mn-exposure (Fuxe et al. 2007). Activation of A_1-receptors inversely regulates glutamate, serotonin and acetylcholine excretion further emerging neuroprotective effects (Cunha 2005). Overall, the reduction in purines like adenosine or inosine might lead to less active A_1-receptors and in turn to an increase of glutamate, serotonin or acetylcholine. Although the increase in glutamate was not very prominent in the injection study, it was observed in the feeding study (both, by in vitro assay (*E.1.2*) and ICR/FT-MS). As described above, too high concentrations of excitatory glutamate can promote neurotic effects in brain tissue. Moreover, an increase in AchE activity was observed in both exposure studies (*E.1.3*), which might be based on an enhanced need for degradation of increased acetylcholine due to reduced adenosine and inosine. A decrease in neural adenosine after chronic exposure of Mn in mice was also described by Villalabos et al. (Villalobos et al. 2001). The effect of Mn on adenosine receptor function and turnover might further be dependent on the brain region as found by these authors. Dorman et al. carried out a chronic inhalation of Mn in rhesus monkeys (Dorman et al. 2008). Correlation of brain Mn with blood guanosine was shown to be negative- meaning the more Mn in the brain, the less guanosine in the blood stream.

Overall, the reduction in physiologically important purines and pyrimidines could further explain the breakdown of neuroprotection during Mn-exposure. Such alterations of purine metabolism upstream of uric acid was also described in a metabolomics study of a PD model in mice (Johansen et al. 2009). This could indicate a further similarity in neurodegenerative mechanisms of both diseases.

One further interesting aspect of these observations regarding the purine and pyrimidine metabolism is the fact that some nucleotides such as GMP and AMP/ADP showed a

log2FC>0 in samples of Mn-exposed animals. Very early studies examined the binding capacity of Mn to nucleotides, and found a strong complex formation of Mn with AMP, ADP and ATP depending on the length of the phosphate residue (Walaas 1958). With Mn predominantly accumulating in mitochondria, this binding capacity with important nucleotides is of greater interest. Hence, it was also shown to be a cofactor of oxidative phosphorylation in mitochondria (Lindberg and Ernster 1954). In rat mitochondria, treatment with Mn^{2+} could prevent the Ca^{2+}-induced inhibition of ATP synthesis (Hillered et al.), whereby this control of ATP production by Mn was also proposed by other authors (Thomas E. Gunter et al. 2006). Moreover, a study on rat hippocampal membranes revealed that modulation of agonist binding on serotonin receptors by GDP and GTP was 10-fold less potent in the presence of Mn^{2+} than in presence of Ca^{2+}. This finding indicates a change in signal transduction complex (i.e. serotonergic receptor) mediated by Mn-nucleotide complexes (Parkel et al. 2011). Overall, these studies substantiate the assumption that the nucleotide status is favored by Mn over the dephosphorylated status (i.e. nucleoside) as also observed herein. A binding of Mn to the respective phosphate group is conceivable resulting in Mn-nucleotide complexes.
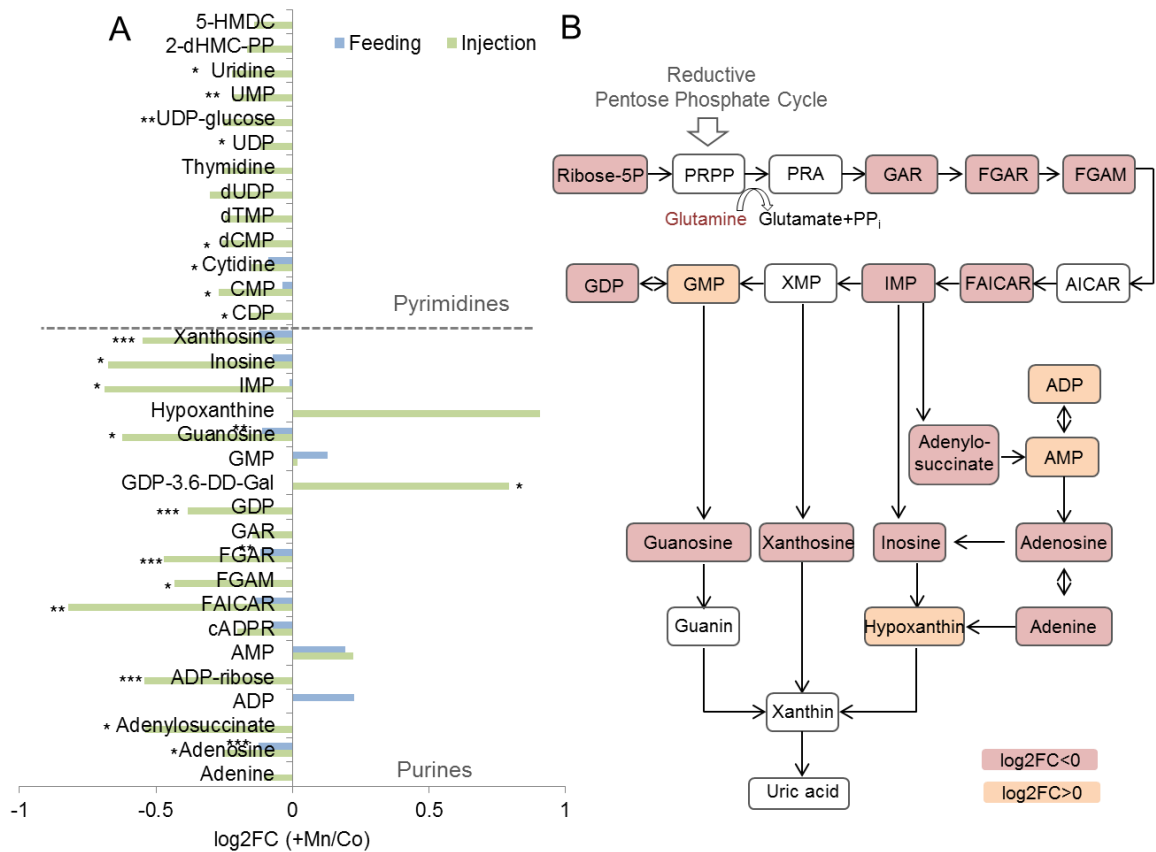
Figure 46 Alterations of metabolites in purine and pyrimidine metabolism in the brain.
(A) Log2 fold changes (FC) of detected metabolites are shown for purines and pyrimidines (Student t-test, *p<0.05, **p<0.01, ***p<0.001). (B) Major steps in purine metabolism were altered due to the single injection of Mn.

B.4.2.2 Alterations in reductive pentose phosphate cycle

As indicated in Figure 46, the precursor metabolite PRPP (5-P-alpha-D-ribose 1-P_2) for purine synthesis comes from synthesis of ribose-5P from the reductive branch of the pentose phosphate cycle (Figure 47). During this cycle, D-glucose is transformed to ribose-5P by various steps. Glucose is known to be one of the main energy suppliers for the brain with neurons using versatile intermediates for their maintenance (Mazzio and Soliman 2003). However, significant changes were in turn observed for this pathway after the single injection of $MnCl_2$. During the production of ribose-5P from D-glucose, NADPH is formed, which is keeping up a reducing milieu. However, this reducing milieu might not be able to be kept up due to the decrease in almost all metabolites of the pentose-phosphate pathway after the single Mn exposure. This is consistent with an *in vitro* study of Mn-treated neurons, which failed to compensate for mitochondrial dysfunction shown by an impaired flux of [1-^{13}C] glucose through pyruvate dehydrogenase (Zwingmann et al. 2003b). This pyruvate dehydrogenase is the rate limiting enzyme in the pentose phosphate pathway and was also shown to be reduced on protein level in the putamen of post mortem PD samples (Dunn et al. 2014b). In line with these findings was the impairment of oxidative energy metabolism after a single Mn injection directly into rat striatum (Brouillet et al. 1993). Moreover, Bowman and coworkers recently applied untargeted metabolomics in striatal cells of a Huntington´s disease model under treatment with $MnCl_2$ by UPLC-IM-MS/MS (Kumar et al. 2015). The results also implicated a disruption of energy metabolism by alterations in the pentose shunt pathway. Dysregulation of glucose metabolism is described as a common feature in the pathogenesis of PD with patients showing glucose hypometabolism (Dunn et al. 2014a). Interestingly, in rodents, selective inhibition of the pentose-phosphate pathway resulted in decreased NADPH levels, which overall globally produced a degenerative effect on dopaminergic neurons (Herken 1990). Due to the similarities of affected brain areas in manganism and PD, these observations can be considered as consistent. They might therefore help to further explain the pathogenic mechanisms occurring in dopaminergic brain areas during Mn-exposure.
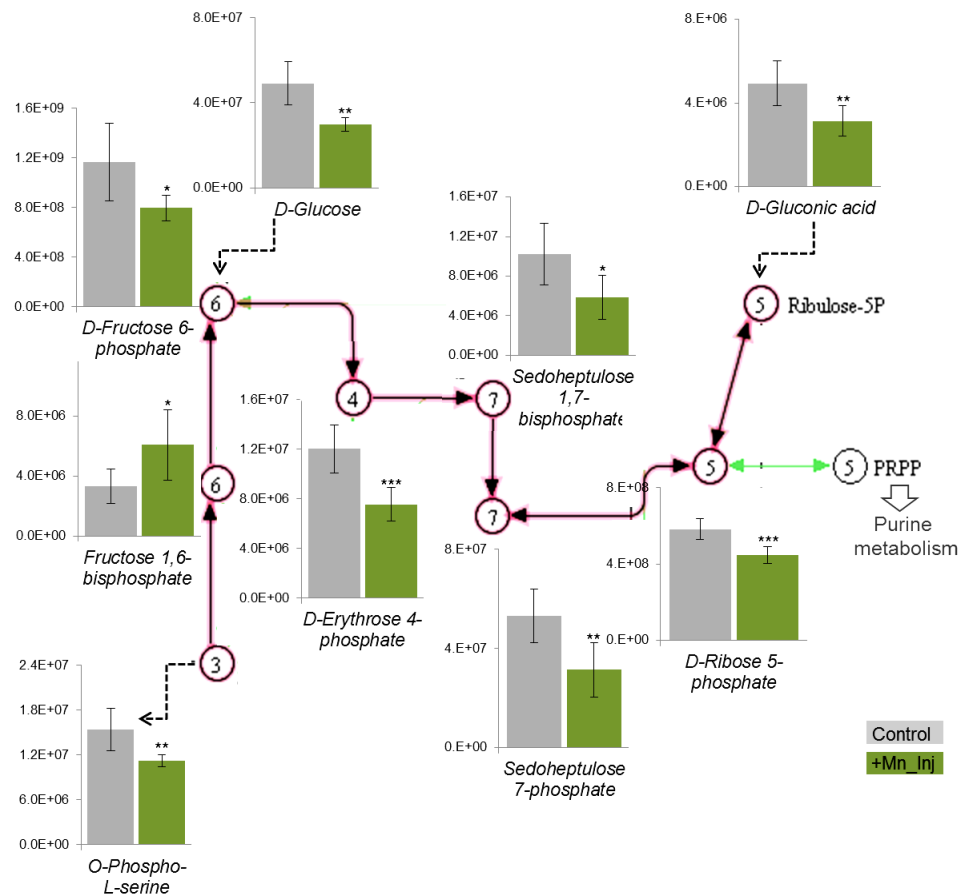
Figure 47 Alterations in the reductive pentose phosphate cycle after injection of Mn.
The pink path shows the different steps of the reductive pentose cycle (numbers indicate C atoms).
Differences in the single metabolites according to detected intensities are shown by column charts.
Dotted arrows represent multi-step reactions.

B.4.2.3 Alterations in glutathione metabolism

As indicated before, glucose serves for various neural reactions in brain. Hence, the pentose phosphate pathway is the predominant source for regeneration of NADPH, which is also needed for glutathione (GSH) cycling in the brain. The major steps of GSH metabolism are illustrated in Figure 48 with determined altered metabolites shown in colors. The tripeptide GSH consists of the amino acids glutamate, cysteine and glycine, and is a major mediator of detoxification of ROS in brain (Dringen 2000). During this, GSH either reacts non-enzymatically with radicals (e.g. superoxide radical anion) or it acts as electron donor for reduction of peroxides via GPx (Singh et al. 1996). The oxidative product is glutathione disulfide (GSSG). Under physiological conditions, there exists a very well balanced ratio between GSH and GSSG with functioning enzymes GPx and GR (glutathione reductase).
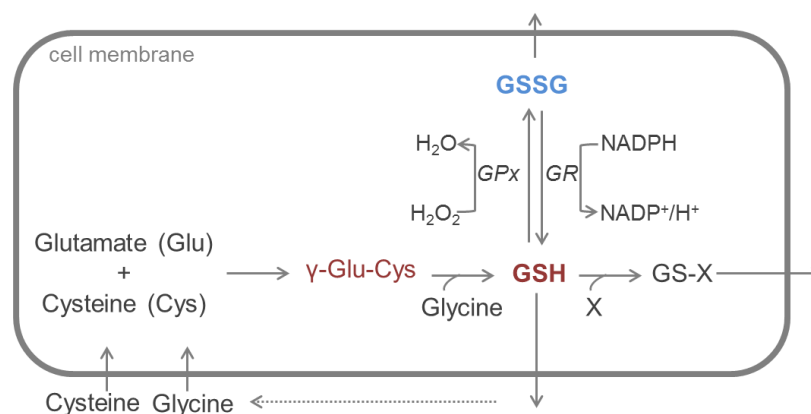
Figure 48 GSH metabolism and alterations due to Mn exposure.
GSH is produced by reaction of glycine with γ-Glu-Cys. X is a substrate of glutathione-S-transferase (GST). Intracellular GSH levels are regulated by a negative feedback loop of produced GSH to γ-Glu-Cys synthetase. Under physiological conditions GSH and GSSG (glutathione disulfide) are balanced by function of GPx (GSH peroxidase) and GR (GSH reductase). Colored words were altered due to Mn-exposure (blue: increased, red: decreased compared to control).

However, under circumstances of oxidative stress, alterations in levels of GSH, GSSG and activity of GPx were observed. Such disturbances are a hallmark of several neurological disorders such as Alzheimer´s disease or Huntington´s Disease, and are also described in PD (Dringen 2000). It is not surprising, that studies in patients suffering of PD showed up to 40% decreased levels of GSH in substantia nigra (Sian et al. 1994). A significant decrease in GSH was also observed after the single injection of $MnCl_2$ in the brain extracts herein (p=0.007). Moreover, the precursor dipeptide γ-Glu-Cys as well as the GSH hydrolysis product L-Cys-Gly-disulfide were significantly lowered in Mn-exposed animals (p=0.042 and 0.009, respectively). A lowered GSH level is thought to be a first indicator of oxidative stress during the progression of PD (Nakamura et al. 1997) and can be seen as such due to the applied Mn exposure. Although an increase in GSSG was only indicative in the injection study, this oxidation product of GSH was significantly increased in the feeding study in the brain of Mn-fed animals (p=0.008). Taking together these findings, Mn-exposure was observed to alter the balance between GSH and GSSG being indicative of neural oxidative stress. Depletion of GSH in striatum and the olfactory bulb was also described in neonatal rats exposed to airborne Mn (M. D. Taylor et al. 2006). An increase in GSSG was detected in that study in the cerebellum of the high dose exposed pups. Based on a similar study previously carried out in rats, the authors claim that these signs of oxidative stress might be reversible. Moreover, the concentrations of Mn, to which animals were exposed to, exceeded the inhalation reference concentrations (US EPA) by a factor of 100-1000. Substantiating the point of reversibility, Hernandez et al. described decreased GSH levels at high Mn concentrations and increased GSH levels at low Mn concentrations *in vitro* in two different neural cell lines (Hernandez et al. 2011a). These observations might also partially explain the

fact that GSH was significantly reduced in the injection but not in the feeding study whereas GSSG was found to be significantly increased in the feeding study but showed only trends in the injection study compared to control. Interestingly, GSH regulation after Mn exposure might be dependent on the brain area. Monkeys exposed to airborne Mn for 65 days showed increased GSH in the putamen and decreased GSH in the caudate in the highest Mn exposure group (Keith M Erikson et al. 2007). Such regional differences get merged when analyzing the whole brain. Moreover, in the mentioned study by Hernandez et al., ascorbate could protect one cell line from Mn-induced neurotoxicity acting as anti-oxidative substrate and as energy supplier for neurons. In the brain of Mn-injected animals, ascorbate was found to be significantly reduced ($p=0.009$), what could have further aggravated oxidative stress events in the brain due to less protection of neurons.

The determined decrease in GSH as observed in the injection study could also be explained by malfunction of enzymes involved in GSH metabolism. Hence, the decrease of GSH precursor accompanied by tendentially increased glutamate is indicative of malfunction of the γ-Glu-Cys or GSH synthetase due to Mn-exposure. The GSH-S-transferase (GST) acts by adding substrates to GSH to reduce cellular oxidative stress. Its expression was shown to be reduced in PD progression (Whitworth et al. 2005). This is consistent with the observed reduction in the GSH hydrolysis product herein. Interestingly, a reduction in expression of that gene encoding the GST homologue in C. elegans led to an increase in dopaminergic neural cell death (Vilar et al. 2007). Taken together, the described alterations in GSH metabolism could be a further explanation of inactive defense against oxidative stress induced by Mn in neural tissue.

B.4.2.4 Alterations in amino acid metabolism

The linkage of purine metabolism with amino acid metabolism was already mentioned above, which is based on the interaction of adenosine with dopamine receptors. Hence, many neurotransmitters are amino acids, which excretion might be affected by this interplay. Similar to observations for the detected nucleotides, major amino acids were reduced in the brain of Mn-exposed rats compared to control. Enzymes of amino acid synthesis, which are known to be modulated by Mn are the tyrosine hydroxylase (TH) as well as the glutamine synthetase (GS). TH is the rate limiting enzyme in dopamine synthesis, whereby a reduction in neural dopamine levels due to Mn-exposure was described in several studies (K. M. Erikson et al. 2008; Guilarte et al. 2006; X. Liu 2006) suspecting an inactive or less active TH. However, the activity of TH might depend on duration of Mn exposure as described by Zhang et al. (D. Zhang et al. 2011). Applying a chronic low-dose concentration of Mn on dif-

ferentiated dopaminergic cells decreased TH activity whilst the acute Mn-treatment (although with higher concentrations) increased TH activity. Herein, not dopamine but it´s precursor amino acid L-tyrosine was detected in both exposure studies and showed reduced concentrations in samples of Mn-exposed animals. The breakdown of dopamine described during Mn-exposure might therefore not solely be based on an inhibition of TH but rather in failure of dopamine synthesis due to less abundant L-tyrosine. This could also explain the controversial findings of Zhang et al. As Mn exposure was related to deposition of the element in the dopaminergic structures within the brain, the mechanisms of dopaminergic dysfunction were examined in versatile studies. One common outcome is that the dopaminergic neurons itself seem not to be injured (Guilarte et al. 2006). There is rather a dysfunction of dopamine synthesis and/or release, which is in line with our findings and which could be based in an early step of synthesis, namely at the stage of L-Tyrosine.

As mentioned above, Mn is cofactor of the GS and is therefore involved in synthesis of glutamine from glutamate by addition of ammonia (Pratap Karki et al. 2013). Deng et al. described an inhibition of GS in astrocytes when treated with Mn – again dependent on applied concentrations (Deng et al. 2012). In the *in vivo* model carried out by Erikson et al., rats were exposed to inhalative Mn in three different concentrations for almost three weeks (K. M. Erikson et al. 2006). Despite the findings by Deng et al., all three applied concentrations of Mn led to the reduction of GS protein levels as well as mRNA in certain brain areas. Consistent with an inactivation of GS by Mn are the findings herein with increased glutamate and reduced glutamine levels in both studies. However, glutamate increase was more prominent in the feeding study (also observed in the *in vitro* assay) while glutamine decrease was only significant in the injection study. Nevertheless, these observations might again depend on duration of Mn-exposure (as discussed in *E.1.2*) explaining the different outcomes.

Among the detected and decreased amino acids, nine belong to the group of the 20 proteogenic amino acids. These alterations could have resulted in a failure of protein synthesis necessary for optimum functioning of the brain. Moreover, these findings are consistent with Bonilla et al. (Bonilla et al. 1994). In that study, mice were daily injected with 5 mg Mn/kg b.w. intraperitoneal for nine weeks resulting in a reduction of 20 free amino acids in the olfactory bulb.
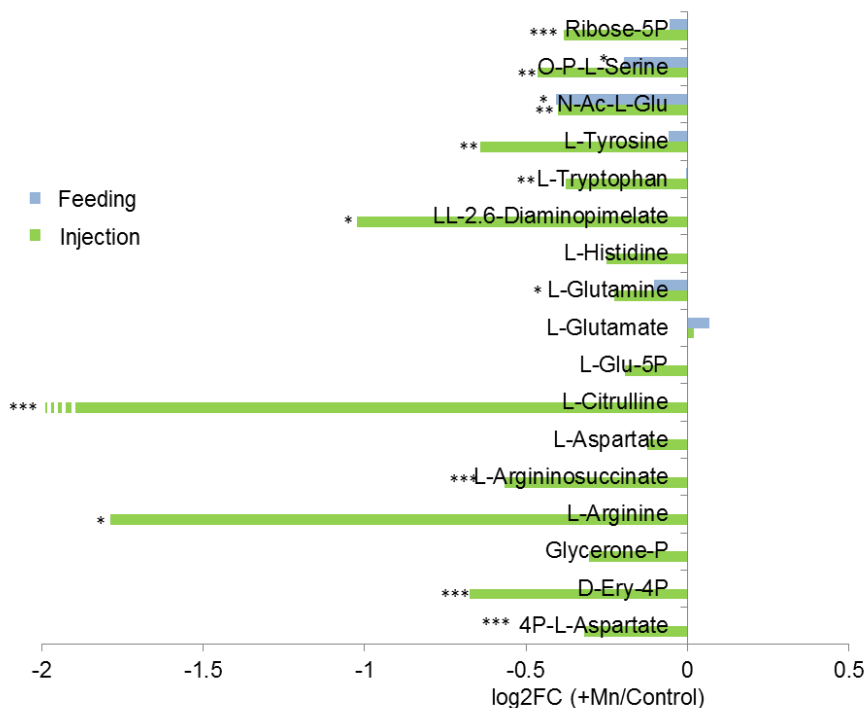
Figure 49 Alterations in amino acid metabolism.
Log2 FC of detected metabolites with respective significance between +Mn and control are shown for injection study (green) and feeding study (blue).

B.4.2.5 Alterations in lipid synthesis

As shown in Figure 50, saturated as well as unsaturated fatty acids were detected in brain extracts, where the majority was again significantly decreased due to the single injection of MnCl$_2$. Neuronal membranes are rich in fatty acids as they possess important roles in neural signaling and maintenance of functionality. Saturated and monounsaturated fatty acids are synthesized in brain whereas polyunsaturated fatty acids (PUFAs) are taken up by diet and get transferred to brain by blood (Bazinet and Laye 2014). Examples for precursor PUFAs from diet are linoleic acid (18:2, ω-6) and α-linoleic acid (18:3, ω-3). During events of oxidative stress in brain, fatty acids are targets for oxidative degradation induced by free radicals, also known as lipid peroxidation (Rassow et al. 2006). Due to the presence of double bonds with highly reactive methylene groups in between, PUFAs can be mainly affected by this peroxidation. The phenomenon of lipid peroxidation has been described for several neurodegenerative diseases, which is reviewed in (Reed 2011). The herein detected reduction overall in PUFAs but also in other fatty acids in the neural tissue of Mn-exposed rats could therefore be indicative of an attack of neural lipids by lipid peroxidation.

Docosahexanoic acid (DHA, 22:6, ω-3) and arachidonic acid (ARA, 20:4, ω-6) belonging to the group of PUFAs are known as potent antioxidant in brain. Hence, the resulting products

from oxidation comprise certain toxicity and were found to be linked to neurodegenerative disorders such as PD (Maruyama et al. 2014). The observed reduction in both, DHA and ARA after the single Mn injection could be a hint for the loss of antioxidative defense mechanisms in brain. Mn-induced lipid peroxidation was also reported by Lebda et al. in brain and liver of rats receiving daily injections of $MnCl_2$ (6 mg/kg b.w.) for 20 days. Interestingly, this lipid peroxidation could be prevented by pretreatment of rats with lycopene, which did not decrease Mn concentrations but exhibited antioxidative properties to examined tissues (Lebda et al. 2012). Moreover, fungal Mn-peroxidase in presence of Mn^{2+} as well as the addition of Mn^{3+} was tested for lipid peroxidation of several PUFAs (Kapich et al. 2011). It turned out that the oxidation rate was independent on degree of saturation as well as that linoleic acid (18:3, ω-3) was most easily oxidized by Mn. Although very little is known about Mn-induced lipid peroxidation it is discussed to involve intermediate steps or molecules as Mn is not able to directly generate hydroxyl radicals from H_2O_2 or superoxide (Farina et al. 2013). The formation of such radicals by other divalent metals was shown for example for Fe^{2+} or Cu^{2+}. An interplay of Mn with these, finally leading to attack of membrane phospholipids, hence, cannot be excluded based on the findings in the feeding study herein (e.g. altered Fe and Cu levels in brain and serum; increased Fe(II)/(III) ratio). Interestingly, in the above mentioned study by Lebda, Fe and Cu homeostasis was also altered in Mn-exposed animals. All in all, the reduction in the detected neural fatty acids herein is in line with the other studies indicating initiation of lipid peroxidation during Mn-induced neurodegeneration.

DHA is known to be metabolized to resolvins and neuroprotectins whereas ARA is transformed to prostaglandins and eicosatetranoic acids. Some of these were also detected by ICR/FT-MS with results shown in the Figure 50. It seems as if the pool of the major PUFAs DHA and ARA was depleted after Mn-exposure whereas some of their lipid mediators were increased compared to control (e.g. 15(S)-HETE, PGB1, ResolvinD2). These lipid mediators are known to be increased in neurodegenerative diseases indicating an activation of inflammatory response via the COX- or LOX-pathway (Bazinet and Laye 2014), where latter was described to be involved for example in AD (Pratico et al. 2004). Depending on its duration and extend, neural inflammation can act as protection for uninjured neurons and for assistance of repair and recovery processes in brain (Farooqui et al. 2007). This might be the case herein, as the impact of Mn was very short so that the production of neuroprotectins could have been ongoing at time point of sampling.

Further interesting is the fact that neural DHA levels can be interrelated to other important metabolisms in brain such as glucose and neurotransmitter cycling. Firstly, reduced levels of DHA in brain were associated with decreased activity of cytochrome oxidase as well as de-

creased GLUT1-mediated glucose uptake in rats (Pifferi et al. 2005). Secondly, dietary intake of PUFAS not only increased DHA but in turn also serotonin and dopamine as well as decreased TH activity (Bondi et al. 2014; Chalon 2006). Therefore, the observed Mn-induced DHA depletion could have promoted a reduction of glucose uptake as well as a decrease in dopamine. Based on this example, various observations after Mn-exposure, which have been facilitated by the analysis of brain extracts by ESI-ICR/FT-MS, could have been brought in a bigger context.
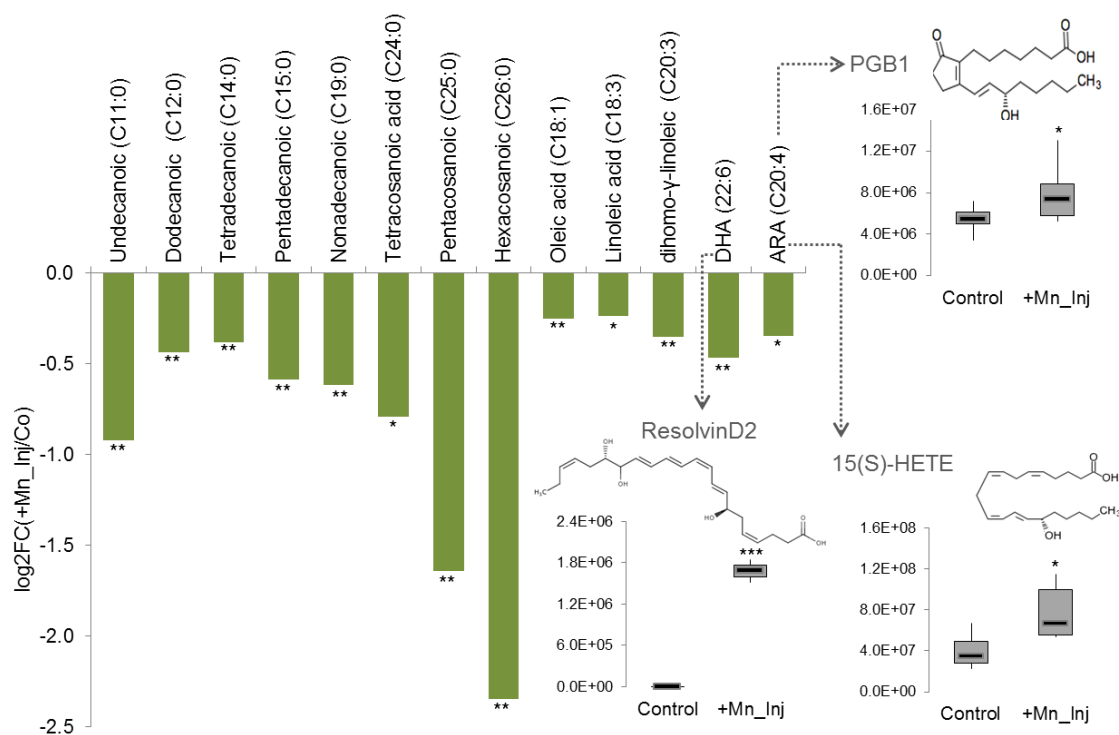
Figure 50 Altered fatty acids and some oxidative metabolites.
Single injection of MnCl2 led to a significant decrease in several un- and saturated fatty acids indicating occurrence of lipid peroxidation in neural tissue (the word acid was left out due to space and in braces indicated are the number of C atoms:number of double bonds). Oxidative metabolites of DHA and ARA such as ResolvinD2, PGB1 and 15(S)-HETE were significantly increased compared to control as sign of inflammatory response.

B.4.3   Conclusions of major alterations in metabolism of the brain

Due to the already above discussed problems with measurement of samples from the feeding study, only some major or important metabolites were included for comparison of changes in metabolic pathways. Nevertheless, those metabolites which were detectable showed the same trend of involved alterations as observed in the analysis of samples form the injection study. A summary of above discussed findings is illustrated in Figure 51 showing only results from the analysis of samples of the injection study regarding to the elaboration criteria (VIP-values ≥1.5 and p-values ≤0.05). In general, fold changes in metabolites between Mn-exposed and control samples were often very low. This could be based in the low concentrations of applied Mn, which might not have resulted in such major changes as working

in really toxicological concentrations. However, very interesting changes in lipid, reductive pentose phosphate, amino acid, nucleotide and GSH metabolism in the brain could be observed after this single low-dose exposure of Mn. Based on the figure and the above discussed connections between these metabolisms, it becomes obvious that multifactorial processes lead to the ongoing inflammatory events in the neural tissue after Mn-epxosure. The application of ESI-ICR/FT-MS therefore facilitated to observe linkages between the various altered metabolisms discussed in literature. This study serves for a detailed overview of the highly complex mechanisms in brain after Mn exposure summarizing the above discussed results.
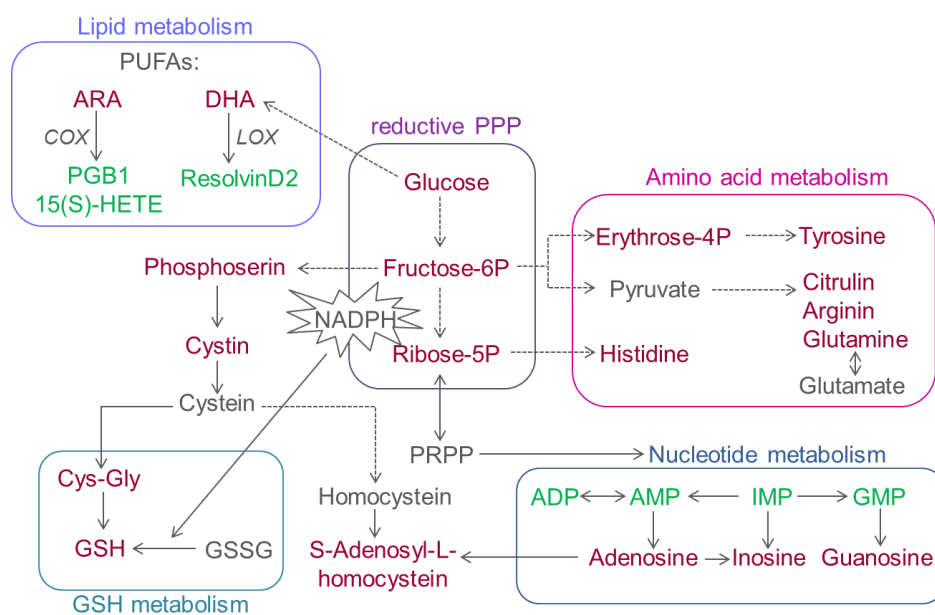
Figure 51 Conclusion of pathway analysis from ICR/FT-MS data (analysis of brain extracts from the injection study).
The interplay of the major altered pathways is shown by discriminative metabolites (green: increased intensities, red: decreased intensities in Mn-exposed animals; gray: not detected).

To our knowledge, only three studies investigating Mn-induced neurodegeneration by application of metabolomic approaches have been carried out so far: the first one was published by Dorman et al. in 2008 where rhesus monkey were exposed to airborne $MnSO_4$ five days a week in different concentrations for 65 days (Dorman et al. 2008). Blood and urine were analyzed by LC-TOF-MS in positive and negative ionization mode. The authors confirmed 27 metabolites with statistically significant expression differences by MS-MS. These were related to oxidative stress and neurotransmission. Some findings were consistent with observations herein, such as a decrease in glutamine, citrullin or adenosylhomocystein. In sum they determined 113 significantly perturbed metabolites with several not found herein. In a second study, mice were treated i.p. with 25 mg/kg $MnCl_2$ for 21 days by co-infusion of ^{13}C-labeled glucose and acetate (Bagga and Patel 2012). Applying ^{13}C-[^1H]-NMR spectroscopy

in brain extracts, for example reduced glutamate was observed in thalamus and hypothalamus, which seems to be controversy to literature. Moreover, glucose oxidation was impaired in glutamatergic neurons substantiating the discussed loss of energy during Mn-exposure. This is in line with the observations herein, where disturbed pentose phosphate cycling also indicated a lowered energy metabolism in brain. A further study carried out by Fordahl et al. (Fordahl et al. 2012) investigated the effects of 1 g Mn/l in drinking water for six weeks on liver, plasma and brain metabolism in rats. Analysis by LC-/GC-TOF-MS revealed in total 98 significantly altered metabolites in these matrices. Most prominent alterations were observed for cholesterol and fatty acid metabolism in the brain such as an increase in oleic and palmitic acid. These findings are controversy to the decreases in lipid metabolism found herein. However, a decrease in major fatty acids seems to be more conceivable with regard to lipid peroxidation and loss of energy production. Also controversy was the described increase in N-Acetylaspartate (NAA), which was found to be correlated with structural damage and neuronal loss according to literature (Demougeot et al. 2001). Herein and also in a Mn-exposure study in monkeys (Guilarte et al. 2006) lowered NAA concentrations were determined in exposed animals, substantiating an alteration in neuronal integrity or density. In line with the work herein was a breakdown of amino acid metabolism in plasma in the study of Fordahl et al. However, it should be emphasized that the applied concentration of Mn in drinking water by the study of Fordahl et al. exceeded the drinking water concentrations of Mn according to WHO guideline for drinking water by a factor of 20000 (recommended level is 0.05 mg/l, (WHO 1996)). Hence, observing major changes in metabolism by application of such high concentrations seems not surprising. The results from the mentioned studies are again an evidence for the different influences on alterations of metabolism attributed to duration and concentration of investigated Mn exposure.

To conclude, the application of direct infusion ICR/FT-MS allowed for analysis of complex metabolites mixtures with very high mass accuracy and resolution. By this, effects on neural mechanisms induced by only slightly increased Mn concentrations were detectable. The application of ICR/FT-MS serves in many areas for untargeted analysis of metabolomic changes for elucidation of all sorts of mechanisms (e.g. host-pathogen interactions (Muller et al. 2013) or systemic diseases such as obesity (Walker et al. 2014)). Hence, also elucidation of neurodegenerative diseases is addressed by such approaches, which is nicely reviewed in (Jové et al. 2014). Lin et al. detected several metabolites in a genetic mutated mice strain of AD by ESI-FT/ICR-MS analysis of hippocampal tissue (Lin et al. 2013). They further identified selected metabolites by MS/MS fragmentation after chromatographic separation. Such counterchecking of detected metabolites by ESI-ICR/FT-MS in comparison with other metabolomics technique such as LC-MS(/MS) would be a future step in the topic of this

work. Not only more metabolites might be detected and already detected metabolites could be assured. Overall, it still remains unknown if observed alterations in metabolite levels are a direct consequence or rather a phenomenon to the cause of the certain disease. This has to be considered with regard to biomarker identification. Even in the case of PD, no fully validated biomarker is currently available although numerous potential ones have been identified (A.-h. Zhang et al. 2013). To find such indicators before the onset of disease, definite elucidation of metabolic pathways and fluxes during disease progression and also in healthy subjects has to be carried out. With regard to Mn-induced neurodegenerative diseases, such approaches are still in the early stages. However, with the work herein, a further step towards the connection of versatile acting mechanisms could be given.

B.4.4   Formula Calculation and Network analysis for deciphering possible Mn-binding compounds

Eventually abundant Mn-complexes in the methanolic brain tissue extracts could have been detected by ESI-ICR/FT-MS. However, these were not annotated by MassTrix as the calculation of formulas is restricted to C, H, O, N, P and S as described in chapter *D.8.2*. The software Formulae1 (FormCalc, written by Dr. M. Frommberger) was applied to calculate compound formulas based on C, H, O, N, S and Mn within the same mass list, which was used for MassTrix annotation (error 0.2 ppm). This calculation was carried out on data from the injection study due to the low number of detected mass signals in the feeding study.

The van Krevelen diagrams in Figure 52A and B should serve for an overweiv on H/C vs. O/C ratios of the calculated formulas by comparing formulas with and without Mn. As discussed in D.8.3.3 (Figure 79) this plot enables a qualitative presentation of the composition of a sample due to the localization of certain areas describing metabolite classes. The Mn-less calculated formulas showed highest density at the upper left and the upper middle area of the plot, which represent areas of small acids and amino acids (Figure 52A). When considering the Mn-containing formulas (Figure 52B), the calculated formulas can be distributed more or less over all areas. However, some very dense areas were outstanding, such as the area of amino acids, the area of small acids as well as the area in the lower left corner. The fact that this region illustrates dehydrated compounds ($-H_2O$) lets suggest the necessity of cleavage of water for the binding of Mn to the various structures.

Figure 52C depicts the number of calculated formulas for each "class of calculated formulas" (CHO vs CHOMn, CHNO vs CHNOMn, CHNOS vs CHNOSMn). The bars show increasing

numbers of calculated formulas with increasing abundance of N or S in the sum formulas both, for Mn-less and for Mn-containing formulas. Interestingly, the ratios of Mn-containing vs Mn-less formulas was highest for S-containing formulas with almost 90% of CHNOSMn. This observation could mean that Mn preferentially binds to S-rich compounds, which is further interesting with regard to its biological meaning.
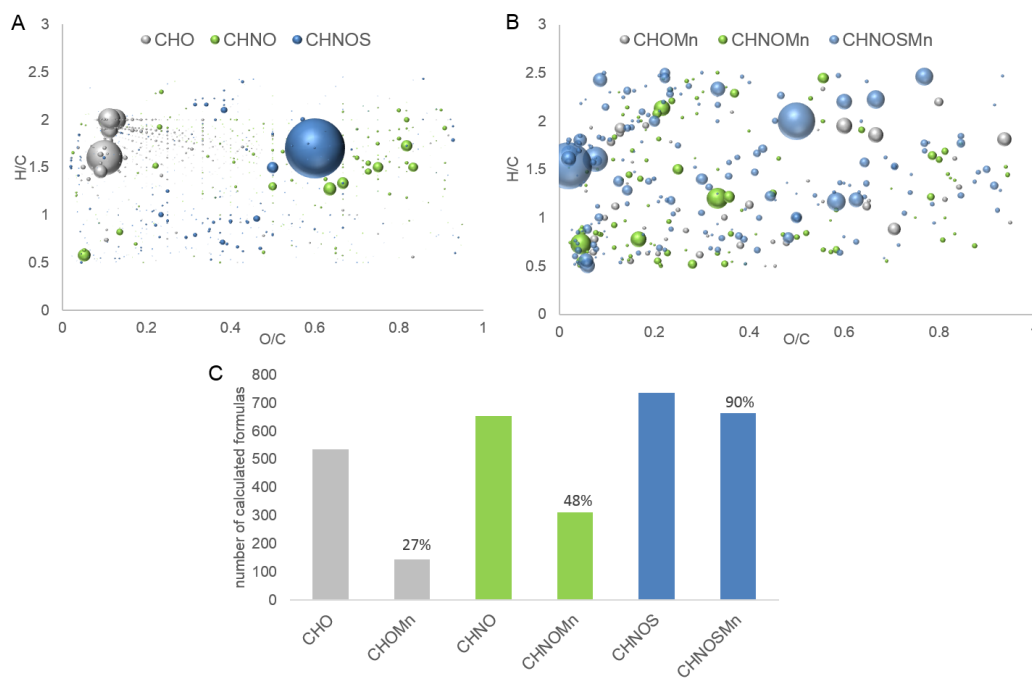
Figure 52 Application of Formulae1 for calculation of eventually occurring Mn-containing formulas. Van Krevelen diagrams showing calculated Mn-less formulas consisting of C, H, N, O and S (A) and showing calculated Mn-containg formulas consisting of C, H, N, O, S and Mn (B). The column plot shows the number of totally calculated formulas and the respective ratio of Mn containing formulas vs Mn-less formulas in %.

For further evaluation of interesting metabolites, the focus was given on S-containing formulas which were classified as amino acid according to the van Krevelen plot. Calculated sum formulas with and without Mn were searched against Chemspider database (http://www.chemspider.com/). By this procedure, every formula had to be analyzed step by step due to the absence of a batch analysis mode. Moreover, there are only very few Mn-containing formulas abundant at all in databases like Chemspider. During one attempt, calculated Mn-less formulas containing H/C ratios from 1.0-1.2 and O/C ratios from 0.6-0.7 (Figure 52A) were examined. One of these formulas was $C_9H_{11}NO_6S$ (M-H$^-$: 260.02347), which gave 32 search results, including the compound O-Sulfo-L-Tyrosine. With regard to this formula, one calculated Mn-containing formula with similar H/C and O/C ratios was $C_{14}H_{17}N_2O_9SMn$ (M-H$^-$: 442.99632). Suggesting that for binding of Mn an elimination of H_2O is necessary, the respective H_2O-containing and Mn-missing formula is $C_{14}H_{19}N_2O_{10}S$. The difference between this formula and O-Sulfo-L-Tyrosine is $C_5H_8NO_4$, which could represent the glutamate ion according to Chemspider based on the sum formula. Therefore, one pos-

sible composition of the above mentioned found Mn-containing formula ($C_{14}H_{17}N_2O_9SMn$) could be the complexation of Mn by the reaction of O-Sulfo-L-Tyrosine with glutamic acid by the loss of H_2O (condensation) and one H for binding of Mn as illustrated in Figure 53A. The mass peaks of both amino acids and their reaction product containing Mn are shown exemplarily by one sample in Figure 53B. Interestingly, also a mass peak, which could represent the dehydrated O-Sulfo-L-Tyrosine could be observed. The final structure of the Mn-glutamyl-sulfo-tyrosine complex as shown in the figure is only a suggestion. Hu et al. studied the influence of peptide side chains on the metal ion binding side in metal ion-cationized peptides by tandem mass spectrometry (Hu et al. 1995). They found out that the immonium and $[a_n\text{-}H]^+$ ions are preferentially formed during fragmentation of Ni^{2+} or Co^{2+} complexes, however, several more ions are formed from Fe^{2+} and Mn^{2+} complexes. However, if the metal is bound to N, the authors propose that tyrosine will coordinate the metal primarily via its aromatic ring. It is known that amino acid side chain groups form weak interactions with metals such as hydrogen bonds, π-π stacking or hydrophobic interactions for recognition of substrates and catalytical functioning of enzymes (Burley and Petsko 1988). However, the shown complex is only a suggestion; for unraveling the exact complex formation, further investigations such as fragmentation analyses or NMR analysis are needed (Sheats et al. 1987). However, it has to be considered that Mn^{2+} or Mn^{3+} cannot be detected directly in solution due to the paramagnetic properties of the ^{55}Mn nucleus (Ronconi and Sadler 2008). Additionally, X-ray absorbance near edge structure spectroscopy of such model complexes would allow the determination of the oxidation state of Mn within these structures (Thomas E. Gunter et al. 2004).

B
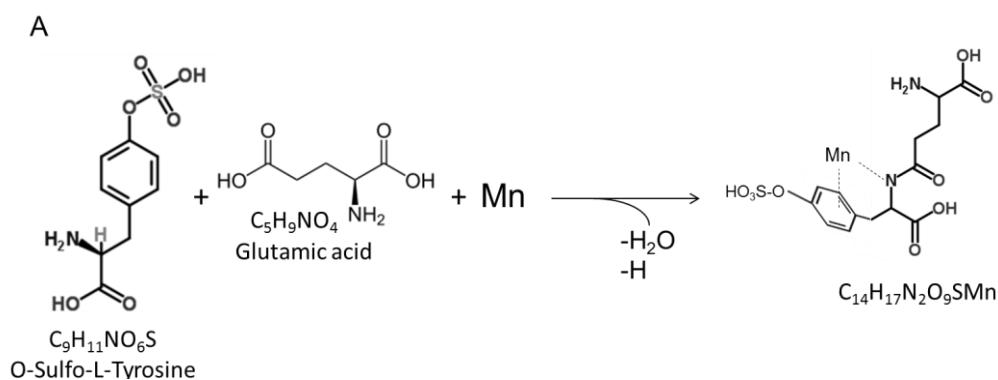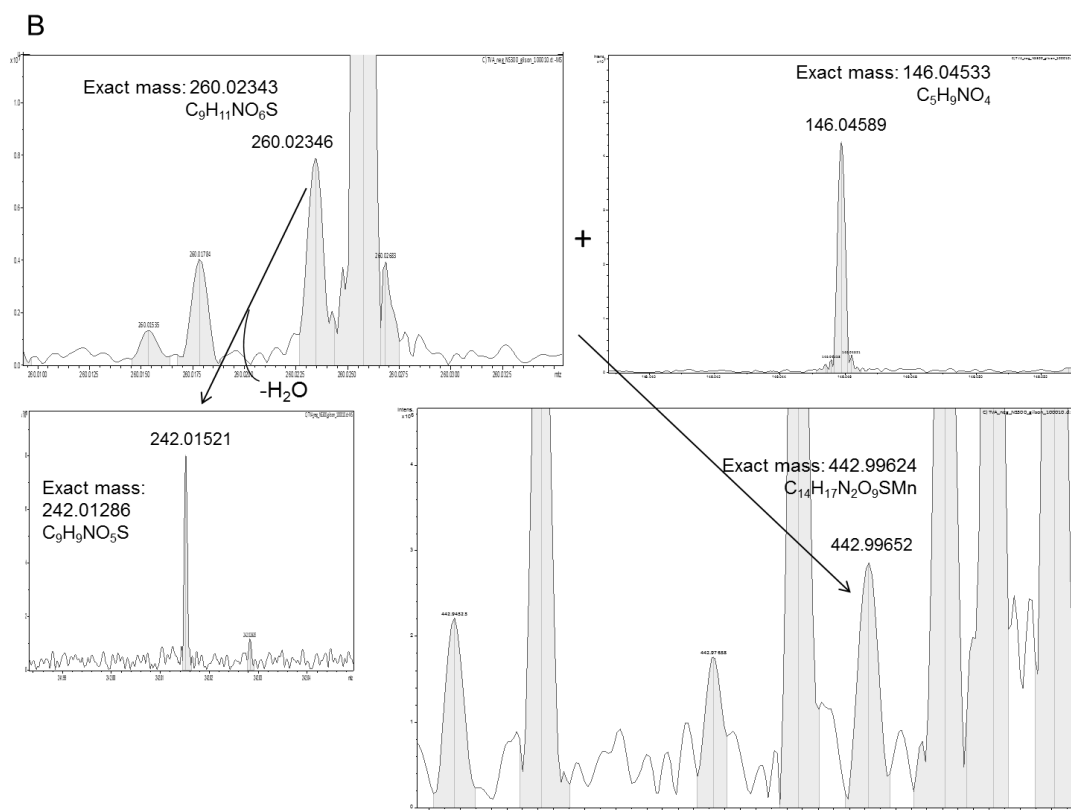
Figure 53 Possible formation of Mn-containing complex based on calculation by FormCalc.
(A) Possible reaction of O-Sulfo-L-Tyrosine with glutamic acid and Mn to the dipeptide
$C_{14}H_{17}N_2O_9SMn$ by the loss of water (condensation of amino acids) and one H due to binding of Mn to
N. The shown structure of the final product is only a suggestion and other structures are possible. (B)
Examples of one sample with the mass peaks of both amino acids and the product as well as the
mass peak of $C_9H_9NO_5S$ (O-Sulfo-L-Tyrosine after loss of H_2O).

Due to the time consuming and less practicable way of searching databases like Chemspider for every calculated structure by FormCalc, another approach was investigated. The theoretical mass, which was calculated for a Mn-containing formula by FormCalc was taken and the mass of the corresponding formula without Mn was subtracted from it to obtain the correct mass for the difference, i.e. Mn (m/z = 54.93804). All masses within the FormCalc matrix were then subtracted by this mass, mimicking the loss of Mn. Additional other reactions were also investigated, such as $+H_2O/-Mn$ (m/z = 36.93750), +H/-Mn (m/z = 53.93022) and +2H/-Mn (m/z = 52.92239). The resulting masses were then uploaded to MassTrix webserver (within an error of 1 ppm) to obtain possible binding molecules for Mn. The annotations were checked for plausibility, which means only molecules were considered, which comprised respective binding sites for Mn, and which could exist in brain. A list of possible Mn-binding annotated molecules is given in Table 14, which also depicts the applied reaction leading to the respective mass. The masses shown were all assigned to the Mn-treated group according to OPLS-DA. The ones with crucial VIP values from OPLS-DA are shown in bold letters. Interestingly, the masses after reaction were also found in the original data ma-

trix (with respect to mass error due to calculations), which were previously all assigned as "unknowns".

Mass [M-H]⁻	Reaction	Mass after reaction [M-H]⁻	Mass from MassTrix annotation	Error (ppm)	Compound acc. to MassTrix	VIP
280.04143	+H₂O/-Mn	243.11393	243.11390	-0.1	**Cyclo(L-Phe-L-Pro)**	**1.6**
	+2H₂O/-Mn	261.12446	261.13174		**L-Phenylalanine-L-Proline**	**1.3**
296.02093	+H₂O/-Mn	259.09343	259.09356	0.5	L-alpha-glutamyl-L-hydroxyproline	
346.03908	+2H/-Mn	293.09890	293.09904	-0.1	**N-Glycosyl-L-asparagine**	**1.7**
349.04643	+H/-Mn	295.11621	295.11603	-0.6	2-Methylaminoadenosine	
384.99915	-Mn	330.06111	330.06089	-0.7	dAMP	
405.04046	-Mn	350.10242	350.10274	0.9	S-(2-Hydroxyethyl)GSH	
438.02891	+H/-Mn	384.09869	384.09833	-0.9	**S-Inosyl-L-homocysteine**	**1.9**
454.00118	+2H/-Mn	401.07879	401.07891	0.3	(R)-4'-Phosphopantothenoyl-L-cysteine	
534.02907	+H₂O/-Mn	497.10157	497.10176	0.4	Oxidized gamma-glutamylcysteine	
679.16369	+2H/-Mn	626.24130	626.24141	0.2	**Tri-N-acetylchitotriose**	**1.6**

Table 14 Further examination of possible Mn-binding compounds in the group of +Mn_Inj. samples. Masses, which were also used for Formulae calculation, were subjected to few reactions as shown in the table. Resulting masses were uploaded to MassTrix webserver for annotation. The obtained compounds were checked for plausibility. Compounds with important VIP values according to OPLS-DA are shown in bold letters.

Among the calculated and annotated compounds in Table 14, over all compounds constituted of mixed amino acids were found. Screening of those molecules according to their molecular structure, Mn would have several possible binding sites. Metal ions were shown to form stable five-membered chelates at the N and O moieties of amino acids within peptides (Laurie 1995). Additional other important binding sites for metal ions within specific amino acids are for example the imidazole ring in histidine, the phenol ring in tyrosine (as discussed above), but also the thiol group in cysteine, or the β- and γ- carboxylate groups of aspartate or glutamate (Shimazaki et al. 2009). The findings from this calculation based structure elucidation underlines the possible Mn-binding structure shown above in Figure 53A. It is further in line with the findings of Mn-speciation in brain (chapter *B.2*), where Mn bound to amino acids was found to be important for transportation of Mn under exposure. However, different matrices (i.e. extracts) were applied for ESI-ICR/FT-MS and SEC-ICP-MS, complicating a direct comparison. Additionally, among the named structures in Table 14, also an alkylated adenosine and dAMP were found. The involvement of Mn on adeno-

sine phosphates was already discussed in chapter *B.4.2.1*. Hence, Mn could also bind to the phosphate residues of these nucleic acid derivatives. Moreover, GSH and cysteine derivatives were calculated according to Table 14. This finding is in line with the outcome of the van Krevelen diagram in Figure 52B and C, where it was shown that from the formulas calculated by FormCalc, Mn preferentially was bound to S-containing molecules. Such a calculation approach could therefore not only help to elucidate some of the occurring "unknowns" but further give hints to possible new Mn-compounds occurring in the brain after exposure. Among the annotated compounds, also some flavonoids such as axillarin or quercetagetin 3,7-dimethyl ether were found, which are not shown in the table. Interestingly, flavonoids in general are discussed to possess neuroprotective abilities with regard to neurodegenerative disorders such as AD or PD (Coyle and Puttfarcken 1993). For some dietary flavonoids, it was already shown that they can cross the blood brain barrier dependent on their lipophilicity (Youdim et al. 2003). It might therefore be susceptible, that Mn is complexed by such flavonoids in terms of neuroprotection as it was already shown to get bound by flavonoids, in particular by quercetin (Dolatabadi 2011). Complex formations of biomolecules such as flavonoids but also amino acids with metals is reviewed in (Vandenbossche et al. 2014) with the purpose of the use of such compounds for water purification of metal contaminations. Investigation of the ability of flavonoids being protective against Mn-induced neurodegeneration is one great future research field, which tends towards possible herbal treatment or prevention strategies of manganism as mentioned in the introduction (chapter *A.3.5.2*).

A general overview on possible reactions in between the matrix of masses was further examined by a mass difference network analysis. Starting from some reference masses, transformations of interest can be applied and possible mass differences are calculated. The resulting network comprises all possible masses or molecules as nodes and the respective connections in between those nodes are called edges, which represent the possible reactions (i.e. mass differences) between the masses. Important masses will be highly connected, while similar structures will be in vicinity to each other. Also subgroups or subfamilies can comprise important information about chemical transformations of masses.

Herein, the data matrix including all masses (the same which was used for FormCalc calculations) was uploaded to NetCalc (in-house written software, (Tziotis et al. 2011). For possible mass transformations, only 24 reactions of interest were allowed. These included Mn-containing mass differences as well as important amino acids or small acids like citrate. The allowed reactions with the resulting frequencies from network calculation are shown in Figure 54.
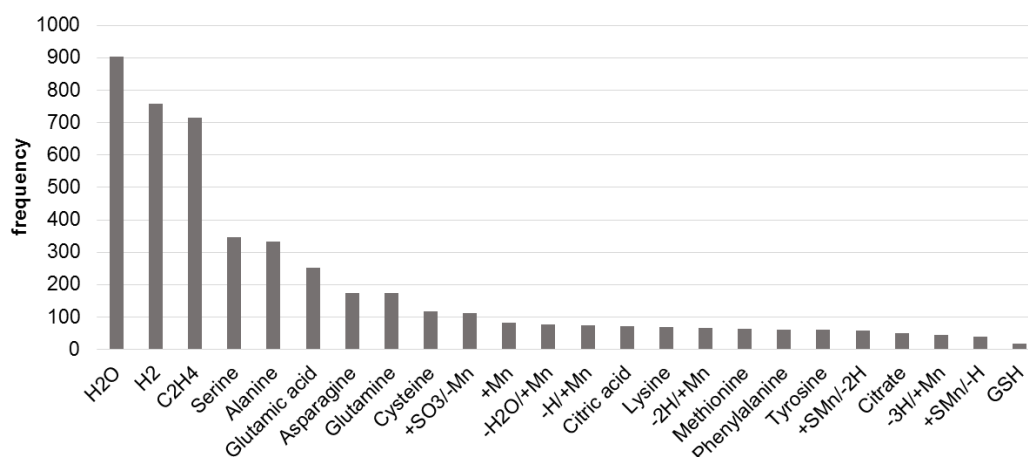
Figure 54 Allowed reactions for calculation of the network with respective frequencies.

From the 9865 masses in the data file, 1007 masses received a sum formula based on the allowed reactions, where 146 contained Mn (see Venn diagram in Figure 55A). The network visualization was carried out with Gephi (http://gephi.github.io/) as described in chapter *D.8.3.4* and is shown in Figure 55B. The coloring of the nodes represents in green sum formulas assigned to the control and in pink sum formulas assigned to the +Mn_Inj group according to VIP value >1.0 from OPLS-DA. The small black arrow indicates a sub-network, where only Mn-containing sum formulas were found showing possible transformations based on the applied reactions (Figure 54). The bridge from the main network to this sub-network is shown in Figure 55C. However, for the shown sum formulas without Mn, no plausible compound could be found by data base searches (Chemspider search with sum formula, My-CompoundID and Metlin search via masses). A similar compound as described above and illustrated in Figure 53 could be described by this network analysis. Figure 55D shows a reaction from $C_{14}H_{18}O_5N_2$ to $C_{14}H_{17}O_5N_2Mn$ by loss of H and addition of Mn. A possible compound for this starting sum formula would be Glutamylphenylalanine as revealed by Chemspider. The structure is similar to the glutamyl-sulfo-tyrosine shown above with an aromatic ring and the glutamyl residue. Hence, by the loss of H, Mn could bind to N and be stabilized by the free electrons from the aromatic ring of phenylalanine, which is concordant with above findings. By application of such network analysis, more reactions can be observed all at once, what could further give insight into possibly formed Mn-complexes. However, this is always depending on the input of allowed reactions.
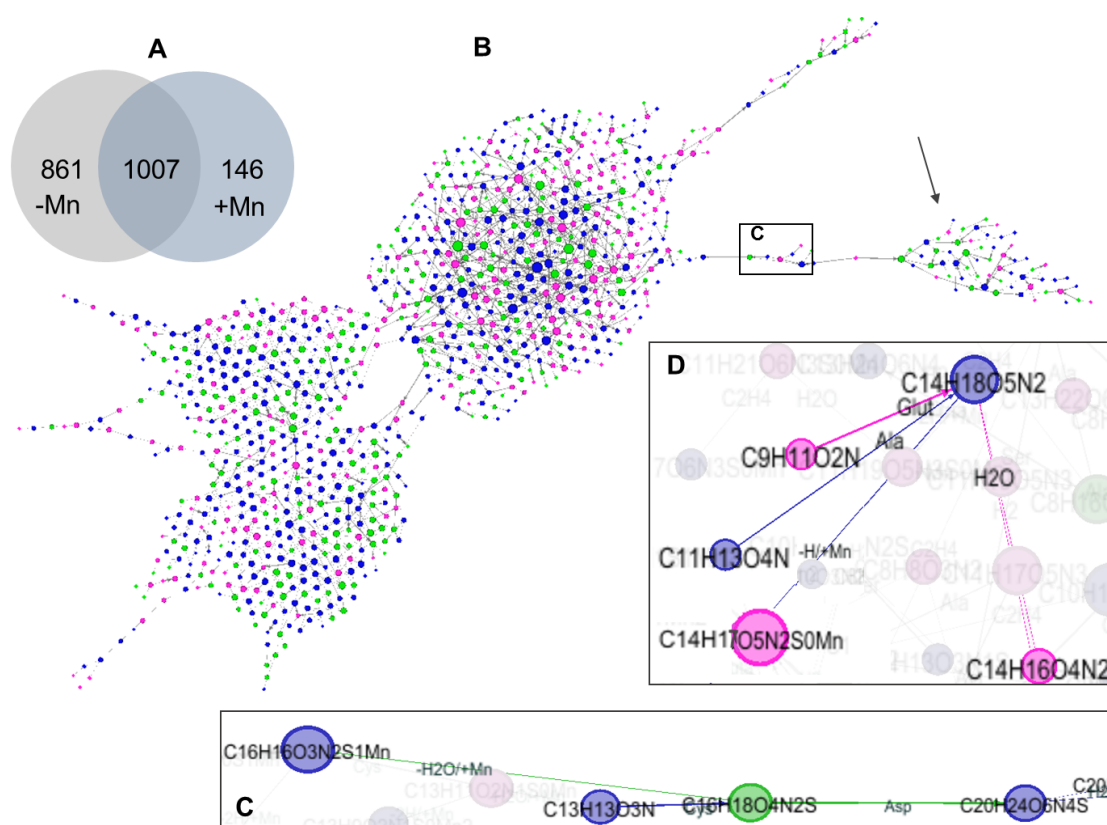
Figure 55 Mass-difference network analysis for deciphering Mn-complexes.
Based on a list of 24 mass differences, a mass-difference network was calculated by NetCalc, where 1007 sum formulas were built with 146 containing C, H, O, N, S and Mn (A). The network was visualized by Gephi (B), comprising also small subnetworks with highly connected Mn-containing sum formulas (small black arrow). Green nodes represent masses from control group and pink nodes from the +Mn_Inj, group according to OPLS-DA. (C) shows the bridge from the main to the subnetwork. (D) shows a reaction to a Mn-containing sum formula from the main network.

To conclude, suggesting that Mn gets stabilized or chelated by amino acids would also explain the reduction in major amino acids as described in alterations of amino acid metabolism in chapter *B.4.2.4*. If a certain amount of naturally occurring amino acids such as tyrosine or alanine is bound to Mn, these mass peaks won´t be annotated due to the lack of such Mn-complexes in available databases. After all, it has to be considered that the found sum formulas are only based on calculations. Deeper investigation of such possible Mn-complexes could be a great task for future research, where ESI-ICR/FT-MS is an excellent tool due to the high mass accuracy. Fragmentation experiments of corresponding synthesized standards would help to underline the possibility of occurrence of the discussed compounds. Concerning this topic, pioneering work was carried out by Nischwitz et al., who investigated Mn-, Fe-, Cu-, and Zn-citrate standards and Mn-citrate from a Mn supplement by ESI-MS/MS (Nischwitz and Michalke 2009).

B.5   Correlation of metallomics with metabolomics data

In this part of the work, certain variables such as total concentrations of elements or Mn-species in serum or brain were correlated with determined metabolites of the brain. The calculated correlations are based on Pearson´s correlations and are illustrated as heatmaps. Different variables as well as Mn-species (serum and brain) were correlated with "most important masses" from ESI-ICR/FT-MS. The term "most important masses" refers hereby to annotated masses with VIP-values ≥ 1.5 from the multivariate analysis (OPLS-DA). Furthermore, variables and Mn-species were correlated to other interesting metabolites, whereby "interesting" means metabolites with biological meaning in Mn-induced neuroinflammation. The focus here was on the metabolic pathways described above. The color code of every heatmap is based on the one shown in Figure 56, where dark red color means strong negative, light blue no, and dark green color strong positive correlation. Metabolites of the heatmaps are listed in the Appendix in Table 28 and Table 29.

Figure 56 Color code for every heatmap shown in this chapter.
Dark red color means strong negative, light blue no, and dark green strong positive correlation based on Pearson´s correlation coefficient.

B.5.1   Correlation heatmaps from the feeding study

The heatmap in Figure 57 shows the correlation of different variables with most important brain metabolites from the feeding study. Those variables were determined as described in chapter *E.1* and include: concentrations of Cu, Mn, and Fe in brain extracts, total brain and serum; concentrations of Fe(II) and Fe(III) in brain extracts; AchE activity; glutamate concentrations. Some interesting clustering behavior could be observed based on the weaker or stronger correlation with most important metabolites in the control or Mn-fed group. AchE activity and glutamate concentrations in the brain extracts as determined by the *in vitro* kits (chapters *B.1.1.2* and *B.1.1.3*) showed a strong positive correlation with the most important metabolites from the Mn-exposed group. Correlations with metabolites from the control group were weaker or negatively or not correlated. These findings substantiate the suggestion that increased Mn concentrations altered AchE and glutamate concentrations in brain leading also to alterations in brain metabolites, which were discriminative for the Mn-exposed group. In general, Cu concentrations in extracts, total brain and overall in serum showed positive correlation with the metabolites from the +Mn_Food group and negative correlation with the metabolites from the control group. The weak correlation of Cu in extracts with most important metabolites of the +Mn_Food group is based on the fact, that the extraction was not selective for Cu as described in chapter D.2.2.1. Fe concentrations in

serum, brain extracts and total brain were found to be negatively correlated with brain metabolites from the +Mn_Food group and positively correlated with the control group. This again is consistent with observations for the total concentrations in one and the other group. More interestingly, the same correlation behavior was true for Fe(III) concentrations in brain whereas Fe(II) concentrations were found to be correlated controversy (positive with +Mn_Food group metabolites, negative with control group metabolites). Hence, the impact of Fe on changes in brain metabolites after Mn-exposure might not be dependent on the total Fe content but rather on the Fe(II) levels in brain. This was already indicated by the linear correlation with Mn concentrations in extracts (chapter *B.1.4.3.1*) and could now also be found by the correlation with brain metabolites.
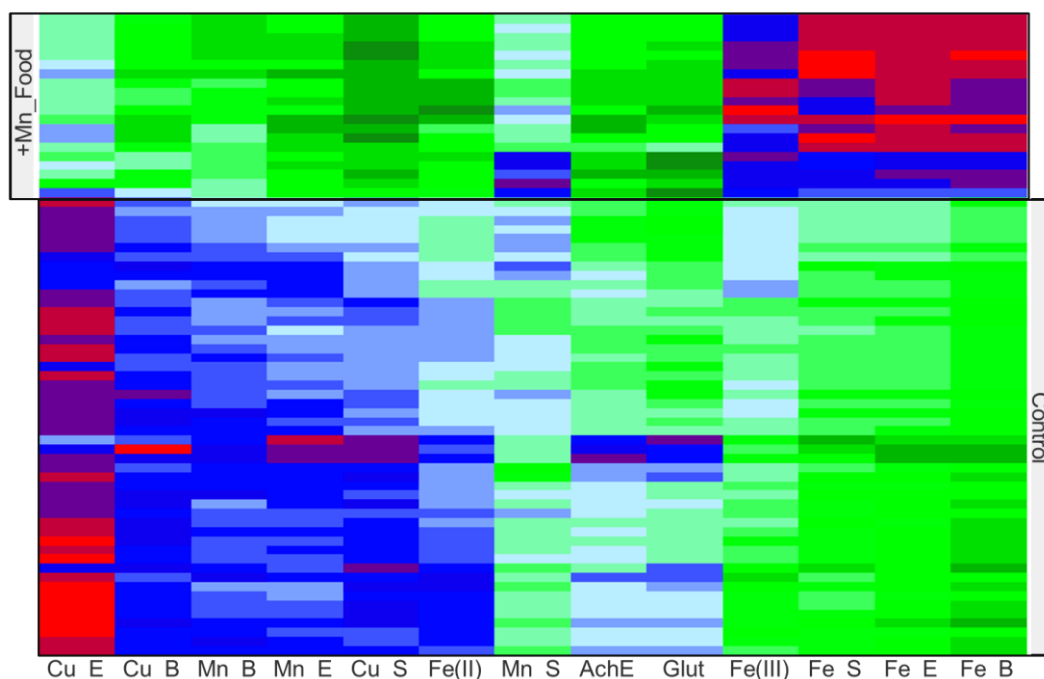
Figure 57 Correlation of variables with most important brain metabolites in the feeding study.
Variables such as concentrations of Cu, Fe, Mn in serum (_S), aqueous brain extracts (_E) and total brain (_B) as well as Fe(II)/(III) concentrations in brain extracts as well as determined AchE activity (AchE) and glutamate concentrations in brain extracts (Glut) were correlated with most important known brain metabolites (+Mn_Food or Control group) from ESI-ICR/FT-MS.

Regarding the variables of Mn concentrations, the correlation heatmap might be helpful in terms of "biomarker discovery". As can be seen in Figure 57, Mn in total brain as well as brain extracts showed a strong positive correlation with metabolites describing the +Mn-fed group and strong negative correlation with metabolites describing the control group – what seems plausible. However, looking at the Mn concentrations in serum, these showed no clear correlation behavior either with the one nor with the other group metabolites, and also some negative correlations with certain metabolites from the +Mn_Food group. This can be seen as strong evidence of the fact that the applied feeding of Mn did not lead to such differences in serum Mn concentrations, which could lead to a clear separation of treated and

untreated group – neither based on comparison of plain total concentrations in serum nor on significant changes in brain metabolites. To investigate the influence of Mn on brain metabolites in more detail, also Mn-species determined in serum (chapter *B.3.3.1*) and brain (chapter *B.2.3.1*) were correlated to the most important brain metabolites of both groups, which is illustrated in the heatmap in Figure 58. According to this heatmap, the fraction Br_C can be seen as a separation between two clusters: the one cluster consistent of Br_A, Br_B, Ser_B, and Ser_C, which showed strong negative correlation with the metabolites defining the Mn-exposed group and strong positive correlation with metabolites defining the control group; and the other cluster consistent of Ser_D, Br_D, Br_F, Ser_A, Ser_E, Br_E and Ser_F, which showed the opposite correlation behavior. This means for example: an increase in serum SEC fraction B (γ-globulin) might implicate an increase in certain brain metabolites, which were discriminative for the control group. Controversy, an increase in serum SEC fraction D (Mn-citrate) might lead to alteration in brain metabolites, which were defining the +Mn_Food group. Brain SEC fractions C (Br_C, Tf) showed no clear correlation to metabolites of one or the other group.
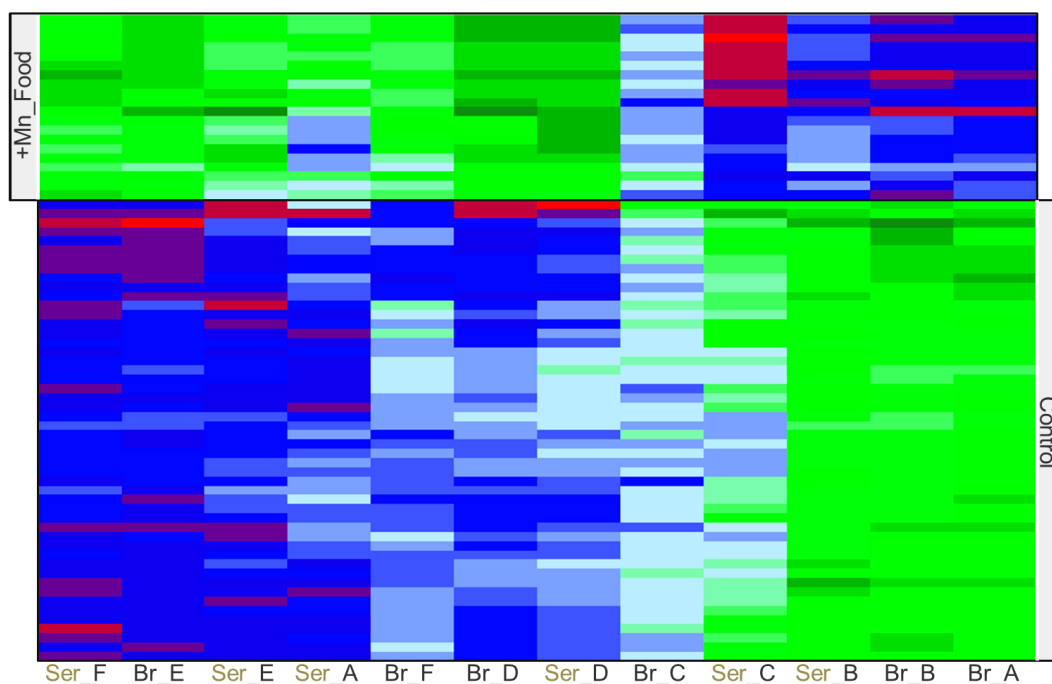
Figure 58 Correlation of Mn-species in serum and brain with most important brain metabolites in the feeding study.
Mn-species (fractions A to F) determined by SEC-ICP-MS in serum (brown letters Ser_) and brain (Br_) were correlated with most important known metabolites (+Mn_Food and Control) from ESI-ICR/FT-MS in methanolic brain extracts.

Except for Ser_A, which was partially positively correlated with some metabolites of the +Mn_Food group, in summary all HMM fractions both from serum and brain were negatively correlated with the brain metabolites defining the Mn-exposed group. On the other hand,

LMM fractions from serum and brain showed positive correlation, which was found to be really strong for fraction D (citrate).

B.5.2   Correlation heatmaps from the injection study

The same correlation studies were also carried out with data from the injection study. The heatmap in Figure 59 shows the correlation of some variables with the most important brain metabolites from ESI-ICR/FT-MS. The variables shown include: concentrations of Mn, Cu, Fe in serum (one hour and four days after injection (_S1 or _S4)), brain (_B) and brain extracts (_E); Fe(II) and Fe(III) concentrations in brain extracts; glutamate concentrations in brain extracts (Glut) as well as AchE activity in brain extracts (AchE). At first sight, clustering behavior is not as prominent as for example in the heatmap of the feeding study (Figure 57). However, division into sum subgroup was possible according to the dashed lines at the bottom of the heatmap. One subgroup encompassed Mn concentrations in serum_1h, in total brain and brain extracts as well AchE activity in brain extracts as well as Fe concentrations in brain extracts and total brain. These variables were found to be positively correlating with mainly all brain metabolites defining the Mn-exposed group and negatively with the ones discriminative for the control group. Controversy, on the very right side of the heatmap, serum concentrations of Cu_1h/4d, Fe_1h/4d and Mn_4d as well as Fe(II) in brain extracts group together. Hence, concentrations of Cu and Fe from every time point of measurement in serum as well as Mn at time point of sacrifice were more or less negatively correlated with those brain metabolites belonging to the Mn-exposed group. The last subgroup consisted of glutamate, Cu in brain extracts and total brain as well as Fe(III). Here correlations with all metabolites of one or the other group were not observable although negative correlation with most metabolites defining the control group seemed to predominate.

The findings therefore substantiate before discussed results, which differed from the feeding study. For example Cu was not increased in serum or brain in Mn-exposed animals in the injection study and was also not positively correlated with the brain metabolites discriminative for Mn-treated animals. The same is true for Fe(II) and Fe(III) concentrations in brain extracts. Interestingly, Mn concentrations in serum were positively correlated with all of the most important brain metabolites of the Mn-treated animals, but only one hour after injection and not at time point of sacrifice.
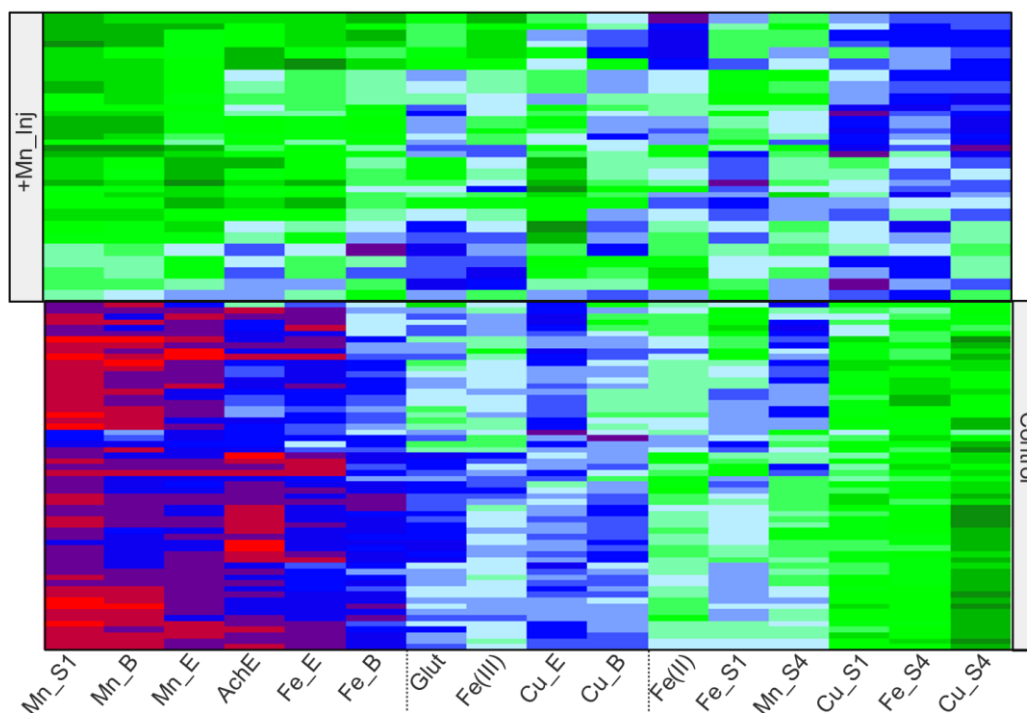
Figure 59 Correlation of variables with most important brain metabolites in the injection study. Variables such as concentrations of Cu, Fe, Mn in serum (_S1: serum1h; _S4: serum4d), aqueous brain extracts (_E) and total brain (_B) as well as Fe(II)/(III) concentrations in brain extracts as well as determined AchE activity (AchE) and glutamate concentrations in brain extracts (Glut) were correlated with most important known brain metabolites (+Mn_Inj or Control group) from ESI-ICR/FT-MS. Dashed lines indicate separation lines between clusters.

In the second step, Mn-species determined in serum and brain were also correlated to the most important metabolites of control and Mn-injected animals, what is illustrated in the heatmap in Figure 60. Here again, at first sight, clustering was not as obvious as in the cor-relation analysis of Mn-species in the feeding study (Figure 58). It rather seemed as if every SEC fraction was negatively correlated with the most important brain metabolites of the con-trol group except for serum_4d SEC fraction A. However, having a closer look, some sub-groups could be determined as indicated by the dashed lines in Figure 60. Interestingly, the citrate fractions (fraction D) from brain as well as serum (both, 1h and 4d) grouped together at the left side, where almost all metabolites from the +Mn_Inj group were found to correlate as strong positive.
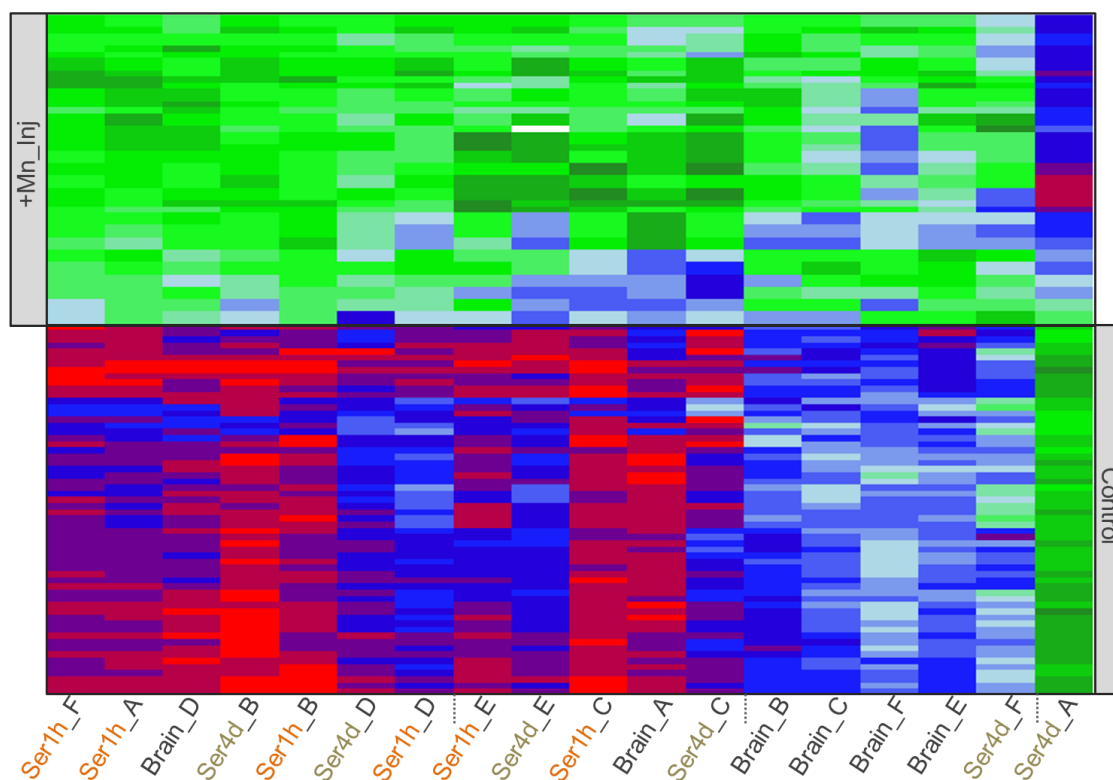
Figure 60 Correlation of Mn-species in serum and brain with most important brain metabolites in the injection study.
Mn-species (fractions A to F) determined by SEC-ICP-MS in serum (orange letters serum 1h, brown letters serum 4d) and brain were correlated with most known important metabolites (+Mn_Inj and Control) from ESI-ICR/FT-MS in methanolic brain extracts.

B.5.3   Discussion and Conclusion

On basis of correlation with all important known metabolites from brain extracts, some interesting observations could be drawn with regard to attempts of reliable measurement parameters of Mn body status. From the heatmaps in Figure 57 and Figure 59 it becomes true that total concentrations of Mn in brain and brain extracts showed positive correlation with the brain metabolites describing the Mn-exposed groups in both exposure studies. In contrast, total Mn concentrations in serum showed none or only weak correlation (partially negative) correlation with the most important metabolites from the Mn-exposed groups in the feeding as well as in the injection study four days after injection. However, one hour after injection, serum Mn concentrations were positively correlated with the brain metabolites from the Mn-injected group. This is even of great interest when thinking about measuring Mn concentrations in blood as indicator of Mn-exposure. As a reminder, in chapter B.1.1, total concentrations of elements in the various body fluids were discussed. It appeared that total concentrations of Mn in serum were only significantly elevated in serum of Mn-treated rats one hour after the *i.v.* injection. However, four days later and in the feeding study, serum Mn concentrations were comparable between control and Mn-exposed rats. This could now be confirmed by the correlation analysis, where Mn in serum was only positively correlated with

brain metabolites from the exposed group one hour after injection. This is therefore strong evidence that total Mn concentrations in serum or blood are only reliable after a short intervention with Mn such as an accident or after Mn-enhanced MRI, where Mn is injected intravenously for better resonance in MRI. Many studies applied the correlation of determined Mn in various matrices with various other determined variables. One interesting study was carried out by Apostoli et al. in a large cohort of occupationally Mn-exposed workers (Apostoli et al. 2000). Mn in air as well as in blood and urine of workers and non-exposed individuals was determined and correlated. Relationship between Mn in blood as well as Mn in urine and atmospheric Mn was significant but only on basis of group comparison. They concluded that Mn in blood and urine could discriminate between exposed and non-exposed people. Moreover, Mn in blood is also linearly related to Mn in atmosphere, but due to high variability, this correlation cannot be used for individual biological monitoring. This becomes even clearer by a study of Hoet et al. where plasma Mn of welders was compared with controls: an increase in after-shift plasma Mn compared to controls was observed, which was also correlated to Mn exposure from air. However, this was only true on the first working day of a week, whereas the relationship between air-Mn and after-shift plasma Mn was strikingly different on the subsequent days (Hoet et al. 2012). This problem with blood Mn concentrations can be underlined with the findings herein, where the correlation heatmaps as well as the total concentrations in serum clearly showed that total Mn concentrations in serum are only indicative after a short intervention with Mn but not under chronic exposures. Moreover, they might only be useful in terms of group comparisons. This might lead to the need of reference values for non-exposed as well as exposed individuals at different duration and concentration of Mn-exposure as well as way of exposure (e.g. oral or inhalative), which seems to be a complex task in future.

An additional prerequisite of the generated heatmaps is the possibility to examine differences in correlation behavior of the various occurring Mn-species. As an example, the correlation of Mn-species determined in the feeding study with some highlighted brain metabolites is illustrated in Figure 61. For comparison, also correlations of total Mn in brain and serum as well as Cu in serum and Fe(II) are given as these variables showed interesting alterations in the feeding study (see chapter *B.1*). In general, LMM Mn-species in serum and brain (fraction D, E and F; indicated by dashed frame with arrows) correlated in that manner, which substantiated findings from injection study as discussed in chapter *B.4.2*. For example, correlations were negative with nucleosides such as inosine, adenosine and guanosine, what is in line with above findings. Moreover, especially SEC fractions D (Mn-citrate) correlated positively with glutamate and negatively with glutamine, underlining the disturbance in glutamate synthesis and also results from the *in vitro* assay (chapter *B.1.2*). Same is true for

observations on the shift in the GSSG/GSH ratio, which was discussed above, as the LMM SEC fractions correlated positively with GSSG but negatively with GSH. The findings for a perturbed lipid synthesis as discussed above is also substantiated by this correlation analysis as LMM SEC fractions correlated positively with detected 15(S)-HETE and prostaglandins, but negatively with their precursors DHA and ARA. HMM SEC fractions were found to be adversely correlated as described for the LMM fractions. Interestingly, Cu in serum, Fe(II) and Mn in brain mostly coincided with correlation behavior of LMM SEC fractions whereas Mn in serum did not. This is again a proof that total concentrations of Mn in serum cannot indicate whether there are already occurring changes in brain metabolisms under these conditions of Mn-exposure.
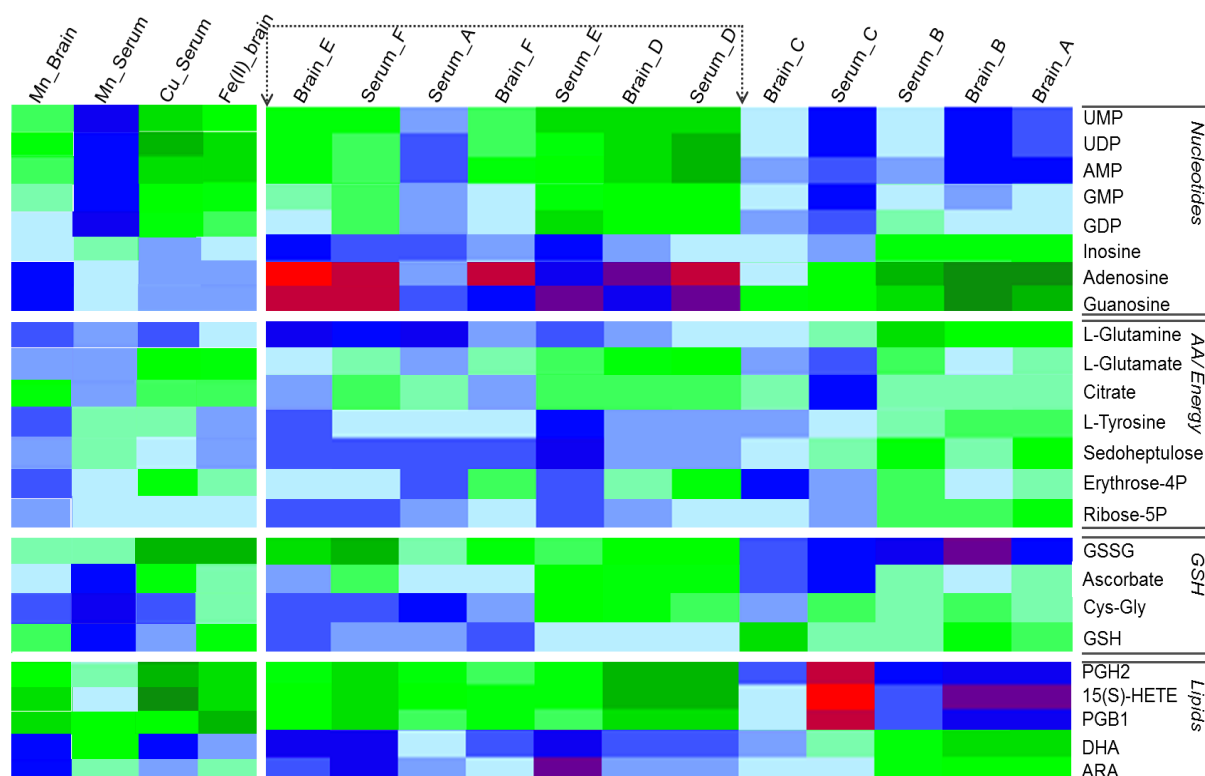
Figure 61 Different correlations from data of the feeding study.
Correlation of Mn-species, Mn in brain and serum, Cu in serum and Fe(II) in brain with some interesting brain metabolites to examine possible differences in correlation behavior of the various Mn-species.

This kind of analysis therefore could substantiate before mentioned and discussed findings. It can further help to elucidate the importance of discrimination between total Mn concentrations and Mn-species or other variables for indication of neural status. Same examination was carried out for the data of the injection study. The results are shown in the Appendix (Figure 93) due to prevention of repetition. In sum, such a clear clustering of LMM and HMM fractions in correlation as given in Figure 61 in the feeding study was not observed. Although differences in the analysis of brain metabolism were clear, the differences in SEC fractions

might not have been high enough to observe clear clustering behavior in these correlation heatmaps. Interestingly, every serum SEC fraction except for inorganic (F) and A clustered together and correlated in similar manner with the metabolites of interest (*Appendix* Figure 93). This could mean that already one hour after injection these formed species influenced changes in the brain similar to the species which occurred four days after injection. The importance of knowledge of the occurring Mn-species was also demanded by Quintanar et al., who suggested the determination of Mn-species in brain cells for investigation of molecular mechanisms (Quintanar 2008).

Coming back to Figure 61, the grouping of LMM SEC fractions overall fractions D from brain and serum (citrate) could be of great interest in terms of biomarker identification of Mn-(over)exposure. With this regard, the usage of a combination of Mn concentrations in serum and Mn-citrate in serum was already discussed as biomonitoring method for Mn-exposed individuals (Michalke and Fernsebner 2013). With respect to the results herein, determining a combination of various variables for getting an idea of the progress of neural injury under Mn-exposure might therefore be advisable. So first of all, the knowledge of the "patients" history is important, such as duration of Mn-exposure and a round figure of Mn concentrations, the individual was exposed to. On basis of that, Mn in serum (and additional elements such as Cu) should be determined. Moreover, Mn-species in serum should be examined. As this procedure requires sophisticated laboratories overall for speciation analysis, an easy and practicable way would be ultrafiltration. This comparable modest fractionation technique was already proposed by Nischwitz et al. ((Nischwitz et al. 2010) and submitted data) applying it on paired serum and CSF samples. After application of a special pre-cleaning protocol of ultrafiltration devices to prevent contaminations, serum can easily be separated in a centrifuge (needed cut off approximately 10 kDa) and Mn concentrations in both fractions can be determined (as well as additional concentrations of other elements such as Cu or Fe). If the concentration in the LMM fraction exceeds a certain value X, also CSF should be analyzed and first therapy strategies such as chelating therapy could be initiated. This biomonitoring scheme is illustrated in Figure 62. The value for X in brackets is based on so far carried Mn-speciation studies, where results more or less came down to a 9% cut off for Mn bound to LMM compounds in serum. However, the number of studies is far to less to give a reliable value. Moreover, reference values need to be determined in healthy individuals. This should preferably be done dependent on country of living as differences in total Mn as well as Mn-citrate in serum were observed for inhabitants of different countries (submitted data).
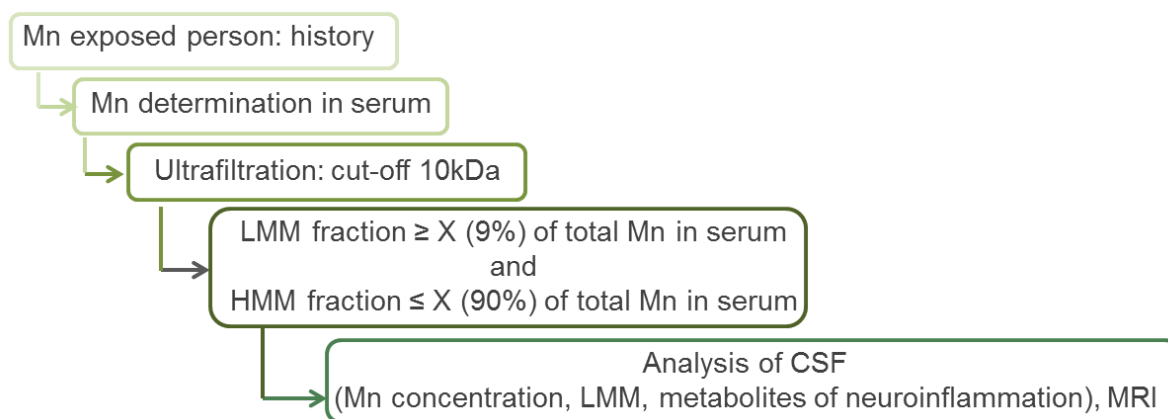
Figure 62 Biomonitoring scheme for Mn-exposed individuals.
Based on the one published in (Michalke and Fernsebner 2013).

Overall, the untargeted study of the brain metabolome under Mn-exposure revealed major alterations in neural metabolisms. These changes of various metabolites might be dependent on different Mn-species, both in serum and brain, which was very good observable in the feeding study. To our knowledge, such analysis was never carried out before in studies of Mn-induced neurodegeneration. The other metabolomics studies discussed above in chapter *B.4.3* indeed included correlations, but these were only based on total Mn concentrations. This can only be useful if there is a reliable detectable increase in total elemental concentrations as described herein. The results of this work showed that the knowledge of Mn-species in serum might give indications of the progress of neural injury and should therefore be considered over, or rather additionally to, total Mn concentration. After all, metalloproteins or metalloenzymes are discussed as possible biomarkers in medicinal chemistry for identification or progress tracking of disease as well as for evaluation of the impact of therapeutic agents (Mounicou et al. 2009). As an example, a family of Zn-dependent proteolytic enzymes (matrix metalloproteinases) was reported as potential diagnostic indicators of cardiovascular diseases (Lopez-Avila and Spencer 2008). The application of analytical techniques as applied in metallomics such as metal-speciation might therefore represent an attractive alternative to the so far used burdensome immunoassays.

B.6   Elemental distribution of Mn, Fe, Cu and Zn in brain by LA-ICP-MS after a single i.v. injection of MnCl$_2$

The task in this part of the work was the development of a LA-ICP-MS method for elemental mapping of Mn, Fe, Cu and Zn within the brain after Mn-exposure. Another aim within this task was to find an appropriate quantification method for LA-ICP-MS of brain tissue. As the single injection of MnCl$_2$ showed, concentrations of Mn in brain were increased compared to not exposed animals. Therefore, this injection study was repeated as described in chapter *D.1* to obtain fresh brain samples. After the single injection of either 1.5 mg Mn/kg b.w. or NaCl in control rats, serum was taken one hour after injection and at the time point of animal sacrifice (four days after injection) to monitor elemental concentrations. Moreover, during the four days between injection and animal sacrifice, feces was collected and analyzed as described before.

B.6.1   Concentrations of Mn, Fe, Cu and Zn in feces and serum

Feces was collected and analyzed by ICP-OES after nitric acid digestion to control excretion of elements (Figure 63). Excretion of Cu, Fe and Zn was comparable between control and Mn-exposed rats. Mn excretion was higher in Mn-exposed rats from day 1 to day 3 after injection, while values were comparable at the time of sacrifice. This showed that the body of the exposed animals seemed to be cleared from Mn after these four days. The findings were comparable to the before carried injection study. The only difference here was a slightly higher excretion of Mn on day 2 compared to day 1, which was not found in the other injection study. This however can be due to the individual excretion behavior or metabolism as obtained values were nicely distributed, what can be seen by the minor standard deviation.
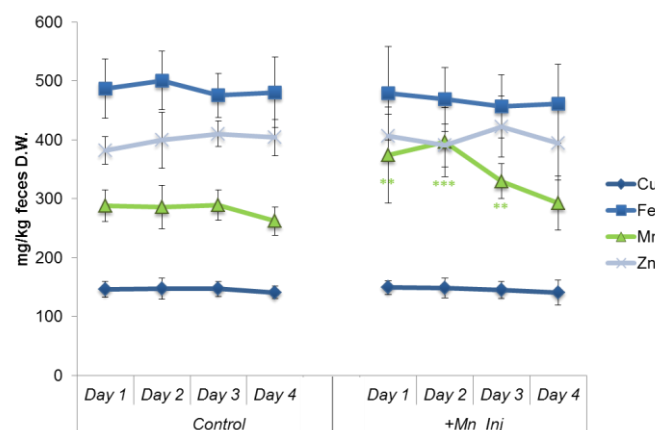
Figure 63 Analysis of feces from the injection study for LA-ICP-MS.
Cu, Zn and Fe excretion was comparable between Mn-exposed and control rats. Mn extraction was higher compared to control in Mn-exposed rats for three days after the injection and was balanced on the fourth day.

Blood was also taken one hour after injection and four days after the injection at time point of sacrifice to monitor Mn levels in serum. As Figure 64 shows, Mn in serum of Mn-exposed rats was increased one hour after injection in a comparable manner than in the previous injection study (~26%). Moreover, the concentrations were balanced four days after injection with slightly lower Mn values in Mn-treated animals. Fe and Zn were comparable between control and Mn-exposed rats both one hour and four days after injection. Concentrations were also comparable with the previous injection study. Regarding Cu, there were some obscurities: very low concentrations of Cu in all animals were detected by ICP-OES. The detected intensities of wavelengths were compared with the applied standard to exclude problems with the detection. Cu was then determined by ICP-MS. However, compared with the previous injection study and also with the feeding study, levels were really low in both, control and exposed animals (around 50 µg/l, usually ≥100 µg/l in rat). Requesting an acci-dently interchange of rats (e.g. mutations for Cu-deficiency) at the rat distributor was not confirmed. This finding had therefore to be accepted as it was.
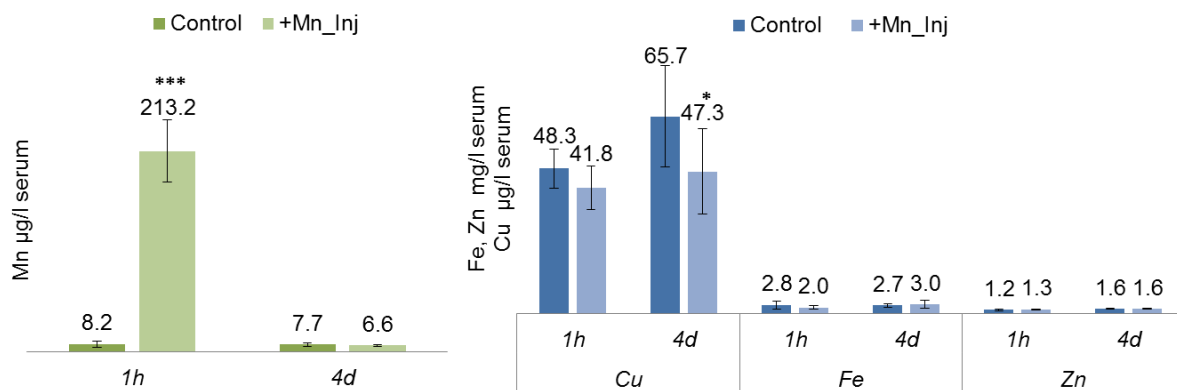
Figure 64 Analysis of serum one hour and four days after injection for monitoring Mn, Fe, Cu and Zn.

B.6.2   Elemental imaging of Mn, Fe, Cu and Zn and quantification attempts

At sacrifice of animals, brains were taken and carefully frozen in liquid nitrogen to prevent breaking of the samples. Brains were embedded, cryosectioned and thawed on microscope slides. In that form they were stored at -20°C until analysis by LA-ICP-MS. Brain slices were ablated line by line in three parts. This splitting was necessary due to relatively long analysis time (up to 24 hours for one slice) to prevent excessive heating of the ICP-MS. Optimum setting of the laser (fluence, energy, spot size etc., see chapter *D.9.3.*) were adopted to op-erating of IPC-MS, especially with regard to prevention of organically overload of the inter-face cones.

The elemental maps shown in Figure 65 were gained by application of Iolite software, where the three separate measurements were put together to one image. On the left side of the figure the Mn-exposed rat brain slice is shown and on the right side the control sample. The upper pictures were taken with the laser included camera in a wideangle mode (A) and in high resolution mode (B), where multiple small pictures were put together to obtain the original size of the brain slice.
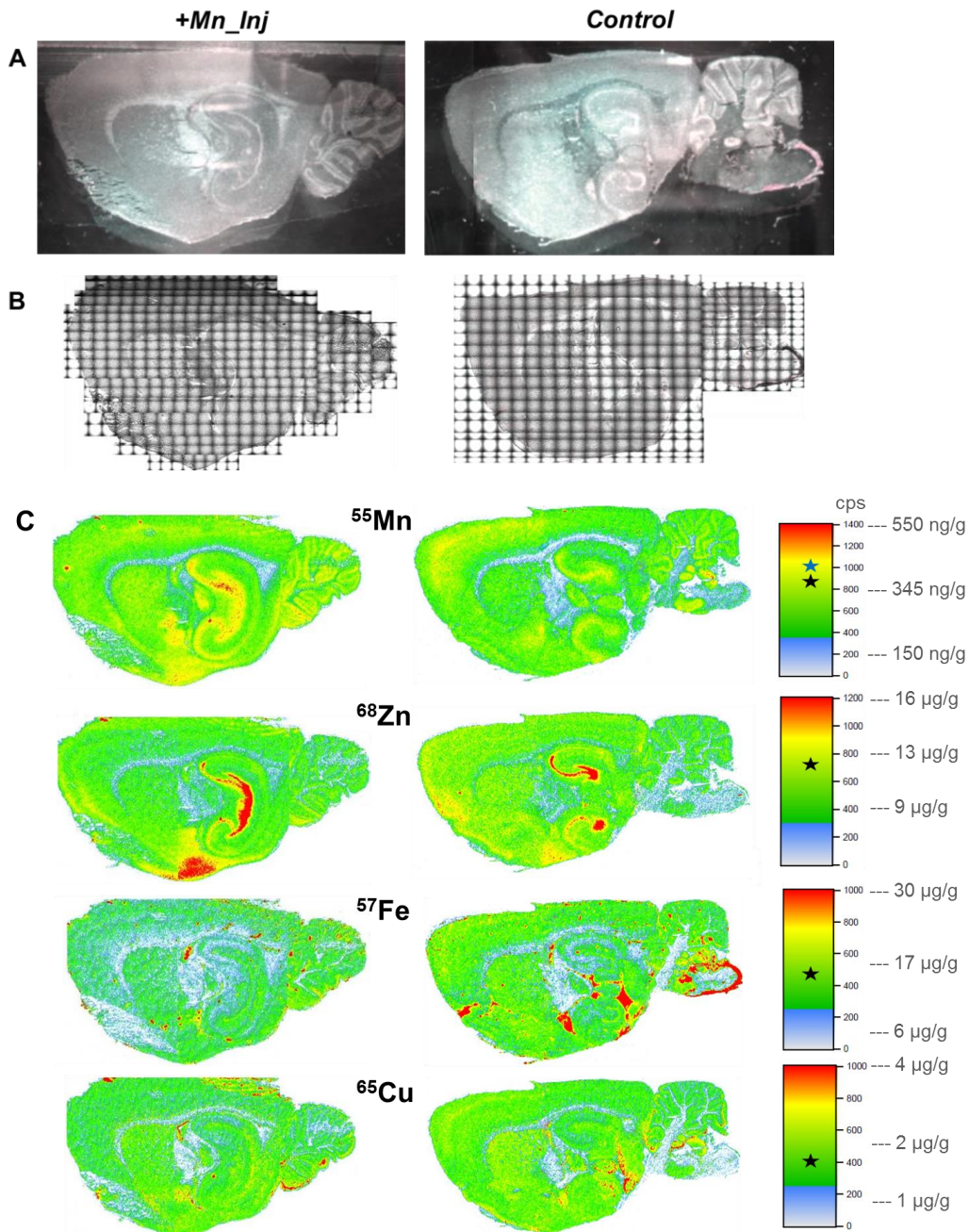
Figure 65 LA-ICP-MS of two brain slices of a control and a Mn-exposed rat.
Pictures of the whole brain slice were taken with the laser camera in wideangle (A) and high resolution (B) mode. (C) shows the elemental distribution of Mn, Zn, Fe and Cu (Mn-exposed and control) within the brain slice) corresponding to the respective color scale bar. The concentrations of each element (per g brain) determined by LA-ICP-MS of standards are also marked. Black stars indicate the concentration of this element found by nitric acid digestion in the injection study (for comparison) (blue star for Mn-exposed rats).

In general, the applied method and settings of LA-ICP-MS were very suitable for preparation of highly resolved elemental maps. Also the splitting of measurement into three parts was not disturbing the final resulting pictures. The concentrations at the color scales at the right of Figure 65 are based on the comparison of determined intensities of ICP-MS with the intensities of ablated standard material. For this, pig brain tissue was spiked with Mn, Fe, Cu and Zn in different concentrations, frozen and cryosectioned as described in chapter *D.9.2*. The stars indicate determined concentrations of the respective element in microwave digested and measured brain samples of the injection study by ICP-MS. Concentrations of Cu, Fe and Zn in total brain were not significantly different in control and +Mn-Inj. samples as indicated by the black star. The blue star indicates the concentrations of Mn in the Mn-treated animals, which was significantly higher in total brain. For comparison of concentrations determined by LA-ICP-MS and aqueous analysis, the "average color" of the respective slice has to be compared to the "position" of the star (i.e. concentration) on the color scale. Basically, the applied quantification method seemed very accurate as the colors of the slices correspond very well to the determined concentrations by aqueous measurement. In terms of Mn, also the difference between the +Mn_Inj (429 ng/g total brain) and control sample (360 ng/g total brain) could be figured out as the Mn-treated sample tended to show more Mn in specific areas, i.e. more "yellow" color (in line with the blue star). The obtained linearity of calibration curves was also very good for all elements (R^2: 0.995 for ^{55}Mn, 0.995 for ^{68}Zn, 0.992 for ^{57}Fe, 0.998 for ^{65}Cu). Moreover, LoDs were calculated as 3σ criterion of the blank measurement, and were 0.08, 1.2, 1.2, and 0.01 µg/g for ^{55}Mn, ^{68}Zn, ^{57}Fe, and ^{65}Cu, respectively. Compared with other detection limits where LA-ICP-MS was applied in soft tissue analysis, these LoDs were very good to work with. For example, Jackson et al. applied a 60 µm spot size ablation on pressed pellets of certified reference material and reported 3.6, 0.12 and 0.66 µg/g for ^{56}Fe, ^{63}Cu and ^{66}Zn (Jackson et al. 2006). It has to be considered that LoDs in LA-ICP-MS are a function of spot size: when increasing the spot size, more material is ablated and intensities are higher, resulting in lower LoD. The disadvantage of an increased spot size, however, is a loss in resolution. Overall, the quantification by matrix-matched standards as applied in this work is very well suited for application as alterations in ablation, material transport and ionization are comparable or the same for the given matrices. Of course, a more practicable method is the application of solution-based calibration by simultaneous introduction of aqueous standard solutions.

For better overview, the ablated brain slice was divided in various brain regions in Figure 66, which is needed for the following discussion about regional distribution of elements:
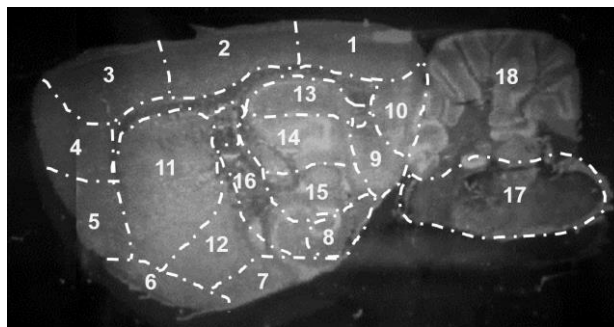
Figure 66 Parasagittal section of rat brain (1.2 mm lateral from the midsagittal plane) with schematic classification of brain regions.
1 visual cortex, 2 somatosensory cortex, 3 motor cortex, 4 agranular insular cortex, 5 piriform cortex, 6 olfactory tubercle, 7 amygdala, 8 substantia nigra, 9 mesencephalic nucleus, 10 superior and inferior nucleus, 11 putamen (striatum), 12 globus pallidus, 13 hippocampus, 14 subthalamic nucleus, 15 thalamic nucleus, 16 internal capsule/cerebral peduncle, 17 brain stem (was cut off in the +Mn_Inj-sample), 18 cerebellum (modified according to (Tarohda et al. 2005)).

As mentioned in the introduction, Mn neurotoxicity was described to be selectively acting on structures of the basal ganglia in the fore- and midbrain, such as globus pallidus, striatum, subthalamic nucleus, and substantia nigra pars reticulate. Additionally to that, other brain regions were discussed, including cortex and hypothalamus (M. Aschner et al. 2009). Contrary to PD, the dopaminergic soma in the substantia nigra pars compacta is usually spared during manganism (Olanow 2004).

Compared to the control sample (Figure 65C), we found higher concentrations of Mn in the area of the olfactory tubercle at the junction to the amygdala (number 6, 7), at the anterior rim of the striatum (number 11), in the globus pallidus (number 12), along the subthalamic and thalamic nucleus (number 14 and 15) as well as in the substantia nigra (number 8) in the sample of the Mn-exposed animal. Moreover, the cerebellum showed higher concentrations of Mn in the +Mn_inj sample than the control one. Contrary, in the control sample, the cortical region (number 2-4) seemed to sequester more Mn than in the sample of the Mn-injected animal.

Notably is the co-accumulation of Mn in areas with high contents of Zn, both in control and in the +Mn-Inj sample. High concentrations of Zn could therefore be found in the areas of the hippocampus, the sub- and thalamic nuclei as well as the substantia nigra and over all the amygdala. In the control sample, these areas also showed high Zn content but in a less extend than the sample of the Mn-treated animal. However, the frontal cortical regions such as the piriform cortex (number 5 in Figure 66) presented higher Zn content in the control rat.

In terms of Fe, the overall Fe content seemed to be lower in the +Mn_Inj sample (overall in the striatum and cortical regions numbers 2-4 and 11 in Figure 66). The highly concentrated Fe in the control sample (red regions) are a reason from blood residues on the brain sample,

which accumulated specifically at rims (see brain stem rim) or cavities (see ventricles). Apart from this finding, Fe seemed to be distributed over the whole brain in similar manner in control and Mn-exposed animals. Cu seemed to be very homogenously distributed over the whole brain. In some areas such as the striatum and the motor cortex (numbers 11 and 3 in Figure 66) it was less concentrated in the +Mn_Inj sample than in control. Moreover, the control sample showed high accumulation of Cu within the convergence zone of mesencephalic and thalamic nucleus and the substantia nigra (numbers 9, 15 and 8 in Figure 66).

Visualization of regional distribution of Mn in the brain during overexposure was carried out in a study by Gallez et al. by autoradiography as well as ICP-MS analysis of digested tissue of 18 different brain regions (similar classification of brain regions as in Figure 66). This study is of great relevance for comparison with the work herein as also a single injection of Mn was carried out in rats (5 µmol/kg ($\approx$27.5 mg/kg) of ^{54}Mn as $MnCl_2$ or Mn-DTPA), and rats were killed one or two weeks later. The results correspond very well to our observations as maximal concentrations of Mn were observed in the following brain regions: hippocampal region, thalamus, colliculi, amygdala, olfactory nuclei and cerebellum (Gallez et al. 1998). In line to the findings herein, the striatum seems not to be the primary area of Mn accumulation after injection of such a low dose. In another study, rats received Mn once a week for four weeks in different concentrations depending on route of administration (p.o., i.p., i.t.) as well as different Mn compounds ($MnCl_2$ or MnO_2). After this longer ("chronic") exposure, Mn was more or less distributed and increased in all parts of the brain with highest regional concentrations in the striatum for i.t. administered $MnCl_2$ (Roels et al. 1997). The preference for accumulation at the striatum might depend on the concentration of Mn as there are two different uptake entries known for Mn (Murphy et al. 1991). When Mn concentration in plasma is low, it enters the brain mainly across cerebral capillaries by a saturation driven process. With increasing plasma Mn concentrations, the influx into CSF is faster than into the brain tissue, and Mn enters the brain via the choroid plexus (adjacent to the striatum, number 11 in Figure 66, within ventricular system). Therefore, the striatum receives more Mn from both, brain capillaries and ventricles, when Mn concentrations are higher, and is therefore the target tissue for further neurological intoxication by Mn.

Another possibility to visualize Mn within the brain is MRI due to the paramagnetic properties of Mn. Newland and coworkers applied $MnCl_2$ inhalative and intravenously in different concentrations in monkeys (Newland et al. 1989). They observed similar regional concentration of Mn within the areas mentioned but suggested a selective affinity of Mn for globus pallidus and the pituitary. Very recently, Criswell et al. examined the T1-weighted MRI signal intensity in the brain of South African Mn mine workers and non-Mn mine workers (Criswell et al.

2015). The highest signal intensities were also found in globus pallidus and striatum (puta-men and caudate) in Mn-mine workers with longest cumulative Mn exposure. After all, the way of exposure and over all the applied concentration of Mn seems to have effects on the preferred brain region, where Mn finally accumulates. But the common affected brain areas (i.e. globus pallidus, hippocampal and thalamic region) overlap in various studies and corre-spond to the findings herein.

To understand the neurotoxic effects of Mn, the basal ganglia (including putamen, globus pallidus, substantia nigra and nucleus subthalamicus) and more particular the dopaminergic system has been focused in various studies by MRI in exposed workers or human and non-human primates (summarized in (Guilarte et al. 2006). Figure 67 serves for an overview of dopaminergic (red), glutamatergic (blue) and GABAergic (green) projections within the ro-dent brain. Interestingly, in the exposed animal, Mn seemed to deposit along the glutama-tergic neurons from hippocampus to substantia nigra (Figure 65C). This underlines the rela-tionship of Mn accumulation within the glutamatergic system as described in chapters *B.1.2* and *B.4.2.4*. Moreover, in the area of the nigrostriatal dopaminergic projections, higher Mn accumulation could be noted. Radioligand studies indicate that the effects of Mn on these dopaminergic systems are rather based on a failure in dopamine release than on destruction of dopaminergic neurons. Therefore, the dopamine reduction observed during manganism leading to the motor function deficits - as observed in PD - seems to be based on an intact but dysfunctional nigrostriatal dopaminergic system (also discussed in chapters *B.1.3* and *B.4.2.4*). The deposition of Mn in these regions found by LA-ICP-MS underlines the interplay of the element with the dopaminergic system. This preferred accumulation of Mn in dopa-minergic cells of the substantia nigra due to chronic Mn exposure was recently also found in situ by X-Ray Fluorescence (XRF) imaging (Robison et al. 2015).
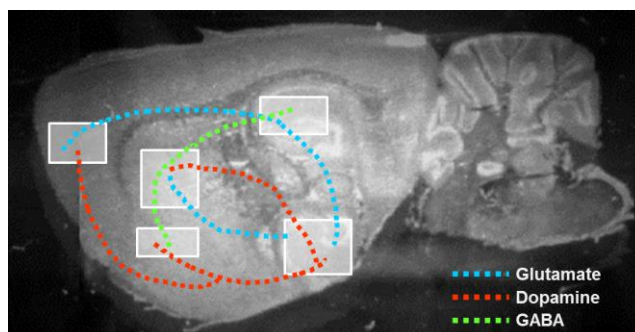
Figure 67 Projection of glutamatergic (blue), dopaminergic (red) and GABAergic (green) neurons within the rodent brain.
For purposes of simplicity, modularity (inhibition or activation) were left out and not all projections are shown. White boxes indicate key nodes within the systems (modified according to (Miller et al. 2013)).

Regarding the distribution of the other metals (Fe, Cu and Zn), the study by Scheuhammer et al. is worth mentioning. Rats were treated with 3 mg/kg b.w. i.p. for 30 days and 19 brain regions were prepared and analyzed by atomic absorption spectrometry after digestion. The authors found increased Mn in the striatum, thalamus and midbrain, which is in line with our findings by LA-ICP-MS. Moreover, they found increases in Cu in some brain areas and decreases of Zn in other brain regions. For Fe, no significant increase or decrease was described in that study, and it seemed to be homogenously distributed. Interestingly, the distribution of Mn and Cu or Fe could be correlated significantly (Scheuhammer and Cherian 1981). The mentioned effects could not be observed herein as Zn seemed rather to be increased and co-accumulating with Mn in the same brain regions. However, a strong accumulation of Zn in the dopaminergic, Mn-rich regions was also found by the XRF analysis of the study by Robison et al. mentioned before. This is concordant with the observations herein. For Fe and Cu the observations herein seem to be controversial to the study of Scheuhammer et al. However, the applied concentration as well as the duration of Mn-treatment in the study by Scheuhammer was higher or longer. For Fe, Criswell et al. also observed a decrease in all brain regions in Mn-mine workers (Criswell et al. 2015). It is assumable that the concentration and duration of Mn-exposure has different effects on the distribution of other trace elements such as Fe, Cu and Zn within the brain. Nevertheless, it is astonishing that already at such a low Mn-exposure these regional differences within the brain and within the examined elements could be detected. The distribution of elements in healthy and common neurodegenerative human brain is excellently reviewed in (Speziali and Orvini 2003).

To our knowledge, elemental imaging by LA-ICP-MS in a model of Mn-exposure has so far only been carried out in *C. elegans*. Wild type L1, drj1.1 deleted and djr1.1, djr1.2 double deleted mutated L1 worms, which are genes involved in PD, were incubated with Mn. The analysis revealed distribution of Mn in the entire worm for the first two, and accumulation of Mn in the gastrointestinal tract in the double deleted mutant (Brinkhaus et al. 2014). Moreover, due to the similarities of manganism and PD, Mn application is frequently used in models of PD. Imaging studies in these include application of EELS (electron energy loss spectroscopy) or XFM (X-ray fluorescence microscopy), and are therefore concentrating on the distribution of Mn on subcellular level. Results indicate accumulation of Mn within mitochondria or the Golgi apparatus giving indices of Mn-induced neurodegenerative mechanisms on cellular level. The various possibilities of imaging techniques in neurodegenerative diseases like PD or AD is nicely reviewed in (Bourassa and Miller 2012). Although LA-ICP-MS was applied in models of PD, the discussion of metal distribution within brain in these studies would extend the scope of this work.

In summary, the developed LA-ICP-MS method showed good resolution and acceptable analysis time. Moreover, the matrix-matched standards seemed adequate for quantification of elemental concentrations. This preliminary study of elemental distribution within brain after Mn-exposure by LA-ICP-MS gave a more explicit overview of elemental concentrations than for example by digestion of tissue or even pieces of tissue, where high metal content overlays regions with low metal content. Of course, analysis has to be repeated in a larger number of samples. Additionally, as described in the Material and Method section, there occurred various problems in cryosectioning, which are the reason for not identical parasagittal slices of control and treated rat brain in Figure 65. Therefore, the comparison of elemental distribution in control and +Mn_Inj is based on preliminary results and has to be taken with care. But these investigations should serve as basis for future work in this area and still, the results for the +Mn_Inj sample correspond well with literature as discussed above. With regard to biological interpretation, future work could also include preparation of metal-tagged antibodies against proteins of interest (e.g. α-synuclein, see (B. Xu et al. 2014)) and analysis by LA-ICP-MS for monitoring eventual involvement of Mn in protein aggregation similar as observed in PD.

C Concluding Remarks and Future Perspectives

The combinatorial application of *metallomics* and *metabolomics* as carried out herein allowed for deeper observations on relationships of metals, metal-species and metabolites in the condition of elevated but non-toxic exposure to Mn.

Investigations on the level of the *metallome* by techniques of elemental analysis revealed Mn-induced shifts

- for Cu and Fe in serum and brain, which were stronger due to subchronic exposure
- in Fe(II)/(III) ratio in brain towards the highly reactive Fe(II), which was for the first time and only observed in the oral subchronic Mn-exposure
- in serum and neural Mn-species depending on exposure conditions, showing importance of LMM compounds such as citrate and amino acids in both body compartments, and
- in regional distribution of Mn, Fe, Cu and Zn in brain after the single acute exposure to Mn.

Investigation on the level of the *metabolome* by a non-targeted ESI-ICR/FT-MS analysis of the brain revealed Mn-induced disturbances in major neural metabolisms such as

- purine and pyrimidine
- amino acids
- energy due to a reduced pentose phosphate pathway
- glutathione, and
- lipid synthesis.

The combination or correlation of both was found to be very powerful to describe differences in changes of neural metabolites depending on total elemental concentrations or Mn-species. In summary, the study helped to substantiate previous knowledge of both, Mn-species formed as well as Mn-induced mechanisms during exposure leading to the observed pathophysiology in manganism or Mn-induced Parkinsonism. Moreover, due to the first-time application of analytical techniques such as IC-ICP-OES and ESI-ICR/FT-MS in a Mn-exposure study, mechanisms occurring during neurodegeneration could be widely enlarged and even be brought together to decipher interrelations. Figure 68 graphically summarizes the herein described findings.

Pilot studies applying such combined approaches were recently also carried out in plasma analysis of stroke patients (Kodali et al. 2012), in urine and serum of hypercholesterolaemic rats (F. Liu et al. 2012) and in mice under arsenic/cadmium exposure (García-Sevillano et al.

2014). These combined analysis might even be more important in future due to more frequently contacts of individuals to metals and metal mixtures via exhaust fumes or the use of metals as nanoparticles, for example in clothing, cosmetics or food industry. The impact of metals or metal mixtures on the development or enhancement of various diseases is not clear yet due to the lack of long-term studies. This will represent a broad investigation field in future research. In these cases, the predominant metal species might be of special interest in terms of target biomarkers for disease diagnosis.

With regard to Mn-induced neurodegeneration, future research should be focused on reliable biomarker identification in serum by combination of elemental and organic analysis. Development of sample preparation protocols, which keep up Mn-species and are applicable in the ESI source, might reveal new complexes of Mn within the body. Such investigations, however, require development of appropriate standards for quantitative and quality assured analytical analysis. Structure elucidation of Mn-complexes by organic MS methods could also be achieved for example in fractions of SEC after the respective sample pretreatment, which would be another powerful 2D approach in terms of biomarker identification. Overall, studies should be fulfilled in human samples to determine reference values of elemental concentrations as well as species, which can be useful in medicinal practice.
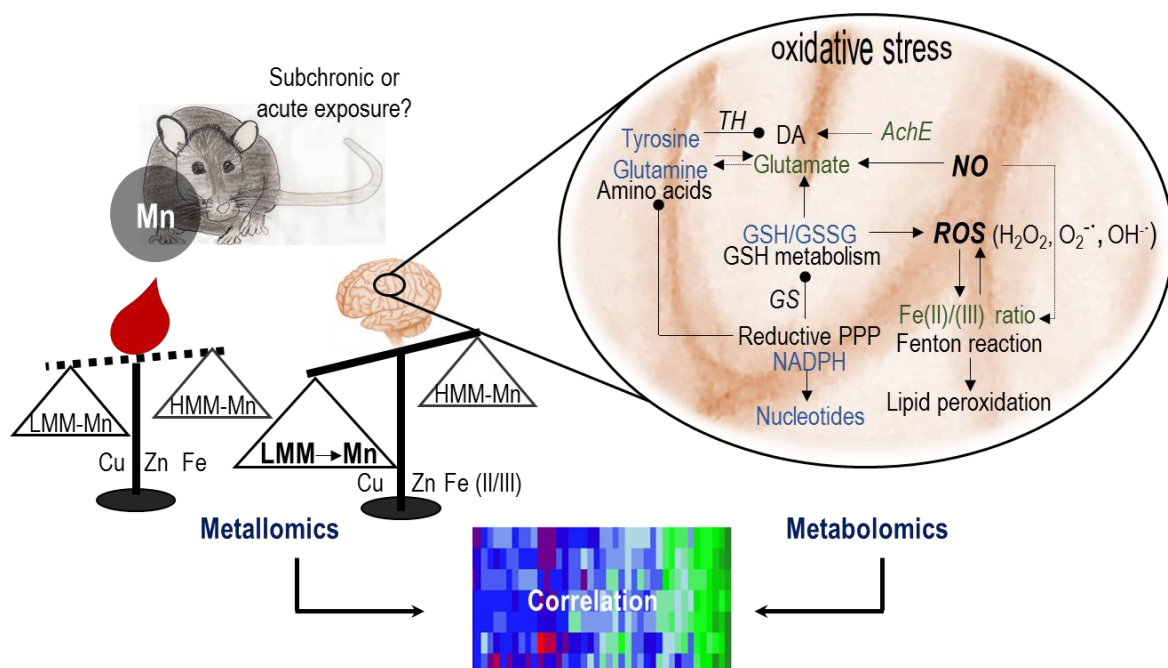
Figure 68 Graphical summary of the main outcome of the thesis.
Application of metallomics in serum and brain showed changes in elemental concentrations as well as Mn-species depending of Mn-exposure, whereas application of non-targeted metabolomics in brain revealed alterations in major neural metabolisms indicating events of oxidative stress. The correlation of both, metallomics and metabolomics, might be useful in terms of biomarker identification during Mn-exposure.

D   Experimental Procedure

D.1   Keeping of animals and Mn-exposure

D.1.1   General conditions

All animal experiments were in accordance with the institutional Animal Welfare Committee as well as the German regulations for experimental animal's treatment as well as approved by the Bavarian federal state government under the file number 55.2-1-54-2531-180-12. For planning the concept of animal treatment or sacrifice, an examined veterinary was consulted. In both animal studies (feeding and injection of Mn), the control and Mn-exposed group consisted of 6 rats. Male Sprague-Dawley rats (RjHan:SD) were chosen due to less hormonal influences compared to female animals (purchased from Janvier (Janvier S.A.S, France)). In the first instance, only the feeding experiment was planned for this work. An appropriate concentration of Mn via the oral route was tested by a preliminary feeding study (*Appendix, chapter E.1*). Due to initial problems with speciation, a further injection study was carried out referring to the one carried out by the last PhD student J. Diederich. Both times, rats were purchased directly after weaning at three weeks of age to ensure sustenance by only mother´s milk, assuming that every rat have had approximately the same status in body trace minerals. The animals were kept in pairs in polycarbonate cages type III under specified pathogen-free conditions at a 12/12 hours light cycle. The cages were embedded by hemp mats to facilitate quantitative collection of feces for analysis of elemental excretion (*Appendix, chapter E.2).* For environment enrichment, paper houses were given in the cages. All animals were supplemented with filtered tap water and fodder ad libitum. The fodder was analyzed with regard to elemental concentrations and was found to comprise an acceptable range of concentrations to be applied in the analysis (*Appendix, chapter E.2*).

D.1.1.1 *Process during the feeding experiment*

Performance of the feeding study and sample taking was carried out in 2012. For the feeding experiment, the control group received a standard diet with 23 mg Mn/kg fodder (R/M AIN 93G, ssniff Experimentaldiäten, Soest, Germany). The test group received the same but Mn-enriched fodder with 500 mg Mn/kg fodder. This concentrations of Mn was still in the range of recommended feeding concentrations according to NRC nutrient requirements of laboratory animals, where the upper limit is given with 1000 mg/kg (NRC 1995). The feeding lasted for 53 days in total, during which time feces was taken weekly for analysis. This feeding ex-

periment was thought to simulate a chronic, low-dose exposure to Mn. It was thought to imitate situations of people living in regions where food or drinking water contains higher Mn concentrations than recommended for daily intake. This feeding experiment was planned to be the only animal study during this thesis. Nevertheless, as speciation pre-trials with these samples had initially not been successful, it has been decided to carry out a further animal experiment by injection of Mn, based on the previous dissertation in the lab of Prof. Michalke, where speciation was carried out successfully (Dr. Johannes Diederich, Dissertation Universität Münster, 2012).

D.1.1.2 Process during the injection experiment

Performance of the injection study and sample collection was carried out in 2013. Animals were kept in pairs and all received the above mentioned standard diet. The aim of giving this fodder was to sustain animals with relatively low concentrations of trace elements for better observation of effects of Mn injection. After an adaption time of two weeks, Mn injection was carried out, where animals had been narcotized with 5% isoflurane. Control animals received 0.1 ml of isotonic 0.9% saline (SteriPharm, Berlin, Germany) intravenously (*i.v.*) through the tail vain. Mn-exposed animals received 0.1 ml of 1.5 mg Mn/kg body weight as $MnCl_2xH_2O$ in 0.9% saline. All solutions were sterile filtered before. The applied injection solutions were prepared from a $MnCl_2$ stock solution (approximately 20 g/l) in isotonic saline, which was measured by ICP-OES for determination of exact concentration of Mn. The factor for dilution for the injection solution of each animal was based on the following calculation:

$$\frac{21.8 \text{ mg/ml (conc. Mn-Stock solution)} * 0.1 \text{ ml (injection volume)}}{1.5 \text{ mg/kg (applicated conc.)} * \text{weight rat (kg)}}$$

Rats were weight before injection and respective dilutions were prepared according to the body weight. One hour after injection, blood was taken from the *vena sublingualis* by punctuation to analyze Mn concentrations in serum. Punctuation means that only a small whole was pierced in this vein by a metal needle and by turning the rat, the blood collected drop wise into an Eppendorf tube. Doing so, the contact of blood to metal needle was as short as possible to prevent contamination of blood with metals from the needle. After the injection, rats were kept as singles in cages for further four days until sacrifice, as Mn concentrations were found to be highest in brain four days after injection (Takeda et al. 1998). During that time, feces were collected every day until sacrifice of animals for monitoring the excretion of elements (*Appendix, chapter E.2*).

D.1.2   Animal sacrifice & Sampling

For sacrifice, animals were deeply narcotized with 5% isoflurane until visible loss of con-sciousness. Sacrifice was carried out by cutting through the *aorta abdominalis* after opening the abdominal cavity with a ceramic scalpel to avoid metal contamination of blood and tis-sue. Right after cutting through the *Aorta abdominalis*, blood was collected in Eppendorf tubes with at least 1 ml per tube. The head was separated from the body and the brain was exposed. It was cleaned with Milli-Q water, weighted and immediately deeply frozen in liquid nitrogen, where it was stored until further treatment for one day. An overview on animal treatment and sampling is shown in Figure 69.
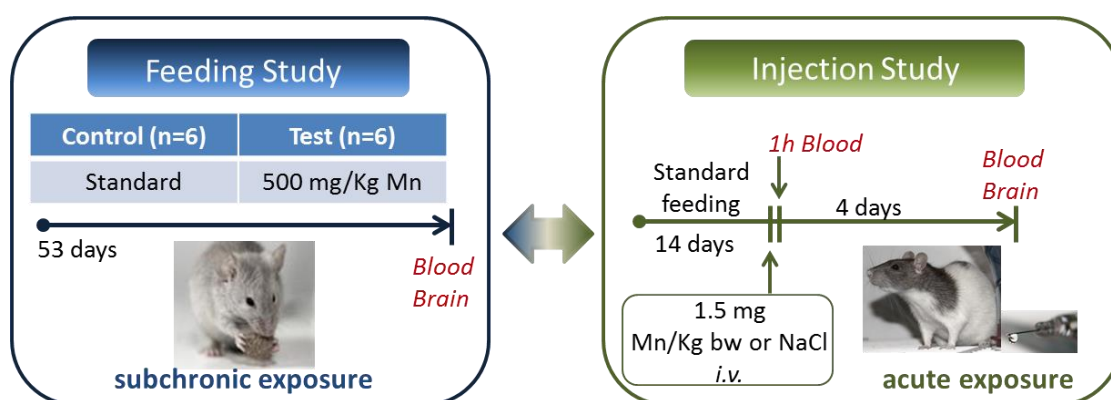
Figure 69 Design of Animal Studies within this work

D.2   Sample preparation procedure

D.2.1   Serum

Blood collected in Eppendorf tubes after punctuation of *vena sublingualis* or after cutting through the *aorta abdominalis* was subsequently centrifuged for 10 minutes at 12000xg and 4°C (Centrifuge 5702R, Eppendorf AG, Hamburg, Germany). The supernatant consisted of serum, which was aliquoted and stored at -80°C until analysis. For determination of whole metal concentrations, ICP-sf-MS measurement was carried as described below.

D.2.2   Extraction of brain tissue

D.2.2.1 Aqueous extraction of brain tissue

For characterization of Mn-species in brain, determination of Fe(II)/(III) in brain as well as for measurement of glutamate and AchE activity in brain, an aqueous extraction of brain tissue was carried out. An extraction protocol adjusted by Diederich et al. (Diederich and Michalke

2011) was applied. This so-called "+N" method included storage of taken brain samples for one day in liquid nitrogen before further processing. The described extraction method was proven to be appropriate for the very labile Mn-species from biological tissue. It was shown to improve extraction efficiency of Mn-species accompanied by higher species stability also after storage of extracts for one month. For eliminating the risk of oxidation, the extraction was carried out in a glove bag (Atmos Bag, Sigma-Aldrich) under Ar atmosphere on ice. Deeply frozen brains were roughly grinded under liquid nitrogen with a PTFE pestle. 0.5-1.0 g of this rough homogenate was transferred into 4 ml of ice cold extraction buffer (10 mM Tris-HCl, pH 7.4), which was previously purged with helium for 3 h. After transfer by 1 ml extraction buffer and homogenization in a 10 ml glass homogenizer (Fortuna, Neolab, Germany), the homogenate was centrifuged in two steps: 5 minutes at 1434 x g at RT and 45 minutes at 20160 x g at 2°C (Biofuge 17 RS, Heraeus-Sepatech, Osterode, Germany). The supernatant was transferred into an Eppendorf tube while the pellet was re-suspended in 1 ml extraction buffer and centrifuged again for 30 minutes at 20160 x g and 2°C. The resulting supernatant was given to the first supernatant and the final volume was filled up to 6 ml with extraction buffer. Extracts were aliquoted and stored at -80°C until analysis. The pellets were stored at 4°C until microwave digestion (*chapter D.2.3.2*). For each brain two extractions were performed yielding 12 extracts per group.

D.2.2.2 Methanolic extraction of brain tissue

For ESI-ICR/FT-MS measurement a methanolic brain extraction was carried out as the aqueous extracts described above were not suitable for the ESI-ICR/FT-MS analysis. These aqueous extracts contained salt from extraction buffer, which would have interfered with the ESI interface disturbing a reliable analysis. The protocol for the methanolic extraction of brain tissue was based on discussion with ESI-ICR/FT-MS-sophisticated colleagues, who have wide experience in analyzing extracts from biological fluids and tissues. They suggested a methanolic extraction by sonication on ice in two cycles. Limitations in time as well as sample amount prohibited investigations on a probably further optimized extraction method. For the extraction, 50 mg of roughly homogenized brain (under liquid nitrogen, see above) were diluted with 500 µl of 50% cold MeOH and sonicated on ice for 20 minutes. The samples were transferred into a 2 ml glass homogenizer with 250 µl of 50% MeOH. Thereafter, the extract was transferred back into Eppendorf tubes with 250 µl of 50% MeOH and again sonicated on ice for 20 minutes. The extracts were centrifuged for 30 minutes at 2°C and 18900 x g (Biofuge 17 RS, Heraeus-Sepatech, Osterode, Germany), and the resulting supernatant was diluted with 70% MeOH 1:10 (v/v). These extracts were stored at -80°C until

measurement, which was carried out the day after the extraction. Due to limitations in the sample amount, only one extract per brain could be carried out.

D.2.3   Nitric acid pressure digestion

For determination of elemental concentrations in a sample such as biological tissue, the matrix consisting of organic material has to be removed to obtain elements in solution. The most applied method is digestion with HNO_3 in closed vessels under pressure. Advantages of these systems are: no evaporation of elements, less external contamination, reduction of digestion time, and improvement of digestion due to the ability to apply temperatures above the boiling temperature of HNO_3. Samples are either weighted into vessels made of PTFE or quartz glass due to the given inert nature of these materials. For thermal excitation, different methodologies are used, such as heating of the vessels in a block of metal in a compartment dryer or by application of microwaves on the material in PTFE vessels in a carousel. A successful digestion is given when the resulting solution has a clear constitution. Important for analytical pure working are cleaning steps before and after the digestion performance applying the same digestion protocol but without sample.

D.2.3.1 Seif apparatus for digestion of brain, feces and fodder

The Seif apparatus developed by Schramel et al. (Schramel et al. 1980) was applied for digestion grinded fodder, feces and homogenized brain tissue. 100 mg of each material was weighted into quartz vessels. After addition of 1 ml distilled HNO_3, the glasses were closed with glass lids and were installed into the Seif apparatus. The digestion was carried out overnight at 170°C in a compartment dryer. After cooling of the devices, samples were filled up to 10 ml with Milli-Q water and stored at room temperature until analysis. For each brain three digestions were performed.

D.2.3.2 Microwave digestion of brain extraction pellets

For microwave digestion of the pellets obtained during aqueous extraction of brain tissue, the pellets were transferred into a quartz glass with 5 ml of distilled HNO_3. These quartz vessels were closed with a specific lid and mounted into PTFE vessels, which were in turn fixed within a carousel. The microwave program consisted of several steps: 0–5 W for 5 minutes, 500 W for 10 minutes, 500–1000 W for 5 minutes, 1000 W for 45 minutes and back to 0 W within 15 minutes. The samples were allowed to cool down and were filled up to 50 ml with Milli-Q water. In that form, samples were stored at room temperature until analysis.

D.2.3.3 Quality control

Each digestion batch included one blank solution (only HNO₃ without sample), which was considered for calculation of elemental concentrations in the samples by a special software (Elana 3.2, HM Informatik AG, Illmenau, Germany; see following *chapter D.3*). Additionally, each digestion batch included digestion of certified reference standard material for quality control. Therefore, bovine liver (CRM 185) was weighted, digested and analyzed in a row with samples.

D.3   Determination of elemental concentrations in samples

All samples were measured by ICP-OES, which is an appropriate method for determination of Mn, Fe, Cu and Zn in standard solution analysis as long as concentrations are adequate with respect to limit of detections of the analyzed elements at ICP-OES (typically 0.5 µg/L for Mn, 1 µg/L for Fe and Cu and 2 µg/L for Zn). Serum and brain extracts as well as extraction pellets were also measured by ICP-sf-MS for determination of Mn as well as for testing the comparability of both instruments. An overview of applied techniques for the various samples is given in Table 15. Before each analysis, serum and extract samples were allowed to thaw at 4°C overnight.

The concentration of elements in the sample solutions were calculated by the instruments respective software (Smart Analyzer Vision/Spectro, WinLab32™/Optima, Element2/Element) based on the before created calibration curve with a certified multi-elemental standard (XGLEN-1686/7, SPEX CertiPrep Ltd., Metuchen, USA). Before, within and after the samples, one blank and one certified multi-elemental standard solution were measured. The final elemental concentration in the samples was calculated on a computerized laboratory data management system (Elana 3.2, HM Informatik AG, Illmenau, Germany). The implied formula of this software aligned concentrations to concentrations in blank, control standards, digestion blank solutions as well as to weight of the samples. Instrument´s operating conditions during solution analysis are listed in the *Appendix, chapter E.4*.

D.3.1   ICP-OES of all samples

For determination of Mn, Cu, Fe and Zn in fodder, feces, digested brains, serum, aqueous extracts and pellets, ICP-OES measurement (Optima 7300DV, Perkin Elmer, Rodgau, Germany or Spectro Ciros Vision, Spectro, Kleve, Germany) was applied. Therefore, samples were diluted in appropriate manner, which is summarized in Table 15. A multi-elemental standard served for calibration of the instruments as well as for calculation of elemental con-

centrations in the samples. Sample introduction was performed by an autosampler (ASX-500, Cetac Technologies, Nebraska, USA or Spectro AS 500, Spectro, Kleve, Germany) connected to a Meinhard nebulizer fitted into a cyclone spraychamber. Before each measurement, 10 blank solutions were measured for stabilization of the instrument. Before, after and in between 12 samples, one blank and one standard solution were measured.

D.3.2 ICP-sf-MS of serum, total brain and brain extracts/pellets

Due to the expected elemental concentrations of Mn being in the lower level as well as for comparability tests, ICP-sf-MS (Element2, Thermo Fisher Scientific, Germany) was chosen as analytical technique for determination of elemental concentrations of Mn in serum, brain extracts and pellets. Sample dilution was 1:20 for serum and 1:10 for brain extracts in Milli-Q water. For internal standardization, 1 µg/l Rh was applied in every case, either by direct addition to samples or by application of the ESI FAST system (Elemental Service and Instruments GmbH, Mainz, Germany), where the internal standard is added continuously during sample introduction by a peristaltic pump. Instrument operating parameters are summarized in the *Appendix, chapter E.4*. Medium resolution was chosen for measurement since it was showing best resolution regarding interferences for the respective elements. Detected isotopes were: ^{55}Mn, ^{63}Cu, ^{65}Cu, ^{56}Fe, ^{57}Fe, ^{64}Zn, ^{66}Zn, ^{68}Zn and ^{103}Rh. A previous peak search before analysis of samples served for setting the mass offset for each isotope for correct mass evaluation. A five point calibration was performed by measurement of a multi-elemental standard with concentrations of 0, 100, 250, 500 and 1000 µg/l containing 1 µg/L Rh as internal standard. Calibrations of at least $R^2=0.999x$ were applied for calculation of elemental concentrations by Elana software.

		Sample	Dilution
ICP-OES		Fodder	1:10E5
		Feces	1:20
		Digested brain	-
	ICP-sf-MS	Serum	1:20
		Aqueous brain extracts	1:10
		Digested Pellets from extraction	-

Table 15 ICP-OES and ICP-sf-MS were applied for determination of total elemental concentrations. Serum, aqueous brain extracts and digested pellets were additionally measured by both due to expected low concentrations of Mn.

D.4   Glutamate concentrations in aqueous brain extracts

D.4.1   Functional principle of the assay

For determination of glutamate concentrations in aqueous brain extracts, the Glutamate Assay Kit of BioVision (California, USA) was applied. According to the manual, the supplied enzyme mix, which is added to the samples, recognizes glutamate with very high specificity. The developing color reaction is dependent on glutamate concentrations in the samples and can easily be measured by a colorimetric method.

D.4.2   Adaption and performance on brain extracts

Due to the distributor´s manual, tissue or cells should have to be homogenized in the supplied assay buffer. Since brain tissue was already homogenized in the Tris buffer mentioned above, dilution experiments were carried out to prove validity of this assay also on the brain extracts. Three different dilutions of aqueous brain extracts (1:5, 1:10, 1:50) were tested to find an optimum fit in between the supplied calibration curve. For reasons of product saving, only a three point calibration curve was carried out. A dilution of 1:10 of brain extracts appeared to have a good concentration of glutamate for application in the assay.

In practice, 50 µl of 1:10 diluted samples or standards or blank (assay buffer) were added in duplets into a transparent 96-well plate. After addition of 100 µl of the reaction mix (90 µl Assay buffer, 8 µl glutamate developer, 2 µl glutamate enzyme mix) according to the distributor´s manual, the plate was incubated at 37°C for 30 minutes under exclusion of light. The optical density was measured at 450 nm using a conventional plate reader (Safire2, Tecan, Crailsheim, Germany). Calculation of glutamate concentrations in the samples was based on the calibration curve carried out by the supplied glutamate standard. The blank value was subtracted from each sample value and concentration of the unknown determined by the calibration equation. The final concentration (mM) is then calculated by dividing the sample amount from the standard curve by the sample volume added to well. At the end, obtained concentrations of glutamate in samples were traced back to gram per brain tissue applied for the respective extraction.

D.5   AchE activity in aqueous brain extracts

D.5.1   Functional principle of the assay

The commercially available AchE Fluorescent Activity Kit of Arbor Assays (Michigan, USA) was applied for determination of AchE activity in aqueous brain extracts. According to the manual, the AchE substrate added to samples or standards reacts with the enzyme by forming a thiol product. The further added proprietary non-fluorescent molecule ThioStar® then covalently binds to this thiol product. The resulting complex is fluorescently active and therefore, fluorescence can be measured at 510 nm after excitation at the range of 370-410 nm. The maximum intensity in the brain extracts was observed at 380 nm, which values were considered for calculation of AchE activity.

D.5.2   Adaption and performance on brain extracts

According to the manufacturer this assay was validated for serum, plasma and erythrocyte membranes. Therefore, also here, dilution experiments had to be carried out to prove validity and the optimum dilution for brain extracts. Again, a 1:10 dilution (v/v) in the supplied assay buffer turned out to be applicable so that measured values were still in the range of detection and the standard curve. 100 µl of each sample or standard were transferred into a black 96-well plate in duplets and 50 µl of the reaction mix was added. The plate was incubated for 20 minutes at room temperature. Thereafter, the fluorescent intensity was determined at 510 nm after excitation at 370-410 nm with a conventional plate reader (Safire2, Tecan, Crailsheim, Germany). Based on the supplied AchE standard, a calibration curve was determined. After subtracting the blank value from the sample values, concentrations were calculated by the equation from the calibration curve (mU/ml). Finally, the dilution factor was implemented and AchE activity was traced back to gram per brain tissue applied for the respective extraction.

D.6   Determination of Fe(II)/(III) status in brain

D.6.1   General considerations

To obtain knowledge about the Fe(II)/(III) ratio after Mn-exposure, ion chromatography for separation of Fe(II) from Fe(III) was hyphenated to ICP-OES as element selective detector. As the aim here was to gain knowledge about the oxidative state of Fe, IEC was chosen as separation technique. The separation principle of IEC is based on the exchange equilibria of charged analyte ions with the oppositely charged stationary phase. Therefore, the column is

equilibrated by the eluent, where charged eluent ions bind to the oppositely charged stationary phase. By application of the sample, the analyte ions compete with the eluent ions for binding sites at the stationary phase. Usually, subsequent change of pH or ionic strength of the eluent leads to elution of the analyte ions by displacement. The retention of the ions is therefore dependent on the pH, the ionic strength of the mobile phase as well as on the nature of the ion exchanger. The herein applied column consisted of a bilayer of anion- and cation resin (quartery ammonium and sulfonic acid, respectively). This column was made for analysis of transition metals and lanthanides in various matrices. In general, IEC often requires eluents with high ionic strength or extreme pH values, where the high salt load can cause problems with the interface to the ICP. Moreover, weakly bound elemental species might be removed; thus, IEC is more suited for covalently bound elemental species of different valence states such as Cr(III)/Cr(VI) or rather Fe(II)/(III).

ICP-OES was chosen as element selective detector due to the fact that Fe was abundant in sufficient concentrations in the brain extracts with regard to detection limits of ICP-OES. The detection limits for Fe in standard solution based analysis (without hyphenation of a column) is about 0.5-1 µg/L at the ICP-OES. Moreover, measurement of Fe was observed to be very robust at the ICP-OES compared to MS based detection (e.g. analysis of Fe at the quadrupole based ICP-MS requires dynamic reaction monitoring due to polyatomic isobaric interferences, what often is problematic due to unpredictable reactions of ions).

D.6.2   Analytical development of IC-ICP-OES

According to literature, the PEEK CS5A together with the guard column CG5A (50 x 4 mm, ThermoScientific, Germany) was able to separate the desired Fe-species. As a test, only the guard column was applied for the analysis and it resulted in the desired separation of Fe(II) and Fe(III). For method development, different eluents as well as different standards were tested. Additionally, chelating agents like ethylenediaminetetraacetic acid (EDTA) and pyridine-2,6-dicarboxylic acid (PDCA) were tested for optimum separation by adding it either to the sample or to the eluent. Examined eluents and standards are summarized in Table 16. Example chromatograms from analytical development are given below.

Standards	Eluents	Flow	Gelating agents
• $FeCl_2$ • NH_4FeSO_4 • Fe(III)citrate • $NH_4Fe(III)$citrate • Spex (Single element Fe standard; liquid)	66mM KOH/5.6mM $KHSO_4$/74mM HCOOH; pH 4.2	isocratic	• EDTA: 1mM in standards • PDCA: 1.5mM in eluent; different concentrations in standards
	250mM NH_4Ac; pH 4.2	isocratic	
	250mM NH_4Ac/ 10mM Tris HAc; pH 7.4	gradient	
	0.8% HCl	isocratic	
	10mM Tris HAc/ 250 mM NH_4Ac; pH varied	gradient/ isocratic	

Table 16   Examined standards, eluents and chelating agents for separation of Fe(II)/(III)

Figure 70 shows the chromatogram of a standard mixture application with the eluent composition based on the column distributor's manual, but modified with respect to concentrations. As standards, $FeCl_2$ and Fe-citrate were applied. A good separation of the standard mixture was observed. However, peak intensities differed although same concentrations were applied. Even more problematic was the fact that K_2SO_4 deposited on the torch and also extinguished the plasma, disqualifying this eluent composition for analysis of brain extracts.
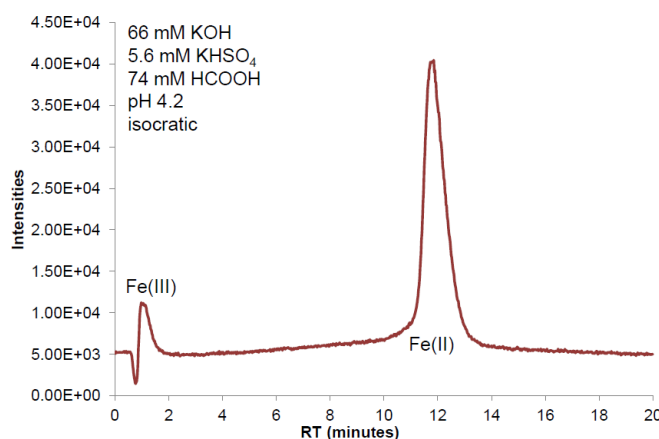
Figure 70   IC-ICP-OES of Fe(II)/(III)-first trials.
Eluent composition based on column´s manual resulted in a good separation, but was not compatible with the plasma.

The chromatograms of standard solutions after switching to a "plasma-suitable" eluent are shown in Figure 71. A gradient with increasing concentrations of H_2O was tested for faster elution of Fe(II). Moreover, 1 mM EDTA was added to the standard solutions as complexing agent. The exemplarily shown chromatograms depict the problem of EDTA in its extreme version: as soon as EDTA was added to the standard solution, Fe(II) was complexed in a manner that retention times were overlapping with the retention time of Fe(III). Although tested in different concentrations, EDTA was disqualified as chelating agent.

10 mM Tris HAc, 250 mM NH$_4$Ac, pH 7.4// 1mM EDTA in standard// gradient
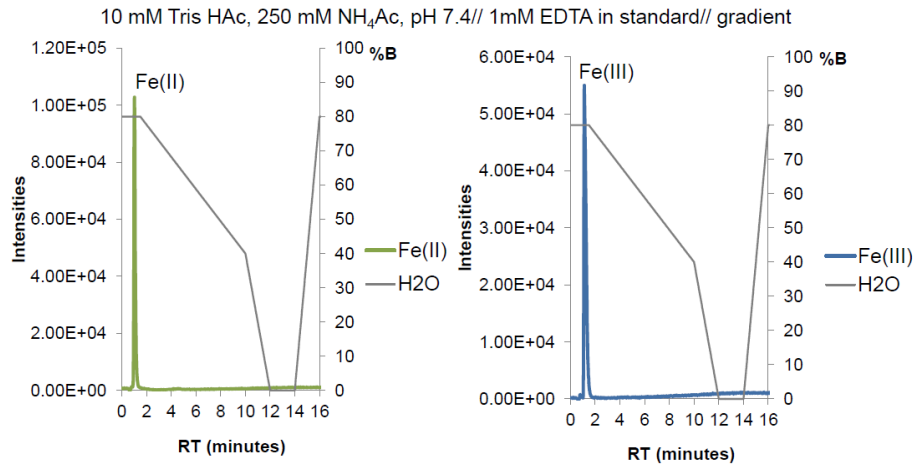
Figure 71 Application of a „plasma-suitable" eluent for separation of Fe(II) and Fe(III).
Gradient elution (grey line) with EDTA added to the standard solutions led to an overlay of Fe(II) and Fe(III) elution.

Another chelating agent applied was PDCA both in eluent (1.5 mM) as well as in the applied standard solutions (1 mM). Figure 72 shows several tested standards under these eluting conditions. It was observed that both FeCl$_2$ (blue line) and Fe-citrate (orange line) standards showed two peaks (for Fe(II) and Fe(III), respectively). The single element standard "Spex" showed only one peak for Fe(III) (pink line), which would be an ideal reference standard for Fe(III). However, these commercial available single-element standards are prepared in low concentrated acid (e.g. HNO$_3$), what disqualifies it to be mixed with the Fe(II) standard or the samples as is would lead to oxidation of Fe(II), which was also observed. For deciphering the origin of the broad peak in almost every applied standard run, H$_2$O was injected (blue line). As the mentioned peak even occurred then, it seemed as if this was a result of the applied gradient (indicated by the grey square). Therefore, it was decided to leave out the gradient and apply an isocratic flow.

10 mM Tris HAc, 250 mM NH$_4$Ac, 1.5 mM PDCA; pH 7.4// 1mM PDCA in standard// gradient
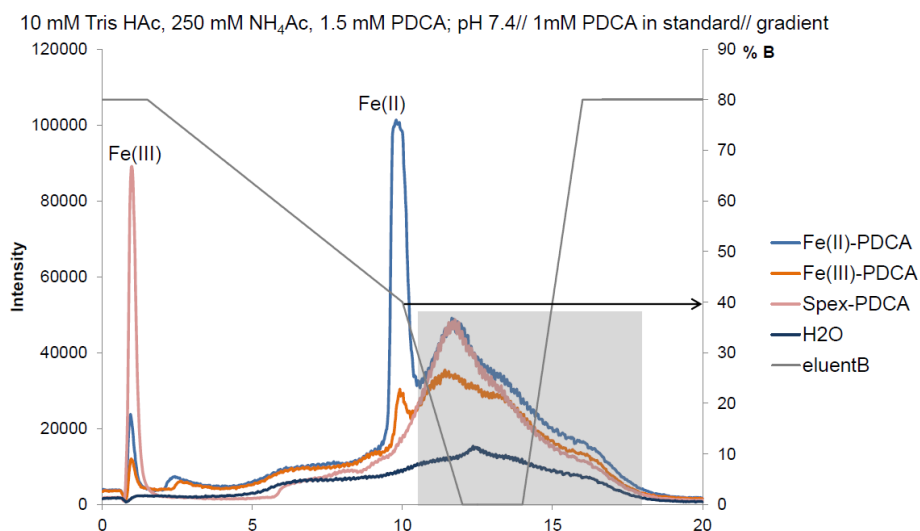
Figure 72 PDCA as chelating agent in eluent as well as standard solutions.
Gradient elution resulted in a formation of a broad peak at the end of chromatogram.

As Fe(II) eluted at around 40% of eluent B (H$_2$O) (black arrow in Figure 72), the isocratic eluting composition was set to 60% eluent A and 40% eluent B. Furthermore, the pH was adjusted to 6.3 to avoid hydroxide formation. This setting finally resulted in a smooth baseline and an elution of Fe(II) at around 5 minutes (blue line, Figure 73). Further tested was the influence of PDCA concentrations in the standard solution itself as illustrated in Figure 73. This test revealed that the standard solution without any PDCA eluted before the complexed ones but still far enough separated from Fe(III), eluting at one minute. Therefore, PDCA was finally only applied via the eluent.
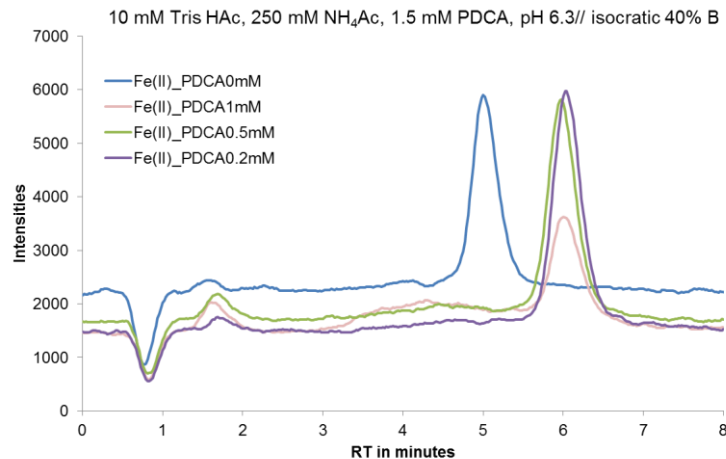
Figure 73 Isocratic elution with 40% B (H$_2$O) and pH of 6.3 revealed a smooth baseline.
PDCA addition to the standard solution had no positive effect compared to Fe(II) standard solution alone and PDCA in the eluent.

The final applied eluting conditions are shown by reference to a sample run (control brain extract) in Figure 74. Elution of Fe(III) and Fe(II) occurred at 1 and 5 minutes, respectively. The Figure illustrates again that adding of PDCA also to the sample solution had no advantageous effect on separation.
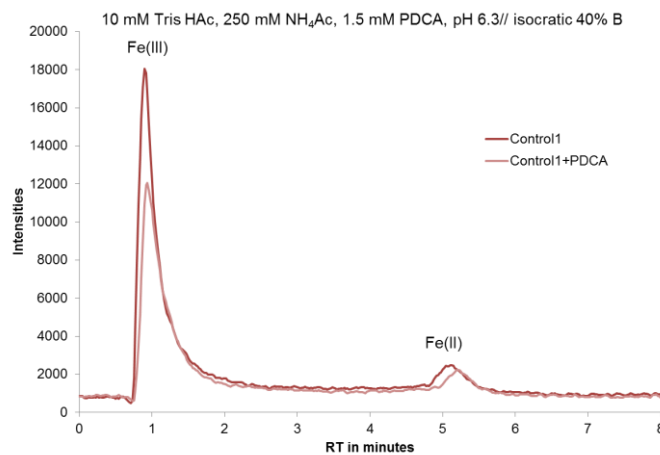
Figure 74 Final eluting conditions shown by application of a control sample (Co1).
Addition of PDCA to the sample (in addition to the eluent) had no advantageous effect.

D.6.3   Chromatographic conditions of IC-ICP-OES

The final applied elution buffer consisted of 10 mM Tris-HAc, 500 mM NH_4Ac and 1.5 mM PDCA at pH of 6.3. After testing of different gradient elution protocols, an isocratic flow of 0.8 ml/min with 40% H_2O (v/v) was found to be sufficient for separation of Fe(II) from Fe(III). A System Gold, 127 NM Solvent Module system (BeckmannCoulter, Germany), was used for eluent delivery, which was further equipped with a Degassext mode DG 4490 (Phenomenex, Darmstadt, Germany) for degassing of eluents. 25 µl of each aqueous brain extract was injected via a syringe filter (0.45 mm, MEMBREX, membraPure Membrantechnik, Reinstwasser, Germany) to filter off any residues, which would have influenced the separation. During operation time, the column was cleaned regularly with 1.5 mM HCl to remove contamination with ions. Before and after each run, a blank run with Milli-Q water was carried out to monitor any potent column carryover.

The HPLC system was directly connected to the sample introduction tube of the Meinhard nebulizer fitted in a cyclone spray chamber of the ICP-OES (Optima 7300DV, Perkin Elmer, Rodgau, Germany), facilitating continuous introduction of the column effluent. The operating parameters for ICP-OES during IC-ICP-OES are listed in Table 17.

Detected wavelength	237.562 nm
Delay time	60 seconds
Read parameters	4 points per peak; 2 replicates
RF Power	1350 V
Nebulizer Gas (Ar)	0.6 ml/min
Plasma Gas (Ar)	15 L/min

Table 17   Operating parameters of ICP-OES during IC-ICP-OES.

To obtain retention times and for calculation of recovery, Fe(II) and Fe(III) standards were applied. Different standard solution of $Fe(II)Cl_2.4H_2O$ were prepared in Milli-Q water in concentrations of 100, 200, 300, 400 and 500 µg/L. Both, external calibration as well as matrix addition analysis was carried out for comparison. The Fe(III) standard was prepared from Fe(III)citrate in acidified (HNO_3) Milli-Q water to ensure release of all Fe(III) from the citrate complex before chromatography. Since the added HNO_3 would have interfered with present Fe(II) in samples by means of oxidation, no matrix addition was carried out for recovery analysis of Fe(III). Instead, external calibration with standard addition served for calculation of recovery of Fe(III). Concentrations of standard solutions were 100, 250, 400, 500 and 750 µg/l with 30% HNO_3 (v/v). Stock solutions of standards (1 g/l) and eluent were prepared freshly before analysis for avoiding oxygen intake during analysis.

D.7   Mn-speciation by SEC-ICP-MS

D.7.1   General considerations and analytical development

Since Mn-species are inherently very labile complexes, an appropriate separation technique for Mn-speciation had to be found. Different approaches were examined, where a few examples of inappropriate applications are shown in the following section. The final applied SEC method is described at the end of the chapter.

Referring to a RP-ICP-MS method carried out by Nischwitz et al. (Nischwitz et al. 2003) three different RP columns were tested for possible separation of Mn-species (Hypersil C4 and Biobasic C4 from ThermoFisher Scientific; Jupiter C4 from Phenomenex). The first task was to evaluate the concentration of MeOH being compatible with the plasma source. A final concentration of 30% MeOH (v/v) in the flow was the highest possible concentration without plasma extinction or observable plasma discoloration. A membrane vaporization system (Spiro, Elemental Scientific, Mainz, Germany) was also tested to be able to apply higher concentrations of organic eluent, but it also brought complications along such as failing ignition of plasma. Different eluent pHs as well as gradients were tested with Mn standards or samples. One example of application of the Jupiter C4 column (Phenomenex, CA, USA) is given in Figure 75. Respective eluting parameters applied are given in Table 18. To reduce the MeOH load into the plasma, post-column dilution with H_2O (0.2 ml/min) was carried out. Chromatograms of Mn-standards and Seronorm™ (animal-based control serum) are illustrated with satisfactory separation of the Seronorm™ sample (light blue line). However, compound characterization was not satisfying indicated by the shown standards in the figure. A reliable assignment of serum compounds was not achieved. As the figure indicates, standards like Mn-citrate (grey line) showed only one peak co-eluting with the inorganic Mn standard (dark blue line) indicating a separation of Mn from the citrate-standard complex. Other tested standards like Mn-Tf showed three peaks (yellow line), although there should only be two peaks (one for inorganic Mn and one protein peak). Moreover, there seemed to be a stacking of major compounds, which finally eluted at the end of the run at increasing MeOH concentrations. The problems with RP-ICP-MS in Mn-speciation should be described by this example. RP-ICP-MS is more suitable for other elemental species like Se-species as they form more stable organo-metallic complexes. Dependent on concentrations of analytes also higher post column dilution would be possible to reduce the organic load in the plasma. Additionally, introducing low concentrations of O_2 can be used for reaction of organic C to be removed from the plasma.

RP conditions for RP-ICP-MS	
Eluent	A: 10 mM Tris HAc, 10 mM NH_4Ac pH6.4
	B: A in 60% MeOH
Flow	0.1 ml/min
Injection V	10 µl

Table 18   Chromatographic parameters of RP applied for samples shown in Figure 75.

—Mn-Citrate   —Mn-Tf   —alpha2-Macrog   —Mn-HSA   —Mn55   —Seronorm
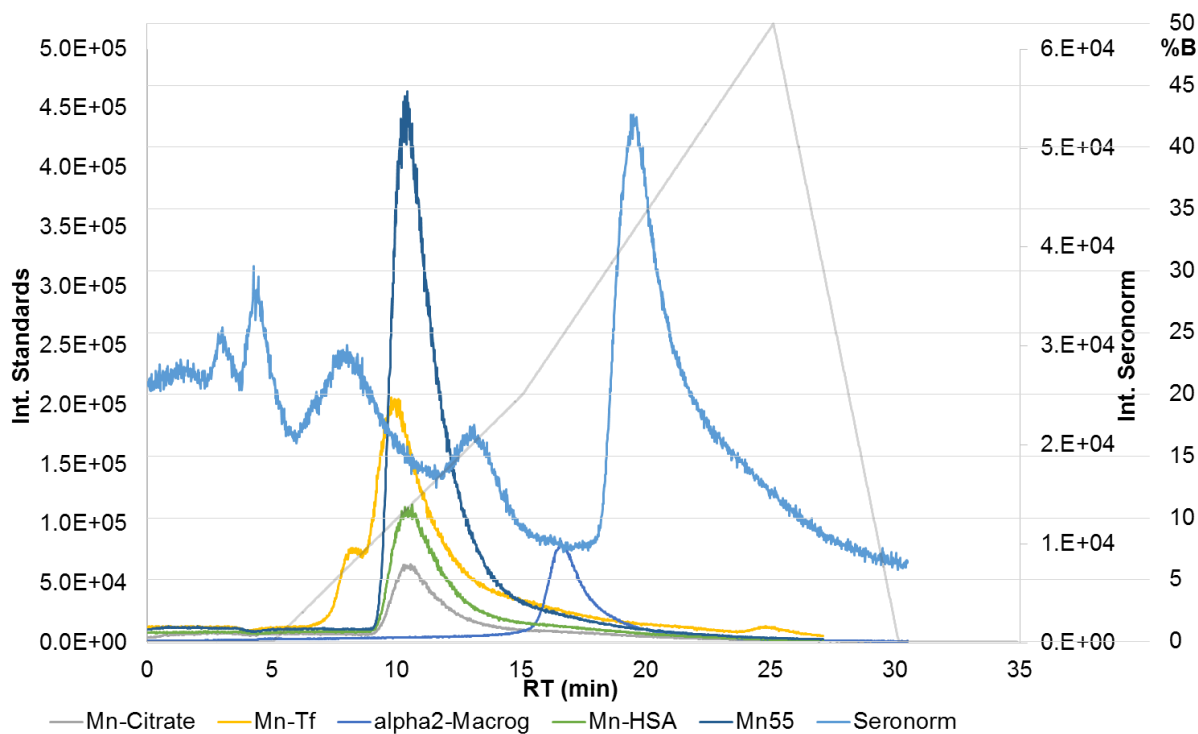
Figure 75 Example of RP-ICP-MS application for Mn-speciation.
Different standards and a Seronorm^{TM} sample (light blue line, second vertical axis) were applied under the shown gradient in Table 18. Assignment of peaks with respect to applied standards was difficult due to co-elution with inorganic Mn (at 11 min) probably due to separation of Mn from standard complexes.

Another approach tested was the hyphenation of IC to ICP-MS for Mn-speciation. Two different columns were examined (BioproQA from YMC America Inc. and AS11 from Thermo Fisher Scientific). Figure 76 illustrates the example of detected Mn and Fe lines from a run applying the BioproQA in gradient elution (Table 19) in following samples: Seronorm^{TM} and serum from the injection trial (control and +Mn_Inj.). It is apparent that the analytical method itself was working as can be seen by the Fe lines, which showed nice separation due to stable complex formation in serum. The problem here again was the characteristic of Mn-species, which seemed to be destroyed during chromatography (by this method). This was also observed for Mn-standards as they showed not reproducible chromatography and retention times could not be assigned clearly. For possible improvement, also column heating and cooling was tested, which neither showed any advantages for separation or improvement in intensity of Mn. The AS11 column showed better chromatograms for Mn in the first

instance but same problems with characterization of the column were observed. This became very obvious by spiking experiments: spiking a standard into a sample led to drifts of peaks or peak splitting or intensity increase in several peaks of the sample. A clear assignment of serum containing proteins was therefore not evaluable. The application of IC for Mn-speciation was therefore also rejected.

IC conditions for IC-ICP-MS	
Eluent	A: 10 mM Tris HAc pH8 B: 20 mM NaCl
Flow	0.5 ml/min
Injection V	25 µl

*Table 19   Chromatographic parameters for IC applied for samples shown in Figure 76.*
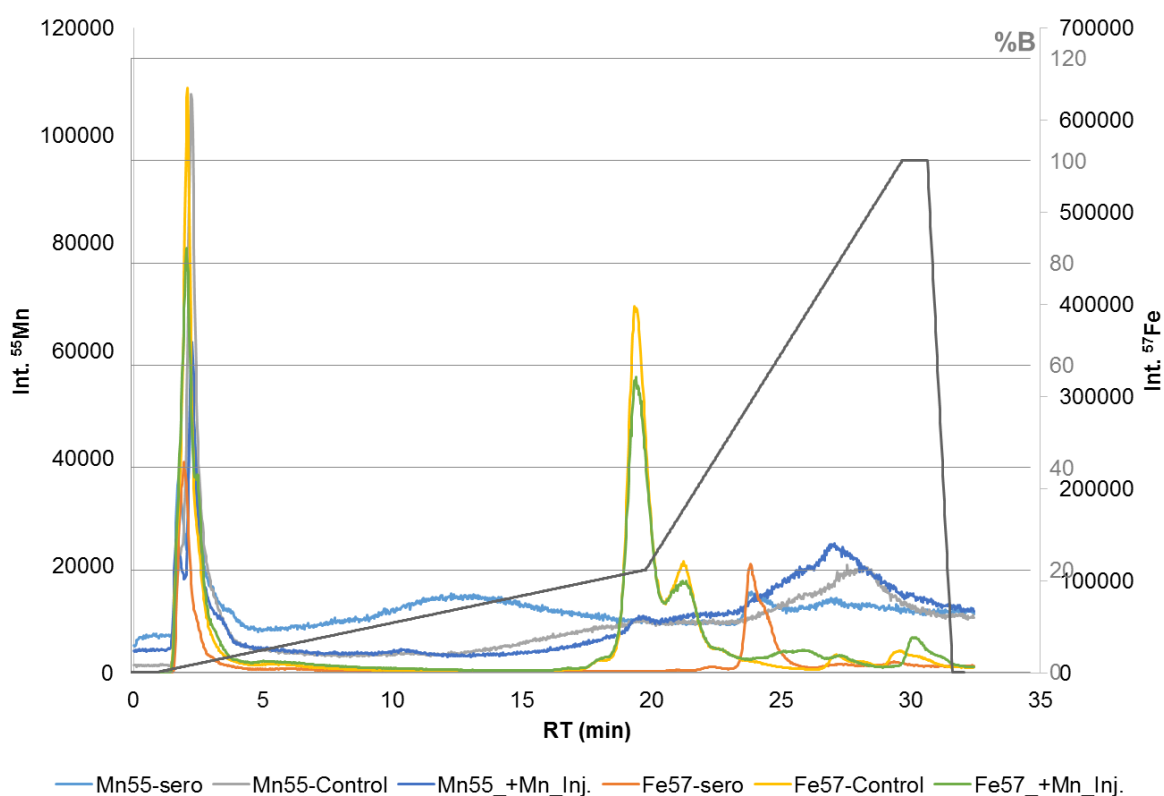
Figure 76 Example of IC-ICP-MS application for Mn-speciation.
Detected lines for ^{55}Mn and ^{57}Fe are shown for Seronorm^{TM}, Control and +Mn_Inj. serum samples of the injection study at the respective gradient (%B, grey line). Compared to Fe (orange, yellow and green lines), which forms stable complexes in serum, Mn separation and detection was not so prominent (light and dark blue/grey lines).

Due to the failures in Mn-speciation by RP- or IC-ICP-MS, the separation technique finally chosen was SEC for the purpose of characterization of Mn-species in brain and serum. SEC was supposed to be a gentle separation technique preserving Mn-complexes in its naturally occurring form. SEC-ICP-MS further was applied in studies of Mn-speciation in various bio-

logical matrices before (Diederich et al. 2012; Michalke et al. 2013; Nischwitz et al. 2008). The stationary phase in SEC is comprised of tightly stacked, small (3-35 µm) and fine-pored (6-200 nm) particles featuring a very big surface on basis of silica gel. The distribution of pore size is strictly controlled and has to be chosen with respect to the separation range of interest. The separation principle is based on hydro- and thermodynamic interactions of molecules at the interface of the stationary and the mobile phase leading to differences in the equilibrium of distribution. Large molecules pass the pores as they are non-retarted in the pores due to size, whereas small molecules can fully sink in and are retained longest by higher interaction with the stationary phase. Depending on how strong intermediate-sized molecules sink in the pores, they will be retained in between (Cammann 2001). The resolution of SEC is commonly very weak and baseline separation is often not given due to a more or less prolonged elution leading to broadening of peaks. In most cases, only size fractions can be determined. The fact that the SEC surface is not completely inherent was shown in some cases, where electrostatic effects or hydrophobic interactions were observed (Szpunar 2000). Increasing the buffer salt could prevent these side effects. However, the recommended concentrations might denature organo-metal complexes, and further are not really compatible with the ICP source. For circumventing the electrostatic or hydrophobic effect, applied eluents need to constitute suitable ionic strength as well as pH. An advantage of SEC is its ability to characterize unknown compounds due to the retention time by alignment with the determined column mass calibration (Michalke 2002). The column mass calibration in turn is not based on molecular size but rather on molecular weight of analyzed standards. The standards for column mass calibration should be chosen in the appropriate size range of expected molecules in the analyzed samples.

To find an optimum SEC-column and/or column combination, various preliminary tests on different columns and column combinations have been carried out in hyphenation to ICP-MS, which are summarized in Table 20. The most important task was a clear separation of the Mn-citrate peak from other Mn-species as this was supposed to be a prominent species formed during Mn-exposure. One major problem hereby was to preserve this species both in the standard as well as in samples during speciation. Furthermore, column suppliers mostly use UV detection for characterization of the columns applying highly salt-loaded eluents, which are not compatible with the plasma. Therefore, eluents have also been tested for high elution capability without applying too high salt-containing buffers.

One tested approach listed in the last row of Table 20 was a pre-separation of Mn-species on a column filled with a heparin based gel. Fractions were collected respective to the sample chromatogram, freeze dried, resolved in eluent in a very low volume and analyzed by the

YMC PackDiol300 hyphenated to the ICP-sf-MS (Element2, Thermo Scientific). The positive effects of this approach would have been firstly, a possible intensity increase due to concentration of samples by freeze drying, and secondly, a more validated description of occurring species due to the 2D-analyis. That approach looked really promising when tested at one brain extract in the first instance due to both, very good separation and high intensities for Mn-species. Unfortunately, these positive effects could only be observed for one brain extract. Repetition of the procedure with other samples had a different outcome. Overall, Mn-citrate was detected in the first instance but not found any more in other extracts. Moreover, characterizing the pre-separating heparin column with standards was not conclusively at all. Although this approach would have represented a very reliable method for determining elemental species due to its 2D structure, it seemed to alter Mn-species in a not predictable way. This was observed overall due to very high intensities of inorganic Mn in every collected fraction from the heparin column. Processes occurring during separation on the heparin column or during freeze drying are not described in detail for Mn-species in literature but seem to be the reason for those inconsistent findings.

Column combination			Eluent	Rejection due to…
Peek: TSK HW75+HW55 100/200x10mm	Peek: TSK HW55 100x10mm	Peek: TSK HW40 250x10mm	50% A: TrisHAc 10mM, NH_4Ac 250mM pH7.4 50% B: H_2O	*No satisfying separation in samples*
Thermo Biobasic SEC300 300x8mm	YMC EcoLab: TSK HW40 700x10mm		80% A: TrisHAc 10mM, NH_4Ac 500mM, 20% MeOH pH7.8 20% B: H_2O	*Although good separation for Fe, Cu and Zn almost no signal detection for Mn; very long analysis time*
Heparin column for pre-separation	YMC PackDiol300		TrisHAc 10mM, NH_4Ac 500mM, NaCl 20mM pH7.6	*Unpredictable changes of Mn-species during procedure (heparin column, freeze drying;)*

Table 20   Tested and rejected SEC column combinations for Mn-speciation.

The finally applied SEC column combinations for characterization of Mn-species in serum and brain extracts are described in the next chapters.

D.7.2   Chromatographic conditions

Characterization of Mn-species was performed in serum as well as in brain extracts by a combination of two columns filled with SEC-material. Since the first column applied for speciation in brain extracts seemed to have lost efficiency after measuring all brain extracts, another first column was applied for speciation of serum samples. Column combinations for each application are described below. The chromatographic conditions were common in both applications (serum and brain extracts).

The applied eluent consisted of 90% Eluent A (50 mM NH$_4$Ac, pH 5.8) mixed with 10% Eluent B (10 mM Tris, 50 mM NH$_4$Ac, 5% (v/v) MeOH, pH 8). The eluent delivery was performed by the metal-free Knauer Smartline HPLC system with an isocratic flow rate of 0.7 ml/min (Knauer, Berlin, Germany). For retention of potent contaminants, a pre-column was installed before the first column (SecurityGuard™, Phenomenex, USA). This pre-column incorporated a small C18 based cartridge in a gold setting, which could easily be inspected for contaminants and was exchanged regularly. After passing the column, the eluent passed a UV detector included in the Knauer system. The UV detection wavelengths were set to 280 nm and 220 nm. Proteins were shown to possess absorption maxima at both wavelengths, which was for example also examined for Mn complexes with HSA or Transferrin (Abe et al. 2008; Chapman et al. 1973). On the other hand, monocarboxylic acids such as citrate possess UV absorption maxima at around 224 nm (Hesse et al. 2002), which was also verified for the Mn-citrate standard herein. In matching the UV signal(s) with the elemental lines from ICP-MS, conclusions about free or protein-bound elements could be drawn. Subsequently to the UV meter, the column effluent entered a Meinhard nebulizer, which was fitted into an in-house-made spray chamber. The injection volume was 25 µl, while each sample had to be injected manually. Automation in Mn-speciation was not possible as there are no total metal-free facilities available for the autosampler. Moreover, chromatographic conditions can change very quickly from one to another sample making a stringent monitoring of sample runs inevitable. Columns were cleaned after each sample by application of 100% B for 10 minutes detecting the wash through. Additionally, columns were cleaned separately overnight by a mixture of 20% 500 mM NaCl and 80% MeOH at 0.1 ml/min in reversed flow to wash off elemental as well as organic contaminations.

The columns were hyphenated to the ICP-MS (Nexion300D, Perkin Elmer, Rodgau, Germany), which was run in dynamic reaction mode (DRC). During this condition, an additional ammonia gas was introduced into the cell resulting in predictive reactions with sample and interfering ions. The reaction with interfering ions was supposed for removing of any po-

lyatomic interferences as described in the *Introduction, chapter A1.2*. Especially for Mn and Fe, this DRC mode was proven to be of advantage for a quantitative analysis. ICP-MS operating parameters during SEC-ICP-MS are listed in Table 21.

Detected masses	Mn 54.938; Fe 56.9354 and 55.9349; Cu 62.9298; Zn 65.9260; Rh 102.905
Dwell Time per amu	300 ms
RF Power	1250 V
RPq	0.8
DRC Cell Gas A (NH_3)	0.7 ml/min
Nebulizer Gas (Ar)	0.94 ml/min
Aux Gas (Ar)	1.2 L/min
Plasma Gas (Ar)	15 L/min

Table 21   ICP-MS (Nexion300D, Perkin Elmer) operating parameters during SEC-ICP-MS.

These parameters were found to be optimum for the measurements. A regular performance check according to manufacturer´s protocol served for quality assurance of the instrumental settings. Therefore, a setup solution (Perkin Elmer SCIEX, Toronto, Canada) containing Al, Cd, Ce, Cr, Cu, In, Pb, Mg, Mn, Rh, Th (1µg/l) and Ba (10 µg/l) was applied. Various parameters like nebulizer and cell gas flows, torch position or auto lens voltages were adjusted. The reference values for good performance are provided by the manufacturer such as [115]In ≥ 50000 cps (counts per second) and Ce/CeO < 2.5%.

For normalization of elemental signals, a post-column supply of Rh solution by an external pump was tested. Unfortunately, back pressure of the columns seemed to be too high so that a useful supply with Rh was not possible. As an alternative, the [103]Rh isotope as such was detected during analysis. Obtained chromatograms for Mn were compared according to peak areas between Rh normalized and not normalized data exemplarily by some samples with PeakFit[TM] v4.11 software (Systat, Erkrath, Germany). Since the resulting peak areas were comparable and the normalization by Rh led to very noisy signals as well as to smeared peak shapes (shown in Figure 77), it was decided to go on without that normalization. Resulting chromatograms were smoothed and fitted to the original signal shape with at least $r^2 \geq 0.99$ in PeakFit[TM]. Obtained percental peak areas were used for calculation of Mn concentrations in comparison with total Mn concentrations in the samples (µg/l for serum or ng/g brain for brain extracts).
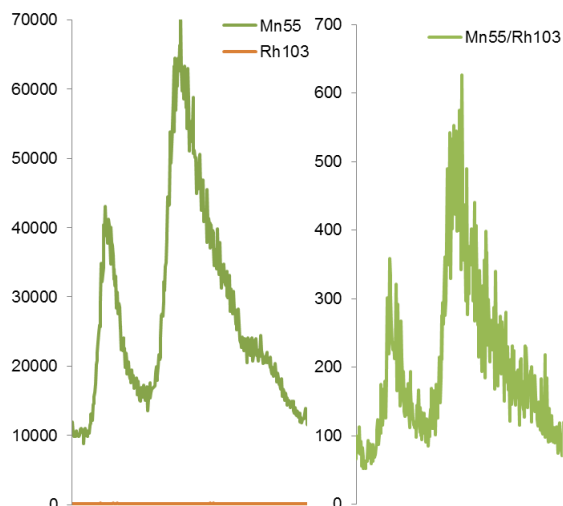
Figure 77 Not normalized vs normalized chromatogram.
The Figure shows an excerpt of a brain extract chromatogram with no normalization on the left side
and with Rh-normalization on the right side, where the signal was very noisy as well as the shoulder
peak was smeared. Unless these effects, peak areas were comparable between normalized and not
normalized chromatograms.

D.7.2.1 Column combination for Mn-speciation in serum

For separation of serum samples two Peek column bodies were combined, whereas the first
one (250x8 mm) was packed with Toyopearl HW55S (TosoHaas, Stuttgart, Germany) for
separation of high molecular mass compounds (HMM) eluting before 19 minutes (separation
range 700-1 kDa). The second column (200x8 mm) was packed with Toyopearl HW40S
(same provider) for separation of low molecular mass (LMM) compounds eluting after 19
minutes (separation range 2000-100 Da). Although LMM compounds and inorganic Mn were
nicely separated from each other as well as from HMMs by this combination, HMM com-
pounds were eluting in one peak. This could not be circumvented by greater dilution since
then, inorganic Mn was merely detectable. However, fraction collection and subsequent
analysis confirmed the peak alignment showing a constitution of the HMM peak of three size
fractions (see also chapter *B.2*).

D.7.2.2 Column combination for Mn-speciation in brain extracts

The two columns combined for separation of Mn-species in brain extracts consisted of a
Biobasic 300mesh column (300x8 mm ID, Thermo, Germany; separation range 700 – 5 kDa)
for HMM compounds eluting before 20 minutes and a 250x8 mm ID peak column filled with
Toyopearl HW40S (TosoHaas, Stuttgart, Germany; separation range 100 – 2000 Da) for
LMM compounds eluting after 20 minutes (same as for serum samples, but freshly packed).

This column combination provided separation of Mn-proteins from each other and from Mn-citrate as well as the latter from inorganic Mn.

D.7.3   Mn-standards and Column mass calibration

To obtain respective retention times and column mass calibration, Mn-standards had to be prepared as there are no commercial available Mn-protein standards. Various proteins and citrate have been mixed with excess Mn in eluent A and allowed to complex at room temperature for one week. Thereafter, standards were stored as aliquots at -20°C until analysis, whereby corresponding working solution were prepared freshly. Furthermore, some standards were applied at the columns without previous mixing with Mn. The standard preparation is illustrated in the following workflow in Figure 78.
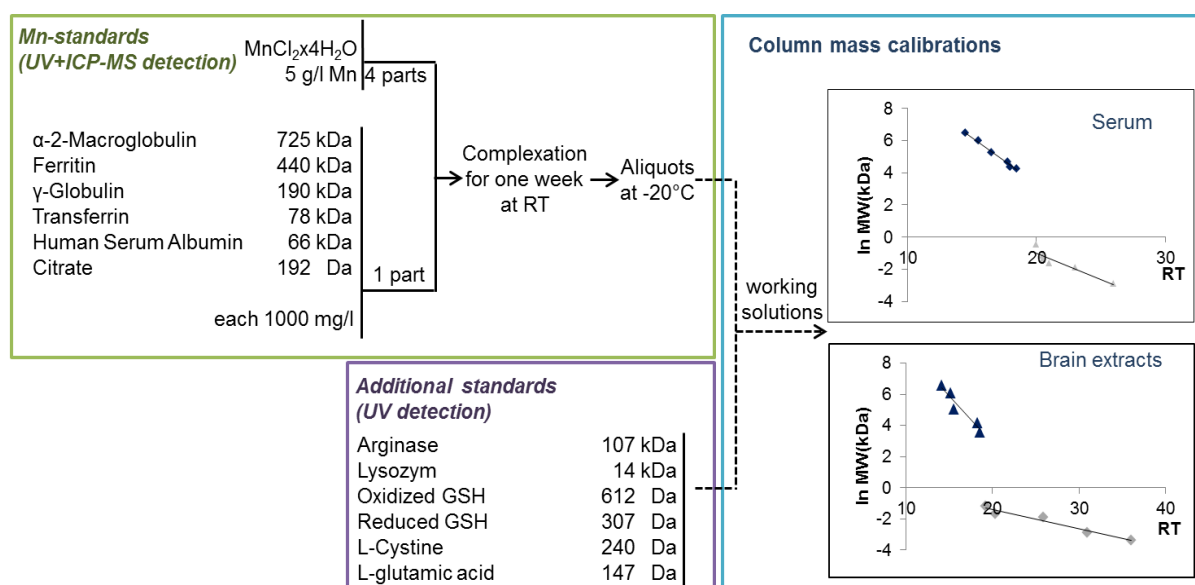
Figure 78 Preparation of Mn-standards and additional standards applied for column mass calibration.

Before elemental detection by ICP-MS, the column eluent passed an UV detector for detection of citrate and disulfide bonds at 220 and 280 nm, respectively. In comparison with the elemental chromatogram, conclusions could be drawn, where Mn was unbound and where it was bound to citrate or proteins. By graphical illustration of ln(MW) against the retention time for each standard, two straight lines were obtained (ln(MW)=a*(RT)+b), describing the separation of each column (column mass calibration). The results are given in *Results and Discussion* at the corresponding chapters (B.*2.1* and *B.3.1*).

D.8   ESI-ICR/FT-MS measurement

Another major task during this work was to get an overview of neural metabolisms, which might be altered due to exposure to Mn. Although there is already knowledge about involved mechanisms during Mn-induced neuroinflammation or neurodegeneration, by application of untargeted ICR/FT-MS a broad overview of changed metabolites can be determined all at once with very high resolutions and mass accuracy (<0.1 ppm). For this purpose, methanolic extractions of the brain tissue were prepared as described in *D.2.2.2*. Samples from the feeding and the injection study had to be measured separately due to the large time lag between carry out of the animal experiments. Measurement conditions as well as data analysis were carried out in accordance to monitor possible common alterations in neural mechanisms after Mn-exposure.

D.8.1   Analytical conditions for ESI-ICR/FT-MS

For acquirement of ultra-high resolution mass spectra, a solariX™ ion cyclotron resonance Fourier transform mass spectrometer (Bruker Daltonics GmbH, Bremen, Germany) containing a 12 Tesla super conducting magnet (magnex scientific Inc., Yarnton, GB) was applied. An Apollo II electrospray source (ESI) (Bruker Daltonics GmbH, Bremen, Germany) served for direct infusion of samples. Before measurement of methanolic brain extracts, external calibration of spectra was carried out by analysis of a 3 mg/l solution of arginine in MeOH with calibration errors below 0.1 ppm (analyzed arginine clusters: [M-H]⁻ m/z 173.10440, 347.21607, 521.32775, 695.43943). Before and after the samples, two spectra of blank MeOH have been recorded to monitor eventually occurring ion memory effects. Between the electrode and the counter electrode an ESI voltage difference of 3500 V was prevalent. To further accelerate ions toward the mass spectrometer, an additional voltage drop of 500 V was maintained between counter electrode and inner cone inside the electrospray. Flow rates of dry gas and of the ESI nebulizer gas were kept at 4 l/min and 2 l/min, respectively. Measurement of samples was carried out in negative ionization mode with a flow rate of 2 µl/min with sample introduction by a Gilson autosampler (sample changer 223, Gilson inc. Middleton, USA), which also provided cooling of the samples at 8°C. Samples were measured in random order. Mass spectra were recorded in a mass-to-charge-ratio of m/z 123-1000 with an ion accumulation time of 300 ms and 300 scans were recorded for one spectrum.

D.8.2   Processing of spectra

The obtained raw spectra were processed with DataAnalysis Version 4.1 (Bruker Daltonik GmbH, Bremen, Germany). Spectra of the MeOH blank solutions were analyzed for contamination such as lipids, but were found to be clean in both measurements. Internal calibration of spectra was carried out by using exact masses of known rat brain metabolites with an error below 0.1 ppm. Thereafter, spectra were exported to peak lists at a signal to noise ratio of 4 and an intensity threshold of 0.01%. An in-house written software (Matrix Generator, M. Lucio) was used for alignment of spectra within an error of 1 ppm. This resulted in a new data matrix including all detected m/z remaining after calibration and exportation. This data matrix was then uploaded to MassTRIX web server (Wägele et al. 2012) in order to perform annotation of masses within an error range of 1 ppm. This software considers C, H, N, O, P and S for finding formulas (including corresponding isotopes) for the respective m/z including correction for the subtracted proton due to ionization mode. Databases such as the human metabolome database (HMDB), Kyoto Encyclopedia of Genes and Genomes (KEGG) or LIPID MAPS are considered for metabolite formulas during the calculation. The resulting KEGG and HMDB IDs have been further applied in the KEGG atlas for analysis of involved pathways (chapter *D.8.2.2*).

D.8.3   Data Analysis

The data matrix resulting from the MassTRIX web server was cleaned in that manner, that only those masses, which were found in more than two out of the twelve samples were considered for further analysis. The final workflow for data analysis of generated ESI-ICR/FT-MS data is shown in Figure 80 at the end of this chapter.

D.8.3.1 *Multivariate statistical analysis*

To obtain group-wise differences, analytical data can either be elaborated by univariate analysis (e.g. t-test, ANOVA) or by multivariate analysis (MVA) (e.g. MANOVA, PCA, PLS). Since univariate techniques bring up parameter-by-parameter differences, they fail to discriminate if single metabolites show only minor differences between groups (Bartel et al. 2013). Therefore, with the use of multivariate analysis also dependencies between the individual metabolites are considered. Via multivariate statistics a group of tools is applied to reduce the dimensionality of large datasets for better visualization and interpretation of results (Madsen et al. 2010).

D.8.3.1.1 Unsupervised methods: HCA and PCA

As an unsupervised multivariate analysis, hierarchical cluster analysis (HCA) was applied to analyze clustering behavior of data. This means to find groups in the data set, which exhibit a similar metabolite intensity profile, regardless of the sample group. Therefore, the open source software Hierarchical cluster explorer© (HCE) 3.5 (Human computer interaction lab, Maryland, USA) was applied with previous normalization of data by unit variance ((X-m)/σ). For clustering itself, Euclidean distances were calculated by the software.

Principal component analysis (PCA) is a further unsupervised method and is mostly used as starting point to elucidate tendencies in a large data set by visualization. During a PCA variables called principal components (PCs) are determined, which represent the majority of the data matrix. The first PC can be seen as a vector through the data set showing the highest variability in the data. The second PC is an orthogonal vector to the first one and describes the maximum amount of the remaining variability. After a certain mathematical factorization of the original data by a coefficient describing the PCs, a score matrix is obtained containing the observations (i.e. samples) in a new coordinate system, which is often illustrated by plotting the first PC against the second PC, called scores plot. In the respective loadings plot, the weight or importance of each variable (i.e. detected mass) contributing to the respective scores is shown.

With PCA being generally applied in MVA, it can be used to find strong subgroupings in a data set (Wheelock and Wheelock 2013). Hence, PCA was also applied for a first visualization of group discriminations or potent outliers herein using SIMCA-P© 9.0 (Umetrics, Umea, Sweden) after scaling of data to unit variance.

D.8.3.1.2 Supervised methods: PLS-DA and OPLS-DA

A step further in data analysis is given by supervised methods. These are of greater interest in hypothesis testing or biomarker discovery within large datasets. Therefore, variables important for separating groups are extracted and correlations between two blocks of data can be found. In this context, two blocks are formed: a X-block containing observations and variables (i.e. oxidative stress markers) and an artificial Y-block containing the class information. The application of partial least square-data analysis (PLS-DA) then helps to extract variables, which are discriminative for one or the other class (Lucio 2008). To get an overview of class separations in the measured samples herein, SIMCA-P© 9.0 (Umetrics, Umea, Sweden) was applied.

Moreover, orthogonal projections to latent structures-data analysis (OPLS-DA) can be seen as an improvement of PLS-DA (Westerhuis et al. 2010). Here, the variance of interest is separated from the variance that is unrelated (i.e. orthogonal) to the defined Y-block (Trygg and Wold 2002). In this way, the variances important for the discrimination between groups are focused into the predictive components while unrelated variances to the tested hypothesis are filtered orthogonally. With regard to the loadings plot, metabolites important for between group differences can be found along the x-axis while metabolites important for within group differences can be found along the y-axis (Wheelock and Wheelock 2013). The strength of OPLS-DA compared to PLS-DA is the use of a single component as a predictor for the class, facilitating the linkage of experimental variables.

In the end, OPLS-DA should reveal variables (i.e. metabolites), which classify the analyzed groups, i.e. which might even be useful as biomarkers. As there are no general rules, a commonly used parameter for defining a cutoff between "unimportant" and "important" variables is the Variable Importance in Projection (VIP) score. As its name implies, the VIP summarizes the importance of each variable in driving the observed group separation (Eriksson et al. 2006). Generally, VIPs>1.0 are often considered to be important. However, Wheelock (Wheelock and Wheelock 2013) recommend to additionally use the p(corr) for variable selection. P(corr) represents the loadings scaled as a correlation coefficient between the model and original data, ranging from -1.0 to 1.0. A value of >0.4-0.5 is commonly applied. In this work, OPLS-DA was carried out to determine discriminative masses, which were important for group separation applying SIMCA-P$^©$ 13.0.3.0 (Umetrics, Umea, Sweden).

D.8.3.1.3 Model quality

In general, all MVA methods are prone for over fitting of data. Hence, cross-validation should be performed, yielding two major variables, which give information about the quality of the model and which should always be considered and reported when applying MVA. One of these variables is the R^2, which is based on the fraction of the original data explained by the model. It is therefore a measure of the overall fit of the model. Additionally, Q^2 is the cross-validated correlation and represents the predictive power of the model with regard to a new dataset (0.9 would implicate a perfect model, while values >0.5 are considered to represent a good model) (Eriksson et al. 2006). With R^2 and Q^2 being similar, an ideal model would be described, where each subject contributes equally and uniformly to the separation of groups. In fact, R^2 is mostly larger than Q^2, but shouldn´t be substantially larger, as this would be a sign of an over fitted model.

D.8.3.2 Pathway mapping

The results from annotation of data via MassTRIX webserver refer to a data base search in LIPID MAPS, HMDB (human metabolome data base) as well as in KEGG (Kyoto Encyclopedia of Genes and Genomes). Therefore, annotated masses receive a corresponding KEGG ID. These have been uploaded to KEGG Mapper (http://www.genome.jp/kegg/tool/map_pathway2.html) to search for involved metabolic pathways and potent differences with regard to the respective organism (rattus norvegicus). Additional given HMDB or LIPID MAPS IDs were also considered and investigated.

D.8.3.3 Formula Calculation

Eventually occurring Mn-containing complexes, which were formed in the brain, might have also been detectable by the ICR/FT-MS measurement. Such complexes are not considered during annotation with MassTRIX. Another software was chosen for formula calculations. The applied in-house written algorithm for calculation of possible Mn-containing formulas is called FormCalc (Frommberger M., unpublished). In general, every desired element can be chosen and ranges for amounts of each chosen element can be set for how often this element can maximally be included in the sum formula. During this work, these ranges were chosen as: 0-100 C, 0-80 O, 0-3 N, 0-2 S and 0-1 Mn within an error window of 0.2 ppm. This calculation was applied on the same mass list matrix, which resulted from matrix generator. Based on the resulting formulas, van Krevelen plots were prepared to monitor specific metabolite groups. This kind of plot sorts the metabolite formulas on two axes such as the ratios of hydrogen to carbon (H/C) to the ratio of oxygen to carbon (O/C). An example is shown in Figure 79. This kind of illustration was applied for an overview if Mn-containing formulas can be assigned to certain classes of compounds as indicated in the figure. Due to this classification, also possible reactions such as decarboxylation or dehydrations can be visualized.
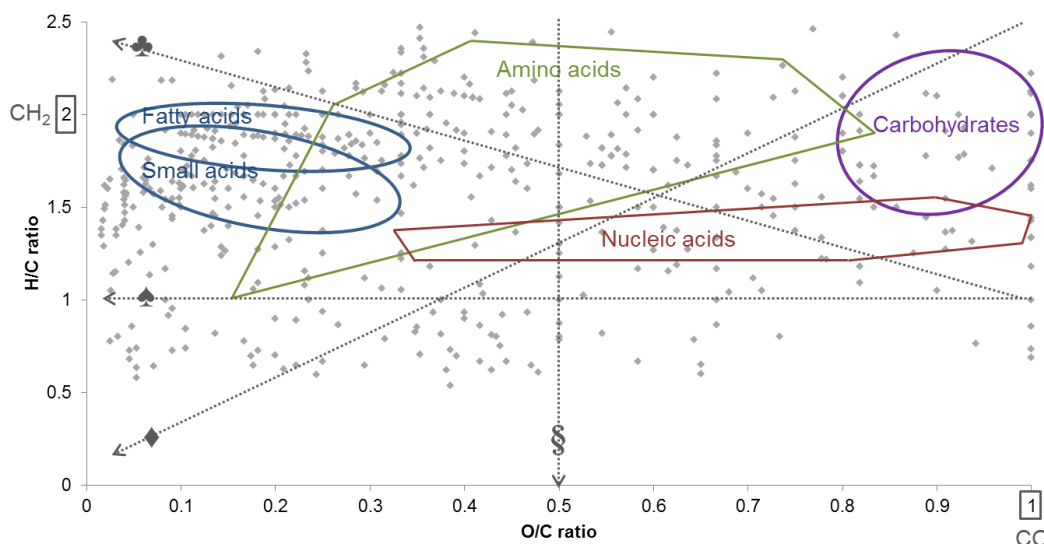
Figure 79 Example of a van Krevelen diagram.
Integrated are the various biomolecular classes such as lipids (fatty/small acids), amino acids, nucleic acids, and carbohydrates. Dashed arrows indicated direction of reaction: ♣ decarboxylation ($-CO_2$), ♠ reduction ($-O$), ♦ dehydration ($-H_2O$), § dehydrogenation ($-H_2$) (modified with permission according to (Hertkorn et al. 2008; Schmitt-Kopplin et al. 2012)).

D.8.3.4 Network analysis

Due to the fact that only a fractional part of detected masses is annotated via MassTRIX webserver, many detected metabolites remain "unknown", which means detected m/z are not assigned to a certain sum formula. This is especially true for Mn-containing compounds, as available databases usually lack in information about such complexes. Therefore, application of mass difference networks can help to unravel sum formulas for masses, which were not annotated, by analyzing possible mass-differences, i.e. specific reactions between metabolites (e.g. loss of H_2O and addition of Mn). The in-house written software NetCalc (Tziotis et al. 2011) was applied for network analysis. By uploading of the respective sample mass list as well as a mass list consisting of masses, which define certain biochemical reactions, all possible mass differences based on the uploaded lists are calculated by NetCalc. Therefore, at least one mass with an exact sum formula in the data matrix has to be known for sure. The calculation was carried out with a network tolerance error of 0.2 ppm and C, H, O, N, S and Mn were considered for elemental formula calculations (allowed reactions are shown in Figure 54).

For visualization of the network, the open source software Gephi (The Open Graph Viz Platform, http://gephi.github.io/) has been applied. The NetCalc output had to be prepared by constructing tables containing nodes and edges, which were imported to Gephi. The nodes table included all masses, which are necessary to describe the applied reactions. The edges in the network represent all possible mass difference reactions between detected masses.

The applied algorithm for network construction was YifanHu, implemented in Gephi. An available plug-in called Noverlap was applied to prevent node overlapping. This can be help-ful in small networks like herein, to examine the nodes more precisely. By this, unknown masses might be clarified through the respective occurring mass difference. Furthermore, interesting information about possible Mn-complexes might be observed.

D.8.3.5 Correlation analysis

In a further step, correlations between different variables as results from the metallomics part (e.g. elemental concentrations in serum or brain, Fe(II)/(III) concentrations in brain, AchE activity in brain, Mn-species in serum or brain) with detected brain metabolites were exam-ined. For the brain metabolites, data from the multivariate analysis (OPLS-DA) were taken (scaled to unit variance and 7-cross validated) and Pearson´s correlations were calculated with the variables of interest. The correlations are shown as heatmaps with a color code, where dark green color means strong positive correlation and dark red color means strong negative correlation.
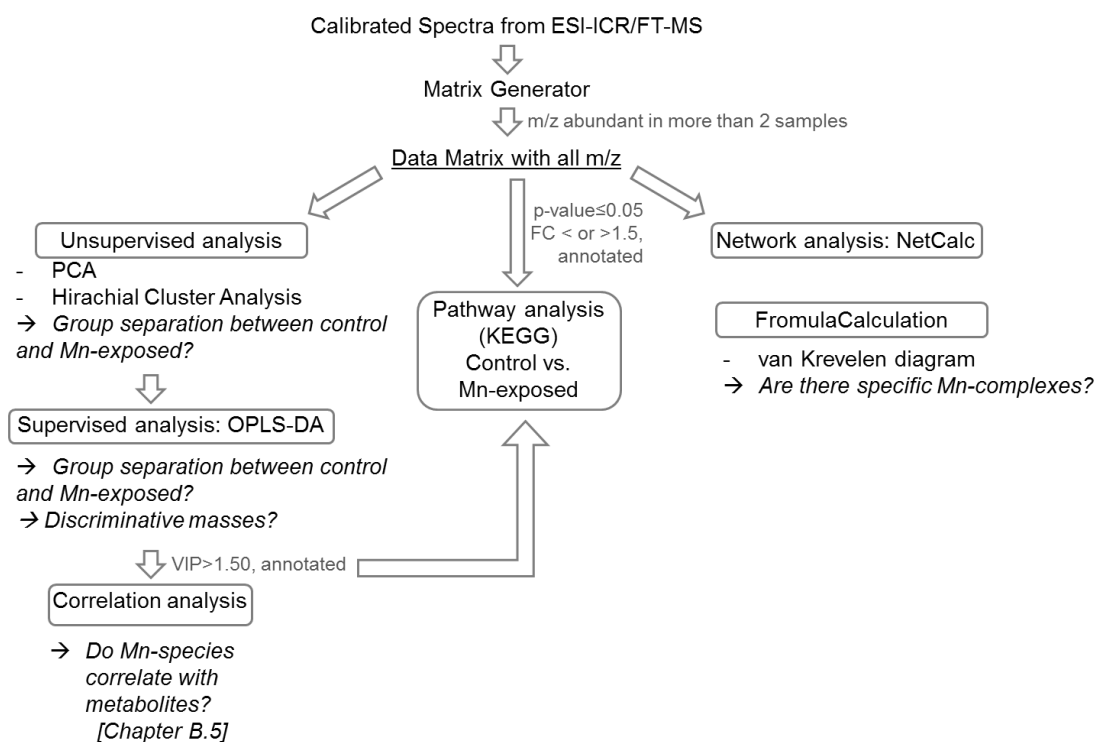

Figure 80 Workflow for data analysis of data obtained by ESI-ICR/FT-MS of methanolic brain extracts.

D.9   Laser ablation-ICP-MS

D.9.1   Animals, sampling and sample preparation

For determination of elemental distribution within the brain after a single $MnCl_2$ injection, a laser ablation system was hyphenated to ICP-MS (LA-ICP-MS). To obtain samples, the same injection study as described in *D.1.1.2* was repeated. In short, 6 male Sprague Dawley rats received 100 µl of a solution of 1.5 mg/kg b.w. $MnCl_2$ in isotonic saline through the tail vain under deep narcotization with isoflurane. For the control group, 6 animals received 100 µl of isotonic saline. Again, for control of Mn injection, blood was taken one hour after injection by punctuation of the *vena sublingualis* and analyzed by ICP-sf-MS as described above. After sacrifice of animals, blood and brains were taken. The brains were weight and subsequently frozen carefully initially in the steam of liquid nitrogen and then totally in liquid nitrogen. This procedure prevented breaking of the brain samples, which was important for cryosectioning. For tissue sectioning, brains were embedded in Tissue-Tek® (O.C.T^{TM}, Sakura Finetek Europe, Netherlands) for more stabilization in small, square shaped cryomolds of PTFE (22x30x20 mm) and frozen at -20°C. Since the aim was a general overview of elemental distribution of Mn, Fe, Cu and Zn in all brain regions along the brain axis, it was decided to carry out sagittal brain sections in the near center of the brain as shown in Figure 81. In this way, all parts of the brain could be observed at a glance on one brain slice. Cryosectioning was performed at a cryostat (CM3050S, Leica Biosystems GmbH, Wetzlar, Germany) with ambient temperature of -20°C by cutting slices of 35 µm of the embedded brain samples.
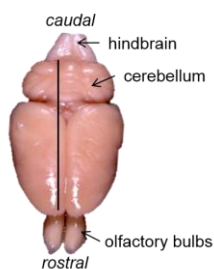
Figure 81 Dorsal view of a rat brain (without embedding medium).
Slices for analysis by LA-ICP-MS were tried to be cut in the near of the middle along the black line.

Slices were thawed on microscope slides (Superfrost Plus^{TM}, Thermo Fisher Scientific, Germany) and stored at -20°C until analysis. The cryosectioning itself brought along some problems due to the relatively big brain compared for example to a mouse brain. The distance between the blade and the sample holder was too small. This led to the need of cutting a peace of the sample edges manually by a razor blade losing some sample. The plan was to perform sections of at least two brain samples per group (Mn-exposed and control). But due

to time and technical problems with the ICP-MS only one slice of one sample per group could be analyzed within this work.

D.9.2   Preparation of standards

Standardization of LA-ICP-MS in biological issues is still a major challenge as the commercial available certified reference materials consist of glass or stone and are therefore not really comparable with the matrix of biological tissue. Matrix-matched standards mostly have to be prepared in-house and need to be adapted to the respective samples. As one possible way to achieve this herein, pig brain was used as matrix for standards. It was believed to be a comparable matrix to rat brain. The pig brain was homogenized by a PTFE pestle and subsequently by a ceramic mortar. These homogenates (n=4) were weight in glass vessels for nitric acid digestion to obtain existing elemental concentrations of Mn, Cu, Fe and Zn by measurement with ICP-OES (procedure for nitric acid digestion by Seif aperture and measurement conditions were the same as described above in *D.2.3.1*).

The existing concentrations in the pig brain were compared with elemental values in the rat brains of the injection trial as similar concentrations of Mn, Fe, Cu and Zn were expected in this samples (repeated injection study). Based on these concentrations, spiking of pig brain was carried out to obtain a five point calibration for Mn, Fe, Cu and Zn with values in between the calibration curve. Each 5 g of homogenized pig tissue was dosed with the respective elemental concentration from single elemental standards. These mixtures were homogenized intensively to ensure total distribution of the elemental standards within the pig tissue. Each homogenate was filled up to 6 g with Milli-Q water to obtain consistent masses. The homogenates were filled in the same square shaped cryomolds of PTFE as used for samples and frozen at -20°C. Additionally, an aliquot of each standard homogenate was preserved for nitric acid digestion. The digested standards were again measured by ICP-OES to verify exact concentrations of the prepared standards. The workflow for standard preparation is illustrated in Figure 82. The frozen standards were also cut at 35 µm thicknesses by the cryostat, thawed on microscope slides and stored at -20°C until analysis by LA-ICP-MS.
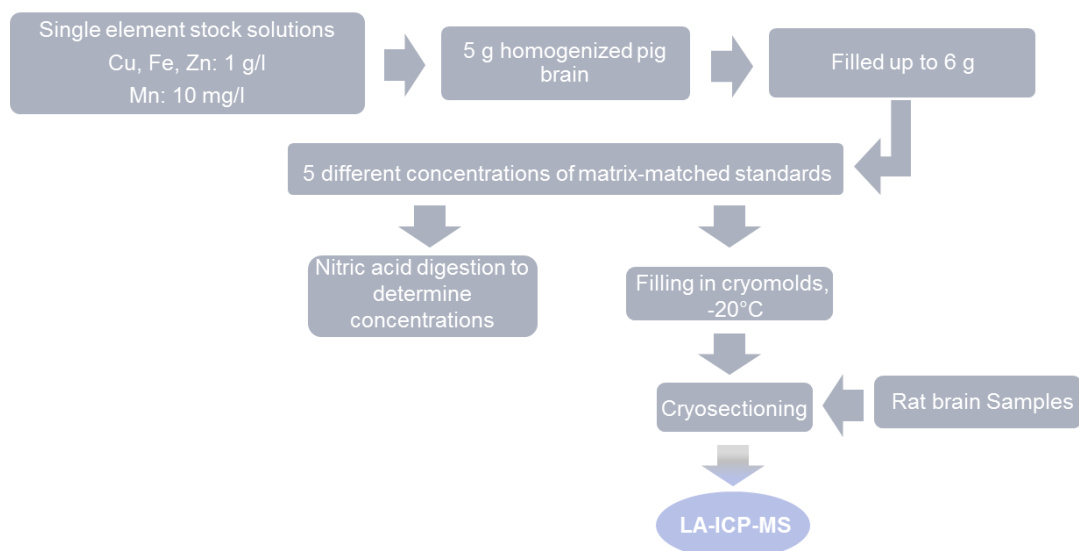
Figure 82 Procedure for preparation of matrix-matched standards for LA-ICP-MS.
Pig brain was doped with four different concentrations of single elemental standards of Mn, Fe, Cu and Zn to obtain a five point calibration. Aliquots were digested to determine concentrations and the rest was frozen in cryomolds, cut in slices and analyzed by LA-ICP-MS in line with samples.

D.9.3   Setup and measurement of LA-ICP-MS

The applied laser ablation system was the solid state laser ESI NWR213 system (Electro scientific industry Europe ltd, Cambridge, UK) supplemented with a Nd:YAG laser operating at 213 nm. This laser ablation unit was hyphenated to the ICP-MS Nexion 300D (Perkin Elmer, Rodgau, Germany). Firstly, it was planned to simultaneously introduce an internal standard (IS) with the ablated material. Delivering an internal standard in parallel with the laser aerosol enables wet plasma conditions (instead of dry plasma conditions), which was shown to be of advantage (O´Connor et al. 2006) by stabilizing the sample introduction into the plasma. Additionally, the ICP-MS measurement can be monitored with regard to mass drifts and intensities. A glass T-peace in front of the ICP-MS torch connected the outlet tube of the laser with the IS aerosol (10 µg/l Rh in 1% HNO_3) from the externally Ar-supplemented spray chamber. However, when running test measurements, this setup appeared to be very unstable showing high oxygen intake, which interrupted plasma conditions and measure-ment. Moreover, further elaboration of generated files normalized to the signal of [103]Rh was not possible by the applied imaging software. At the end, this parallel setup was withdrawn, and the laser outlet tube was connected directly to the torch as applied during general setup. The settings of the ICP-MS as well as the setting for laser ablation are summarized in Table 22. The nebulizer gas (Ar) of the ICP-MS served as gas inlet into the laser system for carry-ing ablated material into the ICP-MS. The nebulizer gas flow was tested for highest signals and was found to be ideal at 1.06 l/min. Laser parameters were also tested by rat brain slic-es and the mentioned parameters in Table 22 were found to be an acceptable compromise

between signal intensities, resolution, sample intake into the ICP-MS and time of measurement. The samples were analyzed line by line and standards were analyzed before and after every measurement with two lines (each ~2000 μm) per standard under same conditions. One brain slice was measured in three steps resulting in a total analysis time of around 23 hours.

Laser parameters		ICP-MS parameters	
Energy	35%	*RF-power*	1250
Fluence	1.90-2.00 J/cm^2	*Isotopes*	^{11}B, ^{55}Mn, ^{57}Fe, ^{63}Cu, ^{65}Cu, ^{66}Zn, ^{68}Zn
Repetition rate	10 Hz	*Dwell time*	50 ms
Spot size	50 μm	*Nebulizer gas (Ar)*	1.06 l/min
Scan speed	50 μm/s	*Plasma gas*	15 l/min
Spacing between lines	50 μm		
Warm up	10 s		
Wash out	15 s		

Table 22   Parameters for laser and ICP-MS during LA-ICP-MS.

D.9.4   Data elaboration and imaging

Every ablated line was exported as single xl file by the ICP-MS software (NexION® software v 3.5). As mentioned above, one slice was analyzed in three parts, where all recorded xl files corresponding to one measurement part were imported into Iolite v2.5 (Paton et al. 2011) as an add-on to Igor Pro (Wavemetrics, Igor Pro 6.34A). According to the manual, the Trace Elements data reduction scheme was applied. For each element (Mn, Fe, Cu, Zn), the baseline was subtracted and the respective measurement time was integrated automatically. Pictures were generated according to the respective aspect ratio (ratio of length to width) of ablated area to obtain correct shaped pictures. If needed, smoothing was performed and pictures were exported at high resolution. The data from analysis of standards were elaborated by Microsoft Excel. The average of the baseline signals (cps) from each element was subtracted from the signals of the measured standard. From the remaining values, the median was calculated for each element. As the standards were measured before and after each analysis, eventually occurring drifts in signal intensities could be monitored. Obtained values for each standard were listed and the average was calculated excluding major outliers (e.g. values near 0 cps due to holes in the standards). These averaged cps values were then plotted against the determined concentration of each element by ICP-OES, and trend lines were calculated. Intensities (cps) from samples could then be applied to the trend line equation and concentration could be calculated. These concentrations were further compared to elemental concentrations in the rat brains determined in the first injection study. Doing so, obtained values by LA-ICP-MS of matrix-matched standards could be compared with expected values and the reliability of the applied standard procedure could be tested.

E   Appendix & Supplementary Data

E.1   Preliminary Feeding study

Based on the initial plan of the doctoral thesis, one feeding study with Mn concentrations at the boarder of sufficient to elevated levels should be carried out. At the beginning it was not clear if the Mn should be administered by water or fodder. A preliminary feeding study was designed to figure out the resulting body concentrations of Mn, taken up by tap water. Group sizes of rats were really small, because the aim was just to get an idea of how concentrations in serum and brain get altered by elevated Mn.

E.1.1   Study design

Male Sprague-Dawley rats (RjHan:SD) were purchased from Janvier (Janvier S.A.S, France) at the age of three weeks directly after weaning as describe in *D.1*. Control rats (n=2) were kept in pairs and received standard fodder (ssniff EF R/M AIN 93G, see *D.1.1*) as well as tap water ad libido. Mn-supplemented rats (n=3) were separated into two cages (one pair and one single) and received the same fodder as well as Mn-enriched tap water (0.2 mg/l) ad libido. The animals were kept in polycarbonate cages type III under specified pathogen-free conditions at a 12/12 hours light cycle. The study lasted for one month. During that time, feces were collected weekly for analysis. Animal sacrifice and sampling was according to the procedures described in *D.1.2*. The only difference was that also liver and kidneys were taken for analysis of elemental concentrations.

E.1.2   Sample preparation

Serum was gained by centrifugation of blood (10 minutes at 12000xg and 4°C) taken from the *vena abdominalis* after deep narcotization of animals with 5% isoflurane and stored at -20°C until analysis.

Liver, kidney and **brain** were taken, weight and suddenly deep frozen in liquid nitrogen. Extraction of brain was carried out as described in chapter *D.2.2.1*. Extraction of liver and kidney was carried out with the same extraction buffer (10 mM Tris, pH 7.4, ice cold and pre-flushed with He). Applied extraction volumes differed from brain extraction and were in analogy to the developed method by Diederich et al. (Diederich and Michalke 2011).

For determination of total elemental concentration in tissues, nitric acid digestion was carried out as described in chapter *D.2.3*. Fodder, feces (freeze-dried), liver, kidney and brain were digested by the described Seif method.

E.1.3   Determination of elemental concentrations in fodder, feces, serum and tissues

Analysis of fodder after nitric acid digestion revealed comparable values to the declared ones for Fe, Cu and Zn (104%, 117%, 105% compared to declared values). The measured concentration of Mn was 72% higher than the declared one giving not optimum experimental conditions with regard to the control group.

The results from analysis of feces are shown in Figure 83. It can be seen that the Mn-exposed animals excreted more Mn throughout the four weeks of treatment with slightly higher excretion the third week. Regarding the other elements, Fe and Zn excretion were slightly higher in Mn-exposed animals compared to control. For Cu excretion, no considerable change was observed.
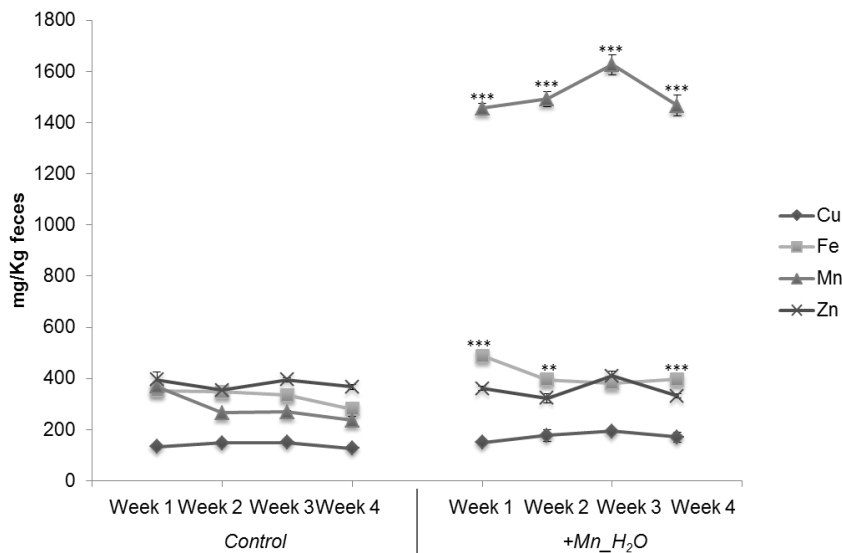
Figure 83 Analysis of feces in the feeding pretrial.
*Feces was collected weekly and analyzed by ICP-OES after freeze-drying and nitric acid digestion (n=5 digestion per sample, Student´s t-test between control and +Mn_H$_2$O *p<0.05, **p<0.01, ***p<0.001).*

Table 23 shows measured concentrations of Mn, Fe, Cu and Zn in serum, total brain, liver and kidney. For extracts only Mn and Fe levels are shown as the extraction protocol was explicitly developed for those two elements. In general, Mn values were higher in brain but the increase was not significantly or very high compared to control (only 5% higher values). Similar to the chronic feeding, serum Mn levels were slightly higher in +Mn_H$_2$O animals but not significant. Regarding Mn levels in liver and kidney, there was no difference in liver and a slight but not significant increase in kidney. For example, Diederich et al. observed an accumulation of Mn also in kidney after a single injection of MnCl$_2$ (Diederich et al. 2012). The shift in Fe towards lower concentrations was also observed in serum, brain, liver, and kid-

ney. Additionally similar to the final carried out feeding study was the significant increase of Cu in serum, brain, liver and kidney. The same was true for the significant decrease of Zn in serum, brain and kidney.

		Control	SD	+Mn_H2O	SD	p-value
		Serum				
µg/l	**Mn**	6.9	0.1	7.3	0.2	n.s.↑
mg/l	**Fe**	4.2	0.3	2.5	0.2	n.s.↓
µg/l	**Cu**	160.5	55.9	893.5	247.1	p=0.004↑
mg/l	**Zn**	1.4	0.1	1.0	0.2	n.s.↓
		Total Brain				
ng/g	**Mn**	406.1	17.6	427.7	23.5	n.s.↑
µg/g	**Fe**	13.3	0.1	10.3	0.5	p=0.004↓
µg/g	**Cu**	1.6	0.2	2.0	0.1	p=0.008↑
µg/g	**Zn**	13.6	0.8	12.9	0.5	n.s.↓
		Brain extract				
ng/g	**Mn**	129.3	16.8	131.8	13.3	n.s.↑
µg/g	**Fe**	5.6	1.0	4.1	0.3	n.s.↓
		Brain extract pellets				
µg/g	**Mn**	227.7	10.3	296.5	16.4	p=0.01↑
µg/g	**Fe**	6.2	2.0	6.7	0.4	n.s.↓
		Total Liver				
µg/g	**Mn**	1.9	0.1	1.8	0.2	n.s.-
µg/g	**Fe**	38.5	18.1	18.3	0.8	p=0.03↓
µg/g	**Cu**	2.4	0.1	4.0	0.3	p<0.001↑
µg/g	**Zn**	25.2	2.4	24.3	1.9	n.s.-
		Liver extract				
ng/g	**Mn**	521.5	88.6	378.1	49.9	n.s.↓
µg/g	**Fe**	24.5	6.1	7.7	0.6	p<0.001↓
		Liver extract pellets				
ng/g	**Mn**	686.4	171.1	935.9	123.4	n.s.↑
µg/g	**Fe**	14.8	2.0	9.2	1.0	p=0.002↓
		Total Kidney				
ng/g	**Mn**	761.8	69.8	784.6	51.4	n.s.↑
µg/g	**Fe**	43.8	2.8	21.2	2.4	p=0.003↓
µg/g	**Cu**	3.4	0.2	4.8	0.4	p=0.02↑
µg/g	**Zn**	26.1	5.4	19.8	0.8	p=0.01↓
		Kidney extract				
ng/g	**Mn**	458.0	55.8	468.0	50.5	n.s.-
µg/g	**Fe**	30.5	3.9	14.8	2.2	p=0.001↓
		Kidney extract pellets				
ng/g	**Mn**	273.8	21.1	262.3	20.5	n.s.-
µg/g	**Fe**	12.6	1.6	7.1	0.6	p=0.04↓

Table 23 Concentrations of Mn, Fe, Cu and Zn in serum brain, liver, kidney as well as tissue extracts (only Mn and Fe are shown)

In summary, alterations in elemental concentrations were already observable by this treatment showing trends of one and the other element in the respective directions (increase or decrease), which were retrospectively in accordance with the finally carried out feeding study. However, the increase of Mn in the brain by only 5% was not sufficient enough for the planned purposes. Another problem – and maybe the reason for the small increase of Mn in brain – was that the animals seemed to drink quite minor amounts of water and therefore didn´t take up very much Mn. We therefore decided to switch from Mn enrichment in drinking water to Mn-enriched fodder as it was then carried out in the final feeding study.

E.2   Elemental Concentrations in Fodder and Feces of Feeding and Injection Study

The standard fodder AIN93G was ordered for feeding of control rats in the feeding study as well as both, control and exposed rats in the injection study. For the exposure of rats in the feeding study this fodder was modified according to our order by 500 mg Mn/kg fodder. For analysis, five samples (a handful of fodder) were drawn, grounded by a ball triturator and nitric acid digested in the Seif apparatus (as described in *Experimental procedure, chapter D2.3.1*). The solutions were analyzed by ICP-OES detecting following elements: Ca, Cu, Fe, K, Mg, Mn, Na, P, and Zn (Figure 84). The unmodified fodder was well in accordance to declared values except slightly higher concentrations for Fe and lower concentrations for Mn. The lower concentrations of Mn were no problem as in general a low supply with Mn was favored for control animals as well as for the exposed animals in the injection study. The measured elemental values for the modified fodder for the exposed group of the feeding study comprised exactly the ordered concentration of Mn and showed slightly higher concentrations of Zn than declared.
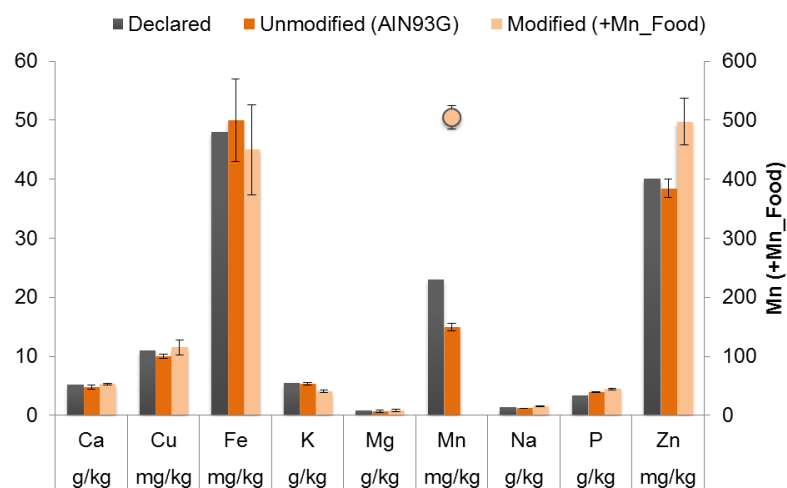

Figure 84 Analysis of fodder for the feeding study by ICP-OES after nitric acid digestion.

As the preliminary route of excretion of Mn is via the bile (up to 97%), feces was collected in both studies to monitor excretion of elements such as Cu, Fe, Mn and Zn. In the feeding study, feces was taken weekly and during the injection study excretion was monitored the four days after the injection of either saline or $MnCl_2$. Collected feces was lyophilized, grounded by a ball triturator and nitric acid digested in the seif apparatus (as described in *Experimental procedure*). Cu, Fe, Mn and Zn levels in the feces were measured by ICP-OES and results for the feeding study are given in Figure 85 while results for the injection study are given in Figure 86.

In the feeding study, Cu excretion in Mn-exposed rats was similar to control animals although it was slightly lower from day 14 on. Similar results were obtained for Zn excretion, which was also slightly lower compared to control rats from day 28 on as Zn excretion seemed to increase in control rats over time. Regarding Fe, excretion was slightly higher in Mn-exposed compared to control rats and it was slightly increasing over time in both groups. Mn excretion was higher in Mn-exposed rats during the whole feeding period with very balanced decreasing values over time. Overall, although receiving same basis of fodder, elemental shifts of Cu and Fe as observed in serum and brain could also be observed in excretion of elements in the corresponding direction (Cu lower, Fe higher excretion). Therefore, the elemental metabolism seemed to respond to the higher oral intake of Mn.
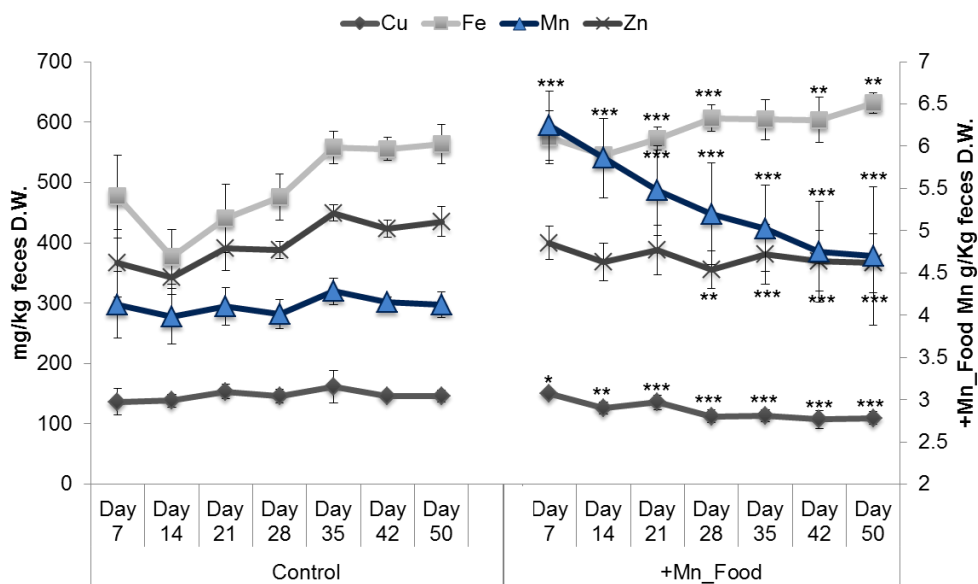

Figure 85 Analysis of feces in the feeding study.
Feces was collected weekly and analyzed by ICP-OES after nitric acid digestion (n=2 digestions per sample, Student t-test between control and +Mn_Food, *p<0.05, **p<0.01, ***p<0.001).

During the injection study, Cu excretion in rats injected with $MnCl_2$ was similar to control animals showing slightly higher values on day two and four. Excretion of Zn was similar. Fe

excretion was also comparable between control and +Mn-Inj animals. Regarding Mn, excretion was higher in Mn-exposed rats with decreasing values from day one on and comparable values on day 4 to control. The results correspond very well to the second injection study carried out for LA-ICP-MS (Figure 63). Overall, Cu, Fe and Zn metabolism seemed not as much disturbed as due to feeding by this single low-dose injection of $MnCl_2$.
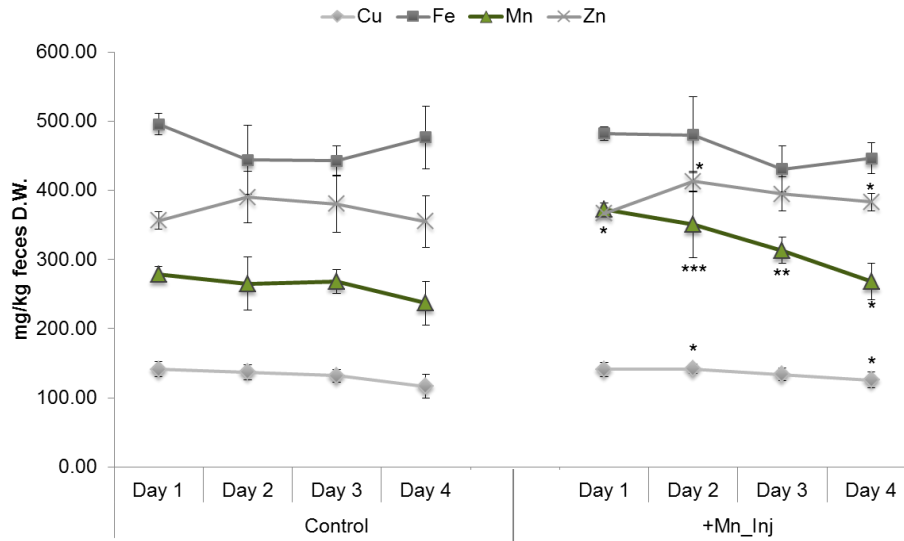

Figure 86 Analysis of feces in the injection study.
Feces was collected every day for four days after injection and analyzed by ICP-OES after nitric acid digestion (n=2 digestions per animal, Student t-test between control and +Mn_Food, *p<0.05, **p<0.01, ***p<0.001).

E.3   Supplementary Tables and Figures

Fraction	LSMEAN		Standard Error		Pr > |t|
	Control	+Mn_Food	Control	+Mn_Food	
A	0.31019	0.36229	0.10418	0.0951	NS
B	0.07564	-0.0214	0.10418	0.0951	NS
C	-0.0135	-0.3389	0.10418	0.0951	NS
D	-0.9287	-0.4655	0.0951	0.0951	*
E	-2.052	-1.0236	0.10418	0.11647	***
F	-1.8529	-1.2307	0.10418	0.0951	**

Table 24 Least square means of interaction effect of serum Mn-species in the feeding study corresponding to Figure 38.
Fractions A-C (HMMs) were not significant (NS) whereas Fractions D-F (LMMs) were obtained to be significantly increased in serum of Mn-fed animals. (NS not significant, *p<0.05, **p<0.01, ***p<0.001)

	Fraction	LSMEAN		Standard Error		Pr > |t|
		Control	+Mn_Inj	Control	+Mn_Inj	
1 hour after injection	A	0.45512	1.79816	0.10372	0.10372	***
	B	0.50187	1.92151	0.11362	0.11362	***
	C	-0.82604	1.22008	0.14668	0.14668	***
	D	-0.60704	0.78371	0.11362	0.11362	***
	E	-1.65103	0.53958	0.14668	0.17965	***
	F	-1.5650	1.08514	0.11362	0.11362	***
4 days after injection	A	0.47554	0.17758	0.07907	0.07907	NS
	B	0.38613	0.61177	0.08662	0.08662	NS
	C	-0.8509	-0.288	0.11182	0.11182	*
	D	-0.6613	-0.4339	0.08662	0.08662	NS
	E	-1.2899	-0.4927	0.11182	0.13695	**
	F	-1.425	-1.3376	0.08662	0.08662	NS

Table 25 Least square means respective to Figure 41 of the general linear model of the injection study.
One hour after injection every fraction was significant whereas four days after injection only Fractions D and E were significant altered between control and +Mn_Inj (NS not significant, *p<0.05, **p<0.01, ***p<0.001).

Least Squares Means for effect Group*Fraction (Feeding study)

Pr > |t| for H0: LSMean(i)=LSMean(j)

Dependent Variable: Mn

i/j	Co_A	Co_B	Co_C	Co_D	Co_E	Co_F	+Mn_A	+Mn_B	+Mn_C	+Mn_D	+Mn_E	+Mn_F
Co_A		<.0001	<.0001	<.0001	0.9996	0.9998	<.0001	<.0001	<.0001	0.3760	0.0052	0.3339
Co_B	<.0001		0.0003	0.0029	<.0001	<.0001	0.0113	0.5290	0.0028	<.0001	<.0001	<.0001
Co_C	<.0001	0.0003		<.0001	<.0001	<.0001	<.0001	0.2348	1.0000	<.0001	<.0001	<.0001
Co_D	<.0001	0.0029	<.0001		<.0001	0.0004	1.0000	<.0001	<.0001	0.1699	<.0001	<.0001
Co_E	0.9996	<.0001	<.0001	<.0001		0.9217	<.0001	<.0001	<.0001	0.0671	0.0586	0.8521
Co_F	0.9998	<.0001	<.0001	0.0004	0.9217		<.0001	<.0001	<.0001	0.8427	0.0004	0.0624
+Mn_A	***<.0001***	0.0113	<.0001	1.0000	<.0001	<.0001		<.0001	<.0001	0.0644	<.0001	<.0001
+Mn_B	<.0001	**0.5290**	0.2348	<.0001	<.0001	<.0001	<.0001		0.5128	<.0001	<.0001	<.0001
+Mn_C	<.0001	0.0028	**1.0000**	<.0001	<.0001	<.0001	<.0001	0.5128		<.0001	<.0001	<.0001
+Mn_D	0.3760	<.0001	<.0001	**0.1699**	0.0671	0.8427	0.0644	<.0001	<.0001		<.0001	0.0002
+Mn_E	0.0052	<.0001	<.0001	<.0001	**0.0586**	0.0004	<.0001	<.0001	<.0001	<.0001		0.8952
+Mn_F	0.3339	<.0001	<.0001	<.0001	0.8521	**0.0624**	<.0001	<.0001	<.0001	0.0002	0.8952	

Table 26 p-values of p-values of two-way ANOVA from the Mn-speciation in brain extracts in the feeding study.
Only Fraction A showed a significant interaction effect (in bold italic). Fractions B-F showed no significant interaction effect between control and +Mn-Inj samples (in bold) (R²=0.91, model p<0.0001).

Least Squares Means for effect Group*Fraction (Injection study)

Pr > |t| for H0: LSMean(i)=LSMean(j)

Dependent Variable: Mn

i/j	Co_A	Co_B	Co_C	Co_D	Co_E	Co_F	+Mn_A	+Mn_B	+Mn_C	+Mn_D	+Mn_E	+Mn_F
Co_A		<.0001	<.0001	<.0001	<.0001	<.0001	0.1205	<.0001	<.0001	<.0001	<.0001	0.2745
Co_B	<.0001		0.0033	<.0001	0.0030	<.0001	<.0001	0.8993	1.0000	0.1113	<.0001	<.0001
Co_C	<.0001	0.0033		0.0002	<.0001	<.0001	<.0001	<.0001	0.0165	0.9967	<.0001	<.0001
Co_D	<.0001	<.0001	0.0002		<.0001	<.0001	<.0001	<.0001	<.0001	<.0001	<.0001	<.0001
Co_E	<.0001	0.0030	<.0001	<.0001		<.0001	<.0001	0.3522	0.0005	<.0001	<.0001	<.0001
Co_F	<.0001	<.0001	<.0001	<.0001	<.0001		<.0001	<.0001	<.0001	<.0001	1.0000	0.1322
+Mn_A	**0.1205**	<.0001	<.0001	<.0001	<.0001	<.0001		<.0001	<.0001	<.0001	<.0001	<.0001
+Mn_B	<.0001	**0.8993**	<.0001	<.0001	0.3522	<.0001	<.0001		0.6445	0.0006	<.0001	<.0001
+Mn_C	<.0001	1.0000	*0.0165*	<.0001	0.0005	<.0001	<.0001	0.6445		0.3037	<.0001	<.0001
+Mn_D	<.0001	0.1113	0.9967	*<.0001*	<.0001	<.0001	<.0001	0.0006	0.3037		<.0001	<.0001
+Mn_E	<.0001	<.0001	<.0001	<.0001	*<.0001*	1.0000	<.0001	<.0001	<.0001	<.0001		0.0401
+Mn_F	0.2745	<.0001	<.0001	<.0001	<.0001	**0.1322**	<.0001	<.0001	<.0001	<.0001	0.0401	

Table 27 p-values of two-way ANOVA from the Mn-speciation in brain extracts in the injection study. Fractions A, B and F did not show a significant interaction effect (in bold). Fractions C, D and E showed a significant interaction effect between control and +Mn-Inj samples (in bold italic) (R^2=0.91, model p<0.0001).
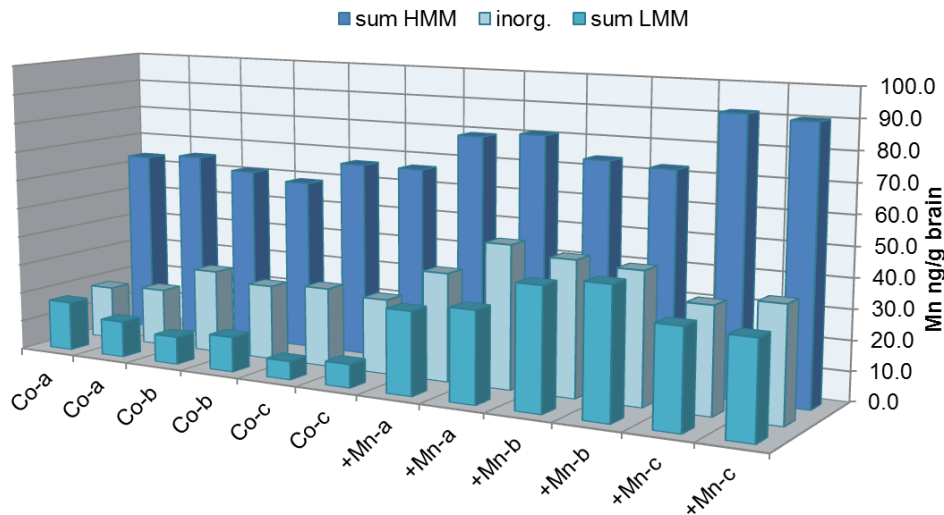
Figure 87 Example for repetition of six brain extract samples (Control a-c, +Mn a-c) for monitoring the LMM SEC fractions.
In general, every SEC peak area was comparable to the first run.
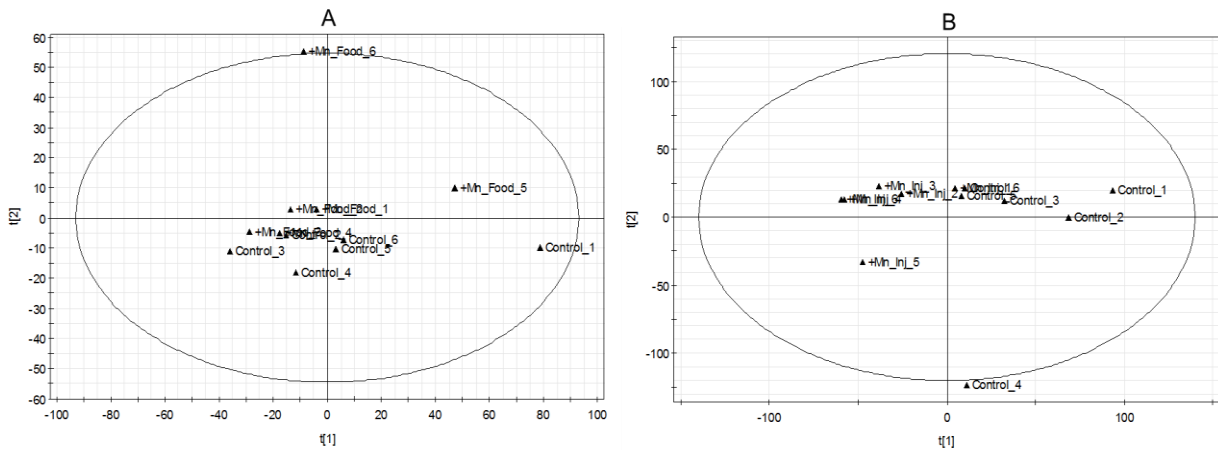
Figure 88 PCA of data from ESI-ICR/FT-MS.
No group separation was observed neither in the feeding (A) nor in the injection study (B).
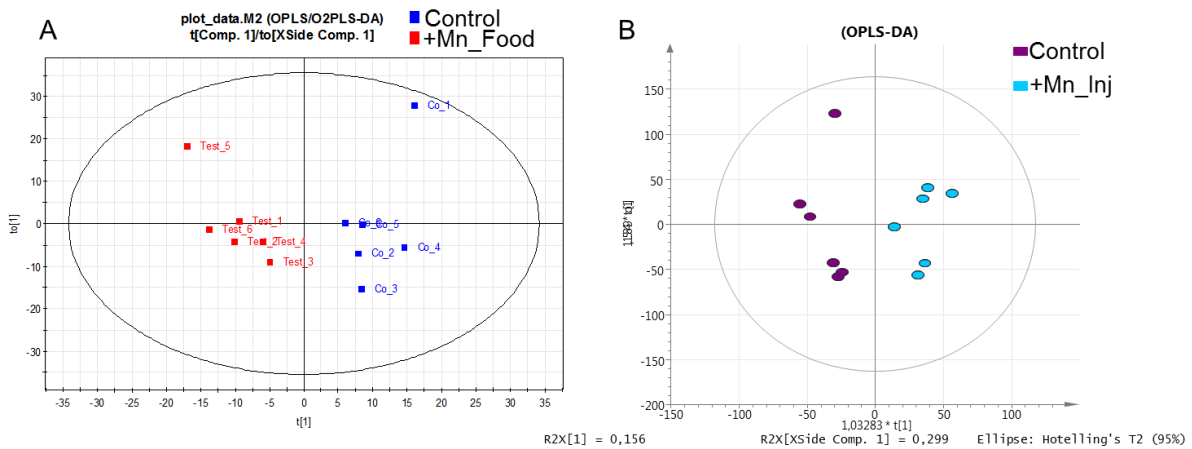
Figure 89 OPLS-DA of data from ESI-ICR/FT-MS.
A good group separation according to component 1 was observed for both, feeding (A) and injection study (B).

Figure 90 Correlation of variables with various interesting metabolites from the feeding study.
Numbers code for metabolites, see list/Table 28 below.

Figure 91 Correlation of species with various interesting metabolites from the feeding study.
Numbers code for metabolites, see list/Table 28 below.

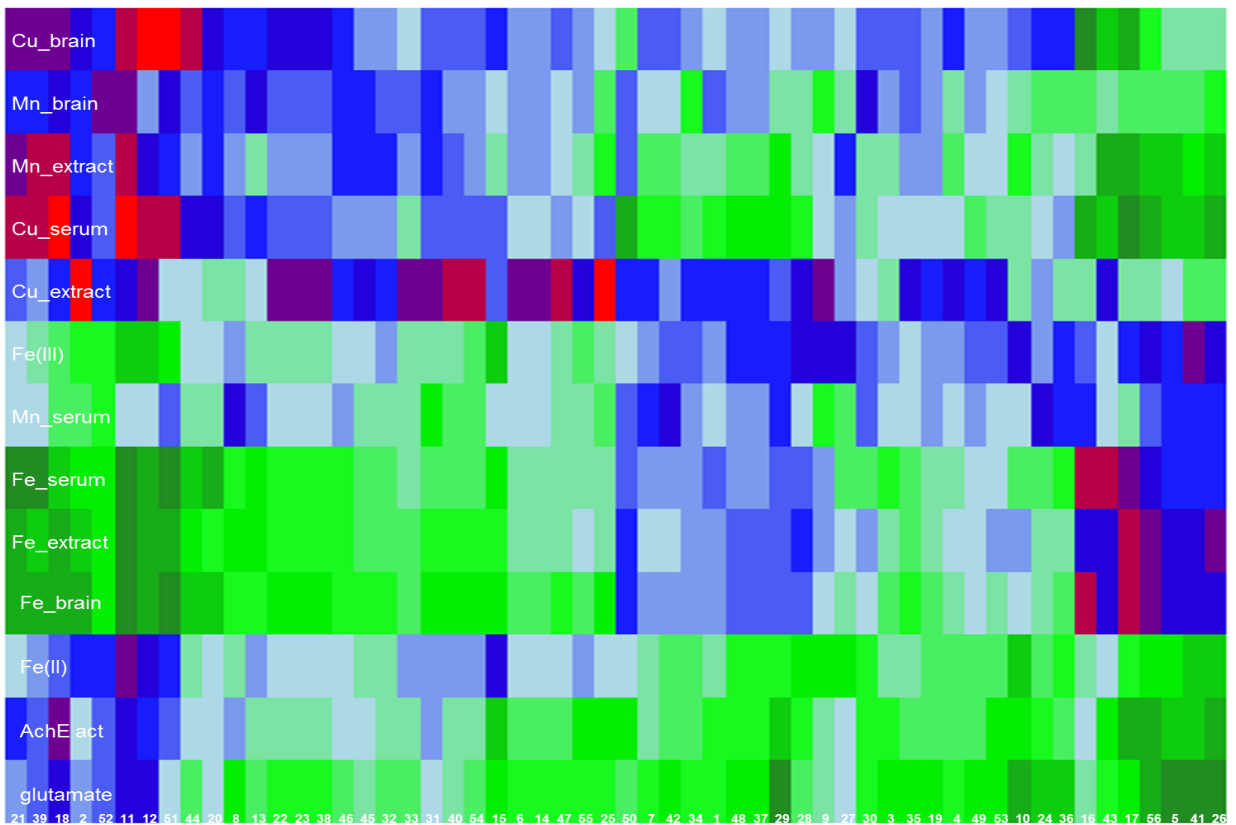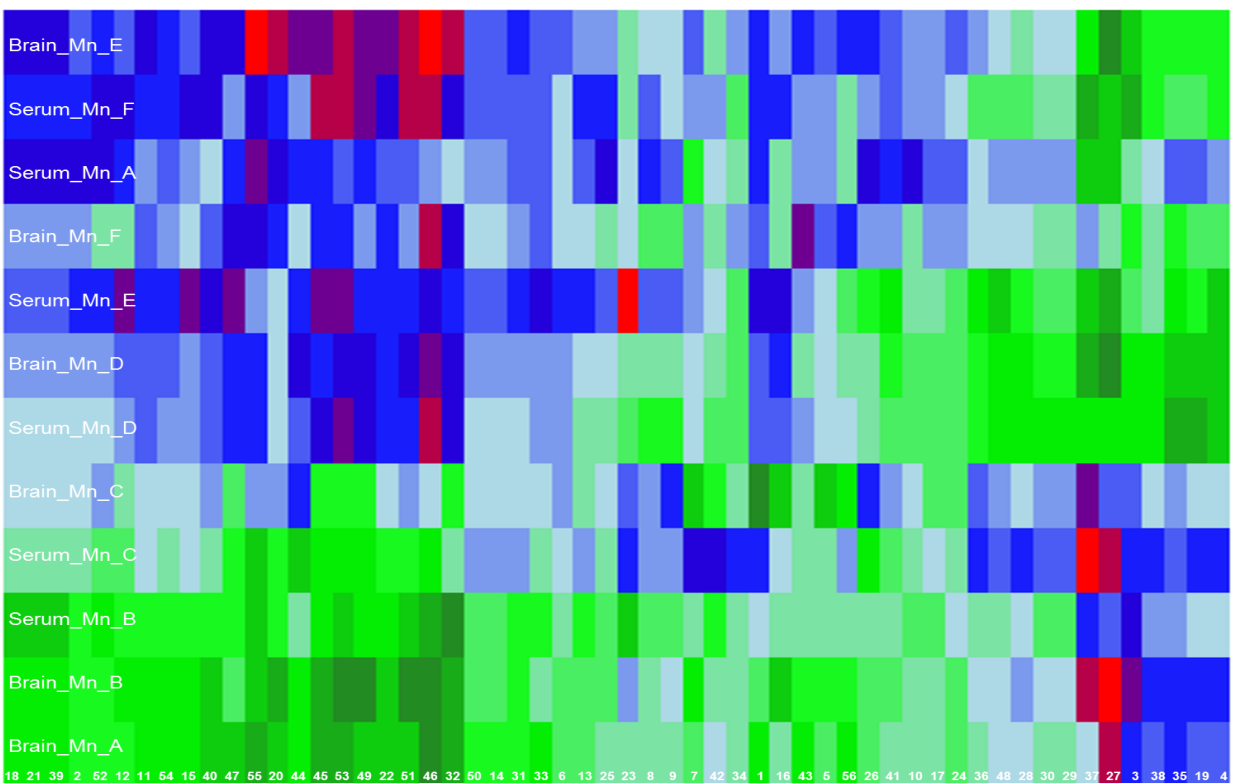| Number Heatmap	Compound	Mass	Class
1	D-Ribose 5-phosphate	229.011873	
2	Glycerone phosphate	168.990752	
3	O-Phospho-L-serine	184.001763	
4	L-Glutamine	145.061881	
5	N6-(L-1,3-Dicarboxypropyl)-L-lysine	275.124862	
6	D-Erythrose 4-phosphate	199.001300	
7	Sedoheptulose 7-phosphate	289.033005	
8	L-Tryptophan	203.082601	
9	L-Tyrosine	180.066630	**Amino Acids**
10	S-Adenosyl-L-homocysteine	383.114333	
11	O-Succinyl-L-homoserine	218.066991	
12	L-Aspartate	132.030242	
13	4-Phospho-L-aspartate	211.996675	
14	Citrate	191.019725	
15	L-Glutamate	146.045903	
16	N-Acetyl-L-glutamate	188.056460	
17	(R)-2-Hydroxybutane-1,2,4-tricarboxylate	205.035363	
18	UMP	323.028590	
19	L-Glutamine	145.061881	
20	UDP-glucose	565.047848	
21	UDP	402.994888	**Pyrimdine**
22	Uridine	243.062255	
23	CMP	322.044575	
24	Cytidine	242.078330	
25	dCMP	306.049620	
26	Hexadecanoic acid	255.232948	
27	Octadecanoic acid	283.264250	
28	(4Z,7Z,10Z,13Z,16Z,19Z)-Docosahexaenoic acid	327.232945	
29	(9Z)-Octadecenoic acid	281.248600	**Fatty acids**
30	(5Z,8Z,11Z,14Z)-Icosatetraenoic acid	303.232949	
31	(6Z,9Z,12Z)-Octadecatrienoic acid	277.217283	
32	(8Z,11Z,14Z)-Icosatrienoic acid	305.248584	
33	9-cis,12-cis-Octadecadienoic acid	279.232950	
34	D-Ribose 5-phosphate	229.011873	
35	L-Glutamine	145.061881	
36	5'-Phosphoribosyl-N-formylglycinamide	313.044320	
37	FAICAR	365.050392	**Purines**
38	ADP	428.026570	
39	AMP	346.055792	
40	GMP	362.050708	
41	Guanosine	282.084386	

42	Inosine	267.073489	
43	Adenosine	266.089471	
44	IMP	347.039814	
45	GDP-3,6-dideoxy-D-galactose	572.080176	
46	GDP-mannose	604.070046	
47	GDP	442.017082	
48	Xanthosine	283.068394	
49	Cyclic ADP-ribose	540.053940	
50	S-2-Hydroxyethyl)glutathione	350.102654	
51	GSH	307.073555	
52	Glutathione disulfide	611.144680	
53	Cys-Gly	177.033946	**GSH**
54	L-Glutamate	146.045903	
55	Ascorbate	175.024825	
56	Glu-Glu	275.088472	

Table 28   Examined metabolites in correlation analysis.
Interesting metabolites based on alterations in metabolisms were applied at heatmaps in Figure 61, and Figure 91.
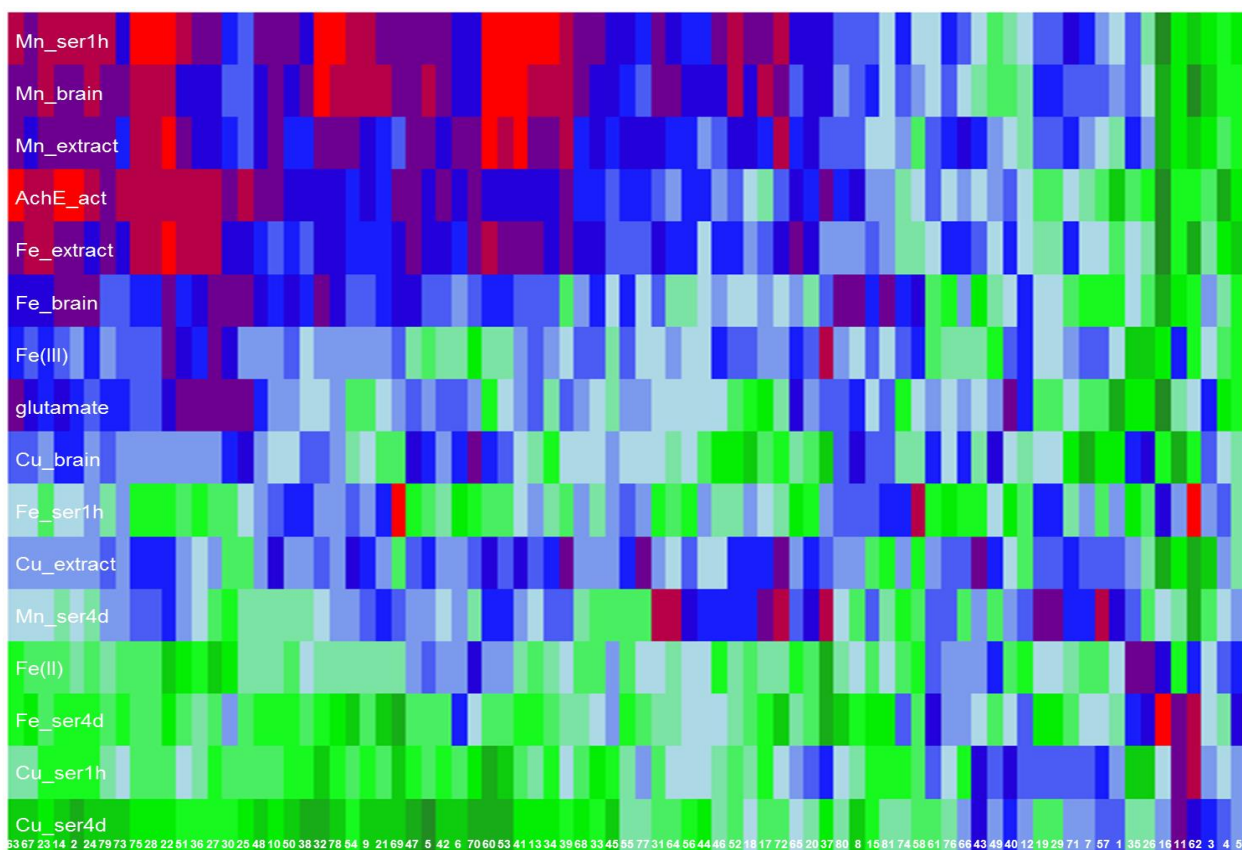
Figure 92 Correlation of variables with various interesting metabolites from the injection study.
Numbers code for metabolites, see list/Table 29 below.
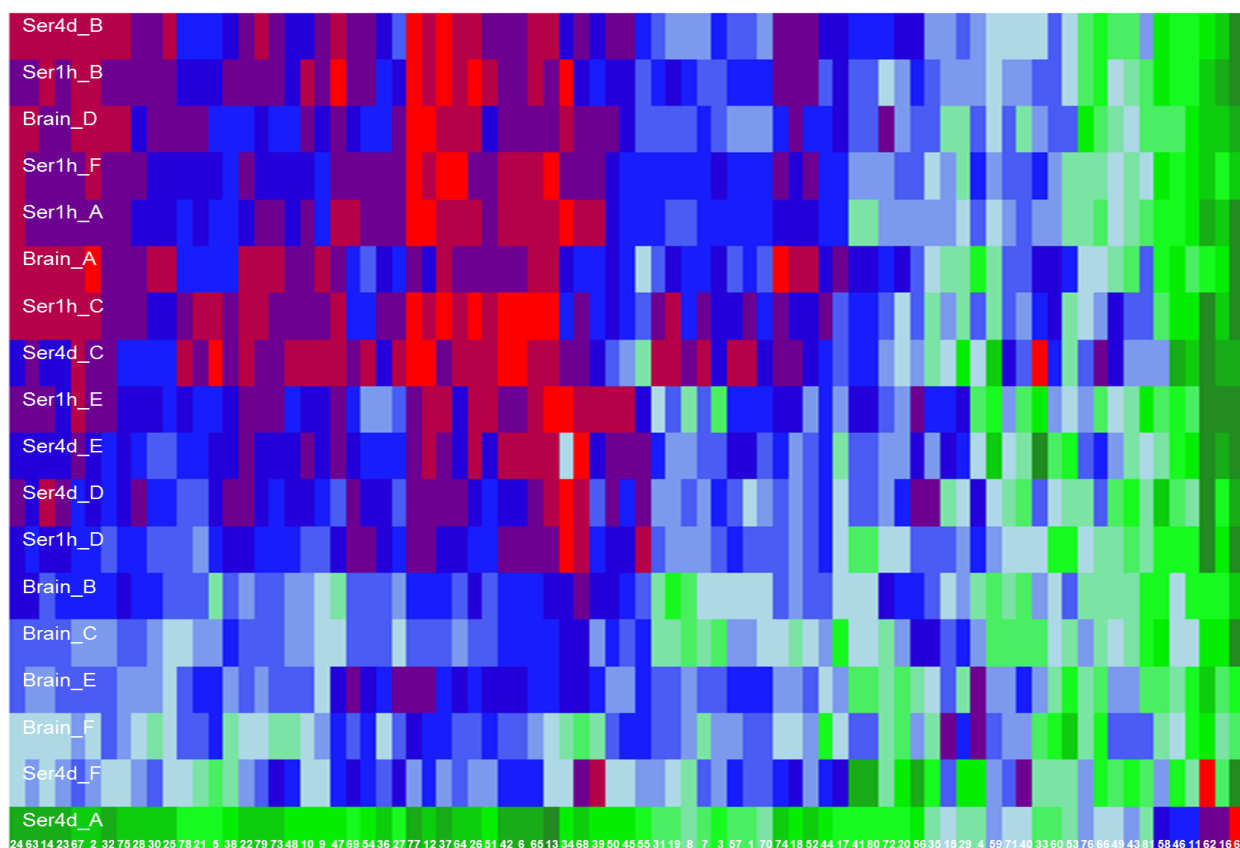
Figure 93 Correlation of species with various interesting metabolites from the injection study. Numbers code for metabolites, see list/Table 29 below

Number heatmap	Compound	Mass	Class
1	D-Ribose 5-phosphate	229.011850	
2	L-Histidine	154.062240	
3	D-Erythrose 4-phosphate	199.001290	
4	L-Tryptophan	203.082580	
5	2-Carboxy(phenylamino)-1-deoxy-D-ribulose 5-phosphate	348.048840	
6	Glycerone phosphate	168.990740	
8	L-Phenylalanine	164.071640	
9	3-Dehydroquinate	189.040400	
10	3-Phospho-D-glyceroyl phosphate	264.952150	Amino acids
11	O-Phospho-L-serine	184.001750	
12	Phosphoenolpyruvate	166.975090	
13	L-Aspartate	132.030240	
14	N-Succinyl-LL-2,6-diaminoheptanedioate	289.104120	
15	LL-2,6-Diaminoheptanedioate	189.088080	
17	L-Citrulline	174.088390	
18	N-(L-Arginino)succinate	289.115340	
19	L-Arginine	173.104370	
20	N-Acetyl-L-glutamate	188.056440	

22	L-Glutamyl 5-phosphate	226.012280	
24	L-2-Aminoadipate	160.061490	
26	UDP-glucose	565.047920	
27	dUDP	386.999820	
28	UMP	323.028590	
29	Uridine	243.062250	
31	Cytidine	242.078320	
32	Deoxycytidine	226.083310	
33	2'-Deoxy-5-hydroxymethylcytidine-5'-diphosphate	416.026600	
34	5-Hydroxymethyldeoxycytidylate	336.060190	**Pyrimidine**
35	dCMP	306.049570	
36	dUDP	386.999820	
37	UDP	402.994920	
39	dTMP	321.049290	
40	Thymidine	241.082980	
41	CDP	402.010860	
42	CMP	322.044580	
43	(4Z,7Z,10Z,13Z,16Z,19Z)-Docosahexaenoic acid	327.232940	
44	Tetracosanoic acid	367.358150	
45	(9Z)-Octadecenoic acid	281.248590	
46	(8Z,11Z,14Z)-Icosatrienoic acid	305.248590	
47	Hexadecanoic acid	255.232940	
48	Octadecanoic acid	283.264240	**Fatty acids**
49	Docosanoic acid	339.326850	
50	(6Z,9Z,12Z)-Octadecatrienoic acid	277.217280	
51	(13Z)-Docosenoic acid	337.311210	
53	(15Z)-Tetracosenoic acid	365.342510	
54	(5Z,8Z,11Z,14Z)-Icosatetraenoic acid	303.232940	
55	Linoleate	279.232940	
56	ADP-ribose	558.064420	
57	D-Ribose 5-phosphate	229.011850	
58	5'-Phosphoribosyl-N-formylglycinamide	313.044330	
59	FAICAR	365.050400	
60	N6-1,2-Dicarboxyethyl)-AMP	462.066790	
61	GDP	442.017110	
62	Guanosine	282.084370	**Purines**
63	GDP-3,6-dideoxy-D-galactose	572.080200	
64	L-Glutamine	145.061870	
65	5'-Phosphoribosylglycinamide	285.049370	
67	5´-AMP	346.055760	
69	Cyclic ADP-ribose	540.053960	
70	IMP	347.039810	
71	Inosine	267.073470	

72	Adenosine	266.089450	
73	Adenine	134.047220	
74	Xanthosine	283.068410	
75	GMP	362.050710	
76	Glutathione	306.076480	
77	Cys-Gly	177.033940	
78	L-Glutamate	146.045890	**GSH**
79	Glutathione disulfide	611.144840	
80	gamma-L-Glutamyl-L-cysteine	249.055040	
81	Ascorbate	175.024810	

Table 29 Examined metabolites in correlation analysis in the injection study.
Interesting metabolites based on alterations in metabolisms were applied at heatmaps in Figure 92 and Figure 93 (left out numbers were annotated as isotopes).

E.4 Operating Parameters of ICP-OES, ICP-sf-MS and ESI-ICR/FT-MS in Standard Analysis

ICP-OES		Optima 7300DV	Spectro Ciros Vision
Detected wavelengths	Ca	317.933	183.801
	Cu	324.752	324.754
	Fe	259.939	259.941
	K	766.49	404.721
	Mg	279.077	279.079
	Mn	257.61	257.611
	Na	589.592	589.592
	P	177.434	177.495
	Zn	213.857	213.856
Delay time		60 seconds	
Read parameters		4 points per peak; 2 replicates	
RF Power, W		1200	1360
Plasma Gas (Ar), l/min		15	14
Nebulizer Gas (Ar), l/min		0.6	0.7
Auxiliary Gas (Ar), l/min		0.5	0.6

ICP-sf-MS	
Detected masses	^{55}Mn, ^{63}Cu, ^{65}Cu, ^{56}Fe, ^{57}Fe, ^{64}Zn, ^{66}Zn, ^{68}Zn, ^{103}Rh
Resolution	Medium (R~4000)
RF Power	1260 W
Plasma Gas (Ar)	15 L/min
Auxiliary Gas (Ar)	1.45 L/min
Sample Gas (Ar)	1.14 L/min

ESI-ICR/FT-MS	
Flow rate	2 µl/min
Mass range	123-1000 m/z
Number of scans	300
Transient time domain	2 MW
Source accumulation	0.01 sec
Ion accumulation time	0.3 sec
Capillary	3600 V
Dry gas flow rate	4 l/min
Dry gas temperature	180 °C
Nebulizer gas flow rate	2 bar
Analyzer entrance	4V

E.5   List of applied Equipment and Materials

Equipment for animal treatment

Canula (stainless steel, plastic)	B. Braun Melsungen AG, Melsungen, Germany
Ceramic scalpel and scissors	Neolab, Heidelberg, Germany
EF R/M AIN 93G (+500 mg/Kg Mn)	Ssniff Spezialdiäten, Soest, Germany
Hugro® Hamp Mats	Hugro GmbH, Saerbeck, Germany
Isotonic saline 0.9%	Steripharm, Berlin, Germany
Polycarbonate cages type III	UNO B.V., PC Zevenaar, Netherlands
PTFE pincetts	Neolab, Heidelberg, Germany

Equipment for sample preparation

Agate grinding vessel	NeoLab, Heidelberg, Germany
Agate mortar and pestle	Neolab, Heidelberg, Germany
Biogue 17RS	Heraeus Sepatech, Osterode am Harz, Germany
Centrifuge 5702R	Eppendorf AG, Hamburg, Germany
CM3050S cryostat	Leica Biosystems GmbH, Wetzlar, Germany
Cryomolds 22x30x20mm	
ESI NWR213 Laser ablation system	Electro scientific industry Europe ltd, Cambridge, UK
Fortuna®Glas homogenizer with PTFE punch	Neolab, Heidelberg, Germany
Freeze-drier	Christ, Osterode am Harz Germany
Glove Bag, Atmosbag	Sigma-Aldrich, Steinheim, Germany
Microwave Multiwave Anton Paar	Paar Physica, Graz, Österreich
PE vessels 15 ml, 50 ml	Greiner Bio-One GmbH, Frickenhausen, Germany
Seif digestion apparatus	Seif-Aufschlusstechnik, Unterschleißheim, Germany
Superfrost Plus™ Microscope slides	ThermoFisher Scientific, Ulm, Germany
Tissue-Tek® embedding medium	O.C.T™, Sakura Finetek Europe, Netherlands

Equipment for analytical analyses

0.45 mm MEMBREX	membraPure Membrantechnik, Reinstwasser, Germany
AchE Fluorescence activity Kit	Arbor Assays, Michigan, USA
Apollo II electrospray source	Bruker Daltonics GmbH, Bremen, Germany
AS11 column	ThermoFisher Scientific, Ulm, Germany
Biobasic C4 column	ThermoFisher Scientific, Ulm, Germany
Biobasic SEC300 column	ThermoFisher Scientific, Ulm, Germany
BioProQA column	YMC America Inc,. Allentown, PA, USA
CG5A column 5x4 mm	ThermoFisher Scientific, Ulm, Germany
Degassext mode DG 4490	Phenomenex, Darmstadt, Germany
EcoLab glass column 700x10mm	YMC America Inc,. Allentown, PA, USA
Element2 ICP-sf-MS	ThermoFisher Scientific, Ulm, Germany
Glutamate Assay Kit	BioVision, Calfornia, USA
HPLC S1000 HPG ceramic pumps, S5000 Manager/Degasser, 2600 LWL DAD	Knauer, Berlin, Germany
HPLC System Gold, 127 NM Solvent Module system	Beckman Coulter, Krefeld, Germany
Hypersil C4 column	ThermoFisher Scientific, Ulm, Germany
Jupiter C4 column	Phenomenex,
NexIon 300D ICP-MS	Perkin Elmer, Toronto, Kanada

Optima 7300DV ICP-OES	Perkin Elmer, Toronto, Kanada
PackDiol300 column	YMC America Inc,. Allentown, PA, USA
PEEK column 100/200/250x8mm	Dionex, Idstein, Germany
Plate reader Safire2	Tecan, Crailsheim, Germany
Sample changer 223 autosampler	Gilson inc., Middleton, USA
SecurityGuard™ pre-column	Phenomenex, Darmstadt, Germany
solariXTM ICR/FT-MS	Bruker Daltonics GmbH, Bremen, Germany
12T superconducting magnet	Magnex scientific Inc., Yarnton, GB
Spectro Ciros Vision ICP-OES	Spectro Analytical Instruments GmbH&Co KG, Kleve, Germany
Spiro vaporization system	Elemental Scientific, Mainz, Germany
Toyopearl HW 40/50/75S SEC material	TosoHaas, Stuttgart, Germany

F   References

Abe, Keita, Chiba, Yuji, and Nishida, Yuzo (2008), 'Facile Uptake of Manganese (III) by Apo-Transferrin: Possible Origin of Manganism', *Zeitschrift für Naturforschung C,* 63 (1-2), 154-56.

Aboud, Asad A, et al. (2012), 'Genetic risk for Parkinson's disease correlates with alterations in neuronal manganese sensitivity between two human subjects', *Neurotoxicology,* 33 (6), 1443-49.

Ala-Korpela, M., Kangas, A. J., and Soininen, P. (2012), 'Quantitative high-throughput metabolomics: a new era in epidemiology and genetics', *Genome Med,* 4 (4), 36.

Andrle, C. M., Jakubowski, N., and Broekaert, J. A. C. (1997), 'Speciation of chromium using reversed phase-high performance liquid chromatography coupled to different spectrometric detection methods', *Spectrochimica Acta Part B: Atomic Spectroscopy,* 52 (2), 189-200.

Antonini, J. M., et al. (2006), 'Fate of manganese associated with the inhalation of welding fumes: potential neurological effects', *Neurotoxicology,* 27 (3), 304-10.

Apostoli, P. (2006), 'Elemental speciation in human risk assessment', (Geneva, Switzerland: WHO).

Apostoli, P., Lucchini, R., and Alessio, L. (2000), 'Are current biomarkers suitable for the assessment of manganese exposure in individual workers?', *Am J Ind Med,* 37 (3), 283-90.

Archibald, Frederick S. and Tyree, Curtis (1987), 'Manganese poisoning and the attack of trivalent manganese upon catecholamines', *Archives of Biochemistry and Biophysics,* 256 (2), 638-50.

Aschner, J. L. and Aschner, M. (2005), 'Nutritional aspects of manganese homeostasis', *Mol Aspects Med,* 26 (4-5), 353-62.

Aschner, M. (2000), 'Manganese: brain transport and emerging research needs', *Environ Health Perspect,* 108 Suppl 3, 429-32.

Aschner, M., Lukey, B., and Tremblay, A. (2006), 'The Manganese Health Research Program (MHRP): status report and future research needs and directions', *Neurotoxicology,* 27 (5), 733-6.

Aschner, M., et al. (2007), 'Manganese: recent advances in understanding its transport and neurotoxicity', *Toxicol Appl Pharmacol,* 221 (2), 131-47.

Aschner, M., et al. (2009), 'Manganese and its Role in Parkinson's Disease: From Transport to Neuropathology', *Neuromolecular Medicine,* 11 (4), 252-66.

ATSDR (2000), 'Toxicological Profile for Manganese', in Agency of Toxic Substances and Disease Registry (ed.), (U.S. Department of Health and Human Services).

Avila, D.S., Puntel, R.L., and Aschner, M. (2013), 'Manganese in Health and Disease', in A. Sigel, H. Sigel, and R.K.O. Sigel (eds.), *Interrelations between Essential and Metal*

Ions and Human Disease (Metal Ions in Life Sciences 13; Dorfrecht: Springer Science+Business Media), 199-213.

Bagga, P. and Patel, A. B. (2012), 'Regional cerebral metabolism in mouse under chronic manganese exposure: Implications for Manganism', *Neurochemistry International,* 60 (2), 177-85.

Balcerzak, Maria, Tyburska, Anna, and Święcicka-Füchsel, Elżbieta (2008), 'Selective determination of Fe(III) in Fe(II) samples by UV-spectrophotometry with the aid of quercetin and morin', *Acta Pharmaceutica* (58), 327.

Barceloux, D. G. (1999), 'Manganese', *J Toxicol Clin Toxicol,* 37 (2), 293-307.

Barrow, M. P., Burkitt, W. I., and Derrick, P. J. (2005), 'Principles of Fourier transform ion cyclotron resonance mass spectrometry and its application in structural biology', *Analyst,* 130 (1), 18-28.

Bartel, J., Krumsiek, J., and Theis, F. J. (2013), 'Statistical methods for the analysis of high-throughput metabolomics data', *Comput Struct Biotechnol J,* 4, e201301009.

Bazinet, R. P. and Laye, S. (2014), 'Polyunsaturated fatty acids and their metabolites in brain function and disease', *Nat Rev Neurosci,* 15 (12), 771-85.

Becker, J. S. (2013), 'Imaging of metals in biological tissue by laser ablation inductively coupled plasma mass spectrometry (LA-ICP-MS): state of the art and future developments', *Journal of Mass Spectrometry,* 48, 255-68.

Becker, J. S., et al. (2005a), 'Imaging of copper, zinc, and other elements in thin section of human brain samples (hippocampus) by laser ablation inductively coupled plasma mass spectrometry', *Anal Chem,* 77 (10), 3208-16.

Becker, J. S., et al. (2005b), 'Determination of phosphorus-, copper-, and zinc-containing human brain proteins by LA-ICPMS and MALDI-FTICR-MS', *Anal Chem,* 77 (18), 5851-60.

Becker, J. S., et al. (2010), 'Scaling down the bioimaging of metals by laser microdissection inductively coupled plasma mass spectrometry (LMD-ICP-MS)', *International Journal of Mass Spectrometry,* 294 (1), 1-6.

Becker, J. Sabine, et al. (2007), 'Laser ablation inductively coupled plasma mass spectrometry (LA-ICP-MS) in elemental imaging of biological tissues and in proteomics', *Journal of Analytical Atomic Spectrometry,* 22 (7), 736.

Becker, J. Sabine, et al. (2009), 'Bioimaging of metals by laser ablation inductively coupled plasma mass spectrometry (LA-ICP-MS)', *Mass Spectrometry Reviews*, n/a.

Becker, J. Sabine, et al. (2004), 'In-gel screening of phosphorus and copper, zinc and iron in proteins of yeast mitochondria by LA-ICP-MS and identification of phosphorylated protein structures by MALDI-FT-ICR-MS after separation with two-dimensional gel electrophoresis', *Journal of Analytical Atomic Spectrometry,* 19 (9), 1236-43.

Bertinet, D. B., et al. (2000), 'Brain manganese deposition and blood levels in patients undergoing home parenteral nutrition', *JPEN J Parenter Enteral Nutr,* 24 (4), 223-7.

Boccard, J., Veuthey, J. L., and Rudaz, S. (2010), 'Knowledge discovery in metabolomics: an overview of MS data handling', *J Sep Sci,* 33 (3), 290-304.

Bondi, C. O., et al. (2014), 'Adolescent behavior and dopamine availability are uniquely sensitive to dietary omega-3 fatty acid deficiency', *Biol Psychiatry,* 75 (1), 38-46.

Bonilla, E., et al. (1994), 'Manganese toxicity: free amino acids in the striatum and olfactory bulb of the mouse', *Invest Clin,* 35 (4), 175-81.

Borgese, L., et al. (2013), 'Metal fractionation in soils and assessment of environmental contamination in Vallecamonica, Italy', *Environmental Science and Pollution Research,* 20 (7), 5067-75.

Bornhorst, J., et al. (2010), 'Manganese inhibits poly(ADP-ribosyl)ation in human cells: a possible mechanism behind manganese-induced toxicity?', *J Environ Monit,* 12 (11), 2062-9.

Bornhorst, J., et al. (2012a), 'Effects of manganese and arsenic species on the level of energy related nucleotides in human cells', *Metallomics,* 4 (3), 297-306.

Bornhorst, J., et al. (2012b), 'Impact of Manganese on and Transfer across Blood-Brain and Blood-Cerebrospinal Fluid Barrier in Vitro', *Journal of Biological Chemistry,* 287 (21), 17140–51.

Boss, C.B. and Fredeen, K.J. (2004) *Concepts, Instrumentation and Techniques in Inductively Coupled Plasma Optical Emission Spectrometry* [online text], Perkin Elmer

Bouchard, M., et al. (2007), 'Neuropsychiatric symptoms and past manganese exposure in a ferro-alloy plant', *Neurotoxicology,* 28 (2), 290-7.

Bouchard, M. F., et al. (2011), 'Intellectual impairment in school-age children exposed to manganese from drinking water', *Environ Health Perspect,* 119 (1), 138-43.

Bourassa, M. W. and Miller, L. M. (2012), 'Metal imaging in neurodegenerative diseases', *Metallomics,* 4 (8), 721-38.

Braunschweig, Juliane, et al. (2012), 'Reevaluation of colorimetric iron determination methods commonly used in geomicrobiology', *Journal of microbiological methods,* 89 (1), 41-48.

Brinkhaus, S. G., et al. (2014), 'Elemental bioimaging of manganese uptake in C. elegans', *Metallomics,* 6 (3), 617-21.

Brouillet, E. P., et al. (1993), 'Manganese injection into the rat striatum produces excitotoxic lesions by impairing energy metabolism', *Exp Neurol,* 120 (1), 89-94.

Bruker, Daltonics 'http://pdf.directindustry.com/pdf/bruker-daltonics-inc/solarix/30029-576686.html'.

Burley, SK and Petsko, GA (1988), 'Weakly polar interactions in proteins', *Advances in Protein Chemistry,* 39, 125.

Calne, D. B., et al. (1994), 'Manganism and idiopathic parkinsonism: similarities and differences', *Neurology,* 44 (9), 1583-6.

Cammann, K. (2001), *Instrumentelle Analytische Chemie: Verfahren, Anwendungen, Qualitätssicherung* (Heidelberg, Berlin: Spektrum Akademischer Verlag).

Caruso, J. A., et al. (2003), 'Group assessment: elemental speciation', *Ecotoxicol Environ Saf,* 56 (1), 32-44.

Cawte, J., Hams, G., and Kilburn, C. (1987), 'Manganism in a neurological ethnic complex in northern australia', *The Lancet,* 329 (8544), 1257.

Chalon, S. (2006), 'Omega-3 fatty acids and monoamine neurotransmission', *Prostaglandins Leukot Essent Fatty Acids,* 75 (4-5), 259-69.

Chapin, Thomas P, Jannasch, Hans W, and Johnson, Kenneth S (2002), 'In situ osmotic analyzer for the year-long continuous determination of Fe in hydrothermal systems', *Analytica Chimica Acta,* 463 (2), 265-74.

Chapman, B. E., MacDermott, T. E., and O'Sullivan, W. J. (1973), 'Studies on manganese complexes of human serum albumin', *Bioinorganic Chemistry,* 3 (1), 27-38.

Chen, C. J. and Liao, S. L. (2002), 'Oxidative stress involves in astrocytic alterations induced by manganese', *Exp Neurol,* 175 (1), 216-25.

Chen, M. K., et al. (2006), 'Acute manganese administration alters dopamine transporter levels in the non-human primate striatum', *Neurotoxicology,* 27 (2), 229-36.

Chen, P., Parmalee, N., and Aschner, M. (2014), 'Genetic factors and manganese-induced neurotoxicity', *Front Genet,* 5, 265.

Christianson, D. W. (2005), 'Arginase: structure, mechanism, and physiological role in male and female sexual arousal', *Acc Chem Res,* 38 (3), 191-201.

Chtourou, Y., et al. (2012), 'Improvement of Cerebellum Redox States and Cholinergic Functions Contribute to the Beneficial Effects of Silymarin Against Manganese-Induced Neurotoxicity', *Neurochemical Research,* 37 (3), 469-79.

Chtourou, Yassine, et al. (2011), 'Manganese Induces Oxidative Stress, Redox State Unbalance and Disrupts Membrane Bound ATPases on Murine Neuroblastoma Cells In Vitro: Protective Role of Silymarin', *Neurochemical Research,* 36 (8), 1546–57.

Comisarow, M.B. and Marshall, A.G. (1974), 'FT-ICR Spectroscopy', *Chemical Physical Letters,* 25, 282-83.

Costa, L.G. and Aschner, M. (2014), *Issues in Toxicology No.22: Manganese in Health and Disease* (London, UK: Royal Society of Chemistry).

Cotzias, G. C. and Papavasiliou, P. S. (1962), 'State of binding of natural manganese in human cerebrospinal fluid, blood and plasma', *Nature,* 195, 823-4.

Couper, James (1837), ' Sur les effets du peroxide de manganèse', *Journal de chimie médicale, de pharmacie et de toxicologie,* (3), 223-25.

Coyle, J. T. and Puttfarcken, P. (1993), 'Oxidative stress, glutamate, and neurodegenerative disorders', *Science,* 262 (5134), 689-95.

Cristoni, S. and Bernardi, L. R. (2003), 'Development of new methodologies for the mass spectrometry study of bioorganic macromolecules', *Mass Spectrom Rev,* 22 (6), 369-406.

Criswell, Susan R., et al. (2015), 'Ex vivo magnetic resonance imaging in South African manganese mine workers', *Neurotoxicology,* 49 (0), 8-14.

Crooks, D. R., Welch, N., and Smith, D. R. (2007), 'Low-level manganese exposure alters glutamate metabolism in GABAergic AF5 cells', *Neurotoxicology,* 28 (3), 548-54.

Crossgrove, J. and Zheng, W. (2004), 'Manganese toxicity upon overexposure', *NMR Biomed,* 17 (8), 544-53.

Crossgrove, J. S. and Yokel, R. A. (2004), 'Manganese distribution across the blood-brain barrier III. The divalent metal transporter-1 is not the major mechanism mediating brain manganese uptake', *Neurotoxicology,* 25 (3), 451-60.

Crossgrove, J. S., et al. (2003), 'Manganese distribution across the blood-brain barrier. I. Evidence for carrier-mediated influx of managanese citrate as well as manganese and manganese transferrin', *Neurotoxicology,* 24 (1), 3-13.

Cunha, R. A. (2005), 'Neuroprotection by adenosine in the brain: From A(1) receptor activation to A (2A) receptor blockade', *Purinergic Signal,* 1 (2), 111-34.

De Ioro, M., Ebbels, T.M.D., and Stephens, D.A. (2007), 'Statistical Techniques in Metabolic Profiling', in D.J. Balding, M. Bishop, and C. Cannings (eds.), *Handbook of Statistical Genetics* (third edn.; Chichester, UK: John Wiley & Sons, Ltd.).

Demougeot, Céline, et al. (2001), 'N-Acetylaspartate, a marker of both cellular dysfunction and neuronal loss: its relevance to studies of acute brain injury', *J Neurochem,* 77 (2), 408-15.

Deng, Y., et al. (2012), 'The protective effects of riluzole on manganese-induced disruption of glutamate transporters and glutamine synthetase in the cultured astrocytes', *Biol Trace Elem Res,* 148 (2), 242-9.

Dettmer, K., Aronov, P. A., and Hammock, B. D. (2007), 'Mass spectrometry-based metabolomics', *Mass Spectrom Rev,* 26 (1), 51-78.

Diederich, J. and Michalke, B. (2011), 'Enhanced extract preparation of native manganese and iron species from brain and liver tissue', *Analytical and Bioanalytical Chemistry,* 399 (5), 1799–806.

Diederich, J., et al. (2012), 'Manganese and iron species in Sprague-Dawley rats exposed with MnCl2 center dot 4H(2)O (i.v.)', *Microchemical Journal,* 105, 115-23.

Dobson, A. W., et al. (2003), 'Oxidative stress is induced in the rat brain following repeated inhalation exposure to manganese sulfate', *Biol Trace Elem Res,* 93 (1-3), 113-26.

Dolatabadi, Jafar Ezzati Nazhad (2011), 'Molecular aspects on the interaction of quercetin and its metal complexes with DNA', *International Journal of Biological Macromolecules,* 48 (2), 227-33.

Dole, R.B. (1997), *Electrospray Ionization Mass Spectrometry-Fundamentals, Instrumentation and Applications* (Chichester: John Wiley & Sons).

Dorman, D. C. and Foster, M.L. (2014), 'Olfactory Transport of Manganese: Implications for Neurotoxicity', in L.G. Costa and M. Aschner (eds.), *Manganese in Health and Disease* (Issues in Toxicology No. 22; London, UK: The Royal Society of Chemistry).

Dorman, D. C., et al. (2008), 'Metabolomic analyses of body fluids after subchronic manganese inhalation in rhesus monkeys', *Toxicol Sci,* 106 (1), 46-54.

Dorman, D. C., et al. (2001), 'Influence of dietary manganese on the pharmacokinetics of inhaled manganese sulfate in male CD rats', *Toxicol Sci,* 60 (2), 242-51.

Dringen, R. (2000), 'Glutathione metabolism and oxidative stress in neurodegeneration', *Eur J Biochem,* 267 (16), 4903.

Dunn, Laura, et al. (2014a), 'Pentose-phosphate pathway disruption in the pathogenesis of Parkinson's disease', *Translational Neuroscience,* 5 (3), 179-84.

Dunn, Laura, et al. (2014b), 'Dysregulation of glucose metabolism is an early event in sporadic Parkinson's disease', *Neurobiology of aging,* 35 (5), 1111-15.

Dusek, P., et al. (2014), 'The neurotoxicity of iron, copper and manganese in Parkinson's and Wilson's diseases', *J Trace Elem Med Biol*.

Eckburg, P. B., et al. (2005), 'Diversity of the human intestinal microbial flora', *Science,* 308 (5728), 1635-8.

Egger, A. E., et al. (2014), 'Quantitative bioimaging by LA-ICP-MS: a methodological study on the distribution of Pt and Ru in viscera originating from cisplatin- and KP1339-treated mice', *Metallomics,* 6 (9), 1616-25.

Ekmekcioglu, C. and Merktl, W. (2006), 'Mangan (Mn)', in C. Ekmekcioglu and W. Merktl (eds.), *Essentielle Spurenelemente: Klinik und Ernährungsmedizin* (1; Wien: Springer Verlag).

Erikson, K. and Aschner, M. (2002), 'Manganese causes differential regulation of glutamate transporter (GLAST) taurine transporter and metallothionein in cultured rat astrocytes', *Neurotoxicology,* 23 (4-5), 595-602.

Erikson, K. A., et al. (2002), 'Manganese accumulates in iron-deficient rat brain regions in a heterogeneous fashion and is associated with neurochemical alterations', *Biological Trace Element Research,* 87 (1-3), 143-56.

Erikson, K. M. and Aschner, M. (2003), 'Manganese neurotoxicity and glutamate-GABA interaction', *Neurochem Int,* 43 (4-5), 475-80.

Erikson, K. M., et al. (2008), 'Duration of airborne-manganese exposure in rhesus monkeys is associated with brain regional changes in biomarkers of neurotoxicity', *Neurotoxicology,* 29 (3), 377-85.

Erikson, K. M., et al. (2006), 'Alterations of oxidative stress biomarkers due to in utero and neonatal exposures of airborne manganese', *Biol Trace Elem Res,* 111 (1-3), 199-215.

Erikson, Keith M, et al. (2007), 'Manganese inhalation by rhesus monkeys is associated with brain regional changes in biomarkers of neurotoxicity', *Toxicological Sciences,* 97 (2), 459-66.

Eriksson, L., et al. (2006), *Multi- and Megavariate Data Analysis - Principles and Applications* (2nd edn.: Umetrics AB).

Fabiani, G., et al. (2007), 'Liver transplantation in a patient with rapid onset parkinsonism-dementia complex induced by manganism secondary to liver failure', *Arq Neuropsiquiatr,* 65 (3A), 685-8.

Fabrizi, C., et al. (1999), 'Activated alpha2-macroglobulin increases beta-amyloid (25-35)-induced toxicity in LAN5 human neuroblastoma cells', *Experimental Neurology,* 155, 252-59.

Farina, Marcelo, et al. (2013), 'Metals, Oxidative Stress and Neurodegeneration: A focus on Iron, Manganese and Mercury', *Neurochem Int,* 62 (5), 575-94.

Farooqui, A. A., Horrocks, L. A., and Farooqui, T. (2007), 'Modulation of inflammation in brain: a matter of fat', *Journal of Neurochemistry,* 101 (3), 577-99.

Fassel, V.A. (1986), 'Analytical Inductively Coupled Plasma Spectroscopies – Past, Present, and Future', *Fresenius J Anal Chem,* 324 (6), 511-18.

Feldmann, Jorg, Kindness, Andrew, and Ek, Paul (2002), 'Laser ablation of soft tissue using a cryogenically cooled ablation cell', *Journal of Analytical Atomic Spectrometry,* 17 (8), 813-18.

Fernández, Beatriz, et al. (2007), 'Direct analysis of solid samples by fs-LA-ICP-MS', *TrAC Trends in Analytical Chemistry,* 26 (10), 951-66.

Fernández Pierna, J. A., et al. (2003), 'A methodology to detect outliers/inliers in prediction with PLS', *Chemometrics and Intelligent Laboratory Systems,* 68 (1–2), 17-28.

Ferraz, H. B., et al. (1988), 'Chronic exposure to the fungicide maneb may produce symptoms and signs of CNS manganese intoxication', *Neurology,* 38 (4), 550-3.

Fiehn, O. (2002), 'Metabolomics--the link between genotypes and phenotypes', *Plant Mol Biol,* 48 (1-2), 155-71.

Finkelstein, M. M. and Jerrett, M. (2007), 'A study of the relationships between Parkinson's disease and markers of traffic-derived and environmental manganese air pollution in two Canadian cities', *Environ Res,* 104 (3), 420-32.

Fitsanakis, V. A., et al. (2006), 'The effects of manganese on glutamate, dopamine and gamma-aminobutyric acid regulation', *Neurochem Int,* 48 (6-7), 426-33.

Fitsanakis, V. A., et al. (2008), 'Measuring brain manganese and iron accumulation in rats following 14 weeks of low-dose manganese treatment using atomic absorption spectroscopy and magnetic resonance imaging', *Toxicol Sci,* 103 (1), 116-24.

Flynn, M. R. and Susi, P. (2009), 'Neurological risks associated with manganese exposure from welding operations - A literature review', *International Journal of Hygiene and Environmental Health,* 212 (5), 459-69.

Foradori, A. C., et al. (1967), 'The discrimination between magnesium and manganese by serum proteins', *J Gen Physiol,* 50 (9), 2255-66.

Forcisi, S., et al. (2013), 'Liquid chromatography-mass spectrometry in metabolomics research: mass analyzers in ultra high pressure liquid chromatography coupling', *J Chromatogr A,* 1292, 51-65.

Fordahl, Steve, et al. (2012), 'Waterborne manganese exposure alters plasma, brain, and liver metabolites accompanied by changes in stereotypic behaviors', *Neurotoxicol Teratol,* 34 (1), 27-36.

Fortune, W.B. and Mellon, M.G. (1938), 'Determination of iron with o-phenanthroline. A spectrophotometric study', *Industrial and Engineering Chemistry,* 10, 60-64.

Francesconi, K. A. and Sperling, M. (2005), 'Speciation analysis with HPLC-mass spectrometry: time to take stock', *Analyst,* 130 (7), 998-1001.

Fuxe, K., et al. (2007), 'Adenosine A(2A) receptors, dopamine D(2) receptors and their interactions in Parkinson's disease', *Mov Disord,* 22 (14), 1990-2017.

Gallez, Bernard, Baudelet, Christine, and Geurts, Muriel (1998), 'Regional distribution of manganese found in the brain after injection of a single dose of manganese-based contrast agents', *Magnetic Resonance Imaging,* 16 (10), 1211-15.

Gao, Guang-xin, et al. (2003), 'Survey on chronic occupational hazards in welders', *Chinese Journal of Industrial Medicine,* 16 (2), 107-07.

García-Sevillano, MiguelÁngel, et al. (2014), 'Use of elemental and molecular-mass spectrometry to assess the toxicological effects of inorganic mercury in the mouse Mus musculus', *Analytical and bioanalytical chemistry,* 406 (24), 5853-65.

Garcia, C. C., et al. (2008), 'Femtosecond laser ablation inductively coupled plasma mass spectrometry: Transport efficiencies of aerosols released under argon atmosphere and the importance of the focus position', *Spectrochimica Acta Part B: Atomic Spectroscopy,* 63 (2), 271-76.

Garcia, Carmen C., Lindner, Helmut, and Niemax, Kay (2007), 'Transport efficiency in femtosecond laser ablation inductively coupled plasma mass spectrometry applying ablation cells with short and long washout times', *Spectrochimica Acta Part B: Atomic Spectroscopy,* 62 (1), 13-19.

Garcia, S. J., et al. (2006), 'Iron Deficient and Manganese Supplemented Diets Alter Metals and Transporters in the Developing Rat Brain', *Toxicological Sciences,* 95 (1), 205–14.

Gavin, C. E., Gunter, K. K., and Gunter, T. E. (1990), 'Manganese and calcium efflux kinetics in brain mitochondria. Relevance to manganese toxicity', *Biochem J,* 266 (2), 329-34.

Gitler, A. D., et al. (2009), 'Alpha-synuclein is part of a diverse and highly conserved interaction network that includes PARK9 and manganese toxicity', *Nat Genet,* 41 (3), 308-15.

Goodacre, R. (2007), 'Metabolomics of a superorganism', *J Nutr,* 137 (1 Suppl), 259S-66S.

Goto, K., et al. (1996), 'An immuno-histochemical study of ferritin in 1-methyl-4-phenyl-1,2,3,6-tetrahydropyridine (MPTP)-induced hemiparkinsonian monkeys', *Brain Res,* 724 (1), 125-8.

Graumann, Rebecca, et al. (2002), 'Oxidation of dopamine to aminochrome as a mechanism for neurodegeneration of dopaminergic systems in Parkinson's disease. Possible neuroprotective role of DT-diaphorase', *Polish journal of pharmacology,* 54 (6), 573-80.

Gray, Alan L. (1985), 'Solid sample introduction by laser ablation for inductively coupled plasma source mass spectrometry', *Analyst,* 110 (5), 551-56.

Gross, J. H. (2013), *Massenspektrometrie - Ein Lehrbuch* (Berlin Heidelberg: Springer Spektrum).

Guilarte, T. R. (2010), 'Manganese and Parkinson's disease: a critical review and new findings', *Environ Health Perspect,* 118 (8), 1071-80.

Guilarte, T. R., et al. (2006), 'Nigrostriatal dopamine system dysfunction and subtle motor deficits in manganese-exposed non-human primates', *Experimental Neurology,* 202 (2), 381-90.

Gunter, R.E., Puskin, J.S., and Russell, P.R. (1975), 'Quantitative magnetic resonance studies of manganese uptake by mitochondria', *Biophysical Journal,* 15 (4), 319.

Gunter, T.E. and Puskin, J.S. (1975), 'THE USE OF ELECTRON PARAMAGNETIC RESONANCE IN STUDIES OF FREE AND BOUND DIVALENT CATION: THE MEASUREMENT OF MEMBRANE POTENTIALS IN MITOCHONDRIAfn1', *Annals of the New York Academy of Sciences,* 264 (1), 112-23.

Gunter, Thomas E., et al. (2006), 'Speciation of manganese in cells and mitochondria: A search for the proximal cause of manganese neurotoxicity', *Neurotoxicology,* 27 (5), 765-76.

Gunter, Thomas E., et al. (2004), 'Determination of the oxidation states of manganese in brain, liver, and heart mitochondria', *Journal of Neurochemistry,* 88 (2), 266-80.

Gunther, Detlef and A. Heinrich, Christoph (1999), 'Comparison of the ablation behaviour of 266 nm Nd:YAG and 193 nm ArF excimer lasers for LA-ICP-MS analysis', *Journal of Analytical Atomic Spectrometry,* 14 (9), 1369-74.

Günther, Detlef and Hattendorf, Bodo (2005), 'Solid sample analysis using laser ablation inductively coupled plasma mass spectrometry', *TrAC Trends in Analytical Chemistry,* 24 (3), 255-65.

Gwiazda, Roberto, Lucchini, Roberto, and Smith, Donald (2007), 'Adequacy and Consistency of Animal Studies to Evaluate the Neurotoxicity of Chronic Low-Level Manganese Exposure in Humans', *Journal of Toxicology and Environmental Health, Part A,* 70 (7), 594-605.

Hare, Dominic, et al. (2009), 'Quantitative elemental bio-imaging of Mn, Fe, Cu and Zn in 6-hydroxydopamine induced Parkinsonism mouse models', *Metallomics,* 1 (1), 53-58.

Hasko, G., Sitkovsky, M. V., and Szabo, C. (2004), 'Immunomodulatory and neuroprotective effects of inosine', *Trends in Pharmacological Sciences,* 25 (3), 152-57.

He, F., Hendrickson, C. L., and Marshall, A. G. (2001), 'Baseline mass resolution of peptide isobars: a record for molecular mass resolution', *Anal Chem,* 73 (3), 647-50.

Heinzmann, Silke S and Schmitt-Kopplin, Philippe (2015), 'Deep Metabotyping of the Murine Gastrointestinal Tract for the Visualization of Digestion and Microbial Metabolism', *Journal of proteome research,* 14 (5), 2267-77.

Herken, Hans (1990), 'Neurotoxin-induced impairment of biopterin synthesis and function: Initial stage of a Parkinson-like dopamine deficiency syndrome', *Neurochem Int,* 17 (2), 223-38.

Hernandez, R. B., et al. (2011a), 'Mechanisms of manganese-induced neurotoxicity in primary neuronal cultures: the role of manganese speciation and cell type', *Toxicol Sci,* 124 (2), 414-23.

Hernandez, R. B., et al. (2011b), 'Mechanisms of Manganese-Induced Neurotoxicity in Primary Neuronal Cultures: The Role of Manganese Speciation and Cell Type', *Toxicological Sciences,* 124 (2), 414-23.

Herrero Hernandez, Elena, et al. (2003), 'Manganese Intoxication: The Cause of an Inexplicable Epileptic Syndrome in a 3 Year Old Child', *Neurotoxicology,* 24 (4–5), 633-39.

Hertkorn, N., et al. (2008), 'Natural Organic Matter and the Event Horizon of Mass Spectrometry', *Analytical Chemistry,* 80 (23), 8908–19.

Hesse, M., Meier, H., and Zeeh, B. (2002), *Spektroskopische Methoden in der organischen Chemie: 102 Tabellen* (6th edn.; Stuttgart: Thieme).

Hillered, Lars, et al. 'Mn2+ prevents the Ca2+-induced inhibition of ATP synthesis in brain mitochondria', *FEBS Lett,* 154 (2), 247-50.

Hoet, P., et al. (2012), 'Manganese in plasma: A promising biomarker of exposure to Mn in welders. A pilot study', *Toxicology Letters,* 213 (1), 69-74.

Hou, X. and Jones, B.T. (2000), 'Inductively Coupled Plasma/Optical Emission Spectrometry', in R.A. Meyers (ed.), *Encyclopedia of Analytical Chemistry* (Chichester: John Wiley & Sons Ltd.), 9468-85.

Hu, Peifeng, Sorensen, Curt, and Gross, Michael L (1995), 'Influences of peptide side chains on the metal ion binding site in metal ion-cationized peptides: Participation of aromatic rings in metal chelation', *Journal of the American Society for Mass Spectrometry,* 6 (11), 1079-85.

Hudnell, H. K. (1999), 'Effects from environmental Mn exposures: a review of the evidence from non-occupational exposure studies', *Neurotoxicology,* 20 (2-3), 379-97.

IOM (2011), 'Dietary Reference Intakes: Vitamin A, Vitamin K, Arsenic, Boron, Chromium, Copper, Iodine, Iron, Manganese, Molybdenum, Nickel, Silicon, Vanadium, and Zinc', in Institute of Medicine (ed.), (Washington DC: National Academy Press).

Iregren, A. (1999), 'Manganese neurotoxicity in industrial exposures: proof of effects, critical exposure level, and sensitive tests', *Neurotoxicology,* 20 (2-3), 315-23.

Jackson, B., et al. (2006), 'Elemental mapping and quantitative analysis of Cu, Zn, and Fe in rat brain sections by laser ablation ICP-MS', *Anal Bioanal Chem,* 384 (4), 951-7.

Jakubowski, N., Moens, L., and Vanhaecke, F. (1998), 'Sector field mass spectrometers in ICP-MS', *Spectrochimica Acta Part B,* 53, 1739-63.

Jeandet, Philippe, et al. (2015), 'Chemical messages in 170-year-old champagne bottles from the Baltic Sea: Revealing tastes from the past', *Proceedings of the National Academy of Sciences,* 112 (19), 5893-98.

Johansen, Krisztina K, et al. (2009), 'Metabolomic profiling in LRRK2-related Parkinson's disease', *PLoS one,* 4 (10), e7551.

Jové, Mariona, et al. (2014), 'Metabolomics of human brain aging and age-related neurodegenerative diseases', *Journal of Neuropathology and Experimental Neurology,* 73 (7), 640-57.

Kaddurah-Daouk, R. and Weinshilboum, R. M. (2014), 'Pharmacometabolomics: implications for clinical pharmacology and systems pharmacology', *Clin Pharmacol Ther,* 95 (2), 154-67.

Kalia, K., Jiang, W., and Zheng, W. (2008), 'Manganese accumulates primarily in nuclei of cultured brain cells', *Neurotoxicology,* 29 (3), 466-70.

Kapich, A. N., et al. (2011), 'Comparative evaluation of manganese peroxidase- and Mn(III)-initiated peroxidation of C18 unsaturated fatty acids by different methods', *Enzyme Microb Technol,* 49 (1), 25-9.

Keane, M., Stone, S., and Chen, B. (2010), 'Welding fumes from stainless steel gas metal arc processes contain multiple manganese chemical species', *Journal of Environmental Monitoring,* 12 (5), 1133-40.

Kebarle, P. (2000), 'A brief overview of the Present Status of the Mechanisms Involved in Electrospray MS', *Journal of Mass Spectrometry,* 35, 804-17.

Kim, Jonghan, et al. (2012), 'Iron-responsive olfactory uptake of manganese improves motor function deficits associated with iron deficiency', *PLoS ONE,* 7 (3), e33533.

Koch, J. and Gunther, D. (2011), 'Review of the state-of-the-art of laser ablation inductively coupled plasma mass spectrometry', *Appl Spectrosc,* 65 (5), 155-62.

Kodali, P., et al. (2012), 'Multiple liquid chromatography separations and nanoESI-ion trap detection of plasma proteins in search of stroke biomarkers: A pilot study', *J Sep Sci,* 35 (17), 2153-61.

Koller, W. C., Lyons, K. E., and Truly, W. (2004), 'Effect of levodopa treatment for parkinsonism in welders: A double-blind study', *Neurology,* 62 (5), 730-3.

Kovacs, D.M. (2000), 'alpha2-Macroglobulin in late-onset Alzheimer´s disease', *Experimental Gerontology,* 35, 473-79.

Krieger, D, et al. (1995), 'Manganese and chronic hepatic encephalopathy', *The Lancet,* 346 (8970), 270-74.

Kumar, Kevin K, et al. (2015), 'Untargeted metabolic profiling identifies interactions between Huntington's disease and neuronal manganese status', *Metallomics,* 7 (2), 363-70.

Kwik-Uribe, C. L., et al. (2000), 'Chronic marginal iron intakes during early development in mice result in persistent changes in dopamine metabolism and myelin composition', *Journal of Nutrition,* 130 (11), 2821-30.

Lai, J. C., Leung, T. K., and Lim, L. (1981), 'Brain regional distribution of glutamic acid decarboxylase, choline acetyltransferase, and acetylcholinesterase in the rat: effects of chronic manganese chloride administration after two years', *J Neurochem,* 36 (4), 1443-8.

Larsen, Erik H. and Sturup, Stefan (1994), 'Carbon-enhanced inductively coupled plasma mass spectrometric detection of arsenic and selenium and its application to arsenic speciation', *Journal of Analytical Atomic Spectrometry,* 9 (10), 1099-105.

Lau, A. and Tymianski, M. (2010), 'Glutamate receptors, neurotoxicity and neurodegeneration', *Pflugers Archiv-European Journal of Physiology,* 460 (2), 525-42.

Laurie, SH (1995), 'The Synthesis, Reactions, Properties and Applications of Coordination Compounds', *Handbook of metal-ligand interactions in biological fluids: bioinorganic chemistry,* 1, 603-19.

Lebda, M. A., El-Neweshy, M. S., and El-Sayed, Y. S. (2012), 'Neurohepatic toxicity of subacute manganese chloride exposure and potential chemoprotective effects of lycopene', *Neurotoxicology,* 33 (1), 98-104.

Lee, E. S., et al. (2009), 'Estrogen and tamoxifen reverse manganese-induced glutamate transporter impairment in astrocytes', *J Neurochem,* 110 (2), 530-44.

Liang, Youxin and Xiang, Quanyong (2004), 'Occupational health services in PR China', *Toxicology,* 198 (1), 45-54.

Liapi, C., et al. (2008), 'Effects of short-term exposure to manganese on the adult rat brain antioxidant status and the activities of acetylcholinesterase, (Na,K)-ATPase and Mg-ATPase: modulation by L-cysteine', *Basic Clin Pharmacol Toxicol,* 103 (2), 171-5.

Lichte, F.E. and Koirtyohann, S.R. (1976), 'Induction Coupled Plasma Emission from a Different Angle', *Federation of Analytical Chemistry and Spectroscopy Society, Philadelphia,* Paper 26.

Lima, P. D., et al. (2008), 'Genotoxic and cytotoxic effects of manganese chloride in cultured human lymphocytes treated in different phases of cell cycle', *Toxicol In Vitro,* 22 (4), 1032-7.

Lin, Shuhai, et al. (2013), 'Hippocampal metabolomics using ultrahigh-resolution mass spectrometry reveals neuroinflammation from Alzheimer's disease in CRND8 mice', *Analytical and bioanalytical chemistry,* 405 (15), 5105-17.

Lindberg, Olov and Ernster, Lars (1954), 'Manganese, a co-factor of oxidative phosphorylation'.

Lipe, G. W., et al. (1999), 'Effect of manganese on the concentration of amino acids in different regions of the rat brain', *J Environ Sci Health B,* 34 (1), 119-32.

Liu, Feng, et al. (2012), 'A combination of metabolomics and metallomics studies of urine and serum from hypercholesterolaemic rats after berberine injection', *Analytical and bioanalytical chemistry,* 403 (3), 847-56.

Liu, X. (2006), 'Manganese-Induced Neurotoxicity: The Role of Astroglial-Derived Nitric Oxide in Striatal Interneuron Degeneration', *Toxicological Sciences,* 91 (2), 521–31.

Lobinski, R., Schaumloffel, D., and Szpunar, J. (2006), 'Mass spectrometry in bioinorganic analytical chemistry', *Mass Spectrom Rev,* 25 (2), 255-89.

Lobinski, R., et al. (2010), 'Metallomics: Guidlines for terminology and critical evaluation of analytical chemistry approaches (IUPAC Technical Report)', *Pure Applied Chemistry,* 82 (2), 493-504.

Lopez-Avila, Viorica and Spencer, Juliet V (2008), 'Methods for Detection of Matrix Metalloproteinases as Biomarkers in Cardiovascular Disease', *Clinical Medicine Insights. Cardiology,* 1, 75.

Lucchini, R. and Zimmerman, N. (2009), 'Lifetime cumulative exposure as a threat for neurodegeneration: need for prevention strategies on a global scale', *Neurotoxicology,* 30 (6), 1144-8.

Lucchini, R. G., et al. (2007), 'High prevalence of Parkinsonian disorders associated to manganese exposure in the vicinities of ferroalloy industries', *Am J Ind Med,* 50 (11), 788-800.

Lucio, M. (2008), 'Datamining metabolomics: the convergence point of non-target approach and statistical investigation.', *Dissertation, TU München*.

Lv, Yingnan, et al. (2014), 'Rationale, design and baseline results of the Guangxi manganese-exposed workers healthy cohort (GXMEWHC) study', *BMJ open,* 4 (7), e005070.

Lynam, D. R., et al. (1999), 'Environmental effects and exposures to manganese from use of methylcyclopentadienyl manganese tricarbonyl (MMT) in gasoline', *Neurotoxicology,* 20 (2-3), 145-50.

Madejczyk, M. S. and Ballatori, N. (2012), 'The iron transporter ferroportin can also function as a manganese exporter', *Biochim Biophys Acta,* 1818 (3), 651-7.

Madsen, R., Lundstedt, T., and Trygg, J. (2010), 'Chemometrics in metabolomics--a review in human disease diagnosis', *Anal Chim Acta,* 659 (1-2), 23-33.

Makarov, Alexei and Szpunar, Joanna (1999), 'Species-selective determination of cobalamin analogues by reversed-phase HPLC with ICP-MS detection', *Journal of Analytical Atomic Spectrometry,* 14 (9), 1323-27.

Mamas, M., et al. (2011), 'The role of metabolites and metabolomics in clinically applicable biomarkers of disease', *Arch Toxicol,* 85 (1), 5-17.

Martinez, H. and Bonilla, E. (1981), 'Water intake and brain choline-acetyltransferase and acetylcholinesterase activites in manganese treated rats', *Neurobehav Toxicol Teratol,* 3 (3), 277-80.

Matzapetakis, M., et al. (2000), 'Manganese citrate chemistry: syntheses, spectroscopic studies, and structural characterizations of novel mononuclear, water-soluble manganese citrate complexes', *Inorg Chem,* 39 (18), 4044-51.

May, T.W. and Wiedmeyer, R.H. (1998), 'A Table of Polyatomic Interferences in ICP-MS', *Atomic Spectroscopy,* 19 (5), 150-55.

Mazzio, E. and Soliman, K. F. (2003), 'The role of glycolysis and gluconeogenesis in the cytoprotection of neuroblastoma cells against 1-methyl 4-phenylpyridinium ion toxicity', *Neurotoxicology,* 24 (1), 137-47.

McDougall, S. A., et al. (2008), 'Postnatal manganese exposure alters dopamine transporter function in adult rats: Potential impact on nonassociative and associative processes', *Neuroscience,* 154 (2), 848-60.

Michalke, B. (2002), 'The coupling of LC to ICP-MS in element speciation: I. General aspects', *Trends in Analytical Chemistry,* 21 (2), 142-53.

Michalke, B. and Fernsebner, K. (2013), 'New insights into manganese toxicity and speciation', *J Trace Elem Med Biol.*

Michalke, B., Halbach, S., and Nischwitz, V. (2009), 'JEM Spotlight: Metal speciation related to neurotoxicity in humans', *Journal of Environmental Monitoring,* 11, 939-54.

Michalke, B., et al. (2013), 'Manganese speciation in paired serum and CSF samples using SEC-DRC-ICP-MS and CE-ICP-DRC-MS', *Anal Bioanal Chem,* 405 (7), 2301-9.

Michalke, B., et al. (2007), 'Manganese speciation in human cerebrospinal fluid using CZE coupled to inductively coupled plasma MS', *Electrophoresis,* 28 (9), 1380-86.

Milatovic, D., et al. (2011), 'Protective effects of antioxidants and anti-inflammatory agents against manganese-induced oxidative damage and neuronal injury', *Toxicology and Applied Pharmacology,* 256 (3), 219-26.

Milatovic, Dejan, et al. (2007), 'Manganese induces oxidative impairment in cultured rat astrocytes', *Toxicological Sciences,* 98 (1), 198-205.

Miliszkiewicz, Natalia, Walas, Stanisław, and Tobiasz, Anna (2015), 'Current approaches to calibration of LA-ICP-MS analysis', *Journal of Analytical Atomic Spectrometry,* 30 (2), 327-38.

Miller, Erin M., et al. (2013), *Dopamine and Glutamate Interactions in ADHD: Implications for the Future Neuropharmacology of ADHD* (Attention Deficit Hyperactivity Disorder in Children and Adolescents).

Mirza, B., et al. (2000), 'The absence of reactive astrocytosis is indicative of a unique inflammatory process in Parkinson's disease', *Neuroscience,* 95 (2), 425-32.

Moos, T. and Morgan, E. H. (2004), 'The metabolism of neuronal iron and its pathogenic role in neurological disease - Review', *Redox-Active Metals in Neurological Disorders,* 1012, 14-26.

Mounicou, Sandra, Szpunar, Joanna, and Lobinski, Ryszard (2009), 'Metallomics: the concept and methodology', *Chemical Society Reviews,* 38 (4), 1119-38.

Muller, C., et al. (2013), 'Molecular cartography in acute Chlamydia pneumoniae infections-a non-targeted metabolomics approach', *Anal Bioanal Chem*.

Murphy, Vincent A, et al. (1991), 'Saturable Transport of Manganese (II) Across the Rat Blood-Brain Barrier', *Journal of Neurochemistry,* 57 (3), 948-54.

Mutkus, L., et al. (2005), 'The in vitro uptake of glutamate in GLAST and GLT-1 transfected mutant CHO-K1 cells is inhibited by manganese', *Biological Trace Element Research,* 107 (3), 221-30.

Nakamura, Ken, Wang, Wenyi, and Kang, Un Jung (1997), 'The Role of Glutathione in Dopaminergic Neuronal Survival', *J Neurochem,* 69 (5), 1850-58.

Newland, M. Christopher, et al. (1989), 'Visualizing manganese in the primate basal ganglia with magnetic resonance imaging', *Experimental Neurology,* 106 (3), 251-58.

Nicholson, J. K. and Wilson, I. D. (2003), 'Opinion: understanding 'global' systems biology: metabonomics and the continuum of metabolism', *Nat Rev Drug Discov,* 2 (8), 668-76.

Nicholson, J. K., Lindon, J. C., and Holmes, E. (1999), ''Metabonomics': understanding the metabolic responses of living systems to pathophysiological stimuli via multivariate statistical analysis of biological NMR spectroscopic data', *Xenobiotica,* 29 (11), 1181-9.

Nikolaev, E. N., Kostyukevich, Y. I., and Vladimirov, G. N. (2014), 'Fourier transform ion cyclotron resonance (FT ICR) mass spectrometry: Theory and simulations', *Mass Spectrom Rev*.

Nischwitz, V. and Michalke, B. (2009), 'Electrospray ionisation with selected reaction monitoring for the determination of Mn-citrate, Fe-citrate, Cu-citrate and Zn-citrate', *Rapid Communications in Mass Spectrometry,* 23 (15), 2338–46.

Nischwitz, V., Michalke, B., and Kettrup, A. (2003), 'Identification and quantification of metallothionein isoforms and superoxide dismutase in spiked liver extracts using HPLC-ESI-MS offline coupling and HPLC-ICP-MS online coupling', *Anal Bioanal Chem,* 375 (1), 145-56.

Nischwitz, V., Berthele, A., and Michalke, B. (2008), 'Speciation analysis of selected metals and determination of their total contents in paired serum and cerebrospinal fluid samples: An approach to investigate the permeability of the human blood-cerebrospinal fluid-barrier', *Anal Chim Acta,* 627 (2), 258-69.

--- (2010), 'Rapid size fractionation of metal species in paired human serum and cerebrospinal fluid samples using ultrafiltration with off-line element selective detection', *Journal of Analytical Atomic Spectrometry,* 25 (7), 1130-37.

Nissen-Meyer, Lise Sofie H and Chaudhry, Farrukh Abbas (2013), 'Protein kinase C phosphorylates the system N glutamine transporter SN1 (Slc38a3) and regulates its membrane trafficking and degradation', *Frontiers in endocrinology,* 4.

Norenberg, Michael D and Martinez-Hernandez, Antonio (1979), 'Fine structural localization of glutamine synthetase in astrocytes of rat brain', *Brain Res,* 161 (2), 303-10.

NRC (1995), *Nutrient Requirements of Laboratory Animals* (4th revised edition edn.; Washington, DC: Nat. Acad. Press.).

O´Connor, C., Sharp, B.L., and Evans, P. (2006), 'On-line additions of aqueous standards for calibration of laser ablation inductively coupled plasma mass spectrometry: theory and comparison of wet and dry plasma conditions ', *Journal of Analytical Atomic Spectrometry,* 21, 556-65.

Okonkwo, J. O., Moja, S. J., and Forbes, P. (2009), 'Manganese levels and chemical fractionation in street dust in South Africa', *International Journal of Environment and Pollution,* 36 (4), 350-66.

Olanow, C. W. (2004), 'Manganese-induced parkinsonism and Parkinson's disease', *Ann N Y Acad Sci,* 1012, 209-23.

Pan, D., et al. (2010), 'Revisiting an old friend: manganese-based MRI contrast agents', *Wiley Interdiscip Rev Nanomed Nanobiotechnol,* (doi: 10.1002/wnan.116).

Parkel, Sven, Tõntson, Lauri, and Rinken, Ago (2011), 'Millimolar Mn 2+ influences agonist binding to 5-HT 1A receptors by inhibiting guanosine nucleotide binding to receptor-coupled G-proteins', *Neurotoxicology,* 32 (1), 25-30.

Paton, C., et al. (2011), 'Iolite: Freeware for the visualisation and processing of mass spectrometric data', *Journal of Analytical Atomic Spectrometry,* 26 (12), 2508-18.

Patti, G. J., Yanes, O., and Siuzdak, G. (2012), 'Innovation: Metabolomics: the apogee of the omics trilogy', *Nat Rev Mol Cell Biol,* 13 (4), 263-9.

Perkin,Elmer
    <http://www.perkinelmer.com/pdfs/downloads/BRO_NexION350ICPMSBrochure.pdf >, accessed 23.01.2015.

--- <http://www.perkinelmer.com/Content/Manuals/GDE_InorganicAnalysis.pdf>, accessed 17.01.2015.

--- <http://www.perkinelmer.com/CMSResources/Images/44-134752BRO_Optima-8x00-Family.pdf>, accessed 15.01.2015.

Pifferi, F., et al. (2005), '(n-3) polyunsaturated fatty acid deficiency reduces the expression of both isoforms of the brain glucose transporter GLUT1 in rats', *J Nutr,* 135 (9), 2241-6.

Pisonero, Jorge, Fernandez, Beatriz, and Gunther, Detlef (2009), 'Critical revision of GD-MS, LA-ICP-MS and SIMS as inorganic mass spectrometric techniques for direct solid analysis', *Journal of Analytical Atomic Spectrometry,* 24 (9), 1145-60.

Pratap Karki, Eunsook Lee, and Aschner, Michael (2013), 'Magnanese Neurotoxicity: a Focus on Glutamate Transporters', *Annals of occupational and environmental medicine,* 25, 4.

Pratico, D., et al. (2004), '12/15-lipoxygenase is increased in Alzheimer's disease: possible involvement in brain oxidative stress', *American Journal of Pathology,* 164 (5), 1655-62.

Quintanar, Liliana (2008), 'Manganese neurotoxicity: A bioinorganic chemist's perspective', *Inorganica Chimica Acta,* 361 (4), 875-84.

Racette, B. A., et al. (2001), 'Welding-related parkinsonism: clinical features, treatment, and pathophysiology', *Neurology,* 56 (1), 8-13.

Racette, B. A., et al. (2005), '[18F]FDOPA PET and clinical features in parkinsonism due to manganism', *Mov Disord,* 20 (4), 492-6.

Ramautar, R., et al. (2013), 'Human metabolomics: strategies to understand biology', *Curr Opin Chem Biol,* 17 (5), 841-6.

Rassow, J., et al. (2006), *Duale Reihe-Biochemie,* eds A. Bob and K. Bob (Stuttgart: Georg Thieme Verlag) 864.

Reed, Tanea T. (2011), 'Lipid peroxidation and neurodegenerative disease', *Free Radical Biology and Medicine,* 51 (7), 1302-19.

Ressler, Thorsten, et al. (2000), 'Quantitative speciation of Mn-bearing particulates emitted from autos burning (methylcyclopentadienyl) manganese tricarbonyl-added gasolines using XANES spectroscopy', *Environmental science & technology,* 34 (6), 950-58.

Riojas-Rodriguez, H., et al. (2010), 'Intellectual function in Mexican children living in a mining area and environmentally exposed to manganese', *Environ Health Perspect,* 118 (10), 1465-70.

Robison, Gregory, et al. (2015), 'Identification of dopaminergic neurons of the substantia nigra pars compacta as a target of manganese accumulation', *Metallomics,* 7 (5), 748-55.

Roels, H., et al. (1987), 'Relationship between external and internal parameters of exposure to manganese in workers from a manganese oxide and salt producing plant', *Am J Ind Med,* 11 (3), 297-305.

Roels, H., et al. (1997), 'Influence of the route of administration and the chemical form (MnCl2, MnO2) on the absorption and cerebral distribution of manganese in rats', *Arch Toxicol,* 71 (4), 223-30.

Rohlman, D. S., et al. (2008), 'Neurobehavioral testing in human risk assessment', *Neurotoxicology,* 29 (3), 556-67.

Ronconi, Luca and Sadler, Peter J (2008), 'Applications of heteronuclear NMR spectroscopy in biological and medicinal inorganic chemistry', *Coordination Chemistry Reviews,* 252 (21), 2239-77.

Roth, Jerome A and Garrick, Michael D (2003), 'Iron interactions and other biological reactions mediating the physiological and toxic actions of manganese', *Biochemical Pharmacology,* 66 (1), 1-13.

Roychowdhury, T., Tokunaga, H., and Ando, M. (2003), 'Survey of arsenic and other heavy metals in food composites and drinking water and estimation of dietary intake by the villagers from an arsenic-affected area of West Bengal, India', *Science of the Total Environment,* 308 (1-3), 15-35.

Sadrzadeh, S. M. and Saffari, Y. (2004), 'Iron and brain disorders', *Am J Clin Pathol,* 121 Suppl, S64-70.

Salmanzadeh, M., et al. (2015), 'Characterization and metals fractionation of street dust samples from Tehran, Iran', *International Journal of Environmental Research,* 9 (1), 213-24.

Salvador, G. A. (2010), 'Iron in neuronal function and dysfunction', *Biofactors,* 36 (2), 103-10.

Santos, Dinamene, et al. (2012), 'The inhibitory effect of manganese on acetylcholinesterase activity enhances oxidative stress and neuroinflammation in the rat brain', *Toxicology,* 292 (2-3), 90–98.

Schaub, T. M., et al. (2008), 'High-performance mass spectrometry: Fourier transform ion cyclotron resonance at 14.5 Tesla', *Anal Chem,* 80 (11), 3985-90.

Scheuhammer, A. M. and Cherian, M. G. (1981), 'The influence of manganese on the distribution of essential trace elements: I. Regional distribution of Mn, Na, K, Mg, Zn, Fe, and Cu in rat brain after chronic Mn exposure', *Toxicology and Applied Pharmacology,* 61 (2), 227-33.

--- (1985), 'Binding of manganese in human and rat plasma', *Biochimica et Biophysica Acta (BBA)-General Subjects,* 840 (2), 163-69.

Schmitt-Kopplin, P., et al. (2012), 'Ulatrahigh Resolution Fourier Transform Ion Cyclotron Resonance Mass Spectrometry for the Analysis of Natural Organic Matter from Various Environmental Systems', in Albert Lebedev (ed.), *Comprehensive environmental mass spectrometry* (ILM Publications).

Schramel, P, et al. (1980), 'Eine neue Apparatur zur Druckveraschung von biologischem Material', *Fresenius' Zeitschrift für analytische Chemie,* 302 (1), 62-64.

Sekirov, I. and Finlay, B. B. (2006), 'Human and microbe: united we stand', *Nat Med,* 12 (7), 736-7.

Seo, Young Ah, Li, Yuan, and Wessling-Resnick, Marianne (2013), 'Iron depletion increases manganese uptake and potentiates apoptosis through ER stress', *Neurotoxicology,* 38, 67-73.

Sheats, John E, et al. (1987), 'Binuclear manganese (III) complexes of potential biological significance', *Journal of the American Chemical Society,* 109 (5), 1435-44.

Shimazaki, Yuichi, Takani, Masako, and Yamauchi, Osamu (2009), 'Metal complexes of amino acids and amino acid side chain groups. Structures and properties', *Dalton Transactions,* (38), 7854-69.

Shinotoh, H, et al. (1995), 'MRI and PET studies of manganese-intoxicated monkeys', *Neurology,* 45 (6), 1199-204.

Sian, Jeswinder, et al. (1994), 'Alterations in glutathione levels in Parkinson's disease and other neurodegenerative disorders affecting basal ganglia', *Ann Neurol,* 36 (3), 348-55.

Sidoryk-Wegrzynowicz, M., et al. (2009), 'Manganese disrupts astrocyte glutamine transporter expression and function', *J Neurochem,* 110 (3), 822-30.

Sidoryk-Wegrzynowicz, Marta and Aschner, Michael (2013), 'Role of astrocytes in manganese mediated neurotoxicity', *BMC Pharmacology and Toxicology,* 14 (1), 23.

Singh, SP, et al. (1996), 'The chemistry of the S-nitrosoglutathione/glutathione system', *Proceedings of the National Academy of Sciences,* 93 (25), 14428-33.

Smith, D., et al. (2007), 'Biomarkers of Mn exposure in humans', *Am J Ind Med,* 50 (11), 801-11.

Smith, E. A., et al. (2013), 'Increased whole blood manganese concentrations observed in children with iron deficiency anaemia', *Journal of Trace Elements in Medicine and Biology,* 27 (1), 65-69.

Smyth, L. T., et al. (1973), 'Clinical manganism and exposure to manganese in the production and processing of ferromanganese alloy', *J Occup Med,* 15 (2), 101-9.

Soga, T., et al. (2003), 'Quantitative metabolome analysis using capillary electrophoresis mass spectrometry', *J Proteome Res,* 2 (5), 488-94.

Speziali, Margherita and Orvini, Edoardo (2003), 'Metals distribution and regionalization in the brain', *Metal Ions and Neurodegenerative Disorders. Singapore: World Scientific Publishing Co. Pte. Ltd*, 15-65.

Spranger, M., et al. (1998), 'Manganese augments nitric oxide synthesis in murine astrocytes: A new pathogenetic mechanism in manganism?', *Experimental Neurology,* 149 (1), 277-83.

Sriram, Krishnan, et al. (2010), 'Mitochondrial dysfunction and loss of Parkinson's disease-linked proteins contribute to neurotoxicity of manganese-containing welding fumes', *The FASEB Journal,* 24 (12), 4989-5002.

Stallings, W. C., et al. (1991), 'Structure-function relationships in iron and manganese superoxide dismutases', *Free Radic Res Commun,* 12-13 Pt 1, 259-68.

Stastny, D., Vogel, R. S., and Picciano, M. F. (1984), 'Manganese intake and serum manganese concentration of human milk-fed and formula-fed infants', *Am J Clin Nutr,* 39 (6), 872-8.

Stone, T. W. (2002), 'Purines and neuroprotection', *Adv Exp Med Biol,* 513, 249-80.

Stookey, L.L. (1970), 'Ferrozine-A New Spectrophotometric Reagent for Iron', *Analytical Chemistry,* 42 (7).

Stredrick, D. L., et al. (2004), 'Manganese-induced cytotoxicity in dopamine-producing cells', *Neurotoxicology,* 25 (4), 543-53.

Sussulini, Alessandra, et al. (2013), 'Quantitative imaging of the tissue contrast agent [Gd(DTPA)]2− in articular cartilage by laser ablation inductively coupled plasma mass spectrometry', *Contrast Media & Molecular Imaging,* 8 (2), 204-09.

Szpunar, J. (2000), 'Bio-inorganic speciation analysis by hyphenated techniques', *Analyst,* 125 (5), 963-88.

--- (2004), 'Metallomics: a new frontier in analytical chemistry', *Anal Bioanal Chem,* 378 (1), 54-6.

Tainer, J. A., Roberts, V. A., and Getzoff, E. D. (1991), 'Metal-binding sites in proteins', *Curr Opin Biotechnol,* 2 (4), 582-91.

Takeda, A. (2003), 'Manganese action in brain function', *Brain Res Brain Res Rev,* 41 (1), 79-87.

Takeda, A., Sawashita, J., and Okada, S. (1995), 'Biological half-lives of zinc and manganese in rat brain', *Brain Res,* 695 (1), 53-8.

--- (1998), 'Manganese concentration in rat brain: manganese transport from the peripheral tissues', *Neurosci Lett,* 242 (1), 45-8.

Tarohda, T., et al. (2005), 'Regional distributions of manganese, iron, copper, and zinc in the brains of 6-hydroxydopamine-induced parkinsonian rats', *Analytical and Bioanalytical Chemistry,* 383 (2), 224-34.

Taylor, M. D., et al. (2006), 'Effects of inhaled manganese on biomarkers of oxidative stress in the rat brain', *Neurotoxicology,* 27 (5), 788-97.

Taylor, Steven W, Luther III, George W, and Waite, J Herbert (1994), 'Polarographic and spectrophotometric investigation of iron (III) complexation to 3, 4-dihydroxyphenylalanine-containing peptides and proteins from Mytilus edulis', *Inorg Chem,* 33 (25), 5819-24.

Templeton, D. M., et al. (2000), 'Guidelines for terms related to chemical speciation and fractionation of elements. Definitions, structural aspects, and methodological approaches (IUPAC Recommendations 2000)', *Pure and Applied Chemistry,* 72 (8), 1453-70.

Thermo,Fisher <http://www.thermoscientific.com/content/dam/tfs/ATG/CMD/CMD%20Documents/BR-30027-Element-2-Element-XR.pdf>, accessed 20.01.2015.

Thomas, R. (2002), 'A Beginner´s Guide to ICP-MS. PartXII - A Review of Interferences', *Spectroscopy,* 17 (10), 24-31.

Thomassen, Y., et al. (2001), 'Chemical speciation and sequential extraction of Mn in workroom aerosols: analytical methodology and results from a field study in Mn alloy plants', *Journal of Environmental Monitoring,* 3 (6), 555-59.

Touitou, Y., et al. (1986), 'Differences between young and elderly subjects in seasonal and circadian variations of total plasma proteins and blood volume as reflected by hemoglobin, hematocrit, and erythrocyte counts', *Clin Chem,* 32 (5), 801-4.

Traeger, J.C. (2000), 'Electrospray Mass Spectrometry of Organometallic Compounds', *International Journal of Mass Spectrometry,* 200, 387-401.

Trygg, J. and Wold, S. (2002), 'Orthogonal Projections to Latent Structures (OPLS)', *Journal of Chemometrics,* 26 (6), 231-35.

Tziotis, D., Hertkorn, N., and Schmitt-Kopplin, P. (2011), 'Kendrick-analogous network visualisation of ion cyclotron resonance Fourier transform mass spectra: improved options for the assignment of elemental compositions and the classification of organic molecular complexity', *Eur J Mass Spectrom (Chichester, Eng),* 17 (4), 415-21.

USEPA (1984), 'Health Assessment Document for Manganese', in U.S.E.A. Agency (ed.), (EPA 600-83-013F; Washington, DC: USEPA).

van der Greef, J., et al. (2013), 'Looking back into the future: 30 years of metabolomics at TNO', *Mass Spectrom Rev,* 32 (5), 399-415.

Vandenbossche, M, et al. (2014), 'Remediation of Heavy Metals by Biomolecules-A Review', *Critical Reviews in Environmental Science and Technology,* (just-accepted), 00-00.

Vankaecke, F., Balcaen, L., and Taylor, P. (2006), 'Use of ICP-MS for isotope ratio measurements', in S.J. Hill (ed.), *Inductively coupled plasma mass spectrometry and its applications* (2nd edn., Analytical Chemistry; Ames, IA, USA: Blackwell), 160-225.

Vilar, R, et al. (2007), 'Association of A313 G polymorphism (GSTP1* B) in the glutathione-S-transferase P1 gene with sporadic Parkinson's disease', *European Journal of Neurology,* 14 (2), 156-61.

Villalobos, V., et al. (2001), 'Effect of chronic manganese treatment on adenosine tissue levels and adenosine A2a receptor binding in diverse regions of mouse brain', *Neurochem Res,* 26 (10), 1157-61.

Vitoulova, E., et al. (2011), 'Characterisation of metal-binding biomolecules in the clam Chamelea gallina by bidimensional liquid chromatography with in series UV and ICP-MS detection', *International Journal of Environmental Analytical Chemistry,* 91 (13), 1282-95.

Wägele, Brigitte, et al. (2012), 'MassTRIX Reloaded: Combined Analysis and Visualization of Tran-Scriptome and Metabolome Data', *PLoS ONE,* 7 (7), e39860.

Walaas, Eva (1958), 'Stability constants of metal complexes with mononucleotides', *Acta chem. scand,* 12 (528), 3.

Walker, Alesia, et al. (2014), 'Distinct signatures of host–microbial meta-metabolome and gut microbiome in two C57BL/6 strains under high-fat diet', *The ISME journal,* 8 (12), 2380-96.

Walter, U., et al. (2003), 'Brain parenchyma sonography discriminates Parkinson's disease and atypical parkinsonian syndromes', *Neurology,* 60 (1), 74-7.

Wang, J. D., et al. (1989), 'Manganese induced parkinsonism: an outbreak due to an unrepaired ventilation control system in a ferromanganese smelter', *Br J Ind Med,* 46 (12), 856-9.

Weber, Günther and Konieczyński, Paweł (2003), 'Speciation of Mg, Mn and Zn in extracts of medicinal plants', *Analytical and bioanalytical chemistry,* 375 (8), 1067-73.

Westerhuis, J. A., et al. (2010), 'Multivariate paired data analysis: multilevel PLSDA versus OPLSDA', *Metabolomics,* 6 (1), 119-28.

Wheelock, A. M. and Wheelock, C. E. (2013), 'Trials and tribulations of 'omics data analysis: assessing quality of SIMCA-based multivariate models using examples from pulmonary medicine', *Mol Biosyst,* 9 (11), 2589-96.

Whitworth, Alexander J., et al. (2005), 'Increased glutathione S-transferase activity rescues dopaminergic neuron loss in a Drosophila model of Parkinson's disease', *Proceedings of the National Academy of Sciences,* 102 (22), 8024-29.

WHO (1996), 'Guidelines for drinking-water quality. Vol. 2', *Health criteria and other supporting information, 2nd ed. Geneva* (World Health Organization).

--- (2005), 'VMNIS, Global database on Anaemia', (Berlin).

--- (2006), 'Elemental speciation in human health risk assessment ', (Environmental health criteria 234; Geneva, Switzerland: Apostoli,P.).

Williams, R.J.P. (2001), 'Chemical selection of elements by cells', *Coordination Chemistry Reviews,* 216-217, 583-95.

Wilson, D. S. and Sober, E. (1989), 'Reviving the superorganism', *J Theor Biol,* 136 (3), 337-56.

Witting, Michael and Schmitt-Kopplin, Philippe (2014), 'Chapter 17 - Transcriptome and Metabolome Data Integration—Technical Perquisites for Successful Data Fusion and Visualization', in Alejandro Cifuentes Carolina Simó and García-Cañas Virginia (eds.), *Comprehensive Analytical Chemistry* (Volume 63: Elsevier), 421-42.

Witting, Michael, et al. (2014), 'DI-ICR-FT-MS-based high-throughput deep metabotyping: a case study of the Caenorhabditis elegans–Pseudomonas aeruginosa infection model', *Analytical and bioanalytical chemistry*, 1-15.

Wörmann, Kilian, et al. (2012), 'Revolution in Diabetes Diagnostics-Metabolomics for Discovering Biomarkers', *Diabetes aktuell für die Hausarztpraxis,* 10 (03), 129-33.

Xu, Bin, Xu, Zhao-Fa, and Deng, Yu (2010), 'Protective effects of MK-801 on manganese-induced glutamate metabolism disorder in rat striatum', *Experimental and Toxicologic Pathology,* 62 (4), 381-90.

Xu, Bin, et al. (2014), 'Alpha-Synuclein is Involved in Manganese-Induced ER Stress via PERK Signal Pathway in Organotypic Brain Slice Cultures', *Molecular Neurobiology,* 49 (1), 399-412.

Xu, K., Bastia, E., and Schwarzschild, M. (2005), 'Therapeutic potential of adenosine A(2A) receptor antagonists in Parkinson's disease', *Pharmacol Ther,* 105 (3), 267-310.

Yokel, R. A. (2009), 'Manganese flux across the blood-brain barrier', *Neuromolecular Med,* 11 (4), 297-310.

Yokel, R. A. and Crossgrove, J. S. (2004), 'Manganese toxicokinetics at the blood-brain barrier', *Health Effects Institute* (2004/03/27 edn.), 7-58; discussion 59-73.

Youdim, Kuresh A., et al. (2003), 'Interaction between flavonoids and the blood–brain barrier: in vitro studies', *Journal of Neurochemistry,* 85 (1), 180-92.

Zacco, A., et al. (2009), 'Analysis of settled dust with X-ray Fluorescence for exposure assessment of metals in the province of Brescia, Italy', *J Environ Monit,* 11 (9), 1579-85.

Zatta, P., et al. (2003), 'The role of metals in neurodegenerative processes: aluminum, manganese, and zinc', *Brain Res Bull,* 62 (1), 15-28.

Zayed, J. (2001), 'Use of MMT in Canadian gasoline: Health and environment issues', *American Journal of Industrial Medicine,* 39 (4), 426-33.

Zhang, Ai-hua, Sun, Hui, and Wang, Xi-jun (2013), 'Recent advances in metabolomics in neurological disease, and future perspectives', *Analytical and bioanalytical chemistry,* 405 (25), 8143-50.

Zhang, D., Kanthasamy, A., and Anantharam, V. (2011), 'Effects of manganese on tyrosine hydroxylase (TH) activity and TH-phosphorylation in a dopaminergic neural cell line', *Toxicol Appl Pharmacol,* 254 (2), 65-71.

Zhang, Surong, Fu, Juanling, and Zhou, Zongcan (2004), 'In vitro effect of manganese chloride exposure on reactive oxygen species generation and respiratory chain complexes activities of mitochondria isolated from rat brain', *Toxicology in Vitro,* 18 (1), 71–77.

Zheng, W., Aschner, M., and Ghersi-Egea, J. F. (2003), 'Brain barrier systems: a new frontier in metal neurotoxicological research', *Toxicol Appl Pharmacol,* 192 (1), 1-11.

Zheng, W., et al. (2011), 'Biomarkers of manganese intoxication', *Neurotoxicology,* 32 (1), 1-8.

Zoriy, M. V., et al. (2006), 'Imaging of Cu, Zn, Pb and U in human brain tumor resections by laser ablation inductively coupled plasma mass spectrometry', *International Journal of Mass Spectrometry,* 257 (1–3), 27-33.

Zwingmann, C., Leibfritz, D., and Hazell, A. S. (2003a), 'Altered metabolic trafficking via glutamine-glutamate-cycle between astrocytes and neurons in manganese neurotoxicity', *Journal of Neurochemistry,* 87, 142-42.

--- (2003b), 'Energy metabolism in astrocytes and neurons treated with manganese: relation among cell-specific energy failure, glucose metabolism, and intercellular trafficking using multinuclear NMR-spectroscopic analysis', *J Cereb Blood Flow Metab,* 23 (6), 756-71.

Curriculum vitae

Katharina Theresa Neth (birth name *Fernsebner*)
Born on 14th of June 1987, Bad Reichenhall

<u>Education and professional experience</u>

04.2012-07.2015	PhD student, Research Unit Analytical Biogeochemistry, Helmholtz Zentrum München
	Focus on elemental analysis, hyphenated techniques and metabolite analysis of brain in Mn-induced neurotoxicology
	Presentation and Publication of research on conferences and in international journals
	Member of the HELENA graduate school

10.2010-04.2012	Studies of Pharmaceutical Sciences, M.Sc., LMU München
	Focus on Drug Monitoring and Instrumental Analytics, Pharmaceutical Biology and Technology
	Master Thesis at the Department of Clinical Chemistry and Biochemistry, Title: "Functional Analysis of Fzd1, Fzd5 and Fzd7 in Wnt/ß-Catenin Signaling of Human Mesenchymal Stem Cells"

04.2007-10.2010	Studies of Pharmaceutical Sciences, B.Sc., LMU München
	Focus on inorganic and organic Chemistry, Biology, Pharmacology
	Bachelor Thesis at the Department of Pharmaceutical Biology, Title: "Comparative functional examination of natural compounds in various highly invasive tumor cell lines"

05.2006	A-Levels, Annette-Kolb-Gymnasium Traunstein

<u>Membership</u>

Since 2012	German Society of Minerals and Trace Elements e.V. (GMS); since 2013 member of the advisory board

Eidesstattliche Erklärung

Ich erkläre an Eides statt, dass ich die bei der promotionsführenden Fakultät Wissenschafts-zentrum Weihenstephan für Ernährung, Landnutzung und Umwelt der Technischen Universi-tät München zur Promotion vorgelegte Arbeit mit dem Titel „Manganese: Species Pattern and Mechanisms of Brain Injury" unter der Anleitung und Betreuung von Prof. Dr. Bernhard Michalke und Prof. Dr. Philippe Schmitt-Kopplin ohne sonstige Hilfe erstellt und bei der Ab-fassung nur die gemäß § 6 Abs. 6 und 7 Satz 2 angegebenen Hilfsmittel benutzt habe.

(x) Ich habe keine Organisation eingeschaltet, die gegen Entgelt Betreuerinnen und Betreuer für die Anfertigung von Dissertationen sucht der die mir obliegenden Pflichten hinsichtlich der Prüfungsleistungen für mich ganz oder teilweise erledigt.
(x) Ich habe die Dissertation in dieser oder ähnlicher Form in keinem anderen Prüfungsver-fahren als Prüfungsleistung vorgelegt.
(x) Ich habe den angestrebten Doktorgrad noch nicht erworben und bin nicht in einem frühe-ren Promotionsverfahren für den angestrebten Doktorgrad endgültig gescheitert.

Die öffentlich zugängliche Promotionsordnung der TUM ist mir bekannt, insbesondere habe ich die Bedeutung von § 28 (Nichtigeit der Promotion) und § 29 (Entzug des Doktorgrades) zur Kenntnis genommen. Ich bin mir der Konsequenzen einer falschen Eidesstattlichen Er-klärung bewusst.

Mit der Aufnahme meiner personenbezogenen Daten in die Alumni-Datei bei der TUM bin ich einverstanden.

München, den 14.09.2015